Immunology *cum grano salis*: The effect of high salt on alternative and pro-inflammatory macrophage activation

Inaugural-Dissertation
to obtain the academic degree
Doctor rerum naturalium (Dr. rer. nat.)

submitted to the Department of Biology, Chemistry and Pharmacy
of Freie Universität Berlin

by
Matthias Gebhardt

from
Nürnberg

2015

prepared in the group of Prof. Dr. Dominik N. Müller
at the Max-Delbrück-Center for Molecular Medicine
from January 2013 until October 2015

Referees: 1. Prof. Dr. Dominik N. Müller
2. Prof. Dr. Christian Freund

Date of thesis defense: 07. April 2016

Content

Acknowledgements

Looking back on my thesis – and I still have to write the discussion – I consider it a successful adventure. I am not talking of this piece of text – that is up to the referees – but of the past three years. I really enjoyed doing science. Personally, this thesis inspired a clear vision for my future and gives me the energy to pursue my aim to become a clinician scientist. As a team member, I am happy to know that this thesis project led to a new publication on the records of our group. I could not have asked for more.

This would not have happened without the great support by so many people. First, I wish to thank my mentors Katrina Binger and Dominik Müller who made it possible for me to work on this thesis project at the MDC. Both of you are great mentors. I thank you for all your valuable advice, discussion and support throughout these three years. And your patience. I hope we stay in contact. I also want to thank Prof. Christian Freund from the FU for being my second referee. I do not take it for granted.

We are a big group. I could list 20 names. But I want to thank simply all of you: for teaching me methods, your technical help, discussing results, helping out, spending long hours together in and outside the lab. And for creating this particularly inspiring, supportive, helpful and welcoming atmosphere typical for our group. Laborpiraten ahoy and always six inches of water under your keel! I really enjoyed being a crew member. Ahoy also to Klaus von der Mark and his former team members to Erlangen – where everything started. With Sabrina and Hendrik and the future disciples I would like to remain with 'Father, forgive them, for they do not know what they do.' Luke (23:34). All the very best for your respective theses.

My thanks to the MDC microarray and flow cytometry core facility members for their expert technical support. I would like to thank Matthias Heinig, Herbert Schulz and Carola Rintisch, Hübner lab, MDC, who taught me the art of native ChIP.

I would like to thank Jakob Völkl and Wolfgang Neuhuber for providing *Sgk1* and *Nfat5* knock out mice, respectively. The inducible Akt experiments would not have been possible without the kind gifts from the Rajewsky lab, MDC. Thanks for this. Thanks to Jonathan Jantsch for exciting my curiosity of the other side: M(LPS) macrophages.

To all the people who spent these three years with me outside the lab:

Thank you!

Abstract

High intake of dietary salt (NaCl), characteristic of the "western" lifestyle, has been linked to hypertension, cardiovascular disease and autoimmunity. These diseases constitute an increasing social health burden and cause a high individual degree of suffering. Despite recent progress, our understanding of the underlying mechanisms remains incomplete. A modest, and physiological relevant, increase in extracellular salt was recently shown to have a pro-inflammatory effect and to boost the polarization of T helper 17 cells and classical, LPS-induced macrophages (M(LPS)) *in vitro*. High dietary salt intake translated to concordant effects *in vivo*, where experimental autoimmunity and clearance of infection were affected. This thesis examines how high salt affects the activation of non-inflammatory, alternative (M2) macrophages, and explores additional mechanisms by which salt affects M(LPS) cells.

In stark contrast to Th17 and M(LPS) cells, high salt dose-dependently decreased the activation of IL-4+IL-13-stimulated (M(IL-4+IL-13)) bone marrow-derived murine macrophages. Genes important for M(IL-4+IL-13) activation and function, including *Mrc1*, *Arg1*, *Ym1*, *Fizz1*, *PD-L2*, *Irf4* and *Klf4* all had a blunted expression in the presence of high salt. This effect was not observed in tonicity control experiments with mannitol or urea, implying a specific action of NaCl. Importantly, this salt-blunted activation also translated to an effect on M2 function; *in vitro*, high salt decreased the ability of M(IL-4+IL-13) macrophages to suppress T cell proliferation. Moreover, mice fed a high salt diet had a reduced M2 activation in an IL-4-dependent *in vivo* activation model following chitin injection, and exhibited delayed wound healing compared with animals fed a normal salt diet.

Different to recent findings with Th17 and M(LPS) cells, using genetic knock out models, the effect of salt on M(IL-4+IL-13) activation was mediated independently of signaling *via* Sgk1 or Nfat5. Genome-wide expression and histone modification analysis were employed (using microarray and ChIP-seq for H3K4me3 and H4ac, respectively) to explore the mechanisms by which high salt affected M(IL-4+IL-13) activation. By combining bioinformatics analysis of the genome-wide data with complementary *in vitro* experiments, high salt was found to reduce both mitochondrial metabolic output and glycolysis of M(IL-4+IL-13) macrophages. This was coupled with a blunting of Akt and mTOR signaling. Experimental restoration of Akt signaling, using a genetic constitutively

active Akt model, rescued the effect of salt on M(IL-4+IL-13) activation. Taken together, these findings indicate a novel mechanism by which high salt reduces full M(IL-4+IL-13) macrophage activation *via* disturbed metabolic signaling pathways and the subsequent impairment of metabolic adaption. For M(LPS) macrophages, high salt was found to increase glycolytic flux which likely supports the metabolic changes normally associated with pro-inflammatory macrophage activation.

Collectively, this thesis provides evidence that high salt reduced the activation of non-inflammatory innate immune cells and contributes to our understanding of the mechanisms by which salt may boost the activation of pro-inflammatory macrophages. It gives supports to the notion that high salt constitutes an important environmental factor, which has differential effects non-inflammatory versus pro-inflammatory immune cells, and may thereby contribute to the development of diseases associated with an imbalance of the immune system.

Zusammenfassung

Die „westliche“ Lebensweise ist durch eine hohe Aufnahme von Kochsalz (NaCl) mit der Nahrung gekennzeichnet. Dies trägt maßgeblich zur Entwicklung von Bluthochdruck, kardiovaskulärer Komplikationen und Autoimmunerkrankungen bei. Diese Krankheitsbilder stellen persönlich und gesellschaftlich eine große Belastung dar. Trotz wesentlicher Fortschritte, versteht man die verantwortlichen Mechanismen bisher nur unvollständig. Vor kurzem konnte gezeigt werden, dass bereits eine geringe Erhöhung der extrazellulären Kochsalzkonzentration, wie sie auch physiologisch zu beobachten ist, *in vitro* zu einer signifikanten Aktivitätssteigerung von entzündlichen Th17 Zellen und von mit LPS aktivierten Makrophagen (M(LPS)) führt. Eine experimentelle Hochsalzdiät bestätigte diese Befunde *in vivo*: Salz verschlimmerte eine induzierte Autoimmunerkrankungen, währen es bei Ansteckung mit dem Protozoon *L. major* zu einer verbesserten Infektionsbekämpfung durch Makrophagen führte. Die vorliegende Doktorarbeit untersucht den Einfluss von Salz auf die Aktivierung nicht entzündlicher, sogenannter M2, Makrophagen.

Im Gegensatz zu Th17 und M(LPS) Zellen wurde die M2 Aktivierung von Makrophagen, die aus Knochenmarksvorläuferzellen stammten, mit den Interleukinen IL-4+IL-13 (M(IL-4+IL-13)) durch Salz abgeschwächt. Der Effekt war dosisabhängig. Die Expression wichtiger M(IL-4+IL-13) Signaturgene, unter anderem *Mrc1*, *Arg1*, *Ym1*, *Fizz1*, *PD-L2*, *Irf4* und *Klf4*, wurde durch Salz unterdrückt. Dies war kochsalzspezifisch und nicht allein auf eine erhöhte Tonizität der Umgebung zurückzuführen, wie durch Kontrollexperimente mit Mannit und Harnstoff gezeigt werden konnte. Auch verschiedene Zellfunktionen wurden durch Salz wesentlich beeinflusst: M(IL-4+IL-13) Zellen, die in der Gegenwart von Salz aktiviert wurden, unterdrückten die Proliferation von T Zellen *in vitro* deutlich schlechter. Außerdem wurde die Aktivierung von M2 Makrophagen *in vivo* in einem Chitininjektionsmodell durch Hochsalzdiät vermindert. Mäuse zeigten unter Hochsalzdiät ebenfalls eine verzögerte Wundheilung.

Wie genetische Modelle zeigten, wirkte Salz im Gegensatz zu Th17 und M(LPS) unabhängig von Sgk1 oder Nfat5 auf die M(IL-4+IL-13) Aktivierung. Um den Wirkmechanismus aufzuklären, wurden die Genexpression und Histonmodifikationen (H3K4me3/H4ac) genomweit mit Microarray und ChIP-seq untersucht. Die kombinierte Analyse der genomweiten Daten und ergänzender *in vitro* Experimente ergab, dass Salz

die mitochondriale und glykolytische Energiegewinnung von M(IL-4+IL-13) Makrophagen in Verbindung mit einer verringerten Aktivierung des Akt-mTOR Signalweges hemmt. Durch die experimentelle Überaktivierung desselben Signalweges wurde der Salzeffekt aufgehoben. Diese Befunde sprechen für einen neuen Mechanismus wie Salz die M2 Makrophagenaktivierung durch sein Eingreifen in metabolische Signalwege und die daraus resultierende gestörte metabolische Zellanpassung beeinflusst. Im Fall der M(LPS) Makrophagen erhöhte Salz die Glykolyse und damit die für entzündliche Immunzelltypen notwendige Anpassung des Zellstoffwechsels.

Zusammenfassend zeigt die vorliegende Arbeit eine verminderte Aktivierung von Zellen des angeborenen Immunsystems durch Salz und identifiziert bisher unbekannte Faktoren, die zur erhöhten Aktivierung entzündlicher Makrophagen durch Salz beitragen dürften. Damit trägt sie zu einem sich abzeichnenden Gesamtbild bei, in dem Salz einen wesentlichen Umweltfaktor für das Gleichgewicht des Immunsystems darstellt und so Gesundheit und Krankheit beeinflussen könnte.

List of figures

List of tables

Abbreviations and symbols

2-DG	2-deoxy glucose
2-NBDG	2-(N-(7-nitrobenz-2-oxa-1,3-diazol-4-yl)amino)-2-deoxyglucose
Aldoa (gene)	Aldolase A
APC	Allophycocyanin
APS	Ammonium persulfate
Arg1 (gene)	Arginase 1
BSA	Bovine serum albumin
caAkt	Constitutively active Akt
Ccl17 (gene)	Chemokine (C-C) ligand 17
Ccl2 (gene)	Chemokine (C-C) ligand 2
Ccl24 (gene)	Chemokine (C-C) ligand 24
Ccl5 (gene)	Chemokine (C-C) ligand 5
Ccl5 (gene)	Chemokine (C-C) ligand 5
Ccng1 (gene)	Cyclin G1
CD	Cluster of differentiation
cDNA	Complementary DNA
Chi3l3 (gene)	Chitinase-like 3
ChIP	Chromatin immunoprecipitation
ChIP-seq	Chromatin immunoprecipitation and sequencing
CoA	Coenzyme A
Cst7 (gene)	Cystatin F
Ctsk (gene)	Cathepsin K
Cy7	Cyanine 7
Da	Dalton
DMEM	Dulbecco's Modified Eagle's medium
DNA	Deoxyribonucleic acid
Dot1l (gene)	Dot1-like histone H3K79 methyltransferase
DTT	Dithiothreitol
E. coli	Escherichia coli
ECAR	Extracellular acidification rate
EDTA	Ethylenediaminetetraacetic acid
Eno2 (gene)	Enolase 2
FC	Fold change
FCCP	Carbonyl cyanide-4-(trifluoromethoxy)phenylhydrazone
FDR	False discovery rate
FITC	Fluorescein isothiocyanate
Fizz1 (gene/protein)	Found in inflammatory zone 1
FSC-A	Forward scatter area
FSC-H	Forward scatter height
g	Acceleration of gravity
GM-CSF	Granulocyte-macrophage colony-stimulating factor
GO	Gene ontology
GPL	General public license
Gr-1	Granulocyte differentiation antigen 1
HAT	Hypoxanthine-aminopterin-thymidine
Hdac4/7 (gene)	Histone deacetylase 4/7

HEPES	4-(2-hydroxyethyl)-1-piperazineethanesulfonic acid
HK2 (gene)	Hexokinase 2
HK3 (gene)	Hexokinase 3
HSD	High salt diet
Hspa1a (gene)	Heat shock 70kDa protein 1 A
HTS	High throughput sampler
I.P.	Intraperitoneal
IFN-β	Interferon beta
IFN-γ	Interferon gamma
IL-10	Interleukin 10
IL-13	Interleukin 13
Il19 (gene)	Interleukin 19
Il1a (gene)	Interleukin 1 alpha
IL-4	Interleukin 4
IL-6	Interleukin 6
IP	Immunoprecipitation
IRF3	Interferon regulatory factor 3
Irf4	Interferon regulatory factor 4
IRS2	Insulin receptor substrate
JAK	Janus kinase
Jmjd3	Jumonji domain containing 3
k	Kilo
kb	kilobase (pairs)
Kdm1a/3a/6b (gene)	Lysine (K)-specific demethylase 1a/3a/6b
Klf4 (gene/protein)	Kruppel-like factor 4
L. major	Leishmania major
Lcn2 (gene)	Lipocalin 2
Ldha (gene)	Lactate dehydrogenase A
LPS	Lipopolysaccharide
Malt1 (gene)	Mucosa-associated lymphoid tissue lymphoma translocation protein 1
MDSC	Myeloid-derived suppression cell
Mgl2 (gene)	Macrophage galactose N-acetyl-glucosamine specific lectin 2
MNase	Micrococcal nuclease
MR	Magnetic resonance
mOsm	Milliosmole
Mrc1 (gene)	Mannose receptor, C type 1
mt	mitochondrial
MTA	Material transfer agreement
MT-CO1 (gene)	Mitochondrially encoded cytochrome c oxidase subunit 1
mTOR	Mechanistic target of rapamycin
NDUFV1 (gene)	NADH dehydrogenase (ubiquinone) flavoprotein 1
Nfat5	Nuclear factor of activated T cells 5
NF-kB	Nuclear factor kappa light chain enhancer of activated B cells
Nos2 (gene/protein)	Nitric oxide synthase 2
NSD	Normal salt diet
OCR	Oxygen consumption rate
OXPHOS	Oxidative phosphorylation
p70S6K	p70S6 kinase
PAA	Polyacrylamide

PB	Pacific blue
PBS	Phosphate buffered saline
Pcgf1 (gene)	Polycomb group RING finger protein 1
Pdcd1lg2 (gene)	Programmed cell death 1 ligand 2
PD-L2 (protein)	Programmed cell death 1 ligand 2
PE	Phycoerythrin
PECs	Peritoneal exudate cells
PerCP	Peridinin chlorophyll
Pfkl (gene)	Phosphofructokinase, liver type
Pgam1 (gene)	Phosphoglycerate mutase 1
PGC-1β	PPARγ-co-activator-1β
PGE_2	Prostaglandin E2
PI	Propidium iodide
PIC	Protease inhibitor cocktail
PKM2	Pyruvate kinase M2
PMSF	Phenylmethylsulfonyl fluoride
PPAR-γ	Peroxisome proliferator-activated receptor gamma
qPCR	Quantitative real-time polymerase chain reaction
Retnla (gene)	Resistin-like alpha
RNA	Ribonucleic acid
Rot+A	Rotenone plus antimycin A
RPMI	Roswell Park Memorial Institute medium
RT	Room temperature
S. mansoni	Schistosoma mansoni
SA	Splice acceptor
Scd1 (gene)	Stearoyl CoA desaturase 1
SDS	Sodium dodecyl sulfate
Sgk1	Serum and glucocorticoid-regulated kinase 1
Slamf1 (gene)	Signaling lymphocytic activation molecule 1
Slc16a6 (gene)	Solute carrier family 16, member 6
Slc2a1 (gene)	Solute carrier family 2, member 1
Slc6a12 (gene)	Solute carrier family 6, member 12
SOCS	Suppressor of cytokine signaling proteins
SPF	Specific pathogen free
SRC	Spare respiratory capacity
STAT6	Signal transducer and activator of transcription 6
TAT	Trans-activator of transcription
TBS	Tris-buffered saline
TCA	Tricarboxylic acid cycle
TCR	T cell receptor
TEMED	Tetramethylethylenediamine
TF	Transcription factor
Tlr2 (gene)	Toll-like receptor 2
TNF	Tumor necrosis factor
Tpi1 (gene)	Triosephosphate isomerase
Tris	Tris(hydroxmethyl)aminomethane
WT	Wildtype

1. Introduction

1.1. New lessons in salt (NaCl) physiology

Cardiovascular disease (CVD) is a leading cause of morbidity and mortality. High dietary salt intake – a hallmark of modern diets – has been blamed to contribute to the development of high blood pressure and CVD (He et al., 2013; He and MacGregor, 2009). Autoimmunity constitutes another major health burden (Marson et al., 2015) and the dramatic increase of autoimmune disorders with western lifestyle suggests the existence of triggering environmental factors (Kleinewietfeld et al., 2013). Whilst both CVD and autoimmunity show strong genetic predisposition (Farh et al., 2015; Housley et al., 2015; Mitchell et al., 2005), the precise mechanisms by which environmental factors might additionally contribute to disease development remain poorly understood (Adler et al., 2014; DiNicolantonio et al., 2013; Klaus, 2012; Kleinewietfeld et al., 2013).

One environmental factor that has changed dramatically with western lifestyle is the excess of salt (NaCl) we consume (O'Donnell et al., 2014, 2015). Na^+ is the dominant extracellular electrolyte (Terry, 1994). The traditional view of body sodium, fluid volume and blood pressure homeostasis assumes that interstitial and intravascular volumes constitute a single extracellular compartment; that plasma and interstitial sodium are in equilibrium without relevant concentration gradients; and that the kidneys have unrestricted access to regulate plasma *and* tissue sodium by blood purification and urinal secretion (Machnik et al., 2010; Titze and Machnik, 2010) (Figure 1 A). In this two-compartment model, some sodium is retained after a sudden increase in sodium intake along with a commensurate amount of water to osmotically neutralize the extra Na^+ and to keep plasma sodium levels within very tight boundaries (Heer et al., 2000; Titze and Machnik, 2010). The kidneys would eventually establish a new steady state of intake and excretion at higher total body sodium and water levels (Titze et al., 2014).

However, careful dietary studies in humans observed a considerable retention of excess sodium at unchanged plasma Na^+ concentrations without the expected increase of total body water (Heer et al., 2000; Rakova et al., 2013; Titze et al., 2002). These and earlier studies shaped the idea of a plasma-*independent* extracellular compartment where Na^+ is stored without water (Heer et al., 2000; Ivanova et al., 1978; Rakova et al., 2013; Titze et al., 2002), thereby extending current textbook knowledge of electrolyte handling and inspiring new hypotheses how mechanistically high salt can cause a lot of trouble.

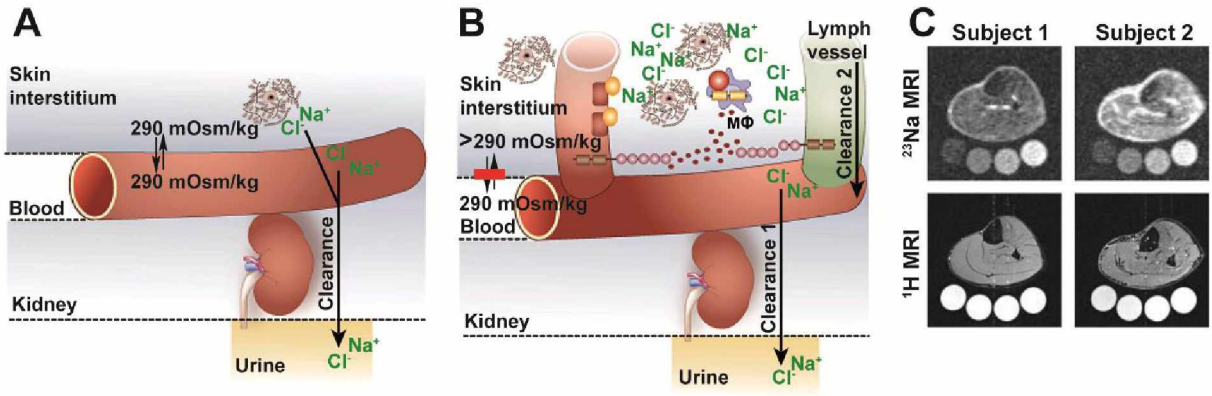

Figure 1. A novel concept of body sodium homeostasis. A: The traditional two-compartment model of body electrolyte, volume and blood pressure homeostasis is based on the concept of electrolyte equilibrium between blood and interstitial volume. Here, blood purification by the kidneys regulates interstitial water and electrolyte balance. **B:** The interstitium is a blood-independent hypertonic sodium storage compartment. Local regulatory networks achieve electrolyte and blood pressure balance together with renal blood purification. Specifically, macrophages act as osmo-sensors and modulate interstitial electrolyte composition via the lymph capillary network (A-B faithfully adapted from (Titze et al., 2014)). **C:** ^{23}Na-MR images of the lower leg (upper panels); tubes with solutions containing 10, 20, 30, and 40mmol/l of NaCl are arranged below the extremity, thereby allowing calibration of tissue Na^+. Tissue Na^+ content is increased in subject2 compared to subject1. Tissue water (lower panels) in the same subjects detected with conventional ^{1}H-MRI. No difference in muscle water content is visible to the naked eye (faithfully adapted from (Kopp et al., 2013a)).

Specifically, the skin interstitium with its high density of negatively charged glycosaminoglycans (GAGs) represents a perfect candidate for sodium storage (Farber, 1960; Farber et al., 1957; Ivanova et al., 1978). Additional animal studies confirmed water-free and GAG-mediated sodium storage in the skin under high dietary intake conditions (Titze et al., 2003; Titze et al., 2004).

A consequence of water-free sodium storage is the creation of hypertonic microenvironments *in vivo* where interstitial sodium concentrations are in considerable disequilibrium compared to blood plasma (Machnik et al., 2010; Machnik et al., 2009; Szabo and Magyar, 1982; Wiig et al., 2013) (Figure 1 B). Tissue hypertonicity then activates kidney-independent networks to regulate electrolyte balance locally. Specifically, macrophages act as on-site hypertonicity sensors, which induce hyperplasia of the lymphatic network via a Nfat5-Vegf-C signaling axis in response to sodium storage. Experimental ablation of this regulatory circuit leads to a significant salt-sensitive blood pressure increase (Machnik et al., 2010; Machnik et al., 2009; Titze and Machnik, 2010; Wiig et al., 2013). Importantly, salt storage is also found in humans (Figure 1 C) and ^{23}Na magnetic resonance imaging (MRI)-

dependent studies suggest striking similarities between experimental animal models and human physiology (Dahlmann et al., 2015; Jantsch et al., 2015; Kopp et al., 2013a; Kopp et al., 2012a; Kopp et al., 2012b; Titze, 2014; Titze et al., 2014).

1.2. Osmotic stress response

How do cells then cope with tonicity-induced stress? Hypertonic solutions cause cell shrinkage by osmotic efflux of water and severe impairment of cellular functions (Burg et al., 2007) (Figure 2 A-B). Most of our knowledge about osmotic stress handling stems from kidney medullary tissue where cells survive and function in extreme hypertonicity (Küper et al., 2007). However, all cells are equipped to deal with a certain degree of osmotic stress irrespective of whether or not they will ever experience it (Burg et al., 2007; Yancey et al., 1982).

DNA damage, cell cycle arrest, oxidative stress and impaired transcription/translation of many genes are all hallmarks of hypertonic stress. Cells restore volume initially by influx of inorganic ions (mainly Na^+ and Cl^-) followed by water at the expense of an unfavorably high intracellular ionic strength (known as regulatory volume increase (RVI)). High intracellular ionic strength interferes with macromolecular function and is responsible for some of the impairments mentioned before (Figure 2 C). Next, energy-demanding active transport replaces intracellular sodium ions with potassium (Burg et al., 2007; Küper et al., 2007).

Cells then initiate long-term adaption by the expression of channels and enzymes that facilitate the uptake and synthesis of compatible organic osmolytes, which do not perturb macromolecules (Figure 2 D). These gradually replace inorganic ions and allow for the recovery of cellular functions while effectively preserving cell volume at the same time. Cells also increase the expression of heat shock proteins during adaption. These act as molecular chaperones to ensure proper protein folding and function (Burg et al., 2007; Küper et al., 2007; Yancey et al., 1982).

Cell shrinkage, ionic strength or the cytoskeleton were all proposed to initiate osmotic stress signaling which is then fed forward to downstream effectors (Burg et al., 2007; Küper et al., 2007). The mitogen-activated protein kinase p38 pathway and the transcription factor nuclear factor of activated T-cells 5 (Nfat5) are tonicity-induced signaling hubs to promote the osmotic stress response (Han et al., 1994; Miyakawa et al.,

1999). Additional upstream signals fine-tune Nfat5 activity by phosphorylation (Ferraris et al., 2002). A PI3K - serum and glucocorticoid-inducible kinase 1 (Sgk1) signaling axis constitutes another backbone of osmo-answer signaling (Lang et al., 2006). This complex response network enables cells to restore cellular functions if tonicity does not exceed a critical threshold (Burg et al., 2007).

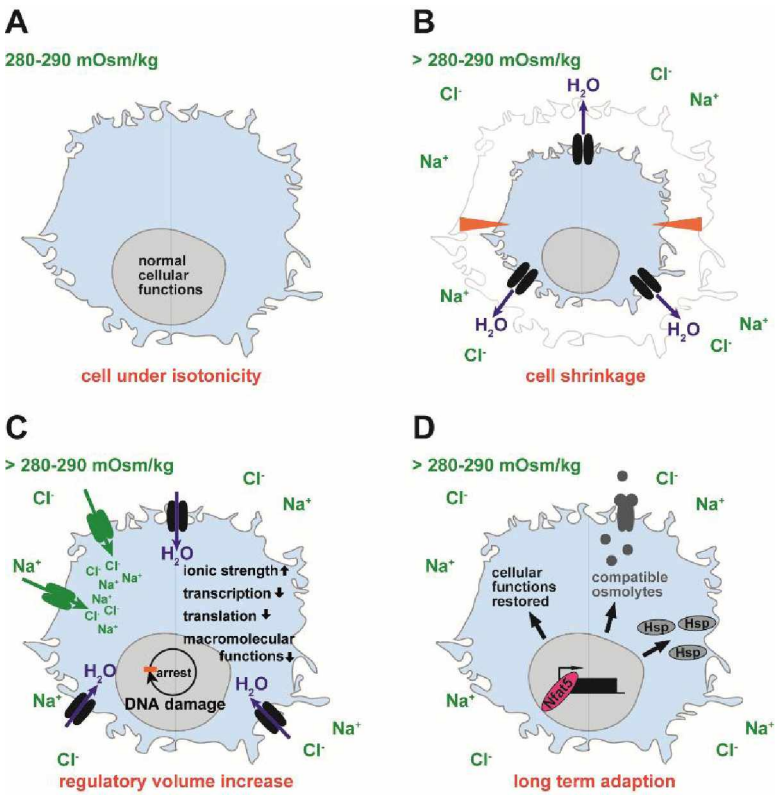

Figure 2. Osmotic stress response. A: Cells in isotonic microenvironments function normally. **B:** Hypertonicity leads to osmotic water efflux and cell shrinkage (red arrowheads). **C:** Cell volume is restored by energy-consuming import of extracellular ions followed by water. High intracellular ionic strength impairs cellular functions, causes DNA damage and cell cycle arrest of proliferating cells. **D:** Osmotic stress signaling via Nfat5 induces the expression of transporters and enzymes for the provision of compatible organic osmolytes. These replace intracellular ions, preserve cell volume and allow for resumption of most cellular functions. Nfat5 additionally induces the expression of heat shock proteins (Hsp) which serve as molecular chaperones for other proteins.

1.3. The macrophage: a whole universe within a cell membrane

Microenvironmental cues greatly influence cellular behaviour and specifically macrophages (Xue et al., 2014). This cell type has come a long way since Elie Metchnikoff first appreciated the importance of these phagocytic cells for host defence (Gordon, 2008). Macrophages fulfill a wide spectrum of functions beyond immunity and immune

regulation (Mosser and Edwards, 2008). They are also first line players in homeostatic regulation ranging from clearance of exhausted erythrocytes and iron recycling (de Back et al., 2014; Kohyama et al., 2009), removal of apoptotic cells (Gordy et al., 2011; Savill et al., 2002), adipose tissue homeostasis (Harms and Seale, 2013; Nguyen et al., 2011; Odegaard et al., 2007; Qiu et al., 2014), to extracellular electrolyte balance (Jantsch et al., 2014b).

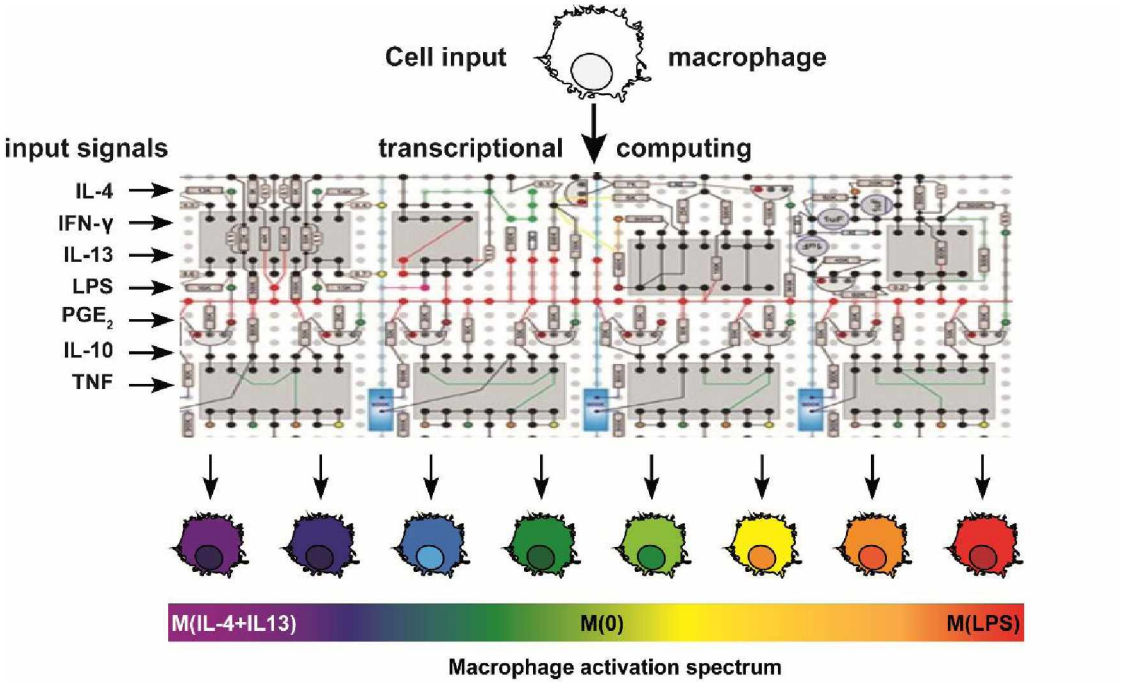

Figure 3. A spectrum model of macrophage activation. Macrophages integrate different stimuli to yield a wide spectrum of activation states beyond the dichotomous assignment into classically activated M1 and alternatively activated M2 macrophages (faithfully adapted from (Xue et al., 2014)).

This functional diversity is reflected by an almost countless number of macrophage phenotypes both *in vivo* and *in vitro*; they literally seem to compute even subtle environmental cues to yield a tailor-made spectrum of activation states (Xue et al., 2014) (Figure 3), ranging from armed-to-the-teeth pro-inflammatory defence cells (often referred to as M1 macrophages) over alternatively activated (often referred to as M2 macrophages) to truly immune-regulatory and function-specific phenotypes (Lawrence and Natoli, 2011; Mosser and Edwards, 2008; Murray and Wynn, 2011a, b). Macrophages should therefore not be forced into the dichotomous scheme of M1 versus M2 activation used before. In this thesis, I will provide extensive methodological information and the exact activation stimuli, e.g. M(IL-4+IL13), M(LPS), wherever possible as recently suggested by the macrophage research community (Murray et al., 2014).

Activation with lipopolysaccharide (LPS) induces prototypic pro-inflammatory macrophages. M(LPS) produce a vast array of bactericidal and pro-inflammatory mediators such as tumor necrosis factor (TNF) and interleukin 6 (IL-6) (Lawrence and Natoli, 2011; Mantovani, 2008; Mosser and Edwards, 2008; Murray et al., 2014; Tugal et al., 2013). The strong induction of *Nos2* and the subsequent NO burst constitute an effective means to combat pathogens (Jantsch et al., 2015; Mantovani, 2008) (Figure 4).

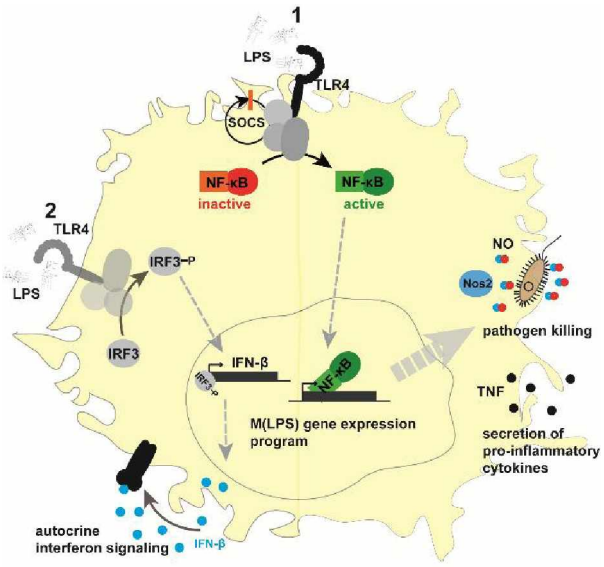

Figure 4. M(LPS) macrophage activation scheme. M(LPS) macrophages are pro-inflammatory immune cells specialized to combat intracellular infections. Recognition of LPS by TLR4 activates NF-κB (1) and IRF3 (2) signaling cascades. Activated NF-κB and phosphorylated IRF3 translocate to the nucleus where they act as transcription factors for the expression of M(LPS) genes. Nos2 and TNF are prominent examples of induced bactericidal and pro-inflammatory genes, respectively. Nitrite oxide (NO) produced from arginine by Nos2 is a major component of the murine armory against intracellular pathogens. The LPS/TLR4 signaling complex initiates negative feedback signaling via SOCS1 at the same time.

The original description of pro-inflammatory macrophages was after activation with interferon gamma (IFN-γ) (Nathan et al., 1983) but LPS by its ability to induce autocrine interferon beta (IFN-β) signaling is sufficient to develop a pro-inflammatory phenotype (Mosser and Edwards, 2008; Toshchakov et al., 2002). LPS is recognized by toll-like receptor 4 (TLR4) (Takeda and Akira, 2004). The LPS/TLR4 complex triggers various downstream signaling cascades (Figure 4): Nuclear factor kappa-light-

chain-enhancer of activated B cells (NF-κB) signaling induce the expression of many M(LPS) effector molecules; the expression of IFN-β is induced via phosphorylation of interferon regulatory factor (IRF) 3 (Bjorkbacka et al., 2004; Lawrence and Natoli, 2011; Mantovani, 2008; Meraz et al., 1996; Mosser and Edwards, 2008; Toshchakov et al., 2002; Tugal et al., 2013; Weintz et al., 2010). Negative feedback signaling via suppressor of cytokine signaling protein 1 (SOCS1) is initiated at the same time to avoid overshooting inflammation (Alexander and Hilton, 2004; Alexander et al., 1999; Fukao and Koyasu, 2003; Song and Shuai, 1998).

Interleukin 4 (IL-4) and interleukin 13 (IL-13) activate completely different pathways to induce alternative activation of M(IL-4+IL-13) macrophages (Gordon, 2003) (Figure 5). Upon binding of these ligands to their respective receptors, receptor-bound Janus kinases (JAKs) phosphorylate STAT6 – the master TF of M(IL-4+IL-14) activation. Phospho-STAT6 homodimers then translocate into the nucleus and induce transcription of the M(IL-4+IL-13) activation program (Gordon, 2003; Martinez et al., 2009; Mosser and Edwards, 2008; Takeda et al., 1996; Varin and Gordon, 2009). Signaling via peroxisome proliferator-activated receptor gamma (PPAR-γ) and a PI3K – Akt – mTOR cascade with subsequent metabolic adaptions (see 1.4) are additional requirements for full M(IL-4+IL-13) activation (Byles et al., 2013; Martinez et al., 2009; Odegaard et al., 2007). Additionally, the TFs Krueppel-like factor 4 (KLF4) (Liao et al., 2011) and interferon regulatory factor 4 (IRF4) (El Chartouni et al., 2010; Satoh et al., 2010) synergize with STAT6. IL-4 signaling also activates a SOCS-dependent negative feedback loop (Dickensheets et al., 2007; Varin and Gordon, 2009) (Figure 5).

Compared to M(LPS), murine M(IL-4+IL-13) macrophages are poor producers of pro-inflammatory cytokines and bactericidal oxygen species (Abramson and Gallin, 1990). They acquire a unique phagocytic receptor and secretory program. Mannose receptor, C type 1 (MRC1 or CD206); arginase 1 (Arg1); chitinase-like protein 3 (Chi3l3 or Ym1) and resistin-like alpha (Retnla or Fizz1) constitute core signature molecules of murine M(IL-4+IL-13) activation *in vitro* and *in vivo* (Goerdt and Orfanos, 1999; Loke et al., 2002; Nair et al., 2005; Nair et al., 2006; Raes et al., 2002; Raes et al., 2005; Stein et al., 1992). The functional implication of these most prominent M(IL-4+IL-13) marker molecules is not well understood except for Arg1 which has been associated with wound healing (see next paragraph) (Anthony et al., 2007; Chang et al., 2001; Jin et al., 1998; Nair et al., 2005; Nair et al., 2006).

Functionally, M(IL-4+IL-13) macrophages are often considered to be prototypic wound-healing macrophages even though contradictory experimental data complicate the assignment of their definite role to date (Deonarine et al., 2007; Martin et al., 2003; Martinez et al., 2009; Mirza et al., 2009; Mosser and Edwards, 2008; Varin and Gordon, 2009). Clearance of helminth infections is another possible *in vivo* function of M(IL-4+IL-13) macrophages. While a direct contribution to pathogen clearance was apparent only in specific infection models, M2 macrophages might still generally help to mount an appropriate immune response by inducing and sustaining eosinophilia during worm infection (Anthony et al., 2007; Martinez et al., 2009; Thomas et al., 2012). For sure, M2 cells possess immuno-suppressive features and contribute to immune homeostasis *in vivo* and *in vitro* where they suppress lethal inflammation or T cell proliferation, respectively (Goerdt and Orfanos, 1999; Gordon, 2003; Herbert et al., 2004; Huber et al., 2010; Martinez et al., 2009; Schebesch et al., 1997).

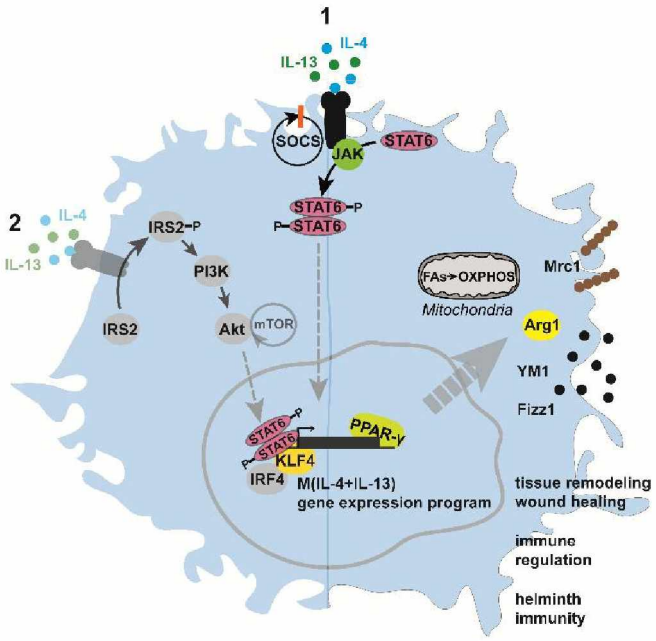

Figure 5. M(IL-4+IL-13) macrophage activation scheme. M(IL-4+IL-13) macrophages are non-inflammatory immune cells important for wound healing, anti-helminth immunity and immune regulation. Upon ligand binding, receptor associated Janus kinases (JAKs) phosphorylate STAT6 which then translocates to the nucleus and acts as master TF of M(IL-4+IL-13) activation (1). The TFs IRF4, KLF4 and PPAR-γ act in concert to yield full activation and metabolic switching. Signaling via insulin receptor substrate 2 (IRS2) – PI3K – Akt regulated by mTOR activity is a second important pathway (2). Mrc1, Arg1, YM1 and Fizz1 are murine core M(IL-4+IL-13) signature proteins.

1.4. Immunometabolism

Adaptions of cellular metabolic programs are crucial for proper immune cell activation (Pearce et al., 2013). Metabolic rewiring is important not only to meet the metabolic needs of highly proliferative cells; it also controls adaptive immune cell effector functions and fate decisions (Chang et al., 2013; McGettrick and O'Neill, 2013; O'Sullivan and Pearce, 2014; O'Sullivan et al., 2014; Shi et al., 2011; Vander Heiden et al., 2009; Warburg et al., 1927). How metabolism also regulates the activation and function of innate immune cells is currently being investigated (Cheng et al., 2014b; Everts et al., 2014; Everts et al., 2012).

Activation of macrophages with either LPS or IL-4+IL-13 induces bold differences in cellular metabolism. M(LPS) increase their glycolytic activity substantially via the TF hypoxia-inducible factor 1-alpha (HIF-1α) compared to M(0) or M(IL-4+IL-13) (Cramer et al., 2003; Newsholme et al., 1986; Rodriguez-Prados et al., 2010). Next to securing energy supply under hostile environmental conditions (NO burst), metabolic re-wiring of M(LPS) also contributes to effector function by tapping metabolic networks to increase the production of bactericidal compounds (Michelucci et al., 2013) and of pro-inflammatory cytokines (Tannahill et al., 2013) (Figure 6 A).

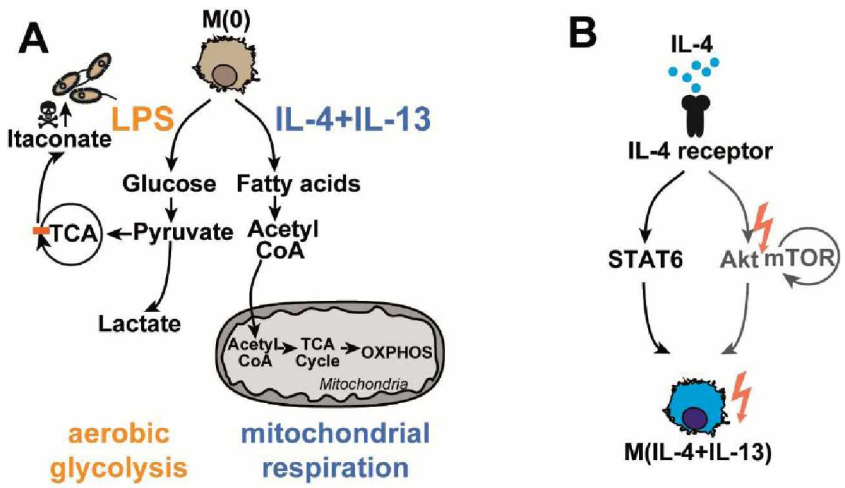

Figure 6. Metabolic re-wiring during macrophage activation. A: Activation of macrophages with LPS (orange) shifts cellular metabolism towards glycolysis and lactate production. Modification of additional metabolic networks, e.g. blocked flow (red bar) through the tricarboxylic acid cycle (TCA), enhances the production of bactericidal metabolites (itaconate). Activation with IL-4+IL-13 (blue) shifts cellular metabolism towards oxidative break down of fatty acids. **B:** Signaling via Akt constitutes a second important cascade for M(IL-4+IL-13) activation next to STAT6. mTOR feeds into Akt signaling and full M(IL-4+IL-13) commitment is impaired if this signaling loop is aberrant (red flashes).

In contrast, M(IL-4+IL-13) utilize primarily oxidative phosphorylation (OXPHOS) to meet their energetic needs (Rodriguez-Prados et al., 2010). Specifically, IL-4 signaling promotes all aspects of mitochondrial fatty acid oxidation from uptake to breakdown via STAT6 and PPARγ-co-activator-1β (PGC-1β) signaling (Huang et al., 2014a; Vats et al., 2006) (Figure 6 A). Early in activation, M2 macrophages break down glucose as their primary substrate for OXPHOS (Tan et al., 2015). Experimental inhibition of these metabolic adaptions blunts the acquisition of a full activation phenotype for both M1 and M2 macrophages (Huang et al., 2014a; Jha et al., 2015; Odegaard et al., 2007; Vats et al., 2006).

Macrophages also integrate whole-organism nutritional status to yield very specific activation phenotypes (Kang et al., 2008; Kratz et al., 2014; Odegaard et al., 2007). It is therefore not surprising that a mechanistic target of rapamycin (mTOR)-Akt signaling loop has been identified downstream of IL-4 which is essential for full M2 commitment; aberrant mTOR signaling causes – via Akt – a pro-inflammatory shift of M(IL-4) activation *in vitro* and *in vivo* (Byles et al., 2013) (Figure 6 B). The mTOR pathway integrates nutrient supply status and other environmental signals to regulate various cell functions (Goberdhan and Boyd, 2009; Haissaguerre et al., 2014) and plays a major role also in the regulation of adaptive immune cells (Chi, 2012; Delgoffe and Powell, 2009).

1.5. Epigenetics and histone modifications

Metabolic regulation of *epigenetics* is one additional mechanism by which metabolism affects cellular function (Lu and Thompson, 2012). Namely, DNA – with its plethora of available genes and regulatory elements – needs to be interpreted according to environmental cues to implement the right transcriptional program at the right spot at the right time. The term *epigenetics* comprises the mechanisms used to superimpose information on DNA *and its usage* without changing the actual sequence (Holliday, 2006; Kouzarides, 2007).

Accessibility of DNA is one critical aspect. Nuclear DNA is tightly packed around histone proteins (Luger et al., 1997) and forms higher order chromatin. The tail domain of histones can be modified by a range of posttranslational modifications such as acetylation and methylation of lysine residues. These modifications shape chromatin structure and DNA accessibility as one *epigenetic* mechanism that regulates downstream DNA-dependent processes. The existence of a language-like histone code was proposed

whereby specific histone modifications or combinations thereof are instructive to regulate transcription (Jenuwein and Allis, 2001; Strahl and Allis, 2000) (Figure 7). To date, many enzymes catalyzing the addition or removal of histone modifications have been identified together with proteins that *interpret* the histone code by binding to specific modifications and recruiting additional effector molecules (Jenuwein and Allis, 2001; Li et al., 2007). Acetylation of histones around the transcription start site (TSS), e.g. histone 4 (H4ac), is associated with actively transcribed genes (Pokholok et al., 2005; Reinke and Horz, 2003). Acetylation reduces the positive charge density of histone tails, interaction forces with negatively charged DNA and thus packing density (Kouzarides, 2007; Weintraub and Groudine, 1976). Trimethylation of histone 3 lysine 4 (H3K4me3) around the TSS is a prototypical methylation mark correlated with activation of gene transcription (Kouzarides, 2007; Li et al., 2007; Pokholok et al., 2005) whereas trimethylation of histone 3 lysine 27 (H3K27me3) is associated with gene silencing (Agger et al., 2007; Schuettengruber et al., 2007). Reversible histone modifications provide plasticity to adapt transcription according to environmental cues. To which extend diet and other lifestyle factors influence cells via epigenetic mechanisms is a question of current research (Alegria-Torres et al., 2011; Jaenisch and Bird, 2003; Smolkova et al., 2014).

Histone modifications are essential for macrophage activation. Irf4 is another essential TF which regulates M(IL-4+IL-13) gene expression programs and activation. *Irf4* expression itself is induced upon M2 activation by the removal of suppressive histone marks (H3K27me3) (Ishii et al., 2009; Satoh et al., 2010). Additionally, experimental interference with the histone code protects from pathological inflammation, indicating that epigenetic mechanisms also regulate pro-inflammatory macrophages (Nicodeme et al., 2010).

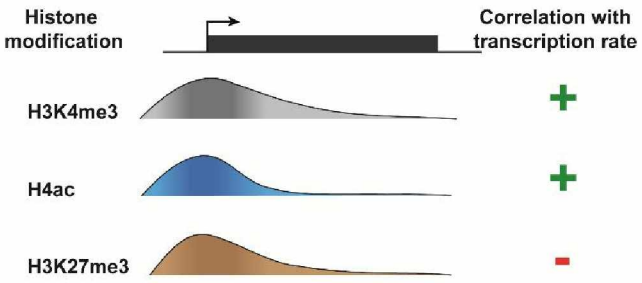

Figure 7. Genome-wide distribution patterns of histone marks and transcription. The distribution of histone modifications on an arbitrary gene relative to its TSS (black arrow). +/-: positive/negative correlation with transcriptional activity (faithfully adapted from (Li et al., 2007)).

1.6. High salt and immune cells

Autoimmune disorders are becoming an increasing health burden in western countries (Kleinewietfeld et al., 2013; Marson et al., 2015). Also, we are becoming increasingly aware how disturbed immune homeostasis contributes to the etiology of high blood pressure and CVD, another scourge for mankind (Dinarello, 2009; Guzik et al., 2007; He and MacGregor, 2009; Saleh et al., 2015). While high dietary salt consumption is associated with blood pressure increase and subsequent CVD (He et al., 2013; He and MacGregor, 2009), the mechanisms by which environmental variables such as salt intake trigger the increasing incidence of autoimmune disorders in western countries remain a critical question of current research (Kleinewietfeld et al., 2013).

Thus, the identification of environmental factors affecting immune cell function and homeostasis is highly desirable. Recent research yielded a new understanding of electrolyte homeostasis *in vivo*: Excess dietary salt is stored in tissues and creates hypertonic microenvironments in interstitial fluid compartments (Machnik et al., 2010; Machnik et al., 2009; Titze and Machnik, 2010; Wiig et al., 2013). The fact that immune cells likely encounter hypertonic, NaCl-loaded environments *in vivo* also in humans, forces us to ask how high salt affects immune cell function. High salt induces highly aggressive Th17 cells *in vitro* and *in vivo* (Kleinewietfeld et al., 2013; Wu et al., 2013). In patients with multiple sclerosis, a Th17-biased autoimmune disorder, high dietary salt intake is associated with disease progression (Farez et al., 2015). Non-inflammatory T cells are also affected; here, high salt impairs the function of regulatory T-cells (Safa et al., 2015).

1.7. Scope of thesis and specific aims

The immune system functions as a fine-balanced clockwork of pro- and anti-inflammatory mechanisms. It is of particular interest to study the effect of high salt on macrophages as: (1) these cells form a physiological tonicity response network *in vivo* (Machnik et al., 2009); (2) macrophages readily migrate along increasing salt gradients (Muller et al., 2013). A comprehensive understanding of how environmental factors influence immune-balance may ultimately translate into novel therapeutic options for common disease entities by comparably simple lifestyle changes.

High salt boosts of M(LPS) activation (Jantsch et al., 2015). In stark contrast, the effects of high salt on anti-inflammatory M(IL-4+IL-13) macrophages and the mechanisms

involved remain elusive. In my thesis, I address this important question (Figure 8) by increasing tonicity during the activation of macrophages with IL-4+IL-13 by an additional 40mM NaCl *in vitro* or by feeding a high salt diet *in vivo*. I hypothesize that the activation of macrophages with IL-4+IL-13 is aberrant under high salt conditions. I further hypothesize that salt-affected activation translates to impaired M(IL-4+IL-13) cellular function *in vitro* and *in vivo*. By applying genome wide research approaches I will generate new hypotheses as to *how* high salt affects M(IL-4+IL-13) and M(LPS) activation beyond our current understanding (Jantsch et al., 2015). I define the following specific aims for my thesis project:

(I) To identify how high salt (additional 40mM NaCl) affects the activation of M(IL-4+IL-13) cells *in vitro*, *ex vivo* and *in vivo*

(II) To investigate whether activation of M(IL-4+IL-13) cells in the presence of high salt alters function *in vitro* and *in vivo*

(III) To generate a comparative genome wide data base of gene expression and activating histone marks under normal and high salt conditions and to use bioinformatics analysis to identify possible mechanisms as to how high salt affects the activation of macrophages by IL-4+IL-13 and LPS

(IV) To verify the mechanisms identified by genome wide analysis (see aim above) with complementary *in vitro* experiments

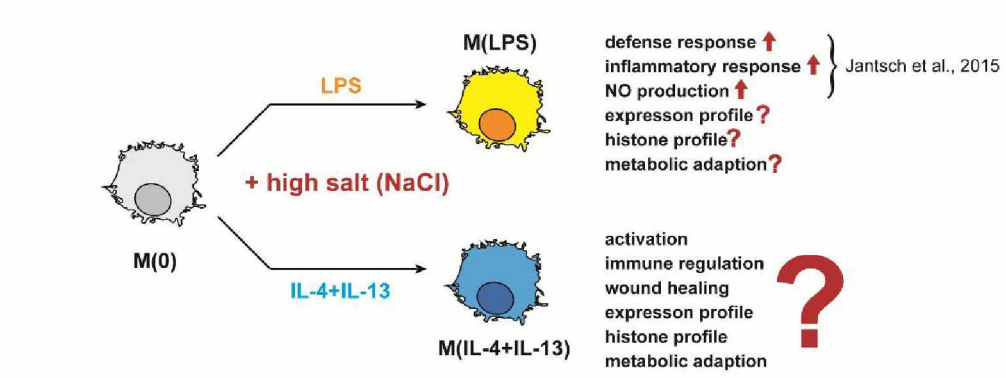

Figure 8. Graphical abstract of thesis research question. High salt (40mM NaCl for *in vitro* experiments) boosts the defense, inflammatory and NO response of murine M(LPS) macrophages (Jantsch et al., 2015). The effect of high salt on M(IL-4+IL-13) macrophage activation and function is largely unknown. The influence of increased salt on genome wide expression, activating histone marks and metabolic adaptions remains elusive for both M(LPS) and M(IL-4+IL-13). The present thesis will address these so far unanswered questions.

2. Experimental animals, materials and methods

2.1. Experimental animals

Primary macrophages were generated from the bone marrow of male ~10-12 week old WT (C57BL/6; Harlan Laboratories), Sgk1 knockout (Sv129J) (Wulff et al., 2002), NFAT5 inducible-knockout (C57BL/6; UBC-Cre/ER^{T2}, Nfat5 fl/fl) (Feil et al., 1997; Kuper et al., 2014) or inducible constitutively active (ca)Akt expression (a kind gift of the Rajewsky lab, MDC, Berlin) mice. Male WT mice were used for *ex vivo*, *in vivo* chitin injection and wound healing studies. Female mice were not included in this study. Mice were fed a normal chow diet (#V1124-300, Ssniff) and tap water unless indicated otherwise. High salt diet was 1% (w/v) NaCl in drinking water and 4% NaCl in chow (#E15431-34, Ssniff). Mice were housed under standard light-dark cycled and SPF conditions. Mice were observed daily. Animal experiments were approved by local authorities.

2.2. Materials

2.2.1. Cell culture

	Manufacturer	Catalogue ID
Adult horse serum	Cell Concepts	#S-HEU03-I
Beta-mercaptoethanol	Sigma	#M3148
DMEM	Gibco	#41966-029
EDTA 0.5M pH 8	Gibco	#15575-038
Fetal bovine serum (FBS) Superior	Biochrom	#S0615
G418	Gibco	#10131-035
HEPES 1M	Gibco	#15630-056
LPS from E. coli O111:B4	Sigma-Aldrich	#L3024
LY294002 Akt inhibitor	Cell Signaling	#9901
Mouse IL-4	R&D Systems	#404-ML-010
Mouse IL-6	Miltenyi Biotec	#130-094-065
Mouse IL-13	Invitrogen	#PMC0134
Non-essential amino acids	Sigma-Aldrich	#M7145
PBS without $CaCl_2$ and $MgCl_2$	Sigma-Aldrich	#D8537
Penicillin-Streptomycin	Gibco	#15140-122
RPMI1640 with L-glutamine	Gibco	#21875-034
RPMI1640 with L-glutamine	Sigma-Aldrich	#R8758
XF Assay media	Seahorse Bioscience	#102365-100
XF Base media	Seahorse Bioscience	#102353-100

2.2.2. Cell lines

Cell line	Cell type/origin	Provider
L929	Sub-clone of parental L strain derived from murine (C3H/An) subcutaneous areolar and adipose connective tissue (Sanford et al., 1948)	ATCC
X-63 GM-CSF	HAT-sensitive Ag8653 myeloma cells transfected with murine GM-CSF cDNA (Stockinger et al., 1996)	National Institute for Medical Research, Division of Molecular Immunology by MTA

2.2.3. qPCR primers and probes

All primers and probes were designed to be species specific for mouse and are indicated 5' → 3'. Primers for ChIP DNA are labelled '*Gene*-ChIP'.

Gene	Sequence
Aldoa	
Forward:	CAGTGAGCAACCCCACTCTGA
Reverse:	GGCAGTGCTTTCCTTTCCTAAC
CD68	
Forward:	TTCTGCTGTGGAAATGCAAG
Reverse:	CAATGATGAGAGGCAGCAAG
Fizz1	
Forward:	CGTGGAGAATAAGGTCAAGGAACT
Reverse:	CACTAGTGCAAGAGAGAGTCTTCGTT
Probe:	TTGCCAATCCAGCTAACTATCCCTCCACTG
Hk2	
Forward:	CAGAAGGTTGACCAGTATCTCTACCA
Reverse:	TCCGGAACCGCCTAGAAAT
Irf4	
Forward:	CGGGCAAGCAGGACTACAA
Reverse:	TCGGAACTTGCCTTTAAACAATG
Ldha	
Forward:	ATGAAGGACTTGGCGGATGA
Reverse:	ATCTCGCCCTTGAGTTTGTCTT
Mrc1	
Forward:	AATACCTTGAACCCATTTATCATTCC
Reverse:	GCATAGGGCCACCACTGATT
Probe:	CGATGTGCCTACCGGCTGCCC
Nfat5	
Forward:	AGCTGGAAATGGAACATTGGA
Reverse:	CGCACAACATAGGGCTCTTCT

Gene	Sequence
Arg1	
Forward:	CCACAGTCTGGCAGTTGGAA
Reverse:	GCATCCACCCAAATGACACA
Probe:	TGGCCACGCCAGGGTCCAC
Eno2	
Forward:	GACGACTGGGCAGCTTGGT
Reverse:	TCAGGTCATCGCCCACTATCT
Gapdh-ChIP	CACCGACCTTCACCATTTTGT
Forward:	GGGCCACGCTAATCTCATTTT
Reverse:	
IL-6	
Forward:	GTTGCCTTCTTGGGACTGATG
Reverse:	GGGAGTGGTATCCTCTGTGAAGTCT
Probe:	TGGTGACAACCACGGCCTTCCC
Klf4	
Forward:	AAACCTATACCAAGAGTTCTCATCTCAA
Reverse:	CCGTCCCAGTCACAGTGGTAA
Mgl2	
Forward:	GAGACAGACTTGAAGGCCTTGAC
Reverse:	GCCACTTCCGAGCCATTG
MyoD-ChIP	GACGCCGCCCCTCAGT
Forward:	TGCAGTCGATCTCTCAAAGCA
Reverse:	
Nos2	
Forward:	GGGCAGCCTGTGAGACCTT
Reverse:	TGCATTGGAAGTGAAGCGTTT
Probe:	TCCGAAGCAAACATCACATTCAGATCCC

Gene	Sequence
Nos2-ChIP	AACCTCACTGAGAGAACAGACAGAAA
Forward:	TTGCAGCTGCTGAGGGATT
Reverse:	
Pgam1	
Forward:	TCGCAGGTACGCAGACCTT
Reverse:	GCTCTGGCAATAGTGTCCTTCA
Slamf1	
Forward:	TGGCTAATGGATCCCAAAGGA
Reverse:	CCATCACACCTCCACCTGTT
Slc2a1	
Forward:	GAGTGTGCTGAAGAAGCTTCGA
Reverse:	GCCGACCCTCTTCTTTCATCT
Ym1	
Forward:	TCCTACTGGAAGGACCATGGAGCA
Reverse:	TCCTGGTGGGCCAGTACTAATTGT

Gene	Sequence
PD-L2	
Forward:	GAGCCAGTTTGCAGAAGGTAG
Reverse:	ATCCGACTCAGAGGGTCAATG
Sgk1	
Forward:	CGGTGGACTGGTGGTGTCTT
Reverse:	GTCGTACATCTCAGCCGTGTTC
Slamf1-ChIP	GCCAGGGTTTGACTGATGTGA
Forward:	GAAGCCAAAGTCAGGTGTTCAGA
Reverse:	
Slc6a12	
Forward:	AGAACTTTACCTCGCCTGTCATG
Reverse:	CGTGGATGCCCGATGTAATAC
18S	
Forward:	ACATCCAAGGAAGGCAGCAG
Reverse:	TTTTCGTCACTACCTCCCCG
Probe:	CGCGCAAATTACCCACTCCCGAC

2.2.4. Antibodies for western blotting

Antigen	Source	Manufacturer	Catalogue ID	
Akt	rabbit	Cell Signaling	#9272	
Arginase 1	mouse	BD Biosciences	#610708	
Beta-actin	mouse	Novus Biologicals	#NB600-501	
Hsp60	rabbit	Cell Signaling	#12165S	
p70/S6K	rabbit	Cell Signaling	#2708	
Phopho-p70/S6K^{Thr389}	rabbit	Cell Signaling	#9234	
Phospho-Akt^{S473}	rabbit	Cell Signaling	#4060	
Phospho-STAT6^{Tyr641}	rabbit	Cell Signaling	#9361	
STAT6	rabbit	Cell Signaling	#9362	
				Conjugation
Mouse IgG	goat	LI--COR	#926-32224	IRDye680CW
Rabbit IgG	goat	LI-COR	#926-32211	IRDye800CW

2.2.5. Antibodies and reagents for flow cytometry

Antigen	Source	Manufacturer	Catalogue ID	Conjugation
B220	rat	BD Pharmingen	#552094	APC-Cy7
CD3	rat	eBioscience	#50-0032-82	eFluor660
CD4	rat	BD Pharmingen	#558107	PB
CD8	rat	BD Pharmingen	#553032	PE
CD11b	rat	BD Biosciences	#553310	FITC
CD16/32	rat	eBioscience	#14-0161-85	-
CD38	rat	Miltenyi Biotec	#130-103-030	APC
F4/80	rat	eBioscience	#17-4801-1631	APC
F4/80	rat	eBioscience	#48-4801-80	PB
Gr-1	rat	Miltenyi Biotec	#130-102-171	PerCP-Vio700
PD-L2	rat	eBioscience	#12-9972-82	PE

	Manufacturer	Catalogue ID
LIVE/DEAD fixable near-IR Dead Cell Stain kit	Life technologies	# L10119
MitoTracker Deep Red FM	Cell Signaling	#8778
2-NBDG	Thermo Fischer Scientific	#N13195
Propidium iodide staining solution	BD Pharmingen	#51-66211E

2.2.6. Antibodies for T cell stimulation

Antigen	Source	Manufacturer	Catalogue ID
CD3	hamster	BD Biosciences	#553057
CD28	hamster	BD Biosciences	#553294

2.2.7. Antibodies and reagents for chromatin immunoprecipitation

Antigen	Source	Manufacturer	Catalogue ID
H3K4me3	rabbit	Cell Signaling	#9751S
H4ac	rabbit	Merck Millipore	#06-866

	Manufacturer	Catalogue ID
Dynabeads Protein A	Invitrogen	# 10002D
Micrococcal nuclease (MNase)	Sigma-Aldrich	#N3755-200U
Proteinase K	Sigma-Aldrich	#P2308-100MG

2.2.8. Kits

	Manufacturer	Catalogue ID
Agilent RNA 6000 Nano kit	Agilent Technologies	#5067-1511
CyQUANT® Cell Proliferation Assay kit	Life Techologies	#C7026
CellTrace CFSE cell proliferation kit	Life Technologies	#34554
EnzyFluo L-lactate assay kit	BioAssay Systems	#EFLCC-100
High capacity cDNA reverse transcription kit	Applied Biosystems	#4368813
Illumina TotalPrep-96 RNA amplification kit	Ambion	#4393543
Lactate fluorometric assay kit	BioVision	#K607-100
LIVE/DEAD fixable near-IR Dead Cell Stain kit	Life Technologies	#L10119
Mouse Ref-8 v2.0 bead chip microarray	Illumina	#BD-202-0202
MinElute PCR Purification kit	Qiagen	#28006
PCR Mycoplasma Test kit I/C	PromoKine	#PK-CA91-1024
QIAamp DNA Mini kit	Qiagen	#51304
Qubit dsDNA HS assay kit	Life Technologies	#Q32854
RNase-free DNase Set	Qiagen	#79254
RNeasy Mini kit	Qiagen	#74106
TruSeq ChIP sample Prep kit	Illumina	#IP-202-1012
XF Cell Mito Stress Test kit	Seahorse Bioscience	#103015-100
XF24 FluxPak	Seahorse Bioscience	#100850-001
XF Glycolysis Stress Test kit	Seahorse Bioscience	#103020-100

2.2.9. Buffers and solutions

Buffer	Application
Base buffer 2x	ChIP
ChIP PIC I 1000x	ChIP
ChIP PIC II 1000x	ChIP
Electrophoresis buffer	SDS-PAGE
Laemmli sample buffer 4x	Western blotting
LiCl buffer	ChIP
MNase digestion buffer	ChIP
MNase reconstitution buffer	ChIP
Nuclei preparation buffer I	ChIP
Nuclei preparation buffer II	ChIP
Nuclei preparation buffer III	ChIP
PBS/BSA	ChIP
Protease Stop I	ChIP

Buffer	Application
Protease Stop II	ChIP
Red blood cell lysis buffer 10x	CFSE co-culture assay
RIPA buffer	ChIP
RIPA buffer 2x	ChIP
TAE buffer	Agarose gel electrophoresis
TBS(-T) 10x	Biochemistry
TE buffer	ChIP
Transfer buffer	Western (tank) blotting

Base buffer 2x:
60mM KCl
15mM NaCl
5mM MgCl2
0.1mM EDTA
15mM Tris-HCl pH 8

ChIP PIC I 1000x
100mg Aprotinin
50mg Leupeptin hemisulfate
ad 5ml with dH_20

ChIP PIC II 1000x
10mg Pepstatin A
ad 10ml with DMSO

Electrophoresis buffer
25mM Tris
190mM glycine
0.1% SDS
pH 8.3

Laemmli sample buffer 4x
62.5mM Tris-HCl, pH 6.8
10% glycerol
1% LDS
355mM beta-mercaptoethanol
0.005% bromophenol blue

LiCl buffer
125ml 1M LiCl
25ml 10% Igepal CA-360
25ml 10% sodium deoxycholate
ad 500ml with dH_2O

MNase digestion buffer
0.32M sucrose
50mM Tris-HCl pH7.4
4mM MgCl2
1mM CaCl2
<u>add directly before use:</u>
Protease Stop II

MNase reconstitution buffer
20mM HEPES-KOH pH 7.4
50mM MgCl2
50% glycerol

Nuclei preparation buffer I
20.538g sucrose
100ml 2x base buffer
ad 200ml with dH_2O
<u>add directly before use:</u>
Protease Stop I

Nuclei preparationbuffer II
4ml nuclei preparation buffer I
160µl 10% Igepal CA-360

Nuclei preparation buffer III
246.456g sucrose
300ml 2x base buffer
ad 600ml with dH_2O
<u>add directly before use:</u>
Protease Stop I

PBS/BSA
50ml PBS
0.25g BSA
50µl 10% Tween20

Protease Stop I
1x ChIP PIC I
1x ChIP PIC II
0.5mM PMSF
5mM sodium butyrate
0.5mM DTT

Protease Stop II
1x ChIP PIC I
1x ChIP PIC II
1mM PMSF
5mM sodium butyrate

Red blood cell lysis buffer 10x
41.5g NH_4Cl
4.2g $NaHCO_3$
10ml 0.5M EDTA
ad 500ml with dH_20

RIPA buffer
10mM Tris-HCl pH 7.6
140mM NaCl
1mM EDTA
0.1% SDS
0.1% sodium deoxycholate
1% Triton X-100

RIPA buffer 2x
20mM Tris-HCl pH 7.6
280mM NaCl
2mM EDTA
0.2% SDS
0.2% sodium deoxycholate
2% Triton X-100
add directly before use:
Protease Stop II

TAE buffer
40mM Tris
20mM acetic acid
1mM EDTA

TBS(-T) 10x
0.2M Tris
1.54M NaCl
(0.5% Tween)
pH 7.6

TE buffer
5ml 1M Tris-HCl pH 8.0
1ml 0.5M EDTA
ad 500ml dH_2O

Transfer buffer
25mM Tris
190mM glycine
20% ethanol
(0.1% SDS for proteins > 80kD)

2.2.10. Reagents and Chemicals

Standard lab chemicals, reagents and solvents were obtained from Carl Roth, Merck and Sigma-Aldrich.

	Manufacturer	Catalogue ID
Agarose	Biozym	#840004
Aprotinin	Carl Roth	#A162.3
BD FACS sheath solution with surfactant	BD Biosciences	#336911
BD FACSFlow	BD Biosciences	#342003
Bovine serum albumin (BSA)	Sigma-Aldrich	#A9430-25G
Chitin	Sigma-Aldrich	# C9752
DTT	Sigma-Aldrich	#43816-10ML
Ethidium bromide 1% solution	Carl Roth	#2218.1
FACS Clean	BD Biosciences	#340345
FACS Shutdown solution	BD Biosciences	#334224
Fast SYBR Green Master Mix	Applied Biosystems	#4385614
Igepal CA-630	Sigma-Aldrich	#I8896-50ML
Isofluran	Baxter	#HDG9623

	Manufacturer	Catalogue ID
Leupeptin hemisulfate	Carl Roth	#CN33.3
Low molecular weight DNA ladder	NEB	#N3233
N-(1-Naphthyl)ethylenediamine dihydrochloride	Sigma-Aldrich	#222488-5G
Odyssey blocking buffer	Li-COR	# 927-50000
Page Ruler Plus Prestained Protein Ladder	Thermo Scientific	#26616
Pepstatin A	AppliChem	#A2205,0010
Phosphatase inhibitor cocktail	Sigma-Aldrich	#P5726-1ML
PMSF	Sigma-Aldrich	#P7626-100MG
Ponceau S solution	Sigma-Aldrich	#P7170-1L
Precision Plus Protein Standard	Bio-Rad	#161-0374/0377
Protease inhibitor cocktail tablets	Roche	#11836145001
QIAzol lysis reagent	Qiagen	#79306
RIPA buffer 10x	Cell Signaling	#9806
RNase-free DNase Set	Qiagen	#79254
Rotiphorese Gel 30 (37.5:1)	Carl Roth	#3029.1
Roti-Quant 5x	Carl Roth	#K015.1
Skim milk powder	Fluka Analytical	#70166-500G
Sodium butyrate	Sigma	#B5887-1G
Sodium deoxycholate	Sigma-Aldrich	#D5760-500MG
Sodium dodecyl sulfate (SDS)	Sigma-Aldrich	#L4509-1KG
Sucrose	Sigma-Aldrich	#S7903-1KG
Sulfanilamide	Sigma-Aldrich	#S9251
TAT-Cre	a kind gift from the Rajewsky lab (MDC, Berlin, Germany)	
TaqMan fast universal PCR master mix 2x	Applied Biosystems	#4367846
TEMED	Carl Roth	#2367.3
Triton-X 100	Merck	#11869.1000

2.2.11. Consumables

	Manufacturer	Catalogue ID
Extra thick blot paper/filter paper	Bio-Rad	#1703966
Fast optical 96-well reaction plate (for qPCR)	Applied Biosystems	#4346906
Filter tips 0.1-10µl	Sarstedt	#70.1130.210
Filter tips 100-1000µl	Sarstedt	#70.762.211
Filter tips 2-200µl	Sarstedt	#70.760.211
Micro Plate PS 96 V-bottom	Böttger	#05-021-0100
Micro-centrifuge tubes 1.5ml	Carl Roth	#4182.1
Microcentrifuge tubes 2ml	Carl Roth	#NA16.1
Microtest plates (F-bottom)	Carl Roth	#9293.1
Microtubes 0.5ml	Carl Roth	#7060.1
Nitrocellulose blotting membrane	Amersham	#106000016
Optical adhesive film (for qPCR)	Applied Biosystems	#4311971
Sterile cell culture dishes 100x20mm	Greiner Bio-One	#664160
Sterile cell culture flask 175cm^2	Greiner Bio-One	#661160
Sterile cell culture flask 75cm^2	Greiner Bio-One	#658170
Sterile cell culture plate 6 well	Greiner Bio-One	#657160
Sterile cell culture plate 96 well (F-bottom)	Greiner Bio-One	#655180

	Manufacturer	Catalogue ID
Sterile cell cultre plate 96 well (F-bottom) black	Greiner Bio-One	#655086
Sterile cell culture plate 96 well (round bottom)	Corning	#3799
Sterile cell scraper M	TPP	#99003
Sterile cell spatula	TPP	#99010
Sterile cell strainer 100µm	BD Falcon	#352360
Sterile cell strainer 40µm	BD Falcon	#352340
Sterile cell strainer 70µm	BD Falcon	#352350
Sterile disposable pasteur pipettes	Carl Roth	#EA66.1
Sterile filter	VWR	#514-0342
Sterile needle 23G x 1 ¼"	B. Braun Melsungen	# 4657640
Sterile needle 26G x 1"	B. Braun Melsungen	#4657683
Sterile needle 27G x ¾" Nr. 20	BD Microlance	#302200
Sterile serological pipette 10ml	Greiner Bio One	#607180
Sterile serological pipette 25ml	Greiner Bio-One	#760180
Sterile serological pipette 5ml	Greiner Bio-One	#606180
Sterile solution basin	BIOLOGIX	#25-0051
Sterile syringe 10ml	B Braun Melsungen	#4606108V
Sterile syringe 20ml	B. Braun Melsungen	#4606205V
Sterile syringe 2ml	B. Braun Melsungen	#4606027V
Sterile syringe 50ml	BD Plastipak	#300865
Sterile syringe 5ml	B. Braun Melsungen	#4606051V
Sterile syringe with needle 1ml	BD Plastipak	#305501
Sterile tissue culture flask 150cm^2	TPP	#90151
Teflon film	DuPont/American Durafilm	#FT FEP 100 C
Tubes 15ml (sterile)	Greiner Bio-One	#188271
Tubes 50ml (sterile)	Greiner Bio-One	#227261

2.2.12. Hardware

	Manufacturer	Catalogue ID
Agarose gel documentation system	Syngene	InGenius LHR
Analytical balance	Sartorius	CPA224S-OCE
Area scan camera (UV gel station)	Lumenera	LW135M
BD FACSAria III	BD Biosciences	
BD FACSCanto II	BD Biosciences	
BD HTS for FACSCanto II	BD Biosciences	
Bioanalyzer	Agilent	Agilent G2938A 2100
Centrifuge	Eppendorf	5424R; 5417R; 5810R
CO_2 cell culture incubator	Heraeus	Function line BB16; BB6060 0_2
Electrophoresis chamber for agarose gels	Renner	Geltray UV transparent
Electrophoresis chamber SDS-PAGE	Bio-Rad	Mini Protean II 2-D cell
Extracellular flux analyzer	Seahorse Bioscience	XF^{e}24
Heat sealer	Rische und Herfurth	Polystar 242
Infrared imaging system	Li-COR	Odyssey 9120
Inverted routine microscope	Nikon	Eclipse TS100
Magnetic separation rack	Life Technologies	CS15000
Microplate reader	Tecan	Spectra Fluor Plus F129005
Mini rotator for 1.5ml test tubes	Biosan	Bio RS-24

	Manufacturer	Catalogue ID
Multimode plate reader	Molecular Devices	Spectramax M5
pH meter	Hanna instruments	HI 2211
Power supply	Bio-Rad	Power Pac 200
Pulse Mixer	Scientific Industries	Vortex Genie 2
qPCR cycler	Applied Biosystems	7500 fast Real-time PCR system
Qubit Fluorometer	Life Technologies	#Q32857
Semi-dry blotting device	Biometra	Fastblot B44
Shaking platform	Heidolph	Polymax 1030
Sonicator	Misonix	Misonix 4000
Spectrophotometer	Peqlab	NanoDrop ND-1000
Tank blotting device	Bio-Rad	Mini Protean II
Thermal cycler	Perkin Elmer	Cetus 480 Thermal DNA cycler
Thermomixer	Eppendorf	Thermomixer comfort
Water bath	Köttermann	#3047

2.2.13. Software

	Manufacturer
7500 Fast System SDS Software	Applied Biosystems
FACSDiva	BD Biosciences
FlowJo version 10	TreeStar
Free Venn Diagram Maker	Mediafreeware
ImageJ/Fiji	GNU GPL
OSYSSEY Application Software version 3.0	Li-COR
Primer Express version 3.0	Applied Biosystems
Prism version 5.01	GraphPad
R	GNU GPL
R package *GOstats*	(Falcon and Gentleman, 2007) GNU GPL
R package *GO.db*	GNU GPL
R package *heatmap.3*	(Zhao et al., 2014) GNU GPL
REVIGO	(Supek et al., 2011); tool online at http://revigo.irb.hr/

2.3. Methods

2.3.1. Generation of conditioned media

Conditioned media containing the macrophage differentiation factor colony-stimulating factor (CSF)-1 was generated by collecting the supernatant from confluent L929 cells cultured for 14 days in DMEM containing 10% (v/v) FBS, 1:100 Non-essential amino acids, HEPES and 1% (v/v) Penicillin-Streptomycin. Supernatants were filtered through a 70µm cell strainer. The quality of each new batch of conditioned media

was assessed by determining the percentage of macrophages generated from WT bone marrow cultures after seven days (see also sections 2.3.2 and 2.3.8).

A cell line secreting granulocyte macrophage colony-stimulating factor (GM-CSF) was obtained by material transfer agreement (MTA) (Stockinger et al., 1996). X-63 GM-CSF cells were expanded in RPMI1640 media containing 5% (v/v) FBS and 1mg/ml G418, as GM-CSF is expressed episomally and might otherwise be lost. Circa $60x10^6$ cells were then washed free of G418 and cultured in 200ml culture medium without G418 for ~48 hours. GM-CSF-conditioned medium was then harvested by collecting supernatants and removing cells by centrifugation. All conditioned media were tested and found to be negative for mycoplasma contamination (by PCR). Aliquots were stored at -20°C and thawed directly prior to use.

2.3.2. Generation and activation of bone marrow-derived macrophages

Bone marrow cells were isolated from the femur and tibia of freshly euthanized mice (by isoflurane inhalation) by flushing with ~10ml of activation media (RPMI1640 containing L-glutamine, 10% (v/v) FBS, 10mM HEPES, 50µM β-mercaptoethanol, 1% (v/v) Penicillin-Streptomycin). Cells were then pelleted and resuspended into monocyte differentiation media (DMEM, 10% (v/v) FBS, 5% (v/v) adult horse serum, 1:100 non-essential amino acids, 50µM β-mercaptoethanol, 20% (v/v) L929 conditioned media containing CSF-1). For macrophage differentiation, $10x10^6$ bone marrow cells were then cultivated in 50ml of differentiation media for seven days in sealed, hydrophobic Teflon® bags at 37°C and 10% CO_2. The yield of bone-marrow derived macrophages (BMDM) from one bag was routinely ~70-100$x10^6$ cells with a macrophage purity of ~85-95%, as determined by the percentage of $CD11b^+F4/80^+$ cells by flow cytometry (Figure 9).

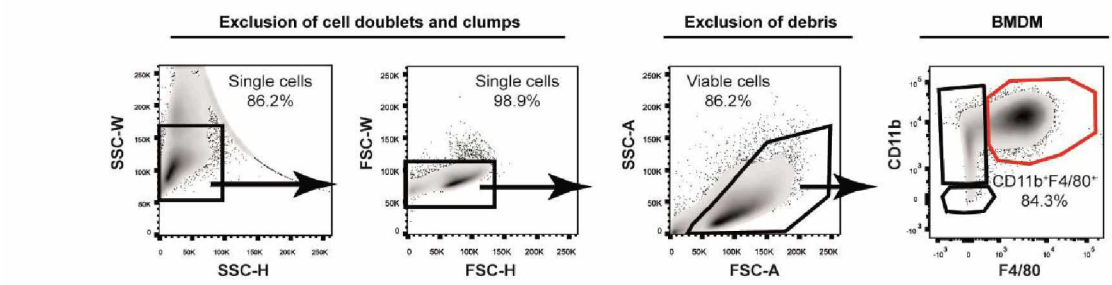

Figure 9. Quality control of bone marrow-derived macrophages (BMDM) generation. For quality assessment of individual BMDM batches, the percentage of (continued on the next page)

$CD11b^+F4/80^+$ double positive cells was determined by flow cytometry after gating for single cells and exclusion of cellular debris. Representative flow cytometry plots are shown.

In some cases, the purity of BMDM was below ~85-95%. Optimization of various experimental variables (e.g. input of undifferentiated bone marrow cells, L929 conditioned media batch, FBS batch, cell culture CO_2 partial pressure) did not affect the purity of BMDM preparations. To substantiate the significance of my findings, the purity of macrophages *before* (new BMDM batch) and *after* activation (see next paragraph) was assessed by flow cytometry. $CD11b^+F4/80^+$ macrophages were highly enriched (>85%) after adhesion to plastic and activation for 24 hours irrespective of the initial BMDM purity (Figure 10). All readouts presented in this thesis were after adhesion and activation for 24 hours; I am confident that the results presented here faithfully report the effect of high salt on highly enriched $CD11b^+F4/80^+$ macrophages.

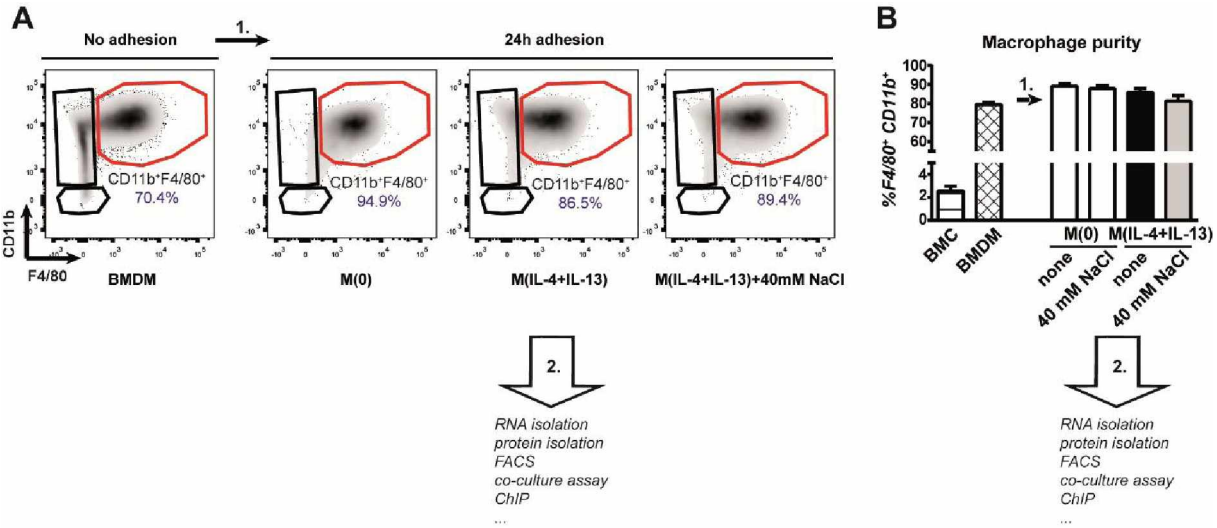

Figure 10. Adhesion/activation for 24 hours increases the purity of BMDM preparations. BMDM with a purity below ~85-95% were adhered to plastic and stimulated with IL-4 and IL-13 (M(IL-4+IL-13)) in the absence (none) or with an additional 40mM NaCl for 24 hours. Unstimulated (M(0)) macrophages were treated similarly. The percentage of $CD11b^+F4/80^+$ double-positive macrophages was assessed *before* and *after* activation by flow cytometry. **A:** Representative flow cytometry plots of $CD11b^+F4/80^+$ double-positive macrophages *before* and *after* adhesion are shown. **B:** Bar graph showing enrichment of $CD11b^+F4/80^+$ double-positive macrophages during activation. (**A+B**): All readouts presented in this thesis were after 24 hours of adhesion/activation.

For activation experiments, the differentiated macrophages were harvested from Teflon bags, pelleted and resuspended into activation media. No CSF-1 was present

for activation experiments. For analysis by qPCR and western blotting, $2x10^6$ differentiated macrophages were plated per well of 6-well plates. For T cell suppression/macrophage functional assays, $20x10^6$ differentiated macrophages were plated into $75cm^2$ flasks. For ChIP-seq, $40x10^6$ differentiated macrophages were plated into $150cm^2$ flasks. In all cases, the differentiated macrophages were first allowed to rest and adhere for two hours. Activation to M(IL-4+IL-13) was performed by the addition of recombinant mouse IL-4 and recombinant mouse IL-13 to the activation media (final concentration 10ng/ml, each). Activation to M(LPS) was by the addition of LPS to the activation media (final concentration 10ng/ml). For the analysis of the effect of salt on macrophage activation, an additional 40mM NaCl was also added to the culture media. Tonicity experiments were performed the same where an additional 80mM urea (which has an equivalent increase in osmolality and passes through the cell membrane) or 80mM mannitol (which has an equivalent increase in tonicity but does not enter the cell) were also added to the culture media. Akt inhibitor LY294002 was used at a concentration of 50nM. Unless otherwise noted, cells were activated for 24 hours at 37°C and 5% CO_2.

2.3.3. Preparation and activation of constitutively active (ca)Akt BMDM

Bone marrow cells were isolated from the femur and tibia of transgenic mice which express a caAkt (N-terminal myristoylation signal-attached) after genetic recombination. These mice have a loxP STOP sequence followed by the caAkt and GFP gene, inserted into the ROSA26 locus. When incubated with recombinant Cre enzyme, the STOP sequence is deleted and caAkt expression is induced (Figure 11). Taking advantage of the inducibility of this model, BMDM were first differentiated (under normal, isotonic conditions) from bone marrow cells from caAkt mice as before, in the absence of any recombinase. This was to ensure normal differentiation of macrophages from caAkt mice identical to WT controls. These were named "caAkt^{inactive}". Following the seven-day differentiation procedure, BMDM were washed three times in serum-free medium to remove proteins. Cells were then resuspended in serum-free medium at a density of $10x10^6$ cells/ml and incubated at 37°C in a water bath for 10 minutes. Meanwhile, recombinant trans-activator of transcription (TAT)-Cre was pre-diluted 1:40 in pre-warmed serum-free media. TAT is a human immunodeficiency virus-derived protein that penetrates cell membranes and guides fusion protein cargo to the nucleus via a nuclear localization

sequence (Dietz and Bahr, 2004; Frankel and Pabo, 1988; Ruben et al., 1989). Then, equal volumes of cell suspension and TAT-Cre were combined to yield a final cell density of $5x10^6$ cells/ml and a 1:80 TAT-Cre dilution and incubated in a water bath (37°C) for 45 minutes. During this time, the excision of the STOP cassette is initiated and thus caAkt expression ("caAkt^{active}") induced (Figure 11). Transduction was quenched by adding media containing 10% (v/v) FBS. Cells were washed once in medium containing 10% (v/v) FBS, resuspended as desired in activation media and plated out. Following incubation with TAT-Cre, BMDM were left for two days to allow for full recombination and caAkt expression. BMDM from WT mice were similarly treated with TAT-Cre and incubated for two days. Finally, caAkt^{active} and WT BMDM were left unstimulated, or stimulated with IL-4+IL-13 alone or with an additional 40mM NaCl for 24 hours. Expression of M(IL-4+IL-13) signature genes was measured by qPCR.

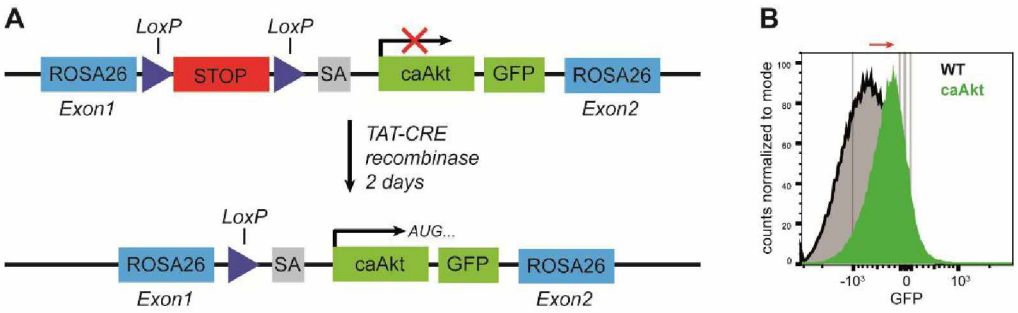

Figure 11. TAT-Cre-mediated recombination of the caAkt locus in BMDM. A: Schematic showing the recombination of the caAkt locus upon Cre incubation. A STOP cassette flanked by LoxP sites inhibits caAkt and GFP expression. When Cre recombinase is added, the STOP cassette is excised and caAkt and GFP are expressed under the control of the ROSA26 promoter. SA: splice acceptor site. **B:** Representative flow cytometry histogram plot showing GFP expression of caAkt^{active} BMDM after Cre recombination compared to wild type (WT) cells treated similarly.

2.3.4. *In vitro* generation of myeloid-derived suppressor cells

Myeloid-derived suppressor cells (MDSC) were differentiated as described previously (Li et al., 2015; Marigo et al., 2010). Briefly, $2.5x10^6$ WT bone marrow cells were cultured for four days in MDSC differentiation media (RPMI1640 with L-glutamine, 10% (v/v) FBS, 1% (v/v) Penicillin-Streptomycin, 10mM HEPES, 20µM beta-mercaptoethanol, 10% (v/v) GM-CSF conditioned media, 40ng/ml IL-6) in 10cm^2 cell culture dishes. The percentage of MDSC among total non-adherent cells (~60%) was determined by flow cytometry after four days.

2.3.5. Griess assay

Griess assays were done in collaboration with Jonathan Jantsch (Regensburg, Germany) to determine nitrite (NO_2^-) in cell culture supernatants of activated macrophages. Briefly, NO, the bactericidal product of Nos2, is oxidized to nitrite in the presence of oxygen. In the assay, NO_2^- from cell culture supernatants then first reacts with sulphanilamide and subsequently N-(1-Naphthyl)ethylenediamine to yield a pink dye which can be quantified by absorbance measurements at 550nm in a colorimetric assay. Sample nitrite concentrations were then derived from a $NaNO_2$ standard curve measured simultaneously.

2.3.6. RNA isolation, preparation of cDNA and qPCR

Activated macrophages were washed once with PBS prior to lysis in Qiazol lysis reagent for isolation of total RNA using an RNeasy RNA isolation kit, according to the manufacturer's instructions. Samples were treated with DNase, according to the manufacturer's protocol and eluted in RNase-free water. RNA quality and concentration were assessed with a spectrophotometer. The integrity of RNA samples for microarray was additionally confirmed on a Bioanalyzer instrument using the Agilent RNA 6000 Nano kit according to the manufacturer's instructions. All RNA samples were stored at -80°C.

The High Capacity cDNA Reverse Transcription Kit was used to transcribe equivalent amounts of extracted RNA into cDNA according to the manufacturer's protocol. cDNA samples were diluted in RNase/DNase-free water to a final concentration of 10ng/µl and stored frozen.

Quantitative real-time polymerase chain reaction (qPCR) was used to quantify gene expression using the relative standard curve method (Marko et al., 2012). TaqMan or SYBR green analysis was conducted according to the manufacturer's instructions, using an Applied Biosystems 7500 Fast Sequence Detection System. qPCR data was analyzed with 7500 Fast System SDS Software. Species-specific primers and probes (where applicable) are detailed in (2.2.3). The expression levels of target genes were normalized to the expression of 18S RNA, unless indicated otherwise. Results were confirmed independently at least three times for *in vitro* BMDM activation. qPCR results of ChIP DNA were normalized to input. Briefly, input Cts were dilution-adjusted to 100% [Ct input – 3.32193] and % input was calculated for each sample [$100*(2^{(\text{adjusted input Ct} - \text{Ct (IP)})})$].

2.3.7. Western blotting

Activated macrophages were once washed with chilled PBS on ice and then scraped into 1x radioimmunoprecipitation assay (RIPA) buffer containing protease and phosphatase inhibitor cocktails and phenylmethanesulfonylfluoride (PMSF) (40µL, 10µL, and 1µL per 950µL RIPA buffer, respectively). Protein was extracted by freeze-thawing in RIPA buffer over night at -20°C, followed by centrifugation at 4°C for 15 minutes at 20000x*g* to pellet insoluble cellular debris. Supernatants were stored at -80°C. Total protein was determined by Bradford assay. Briefly, protein lysates were diluted 1:100 in PBS before addition of 1x Roti-Quant Bradford reagent. Absorbance was measured at 595nm wavelength with an absorbance plate reader. Protein concentrations were derived from a BSA standard curve measured in parallel.

Equal amounts of total protein were denatured by incubation at 95°C for five minutes in 1x Laemmli buffer and loaded onto polyacrylamide (PAA) gels for sodium dodecyl sulfate polyacrylamide gel electrophoresis (SDS-PAGE) to separate proteins according to their molecular mass. A discontinuous PAA gel system consisting of stacking and separation gel was used. Samples were run at 80V or 120V in the stacking or separation gel, respectively.

After electrophoresis, proteins were transferred from the gel to a piece of nitrocellulose membrane by tank blotting using a Mini Trans-Blot® Cell. Membranes were equilibrated in transfer buffer for 15 minutes prior to blotting; transfer was at 250mA for 75 minutes on ice and in ice-cold transfer buffer. Transfer efficiency of equal amounts of total protein per lane was checked by reversible staining of membrane-bound protein with Ponceau S stain. Ponceau S staining was then washed off with TBS-T buffer.

Membranes were then blocked with 3% (w/v) BSA or 5% (w/v) milk in TBS-T for 1-2 hours at room temperature (RT) to saturate all non-specific protein binding sites. Membranes were then incubated with primary antibodies (detailed in 2.2.4) diluted in blocking solution according to the manufacturers' protocols at 4°C over-night with gentle agitation. After thorough washing with TBS-T, the membranes were incubated for two hours with fluorophore-conjugated secondary antibody (detailed in 2.2.4) against primary antibody host species diluted 1:5000 in ODYSSEY Blocking buffer. After washing with TBS-T, secondary antibodies were excited and read on an infrared scanner. Where applicable, densitometric quantification of protein bands was performed with the program ImageJ (Schneider et al., 2012).

2.3.8. Flow cytometric analyses

All staining of cells for flow cytometry was done at 4°C or on ice with chilled reagents. Single cell suspensions were used for flow cytometric analyses. Where applicable, adherent macrophages were prepared into single cell suspensions by incubation in ice-cold PBS/2mM EDTA for 15 minutes, before gentle scraping. Activated macrophages or BMDM were then pelleted and resuspended in PBS/2mM EDTA with 0.5% (v/v) FBS, which contained a murine Fc receptor-blocking antibody 1:100. Cells were incubated with Fc-blocking antibody on ice for 10 minutes. Next, cells were washed once with PBS, pelleted by centrifugation and resuspended in PBS/2mM EDTA with 0.5% (v/v) FBS, containing diluted antibodies (detailed in 2.2.5) according to application: α-PD-L2-PE 1:200, α-F4/80-APC 1:100, α-F4/80-PB 1:100, α-CD11b-FITC 1:100, α-CD38-APC 1:100, and α-Gr-1-PerCP-Vio700 1:100.

Macrophages were incubated with fluorescently-labelled antibodies in the dark for 20 minutes, washed once with PBS/2mM EDTA with 0.5% (v/v) FBS, resuspended and data was acquired on a BD FACSCanto II instrument operated by FACSDiva software. Flow cytometric analyses of macrophage:T cell co-culture assays were performed similarly. Briefly, CFSE-labeled T cells were pelleted after 4.5 days and resuspended in PBS containing LIVE/DEAD fixable near-IR dead cell stain 1:1000. After incubation in the dark for 10-15 minutes, cells were washed once with PBS and stained in PBS/2mM EDTA with 0.5% (v/v) FBS containing α-CD8-PE 1:200 and α-CD4-PB 1:400 for 20 minutes in the dark. After washing, data was acquired and proliferation was determined by CFSE dilution of gated $CD4^+$ and $CD8^+$ T cell populations. Dead cells and debris were excluded from the analysis by gating.

For cell viability analyses, macrophages were first counted manually using a haemocytomer, and then propidium iodide (PI) staining solution was added to a final concentration of 1µg/ml prior to data acquisition.

Mitochondrial mass of activated macrophages was analyzed using MitoTracker Deep Red. Single-cell suspensions were incubated with dye diluted in PBS at a final concentration of 50nM for one hour, washed and then measured by flow cytometry.

To measure glucose uptake of activated macrophages, cells were first exchanged into glucose-free media (also without interleukins and additional salt) containing 30µM 2-(N-(7-nitrobenz-2-oxa-1,3-diazol-4-yl)amino)-2-deoxyglucose (2-NBDG)

and incubated for one hour at 38°C, washed, and then subjected to flow cytometric analysis.

A BD FACSCanto II HTS device for automatized sample acquisition was used where applicable. Data analysis and plotting were performed with the FlowJo software version 10.

2.3.9. Isolation and stimulation of peritoneal macrophages

WT mice were euthanized and 5ml of ice-cold PBS, 3% (v/v) FBS was injected into the peritoneal cavity. After gentle massage, the lavage fluid was recovered using a syringe and needle. Peritoneal exudate cells (PECs) were then pelleted by centrifugation and resuspended in activation media. Peritoneal cells were allowed to attach for two hours to enrich for plastic-adherent cells, before washing once with media. Cells were then left unactivated (M(0)) or stimulated with IL-4+IL-13 (10ng/ml, each) alone or with an additional 40mM NaCl for 24 hours. Signature gene expression was by qPCR.

2.3.10. Cell viability assay (DNA content)

BMDM were plated in flat-bottom 96-well plates at a density of 50,000 cells per well, allowed to adhere for two hours and activated as described before. After 24 hours, the culture media was removed, cells were washed once with PBS, and the DNA content of each well was determined using the CyQUANT® Cell Proliferation Assay Kit according to the manufacturer's instructions and a fluorescence plate reader. Here, DNA quantification is via a dye that exhibits strong fluorescence enhancement when bound to DNA with a wide linear range. Total cell numbers were derived from a standard curve of similarly treated and serially diluted M(0) macrophages.

2.3.11. *In vivo* activation of M2 macrophages by chitin injection

Age-matched WT mice were randomly assigned to receive a high salt diet (4% NaCl in chow plus 1% in the drinking water; HSD) or normal-salt diet (0.4 % in chow plus tap water; NSD) for 14 days. On day 14, chitin was prepared as described before (Byles et al., 2013; Satoh et al., 2010). Briefly, chitin was washed with sterile PBS three times and sonicated in PBS for 30 minutes on ice. Homogenized chitin was diluted to a final concentration of 4µg/ml in sterile PBS and large particles were removed by filtering

through a 100µm cell strainer before I.P. injection of 200µl (800ng chitin/mouse) of the homogenized chitin preparation. After injection, mice were housed for an additional two days with HSD or NSD, sacrificed and PECs were collected as described before (see 2.3.9) and pelleted.

To analyse the expression of M(IL-4+IL-13) signature genes in crude, unsorted PECs, based on a recently published method (Byles et al., 2013; Satoh et al., 2010) (experiment 1), cells were resuspended into media (RPMI1640 with L-glutamine, 1% (v/v) Penicillin-Streptomycin) and then allowed to adhere to 6-well plates for two hours at 37°C, 5% CO_2. Non-adherent cells were removed by extensive washing with PBS and adherent PECs were then lysed in Qiazol followed by RNA isolation and qPCR. All expression data were normalized to the macrophage marker gene CD68 in experiment 1. CD68 is a reliable marker gene for peritoneal macrophages in the chitin injection model applied here, irrespective of the dietary regime (Figure 12).

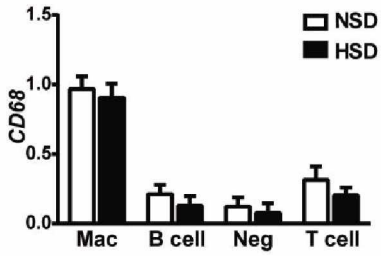

Figure 12. CD68 is a reliable peritoneal macrophage marker. Peritoneal cells were sorted by FACS from mice fed a normal (NSD) or high salt diet (HSD) for 16 days into macrophages ("Mac"), B cells, negative cells ("Neg"), or T cells using a panel of suitable surface markers. The final purity of each sorted population was >85%. CD68 expression was determined in populations by qPCR.

For experiment 2, PECs were resuspended into PBS/2mM EDTA with 0.5% (v/v) FBS and then stained with the following diluted antibodies (detailed in 2.2.5): α-CD11b-FITC 1:100, α-F4/80-PB 1:100, α-CD3-eFluor660 1:100, α-B220-APC-Cy7 1:100 for 20 minutes in the dark. Stained PECs were then washed, analysed and sorted on a BD FACSAria instrument. To sort, doublets were first excluded by FSC-A vs. FSC-H analysis, and then gated as desired. All sorted samples were re-analysed and macrophages had a purity >85%, whilst all other populations had purities >90%. Analysis of flow cytometry data was performed with the FlowJo software version 10. Sorted cells were immediately put into Qiazol solution and stored at -80°C for RNA extraction and subsequent gene analysis by qPCR.

2.3.12. *In vivo* wound healing

Fourteen age-matched WT mice were randomly assigned to receive a high salt diet (4% NaCl in chow plus 1% in the drinking water; HSD) or normal-salt diet (0.4% in chow plus tap water; NSD) from the day of wounding onwards. Each mouse was subjected to two 8-mm excisional wounds, one on each side of the midline of the back on day 0 of the respective diets. Thereafter, mice were treated by the same regime. Wounds (length × width) were measured on day 0, 3, 5, 7, 10, 12 and 14, and the percent total wound area was calculated as the percentage of wound area compared to day 0 of the respective animal. One wound in each group was excluded from analysis, as a piece of the bedding stuck to the wound and affected the healing process. Wound measurements were done without knowledge of the dietary group assignment. At the end of the assay (14 d), skin samples were taken from the site of the wounds and RNA extracted for gene expression analysis as described above. Mice on HSD consumed significantly more drinking water; despite a slightly reduced food intake, their body weight remained similar to that of mice on NSD until the end of the experiment, indicating no gross adverse health effect of HSD treatment (Figure 13). The wound healing experiment was performed in collaboration with Prof. Karl Hilgers (Erlangen, Germany).

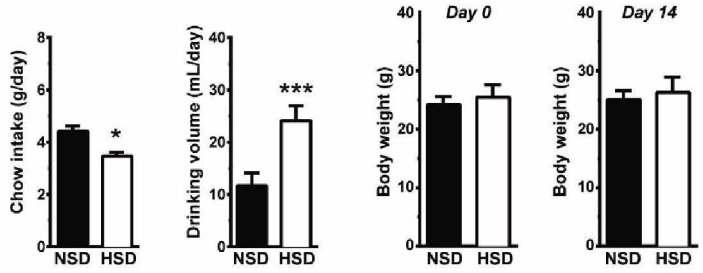

Figure 13. Eating and drinking behaviour of mice during wound healing. The total chow intake and drinking volume was measured over 14 days of wound-healing whilst on normal salt diet (NSD) and high salt diet (HSD). The body weight of the mice was also measured at day 0 and at the end of the time course. *$p<0.05$; ***$p<0.001$.

2.3.13. *In vitro* co-culture suppression assay

Spleens were dissected from WT mice, submerged in chilled assay media (RPMI1640 containing 10% (v/v) FBS, 1% (v/v) Penicillin-Streptomycin) and cut into pieces. To prepare single cell splenocyte suspensions, spleens were pushed through a 70µm cell strainer. Cells were pelleted by centrifugation and then resuspended in red blood cell lysis

buffer for 3 minutes. Red blood cell lysis was quenched with the addition of assay media. Cells were washed once with PBS to remove FBS, before labeling with 0.5-1µM carboxyfluorescein succinimidyl ester (CFSE) at a final cell density of $10x10^6$ cells/ml in PBS for 5 minutes. CFSE is a membrane-permeable fluorescent cell staining dye that covalently binds to intracellular lysine residues. Due to covalent binding to proteins, CFSE is retained within cells for very long periods and equally distributed during subsequent cell divisions. This is the principle of cell proliferation monitoring using CFSE (Figure 14) (Quah and Parish, 2010; Quah et al., 2007). The labeling reaction was stopped with chilled assay media and splenocytes were washed with assay media for two more times.

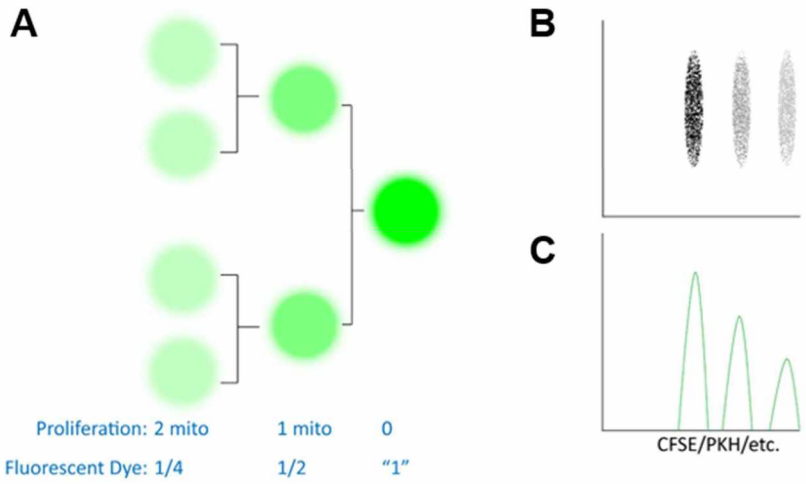

Figure 14. The principle of cell proliferation monitoring using CFSE and flow cytometry. A: CFSE is equally distributed among daughter cells with each mitosis (mito). **B+C:** When analyzed by flow cytometry, cells of different cell generations from (**A**) form distinct populations 'clouds' in dot-plot view (**B**) or individual peaks in histogram view (**C**). (faithfully adapted from http://www.stmichaelshospital.com/research/facilities/images/Figure-3-Cell-Cycle.jpg; 05. August 2015).

Labelled cells (250,000/well) were first stimulated alone in 96-well plates in 150µl/well of isotonic assay media with plate-bound α-CD3 and α-CD28 for 24 hours. 96-well plates had been coated with PBS-diluted α-CD3 (0.5mg/ml) and α-CD28 (0.2mg/ml) for 2h at 37°C before. Initially, the amount of coating antibody was optimized to yield robust proliferation (Figure 15 A) without causing activation-induced cell death (Green et al., 2003). Simultaneously (and separately), BMDM were left unstimulated (M(0)) or activated to M(IL-4+IL-13) alone or with an additional 40mM NaCl for 24 hours (see 2.3.1). On the next day, M(0), M(IL-4+IL-13), and M(IL-4+IL-13)+40mM NaCl activated macrophages were detached with PBS/2mM EDTA and gentle scraping. As it has

previously been shown that salt affects T cell activation and function (Kleinewietfeld et al., 2013), M(IL-4+IL-13) macrophages activated in high NaCl were washed thoroughly (3 x PBS) to remove excess salt (i.e the T cells did not experience hypertonic conditions). M(0) and M(IL-4+IL-13) macrophages stimulated in isotonic media were treated similarly. After washing, macrophages were added to 96-well plates containing the CFSE-labelled splenocytes at macrophage:splenocyte ratios of 1:3, 1:6, 1:12, 1:24, and co-cultured for an additional 3.5 days in 250µl/well isotonic assay media. T cells showed robust proliferation on day 4 during assay optimization (Figure 15 B). The proliferation of T cells was determined after 4.5 days as described above (see 2.3.8).

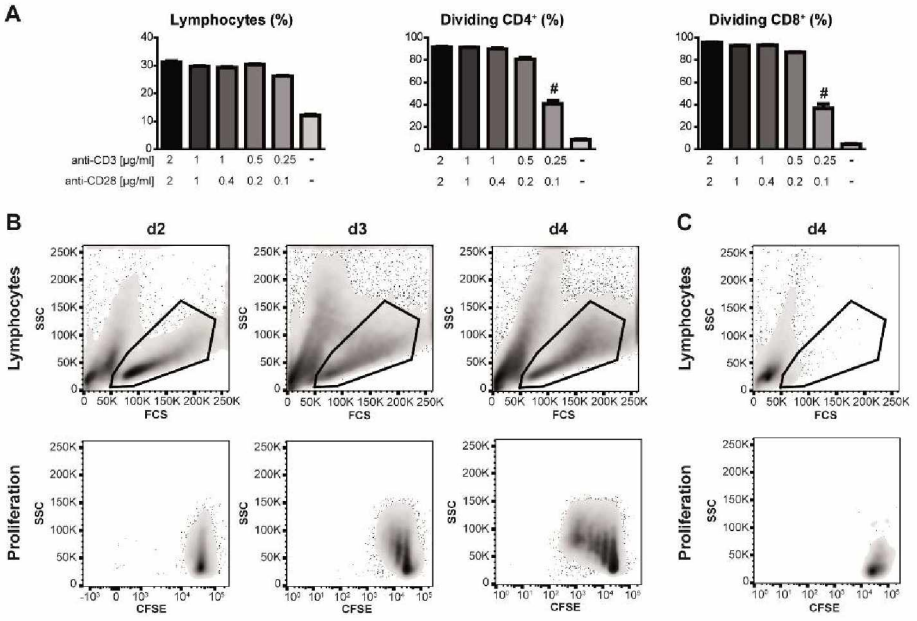

Figure 15. Optimization of CFSE proliferation assay conditions. A: The percentage of total lymphocytes and of proliferating $CD4^+$ and $CD8^+$ T cells at different coating antibody concentrations is shown. #$p<0.05$ vs 0.5µg/ml α-CD3+0.2mg/ml α-CD28. **B:** T cell proliferation at optimum antibody concentrations over time is shown. No cell division was observed until day 2. Most cells had undergone subsequent rounds of mitosis on day 4. **C:** No cell proliferation is detectable in the absence of antibody coating.

Myeloid-derived suppressor cells (MDSCs) have recently been described as a T cell-suppressive immature myeloid-lineage cell population (Gabrilovich and Nagaraj, 2009; Katoh and Watanabe, 2015; Li et al., 2015; Marigo et al., 2010). MDSCs are a $CD11b^+Gr\text{-}1^+$ double-positive cell population that constitutes ~20% of total mouse bone marrow cells (Gabrilovich and Nagaraj, 2009). To exclude that MDSCs possibly influence the macrophage/T cell co-culture assay described here, the percentage of MDSCs was determined in freshly prepared batches of BMDM before and after activation of

macrophages used for co-cultures. MDSCs were also generated *in vitro* (see 2.3.4) as a suitable positive control for flow cytometric analysis (Figure 16 A). MDSCs were determined as the granulocyte differentiation antigen 1 (Gr-1) positive subpopulation of total $CD11b^{+}F4/80^{-}$ cells (Figure 16 B). MDSCs were successfully induced *in vitro* (~60%) and showed an abundance in total bone marrow (~30%) similar to observations by others (Gabrilovich and Nagaraj, 2009); importantly, MDSCs were virtually absent from BMDM preparations both before and after (<0.5%) macrophage activation (Figure 16 C). The suppression assays presented here were conducted at splenocyte:macrophage ratios of 1:3, 1:6, 1:12 and 1:24 (with 250,000 splenocytes in each condition). Based on the calculated 0.2% abundance of MDSCs in both M(IL-4+IL-13) stimulated conditions (Figure 16 C), co-culture assays potentially contain approximately 167, 83, 41 and 20 MDSCs, in each respective dilution. This is in comparison to the ~83,000, 42,000, 21,000 and 10,000 macrophages. Thus, potential MDSCs contamination is not significantly confounding the co-culture assay results.

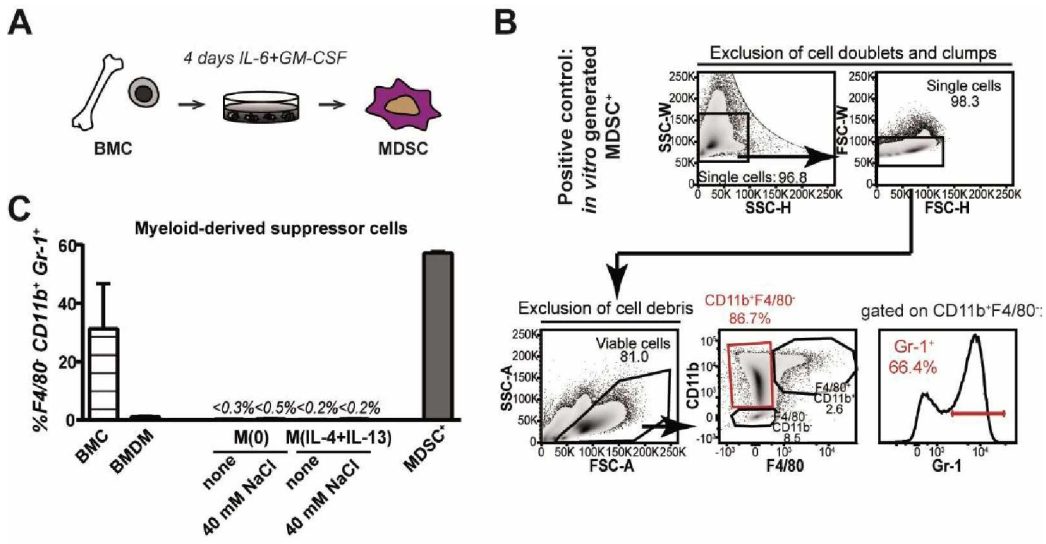

Figure 16. MDSCs are absent from BMDM and activated macrophages. A: Schematic showing the *in vitro* generation of MDSCs by incubation of bone marrow cells (BMC) with IL-6 and GM-CSF. **B:** To quantify MDSCs, the percentage of $Gr\text{-}1^{+}$ cells was determined within total $CD11b^{+}F4/80^{-}$ cells (red rectangle) after removal of doublets and dead cells. Flow cytometry plots from the *in vitro* generation of MDSCs are shown. **C:** BMDM were generated from freshly isolated bone marrow cells (BMC) and stimulated with IL-4 and IL-13 (M(IL-4+IL-13)) in the absence (none) or with an additional 40mM NaCl for 24 hours. Unstimulated (M(0)) macrophages were treated similarly. The percentage of MDSCs was determined in each sample as described in (**B**) with *in vitro* generated MDSC as a positive control ($MDSC^{+}$).

2.3.14. Microarray

Total RNA was extracted as described above (2.3.6) from M(0), M(IL-4+IL-13), and M(LPS) macrophages activated with and without an additional 40mM salt (N=2 per group) and analysed using the Illumina Mouse Ref-8 v2.0 array. Amplified cRNA for array hybridization was prepared using a commercial RNA amplification kit. All microarray experiments were performed at the MDC core facility and according to the manufacturers' recommendations.

2.3.15. Chromatin immunoprecipitation (ChIP) and sequencing

Twelve ChIP-seq experiments were performed to determine genome wide histone modification (H3K4me3 and H4ac) levels of murine primary BMDM after 24 hours IL-4+IL-13 (10ng/ml each) or LPS (10ng/ml) stimulation in the presence or absence of 40mM NaCl. Unstimulated M(0) macrophages were treated similarly. The procedure was modified from (Barski et al., 2007) (Figure 17 A).

Per group, $40x10^6$ BMDM were harvested by incubation with PBS/2mM EDTA and gentle scraping. Cells were pelleted and stored at -80°C. To isolate nuclei, cell pellets were thoroughly resuspended in 1ml ice-cold nuclei preparation buffer I. 1ml of ice-cold nuclei preparation buffer II was added and cells were incubated on ice for 10 minutes. 15ml tubes containing 10ml of ice-cold nuclei preparation buffer III were prepared and the cell suspension was carefully overlain. Nuclei were pelleted by centrifugation through this sucrose cushion for 20 minutes at 4°C.

Subsequently, supernatants were removed and nuclear pellets resuspended in 1ml MNase buffer. Reconstituted MNase was added and the samples were digested at 37°C to yield native chromatin samples consisting mainly of mono-nucleosomes. The amount of MNase used for digestion and incubation time were optimized with each new enzyme batch. Effective preparation of mono-nucleosomes was confirmed by electrophoresis of digested DNA samples on 2% agarose gels containing ethidium bromide (Figure 17 B). MNase treatment was stopped by adding 20µl 0.5M EDTA. 1ml of chilled 2x RIPA buffer was added to each sample followed by thorough mixing to release chromatin from nuclei. Nuclear debris was removed by centrifugation and collecting of native chromatin supernatants.

In the meantime, Protein A Dynabeads were coated with antibody for immunoprecipitation (IP). Briefly, 50µl Dynabeads were washed once with PBS/BSA using a magnetic separation rack. Dynabeads were coated with 5µl anti-H3K4me3 or 3µl anti-H4ac antibody in 500µl PBS/BSA with gentle agitation for 6-8 hours at 4°C. Next, antibody-coated beads were washed twice with ice-cold PBS/BSA before 600µl of native chromatin were added and precipitated over night at 4°C with gentle agitation. 60µl of chromatin were kept as input and stored at -20°C.

The next day, all IP samples were washed thoroughly at 4°C with gentle agitation in 1ml of the respective buffers as follows: twice RIPA buffer, twice RIPA buffer with 0.3M NaCl, twice LiCl buffer, once TE buffer with 0.2% Triton X-100, and once TE buffer. Next, all samples including input were digested with proteinase K (100µl TE buffer, 5µl 20% SDS, 5µl proteinase K (10mg/ml stock) per sample) for 4 hours at 65°C and thorough agitation. A MinElute PCR Purification kit was used to purify immunoprecipitated DNA after proteinase K digestion. The specificity of immunoprecipitation was confirmed with known active (*Gapdh)* and inactive (*MyoD1*) genes by qPCR and DNA concentrations were quantified sample-wise using a Qubit device and high sensitivity dsDNA assay kit, according to the manufacturer's instructions. 50ng purified DNA was used to construct ChIP-seq libraries using a TruSeq ChIP Sample Prep kit according to the manufacturer's protocol. After cluster generation, sequencing was performed using the Illumina HiSeq 2000 platform. Library preparation and sequencing were performed in collaboration with the Hübner lab (MDC, Berlin, Germany). Additionally, independent ChIP experiments were performed to confirm genome-wide results at specific gene loci using qPCR.

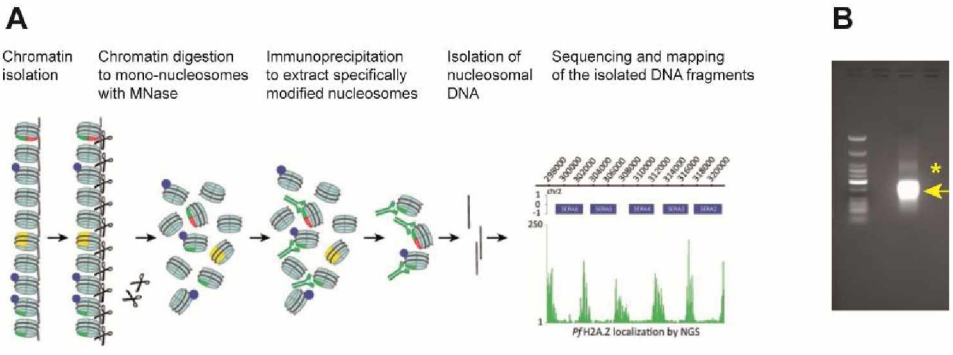

Figure 17. Native chromatin immunoprecipitation using MNase digestion. A: Schematic depicting the work flow of native chromatin immunoprecipitation (faithfully adapted from (Hoeijmakers et al., 2012)). **B:** Representative 2% agarose gel of MNase-digested DNA. As desired, mono-nucleosomal DNA is abundant (yellow arrow) with very little contamination by di-nucleosomal DNA (yellow asterisk).

2.3.16. Data analysis of microarray and ChIP-seq

M(IL-4+IL-13) and M(LPS) signatures of genes which were differential upon activation of BMDM for expression, H3K4me3, H4ac or various combinations were determined *de novo* using the available microarray and ChIP-seq data in close collaboration with Matthias Heinig and statisticians from the Hübner lab (MDC, Berlin, Gemany). Briefly, microarray data were quantile normalized on a probe level (25,697) without background correction. Quality control using principle component analysis did not reveal any batch effects (not shown). Differential gene expression analysis was then performed using analysis of variance in linear models using false discovery rate (FDR) to control for multiple testing (Benjamini et al., 2001). For ChIP-seq, short reads were mapped to the mouse reference genome (mm9) using the Bowtie algorithm; only reads mapped uniquely were retained. SAMtools was used to remove duplicate artefact reads (Li et al., 2009). All ChIP-seq data conformed the ENCODE consortium quality metrics (Landt et al., 2012). ChIP-seq promoter occupancy was quantified in TSS regions (±2kb) based on gene annotation from Ensembl release 62 for either M(0) and M(IL-4+IL-13) or M(0) and M(LPS) activated macrophages in two biological replicates per condition. Differential occupancy analysis was performed on the raw read counts using DESeq negative binomial regression model. The false discovery rate was controlled using the Benjamini Hochberg method (Benjamini et al., 2001). For further analysis and visualization, read counts were normalized using a quantile based scaling factor (Schulte et al., 2010). Finally the data was integrated with the gene expression data using the probeset to Ensembl mapping from the bioconductor package illuminaMousev2.db. Using this approach, a set of 3560 or 7030 genes which were differential (FDR<0.05) for expression, H3K4me3, H4ac or various combinations was identified as M(IL-4+IL-13) or M(LPS) signature, respectively.

Further analysis was based on the subset of all signature genes which were differential (FDR<0.05) for gene expression, i.e. 2604 (M(IL-4+IL-13)) or 4029 (M(LPS)) genes. Fold-changes (FC) were calculated for these genes using mean microarray expression data. Next, for genes with a FC>1.3 (induced and reduced) upon activation, gene ontology (GO) term analysis was performed using the GOstats R package (Falcon and Gentleman, 2007) to characterize biological processes affected by activation. For visualization, significant (FDR<0.05) (Benjamini et al., 2001) GO results were further processed using the Reduce and Visualize Gene Ontology (REVIGO) online tool which reduces the number of redundant GO terms according to their significance and semantic

similarity (Supek et al., 2011). REVIGO attributes a dispensability value ranging from 0 (not dispensable) to 1 (very dispensable) to each term. Terms with dispensability values below cut-offs indicated in figure legends were chosen for presentation.

To unveil the effect of high salt on macrophage activation, salt-sensitive M(IL-4+IL-13) or M(LPS) genes were identified among all activation-induced genes (FC>1.3 vs M(0)) by setting a FC limit of 1.2 when comparing M(IL-4+IL-13) or M(LPS) macrophages activated in the absence or presence of an additional 40mM NaCl. As, compared to the large differences usually expected when comparing pharmacological inhibitors or gene knockout models, more subtle differences were expected with this smaller environmental perturbation, this relatively low FC cut-off was chosen. 302 or 432 salt-sensitive genes were identified for activation with IL-4+IL-13 or LPS, respectively. The lists of salt-sensitive genes were then again analysed for the enrichment of GO pathways as described above. A FDR cut-off of 0.1 was accepted for salt-sensitive M(IL-4+IL-13) genes.

Heatmaps for illustration of the salt effect on M(LPS) glycolysis genes were generated using the heatmap.3 R package (Zhao et al., 2014). Plots showing the distribution of gene expression and histone mark changes upon BMDM activation (Figure 39 B) were generated in R using the *density* function.

2.3.17. Metabolic studies

Extracellular flux analysis was performed to determine the effect of NaCl on the mitochondrial respiratory capacity (oxidative phosphorylation, OXPHOS) and glycolysis. To do so, mitochondrial and glycolytic stress tests were performed with an extracellular flux analyzer. Macrophages were first seeded at a density of $1x10^5$ cells/well of an XF24 cell culture microplate and stimulated with or without IL-4+IL-13 in the absence or presence of 40mM NaCl for 24 hours.

For analysis of OXPHOS, a XF Cell Mito Stress Test Kit was used, according to the manufacturer's directions. Briefly, cells were exchanged into XF Base media containing 11mM glucose and 1% (v/v) FBS. Five consecutive measurements of the oxygen consumption rate (OCR) were then obtained under basal conditions, after which the following compounds (all from the XF Cell Mito Stress Test kit) were added sequentially (five measurements each): 1µM oligomycin, to inhibit mitochrondrial respiration; 1.5µM fluoro-carbonyl cyanide phenylhydrazone (FCCP), a mitochondrial uncoupler to elucidate

maximal respiration; 100nM rotenone plus 1μM antimycin A, to inhibit the electron transport chain and measure the amount of non-mitochondrial respiration.

For analysis of glycolysis, a XF Glycolysis Stress Test kit was used, according to the manufacturer's directions. Briefly, cells were exchanged into XF Assay media with no glucose and 1% (v/v) FBS. Three consecutive measurements of the extracellular acidification rate (ECAR) were then obtained under basal conditions, after which the following compounds (all from the XF Glycolysis Stress Test kit) were added sequentially (5 measurements each): 10mM glucose, to initiate glycolysis; 1μM oligomycin, to inhibit mitochrondrial respiration and 50mM 2-deoxy-glucose (2-DG), to inhibit glycolysis. Extracellular flux analyses were performed by Katrina Binger. Basal OCR, ECAR, SRC and glycolysis were calculated as per the manufacturer's directions.

2.3.18. Mitochondrial content analysis

The analysis of mitochondrial mass by flow cytometry is described in 2.3.8. Additionally, a previously described qPCR assay was used to determine the effect of salt on mitochondrial content (Guo et al., 2009). Macrophages were activated as before to M(0) or M(IL-4+IL-13) with or without additional 40mM NaCl. Next, total DNA was extracted with the QIAamp DNA Mini Kit according to the manufacturer's instructions. The abundance of two respiratory chain enzymes – one mitochondrial (cytochrome c oxidase subunit 1; MT-CO1) and one nuclear (NADH dehydrogenase (ubiquinone) flavoprotein 1; NDUFV1) – were determined by qPCR and the ratio of mitochondrial DNA to nuclear DNA expression was used as a measure of relative mitochondrial content. The following primers were used (Guo et al., 2009):

Gene	Sequence	Gene	Sequence
MT-CO1		*NDUFV1*	
Forward:	5-TGCTAGCCGCAGGCATTAC-3	Forward:	5-CTTCCCCACTGGCCTCAAG-3
Reverse:	5-GGGTGCCCAAAGAATCAGAAC-3	Reverse:	5-CCAAAACCCAGTGATCCAGC-3

2.3.19. Glucose uptake analysis

See flow cytometry experimental section (2.3.8) for details.

2.3.20. Lactate production

BMDM were seeded at a density of $2x10^6$ cells per 6-well, allowed to attach for two hours and activated as described before (2.3.2). After activation, cells were washed twice with pre-warmed PBS. Cells were then incubated in 1ml of FBS-, LPS-, and interleukin-free medium (RPMI1640 with L-glutamine containing 0.5% (w/v) BSA, 10mM HEPES, 50µM beta-mercaptoethanol, 1% (v/v) Penicillin-Streptomycin) for 1-2 hours. Supernatants and cell lysates were then collected for extracellular and intracellular lactate measurements, respectively, using the EnzyFluo L-lactate assay or Lactate fluorometric assay kit according to the manufacturers' instructions. Data were normalized sample-wise to total protein concentrations, determined by Bradford assay (2.3.7) of recovered cell lysates.

2.3.21. Statistical analysis

Data is presented as mean±SEM. Where applicable, outliers were excluded by the extreme studentized deviate method. Normality of data was assessed according to the Kolmogorov-Smirnov test. Unless otherwise indicated, two groups were compared by either two-sided Student's t-tests (parametric) or a Mann-Whitney U-tests (for non-parametric data). For analysis of more than two groups one-way ANOVA (parametric) or Kruskal-Wallis (non-parametric) test was performed and for all significant outcomes a Tukey's or Dunns' (respectively) multiple comparison test was performed. The number of animals for *in vivo* experiments was chosen based on analysis of previous studies (Byles et al., 2013; Kleinewietfeld et al., 2013; Liao et al., 2011).

3. Results

3.1. High salt blunts M(IL-4+IL-13) macrophage activation

3.1.1. High salt decreases expression of M(IL-4+IL-13) marker genes

Stimulation of macrophages with LPS under high salt conditions (additional 40mM NaCl) leads to a significant increase of inflammatory gene expression (Figure 18 A) and enhanced production of antimicrobial effector molecules (Figure 18 B). The salt-induced boost of M(LPS) activation has been described in greater detail elsewhere (Jantsch et al., 2015).

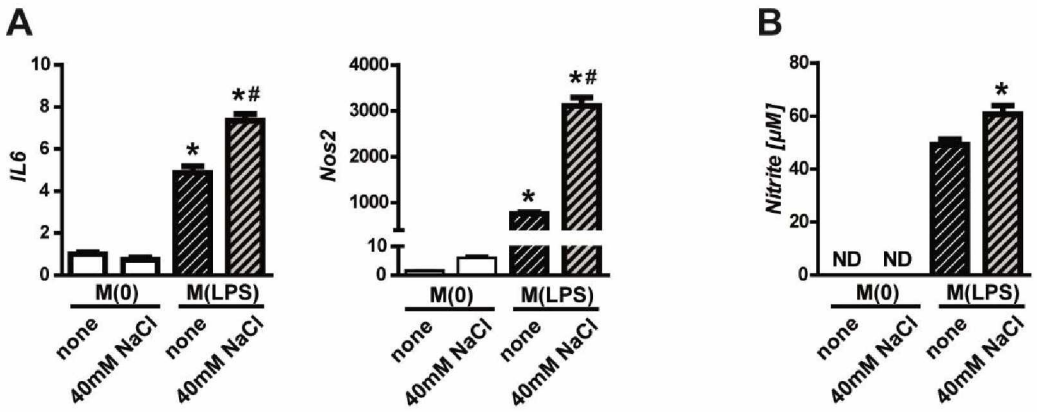

Figure 18. High salt boosts activation of M(LPS) macrophages. A: Macrophages were stimulated with 10ng/ml LPS in the absence (none) or with an additional 40mM NaCl for 24 hours. Unstimulated (M(0)) macrophages were treated similarly. The expression of M(LPS) signature genes was determined by qPCR. *p<0.05 vs M(0); #p<0.05 vs M(LPS). **B:** Macrophages were stimulated as in (**A**) and nitrite was determined in cell culture supernatants as a surrogate for NO production with Griess reagent. *p<0.05 vs M(LPS). ND: not detected.

To test the effect of high salt on the IL-4+IL-13-dependent activation of M2 macrophages, adherent bone marrow derived macrophages (BMDM) were incubated with IL-4+IL-13 (10ng/ml each) for 24 hours in culture medium in the absence (isotonic; $[Na^+]_{media}$≈139mM, $[Cl^-]_{media}$≈109mM) or in the presence of an additional 40mM NaCl (hypertonic; $[Na^+]_{media}$≈179mM, $[Cl^-]_{media}$≈149mM) (Figure 19 A). RNA was isolated from activated macrophages and the expression of a panel of typical murine M(IL-4+IL-13) activation marker genes was determined by qPCR. In complete contrast to M(LPS), high salt significantly blunted the IL-4+IL-13-induced expression of *Arg1*, *Mrc1*, *Ym1* and *Fizz1* (Figure 19 B). Additionally, high salt blunted the expression of the M(IL-4+IL-13)-induced

transcription factors *Klf4* and *Irf4* (Figure 19 C). The blunted expression of Arg1 by high salt was also confirmed on protein level by western blotting (Figure 19 D).

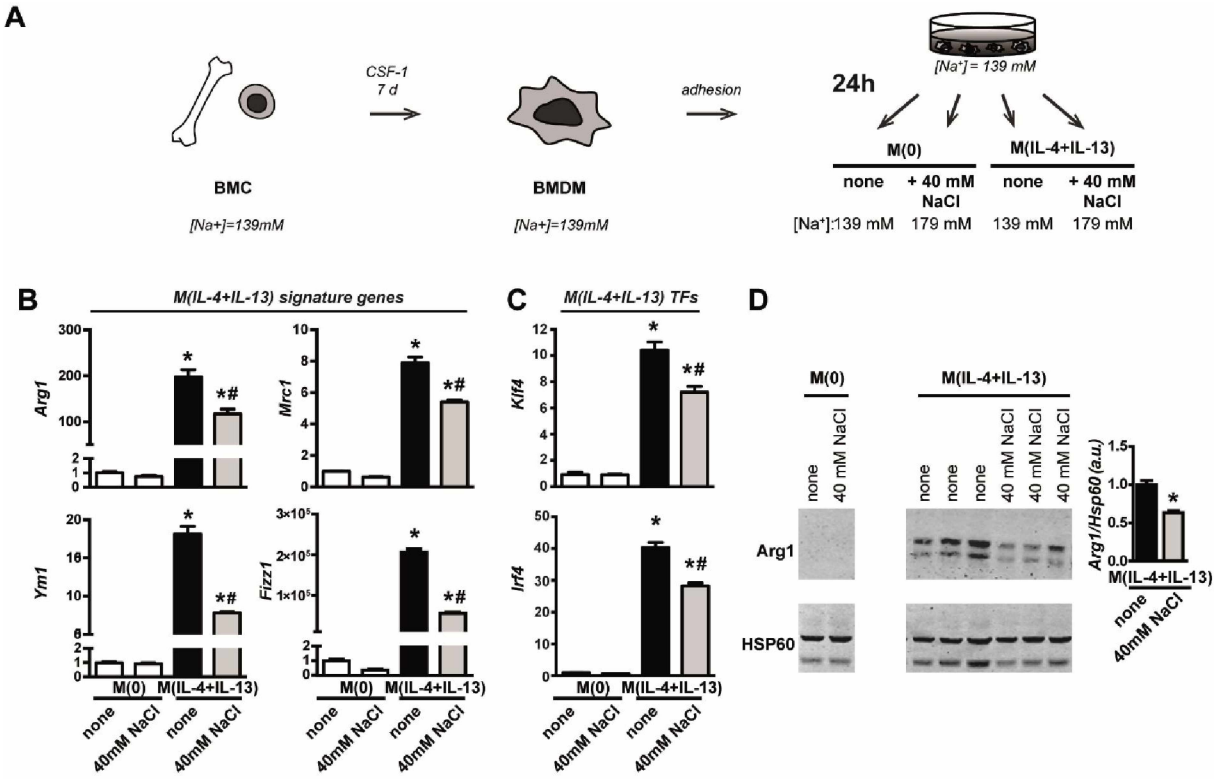

Figure 19. High salt blunts the expression of M(IL-4+IL-13) signature genes of BMDM. A: Schematic of *in vitro* stimulation of macrophages. Indicated is the final media concentration of Na^+ per condition, where 139mM is normal, isotonic media. BMDM were typically incubated as indicated for 24 hours. Abbreviations: BMC, bone marrow cells; BMDM, bone marrow-derived macrophages. **B+C:** Macrophages were stimulated with IL-4+IL-13 (M(IL-4+IL-13)) in the absence (none) or with an additional 40mM NaCl for 24 hours. Unstimulated (M(0)) macrophages were treated similarly. The expression of M(IL-4+IL-13) signature genes was determined by qPCR. *p<0.05 vs M(0); #p<0.05 vs M(IL-4+IL-13). **C:** Protein levels of Arg1 were determined by western blotting after treatment as in (**A**). Hsp60 loading control is also shown. Bar graph shows the quantification of the relative levels of Arg1 normalized to M(IL-4+IL-13) lysates. *p<0.05.

To test, whether the blunting of M(IL-4+IL-13) marker gene expression by high salt was dose-dependent, BMDM were activated in the presence of an additional 10, 20 or 40mM NaCl. The concentration range was chosen according to interstitial hypertonicity levels observed *in vivo* under high dietary salt intake (Jantsch et al., 2015; Machnik et al., 2009; Wiig et al., 2013). Blunting of signature genes by high salt was dose-dependent (Figure 20). *Arg1* expression was significantly blunted by 20 and 40mM NaCl. 10mM NaCl were sufficient to significantly reduce *Mrc1* expression and 20 and 40mM NaCl showed an

even stronger effect. *Fizz1* and *YM1* showed the clearest dose dependency with higher salt concentrations leading to significantly stronger blunting effects.

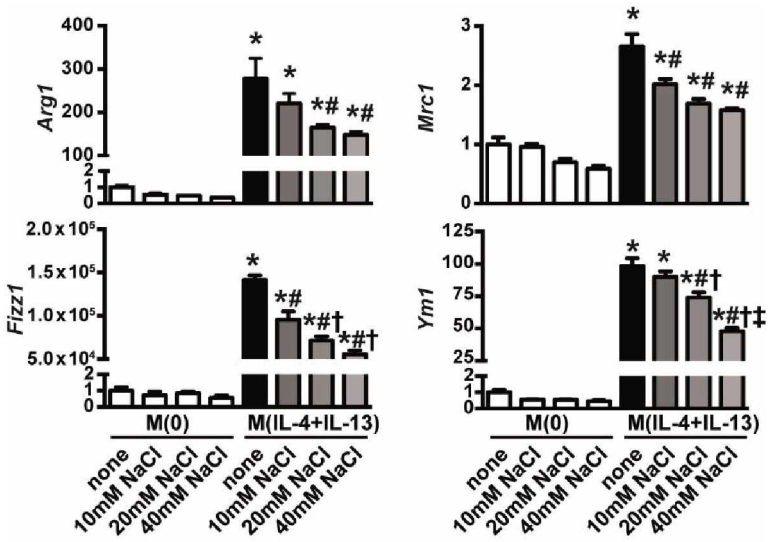

Figure 20. High salt blunts M(IL-4+IL-13) marker gene expression dose-dependently. BMDM were stimulated with IL-4+IL-13 (M(IL-4+IL-13)) in the absence (none) or increasing concentrations of additional NaCl (10, 20 and 40 mM). Unstimulated (M(0)) macrophages were treated similarly. The expression of M(IL-4+IL-13) signature genes was determined by real-time qPCR. * $p<0.05$ vs M(0); # $p<0.05$ vs M(IL-4+IL-13) none (no additional salt); †$p<0.05$ vs M(IL-4+IL-13)+10mM NaCl; ‡$p<0.05$ vs M(IL-4+IL-13)+20mM NaCl.

To corroborate the physiological relevance of these findings, the effect of high salt on M2 polarization was also determined with *ex vivo* peritoneal macrophages. Macrophages were isolated from the peritoneal cavity of WT mice by lavage and allowed to attach to cell culture plastic dishes, followed by washing in order to enrich adhesive cells (Figure 21 A). The composition of peritoneal cells was assessed by flow cytometry before and after attachment by flow cytometry (Figure 21 B). Initially, macrophages ($CD11b^+F4/80^+$) constituted circa 52% of total peritoneal cells. B ($B220^+$) and T ($CD3^+$) cells accounted for approximately 48% and 15% of non-macrophage ($CD11b^-$ $F4/80^-$) cells, respectively; the identity of $CD11b^-F4/80^-B220^-CD3^-$ cells (28%) was not further investigated. Surprisingly, plastic attachment removed peritoneal T cells (Figure 21 B; red box) but not peritoneal B and $CD11b^-F4/80^-B220^-CD3^-$ cells. The percentage of macrophages was approximately 50% before and after adhesion (not shown). Therefore, all gene expression data were normalized to CD68, a macrophage specific marker gene (Byles et al., 2013) (Figure 12). Activation of peritoneal cells with IL-4+IL-13 induced robust expression of the marker genes *Arg1*, *Mrc1*, *Fizz1* and *Ym1* (Figure 21 C) albeit the

magnitude of induction differed from BMDM (Figure 19 B). Similar to BMDM, activation in the presence of an additional 40mM NaCl blunted the induction of *Mrc1*, *Fizz1* and *Ym1* significantly, whereas *Arg1* was not affected here (Figure 21 C).

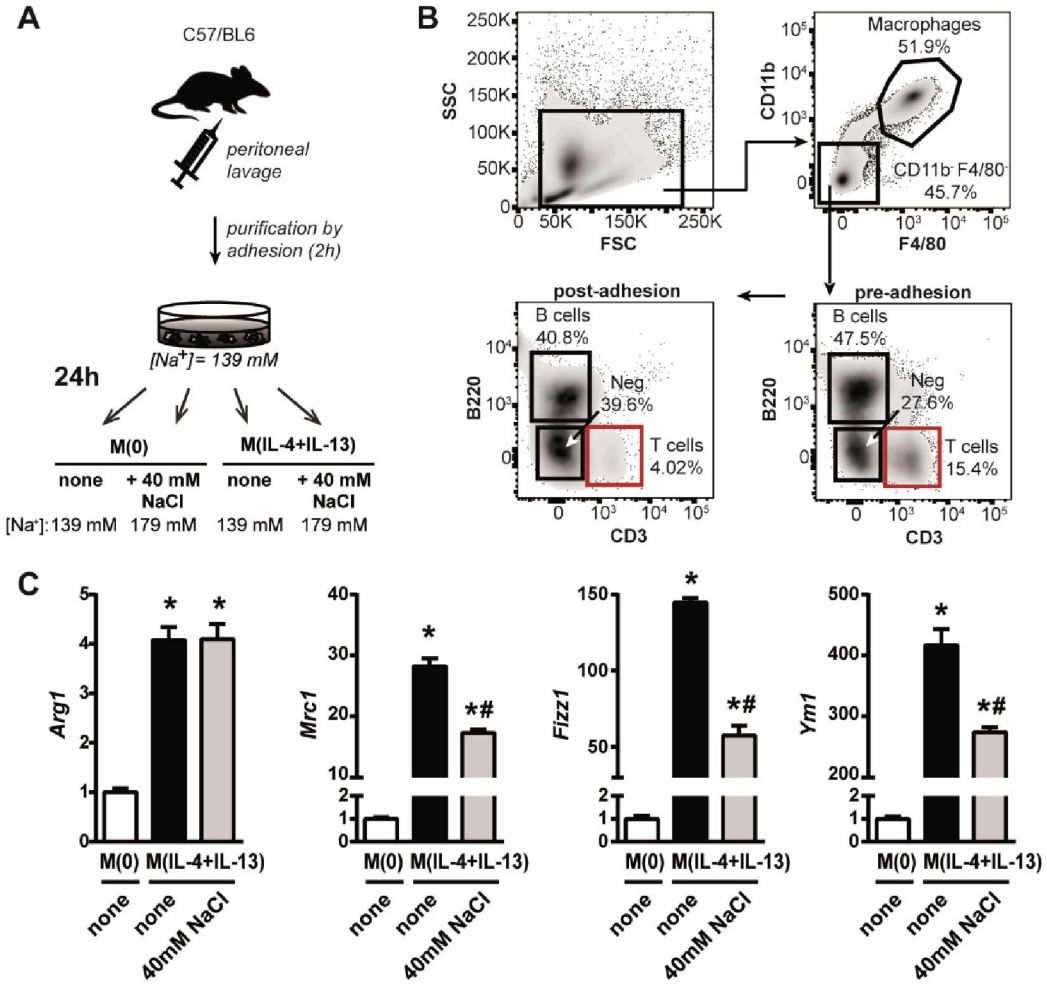

Figure 21. High salt blunts activation of *ex vivo* peritoneal macrophages. A: Resident peritoneal immune cells were isolated from WT mice by lavage. Adhesive cells were enriched by attachment to plastic for two hours and washing before activation. **B:** Representative flow cytometry plots showing the staining of peritoneal lavage cells for macrophages ($CD11b^+F4/80^+$) and further characterization of $CD11b^-F4/80^-$ cells *before* and *after* plastic adhesion: $B220^+$ (B cells); $CD3^+$ (T cells, red box), $CD11b^-F4/80^-B220^-CD3^-$ (Neg: negative cells). C: The expression of M(IL-4+IL-13) signature genes by unstimulated (M(0)) peritoneal lavage cells or after stimulation with IL-4+IL-13 (M(IL-4+IL-13)) in the absence (none) or with an additional 40mM NaCl as determined by qPCR. Expression data were normalized to CD68. *p<0.05 vs M(0); #p<0.05 vs M(IL-4+IL-13).

3.1.2. NaCl blunts M(IL-4+IL-13) activation independent of tonicity, early STAT6 signaling, osmo-pathways or general macrophage fitness

Any compound unable to freely cross cell membranes increases tonicity if present at concentrations higher than physiological, without commensurate decrease of other osmolytes (Irarrazabal et al., 2008). Cells have evolved strikingly uniform mechanisms to adapt to high tonicity, or osmo-stress, caused by very different agents (Burg et al., 2007; Yancey et al., 1982). To test whether the blunting of M(IL-4+IL-13) signature gene expression was salt-specific or merely due to increased tonicity, BMDM were stimulated for 24 hours with IL4+IL13 in the absence or presence of 40mM NaCl as before, or with two different non-ionic tonicity controls: mannitol, which increases tonicity without entering the cell, and urea, which increases osmolality of the bathing solution and enters the cell. Neither the presence of an additional 80mM mannitol nor urea (40mM NaCl in aqueous solution dissolves into 80mM of effective osmolytes) during the activation of macrophages with IL-4+IL-13 blunted marker gene expression significantly compared to 40mM NaCl (Figure 22). Therefore, high NaCl acts on macrophage activation specifically and independent of tonicity. Additional activation experiments using 40mM sodium gluconate instead of a sodium chloride salt showed that Na^+ alone was sufficient to blunt M(IL-4+IL-13) marker gene expression (not shown).

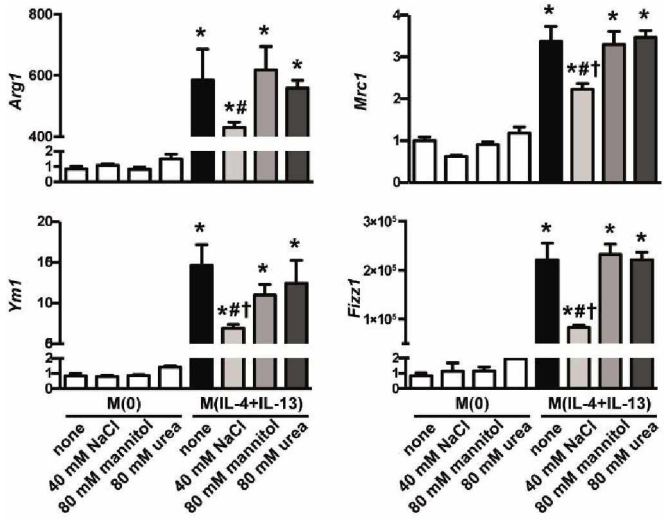

Figure 22. High salt blunts M(IL-4+IL-13) marker gene expression indepenent of tonicity. Macrophages were stimulated as before or with an additional 80mM mannitol or urea as tonicity controls. Signature gene expression was analyzed by qPCR. *p<0.05 vs M(0); #p<0.05 vs M(IL-4+IL-13) none and M(IL4+IL-13)+mannitol; †p<0.05 vs M(IL-4+IL-13)+urea.

Instant phosphorylation of STAT6 is a crucial proximal signaling event upon IL-4/IL-13 receptor binding (Gordon and Martinez, 2010; Mishra et al., 2011). Phosphorylation of STAT proteins is often a quick and transient phenomenon, however, maintenance of high phosphorylation levels over several hours has been described specifically for STAT6 (Comfort and Haugh, 2008). In order to identify mechanisms by which high salt affects M(IL-4+IL-13) activation, early and late STAT6 phosphorylation was examined by western blotting in the absence or in the presence of an additional 40mM NaCl or 80mM mannitol as a tonicity control (Figure 23). To investigate early STAT6 signaling, cells were pre-incubated with an additional 40mM NaCl or 80mM mannitol for five minutes before IL-4+IL-13 were added and STAT6 phosphorylation determined at 15, 30 or 60 minutes.

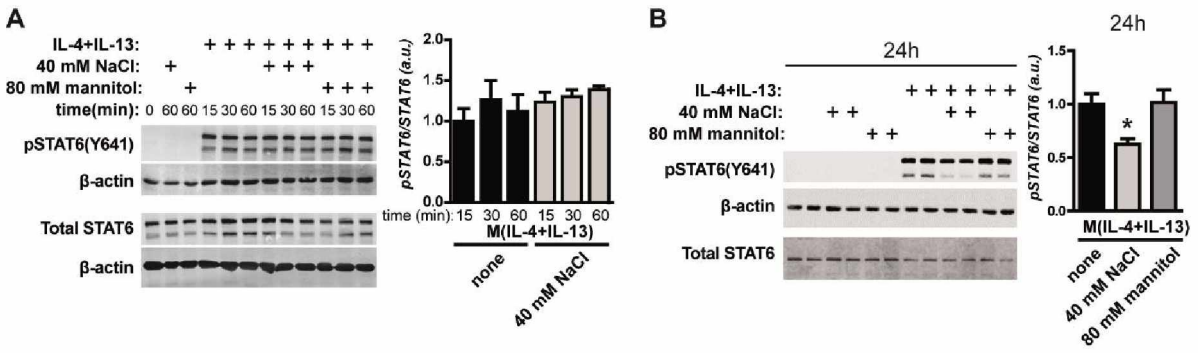

Figure 23. High NaCl mildly reduces late but not early STAT6 phosphorylation. The effect of NaCl on the phosphorylation of STAT6 was determined by western blotting. **A:** To examine early signaling, macrophages were serum-starved overnight and then pre-treated with an additional 40mM NaCl or 80mM mannitol for five minutes prior to stimulation with IL-4+IL-13 for 15, 30 or 60 minutes. The levels of phosphorylated and total STAT6 were determined in separate blots with β-actin used as loading control. The bar graph shows the quantification of relative levels of pSTAT/STAT for each time point, normalized to t=15 of M(IL-4+IL-13) lysates. **B:** For late signaling, macrophages were incubated with IL-4+IL-13 in the absence (none) or in the presence of an additional 40mM NaCl or 80mM mannitol for 24 hours. The levels of phosphorylated and total STAT6 were determined as in (**A**). The bar graph shows the quantification of relative levels of pSTAT/STAT normalized to M(IL-4+IL-13) lysates. *p<0.05 vs M(IL-4+IL-13)+40mM NaCl and M(IL-4+IL-13)+80mM mannitol.

STAT6 phosphorylation was undetected in the absence of IL-4+IL-13 (Figure 23 A; lanes 1-3). STAT6 phosphorylation was high after the addition of IL-4+IL-13 at all three time points (Figure 23 A; lanes 4-6) irrespective of the presence of an additional 40mM NaCl (Figure 23 A; lanes 7-9) or an additional 80mM mannitol (Figure 23 A; lanes 10-

12). The bar graph shows the quantification of relative levels of pSTAT/STAT for each time point, normalized to t=15 minutes of M(IL-4+IL-13) lysates for M(IL-4+IL-13) and M(IL-4+IL-13)+40mM NaCl.

Late STAT6 phosphorylation in response to IL-4+IL-13 was determined after 24 hours of co-incubation without (none) or an additional 40mM NaCl or 80mM mannitol (Figure 23 B). At this later time point, the presence of 40mM NaCl (Figure 23 B; lanes 9-10) decreased STAT6 phosphorylation compared to isotonic activation (Figure 23 B; lanes 7-8) independent of tonicity (Figure 23 B; lanes 11-12). The bar graph shows the quantification of relative pSTAT6/STAT6 levels normalized to M(IL-4+IL-13) at 24 hours. Collectively, high salt does not affect early signaling events upon IL-4+IL-13 stimulation but significantly decreases relative levels of pSTAT6/STAT6 at late time points independent of tonicity.

A Sgk1–Nfat5 tonicity-response signaling axis was found to be responsible to mediate the effects of high salt on T cells (Kleinewietfeld et al., 2013; Wu et al., 2013) and pro-inflammatory M(LPS) macrophages (Jantsch et al., 2015). To investigate whether the same signaling axis is essential to mediate the high salt effect on M(IL-4+IL-13) macrophage activation, BMDM were generated from *Sgk1* and *Nfat5* knock out mice to test whether deficiency of these signaling molecules rescues the salt effect on M(IL-4+IL-13) activation.

First, the responsiveness of both *Nfat5* and *Sgk1* to osmotic stress was confirmed in our BMDM cell culture system where an additional 40mM NaCl significantly enhanced the expression of both genes in resting (M(0)) and activated (M(IL-4+IL-13)) WT macrophages (Figure 24 A). In stark contrast to other cell types (M(LPS) and Th17 cells), the genetic knock out of *Nfat5* or *Sgk1* did not significantly influence the effect of high salt on M(IL-4+IL-13) marker gene expression (Figure 24 B and C, respectively). *Arg1*, *Mrc1*, *Fizz1* and *Ym1* all showed significantly reduced expression in the presence of an additional 40mM NaCl in activated BMDM generated from *Nfat5* knock out bone marrow (Figure 24 B). *Sgk1* knock out rescued the salt effect on *Arg1* expression. However, it did not affect the high salt-dependent blunting of the expression of the remaining signature genes *Mrc1*, *Fizz1* or *Ym1* (Figure 24 C). These results suggest that Sgk1-Nfat5 signaling is not mediating the blunting effect of high salt on M(IL-4+IL-13) activation and that other mechanisms are responsible. The elucidation of these mechanisms will be the focus of later sections of the present thesis.

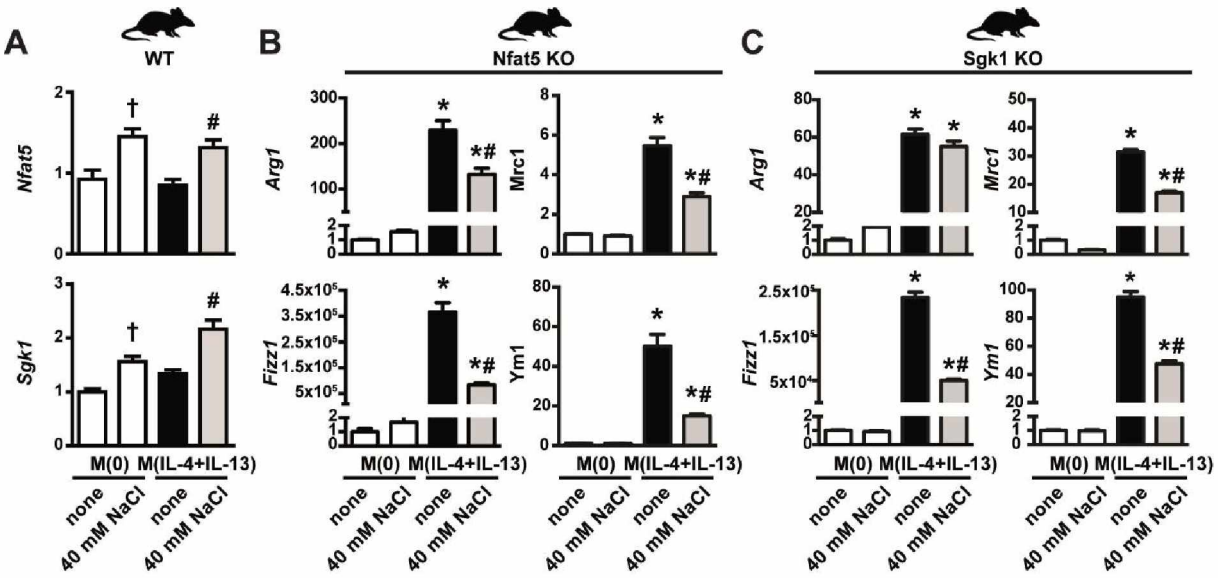

Figure 24. *Nfat5* and *Sgk1* knock out do not rescue salt-blunted M(IL-4+IL-13) activation. Macrophages from the respective wildtype or gene-deficient mice were stimulated with IL-4 and IL-13 (M(IL-4+IL-13)) in the absence (none) or with high salt for 24 hours. Unstimulated (M(0)) macrophages were treated similarly. **A:** The expression of genes known to mediate cellular responses to tonicity was determined by qPCR. †p<0.05 vs none; #p<0.05 vs M(IL-4+IL-13) none. **B and C:** Cells were isolated from the bone marrow of *nfat5* myeloid-specific knock out or *sgk1* total knockout mice, and differentiated into macrophages. *Nfat5* KO (**B**) or *sgk1* KO (**C**) macrophages were then stimulated as in (**A**). The expression of M(IL-4+IL-13) signature genes was determined qPCR. *p<0.05 vs M(0); #p<0.05 vs M(IL-4+IL-13) none (no additional salt).

In response to this unexpected result, the effect of an additional 40mM NaCl on M(0) and M(IL-4+IL-13) viability was investigated using several independent methods to exclude that the effect of high salt on M(IL-4+IL-13) activation was caused merely by impaired macrophage viability. As before, BMDM were left untreated or activated with or without an additional 40mM NaCl for 24 hours prior to analysis. Cells were then harvested and the exclusion of the cell viability dye propidium iodide was analyzed by flow cytometry. Dead cells were detected in all four groups but importantly no significant difference was evident between M(IL-4+IL-13) and M(IL-4+IL-13)+40mM NaCl; high salt significantly affected the viability of untreated macrophages, however (Figure 25 A). Assessing cell counts by DNA content after activation in the presence or absence of an additional 40mM NaCl confirmed the aforementioned results independently (Figure 25 B). Additionally, manual counting of cells was performed with a haemocytometer (Figure 25 C). As before, no significant effect of high salt on cell numbers was detectable.

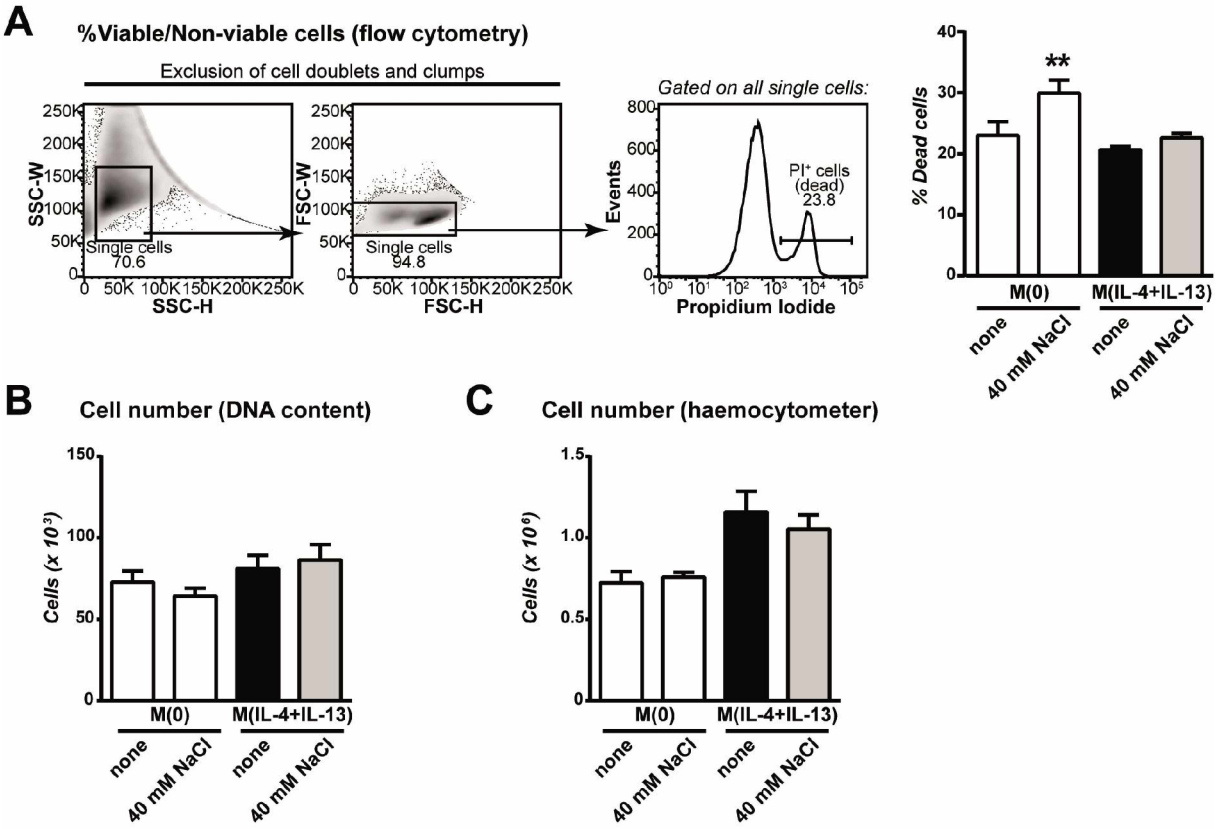

Figure 25. High salt does not decrease M(IL-4+IL-13) cell viability. A: The viability of unstimulated (M(0)) or IL-4+IL-13 stimulated macrophages alone or with an additional 40 mM NaCl was examined by monitoring the exclusion of a viability dye (Propodium Iodide; PI) by flow cytometry. The quantification is shown to the right. **p<0.01 vs M(0) none. **B and C:** The number of cells following incubation for 24 h as in **A** was determined by measuring DNA content (CyQUANT) relative to a standard curve of known cell numbers (**B**), or by manually counting with a haemocytometer (**C**).

In summary, the results demonstrate that the high salt concentrations used throughout this thesis for *in vitro* experiments do not significantly reduce M(IL-4+IL-13) macrophage viability. Of note, others have recently also shown a quick restoration of cellular volume within 30 minutes specifically for macrophages upon a tonicity increase by 200mOsm (Ip and Medzhitov, 2015).

3.1.3. High salt affects M2 macrophage activation *in vivo*

Before setting out to identify possible mechanisms by which high salt affects M(IL-4+IL-13) activation, I next addressed the functional and *in vivo* relevance of the findings presented so far. Reese et al. described an IL-4-dependent and widely used *in vivo* model of M2 macrophage activation by peritoneal injection of homogenized chitin (Byles et al., 2013; Reese et al., 2007; Satoh et al., 2010), a natural polymer found in parasitic

nematodes and nematode egg shells (Perrigoue et al., 2008). Here, the experimental procedure was adapted to investigate whether high salt affects M2 macrophage activation *in vivo*. WT mice were fed a normal salt diet (NSD) or high salt diet (HSD) for 14 days prior to intraperitoneal (I.P.) injection of homogenized chitin. The respective diets were continued for two more days after injection. Peritoneal exudate cells (PECs) were then isolated by lavage (Figure 26). In experiment 1, total PECs were allowed to attach to cell culture plastic for two hours to enrich adherent cells, i.e. macrophages. Elicited macrophages ($CD11b^+F4/80^+$) were not the dominant PEC cell population in the I.P. chitin injection model before adhesion; additionally among $CD11b^-F4/80^-$ cells, peritoneal B ($CD19^+$) and T ($CD3^+$) cells were observed (Figure 27 A). These results are in agreement with observations made by others (Satoh et al., 2010). Adhesion to plastic for two hours followed by extensive washing repeatedly led to a significant enrichment of $CD11b^+F4/80^+$ macrophages and a loss of peritoneal T cells while peritoneal B cells could not be removed (Figure 27 B). Therefore, M2 marker gene expression of PECs was analysed relative to CD68, an approved macrophage marker (Byles et al., 2013) (Figure 12).

In experiment 1, HSD led to a significant reduction of the M2 signature genes *Mrc1* and *Fizz1*. *Arg1* expression was not affected by HSD and *Ym1* showed large variability between individual samples (Figure 28).

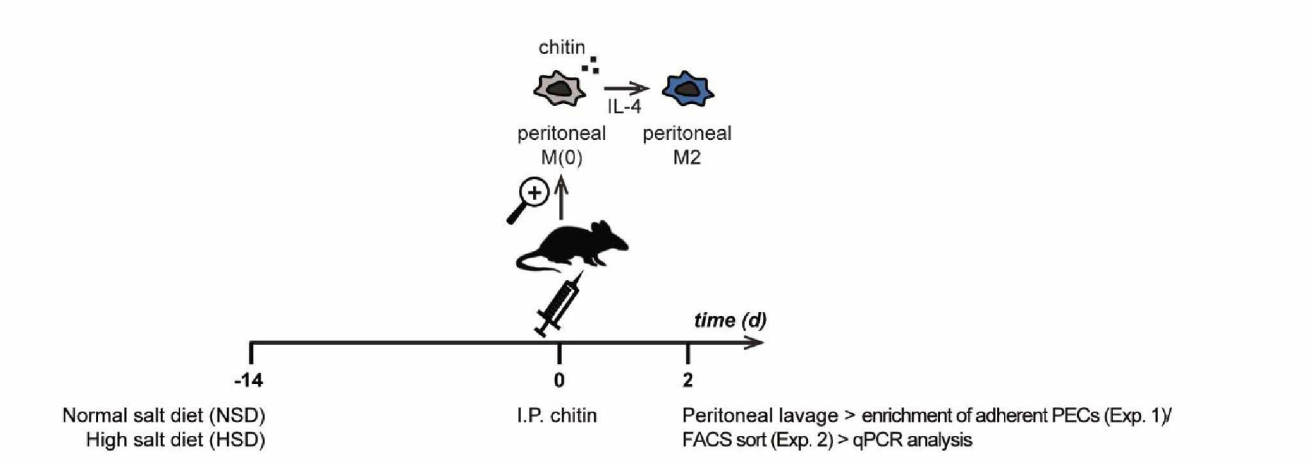

Figure 26. Study design to investigate the effect of high salt on M2 activation *in vivo*. Mice were fed a normal salt diet (NSD) or a high salt diet (HSD) for 14 days, at which point homogenized chitin was injected intraperitoneally (I.P.). After 2 days, peritoneal exudate cells (PECs) were collected by lavage, enriched for adherent cells (macrophages) by attachment to plastic (experiment 1) or the desired immune cell populations were purified by fluorescence-activated cell sorting (FACS) (experiment 2). Gene expression of M2 marker genes was then analysed by qPCR. Exp. 1/2: experiment 1 or 2, respectively.

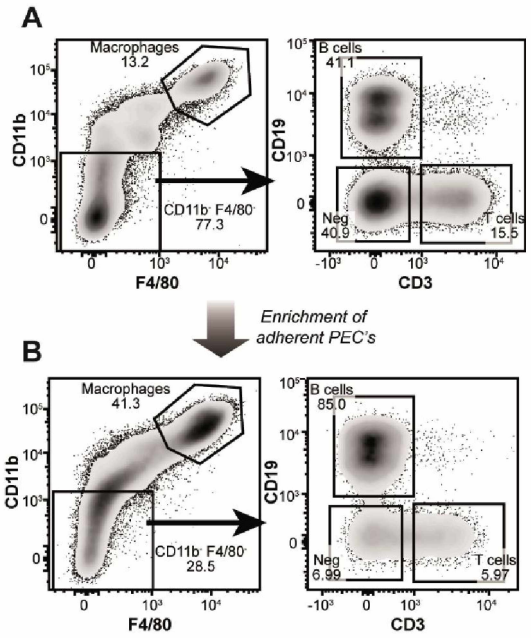

Figure 27. Plastic-adhesion of PECs enriches macrophages. Mice were fed a NSD or HSD for two weeks, at which point chitin was injected intraperitoneally (I.P.). After 2 days, PECs were collected by lavage and left to adhere to tissue culture plates for 2 hours, before extensive washing and isolation of RNA for gene expression analysis by real-time qPCR. The proportion of macrophages ($F4/80^+CD11b^+$), B cells ($F4/80^-CD11b^-CD19^+$), T cells ($F4/80^-CD11b^-CD3^+$) and "Neg" cells (F4/80-CD11b-B220-CD3-) among PECs was analysed by flow cytometry before adhesion (**A**), and after adhesion to tissue culture plates for two hours (**B**). After adhesion, a 3-fold enrichment of macrophages was routinely observed.

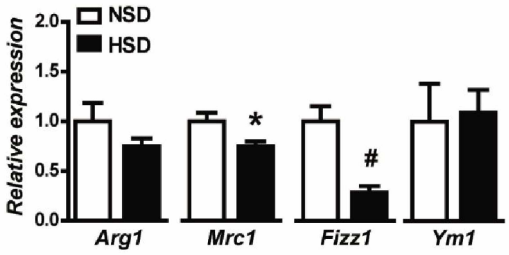

Figure 28. High salt diet reduces M2 macrophage activation *in vivo*. The expression of M(IL-4+IL-13) genes in adhered PECs relative to CD68 as described in (Figure 27) was determined by qPCR. NSD: normal salt diet; HSD: high salt diet. *p<0.05, #p<0.001.

These data were encouraging and suggested an effect of high dietary salt on M2 macrophage activation in an IL-4-dependent model *in vivo*. To corroborate these findings, the I.P. chitin experiment was modified slightly and repeated independently (Figure 26; experiment 2).

First, the effect of dietary salt intake on the percentage and number of macrophages among total PECs after chitin administration was investigated in detail. No significant differences were observed between the two dietary groups (Figure 29).

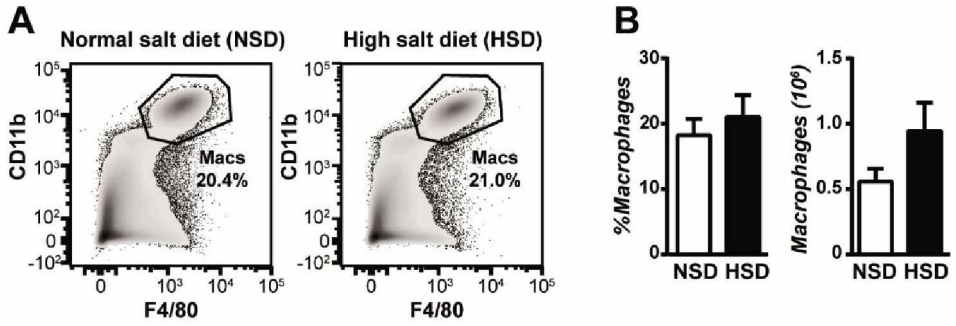

Figure 29. Dietary salt has no effect on the amount of chitin-elicited macrophages. A: Representative flow cytometry plots showing staining for macrophages ($CD11b^+F4/80^+$) of PECs from mice on NSD and HSD two days after chitin injection. **B:** Quantification of the proportion and actual number of macrophages in PECs from (**A**).

Next, to yield a pure peritoneal macrophage preparation free of other contaminating cell types, this time (experiment 2) fluorescence-assisted cell sorting (FACS) was used to purify different PEC populations after lavage. Macrophages ($CD11b^+F4/80^+$), B cells ($CD11b^-F4/80^-B220^+$), T cells ($CD11b^-F4/80^-CD3^+$) and negative cells ($CD11b^-F4/80^-B220^-CD3^-$) could be sorted at a purity of 85%, 91%, 97% and 99%, respectively (Figure 30). RNA was then isolated individually from the four cell populations and used for gene expression analysis of M2 signature genes by qPCR. *Arg1* and *Fizz1* were detected specifically in sorted macrophages while *Mrc1* and *Ym1* were expressed at considerably high levels in 'negative cells' (Figure 31). Interestingly, in our model, *Mrc1* – considered a typical M2 macrophage marker gene – was highly expressed in 'negative cells' and only at much lower levels similarly in both B cells and macrophages; Mrc1 expression was not detected in T cells (Figure 31). Feeding mice a HSD for 14 days prior to chitin injection significantly reduced the expression of *Arg1* and *Fizz1* in experiment 2. *Mrc1* expression was not affected by dietary salt intake in macrophages but significantly lower in negative cells (Figure 31). One may speculate that the contradictory results concerning *Mrc1* expression from experiment 1 might be due to contamination of macrophages with negative cells.

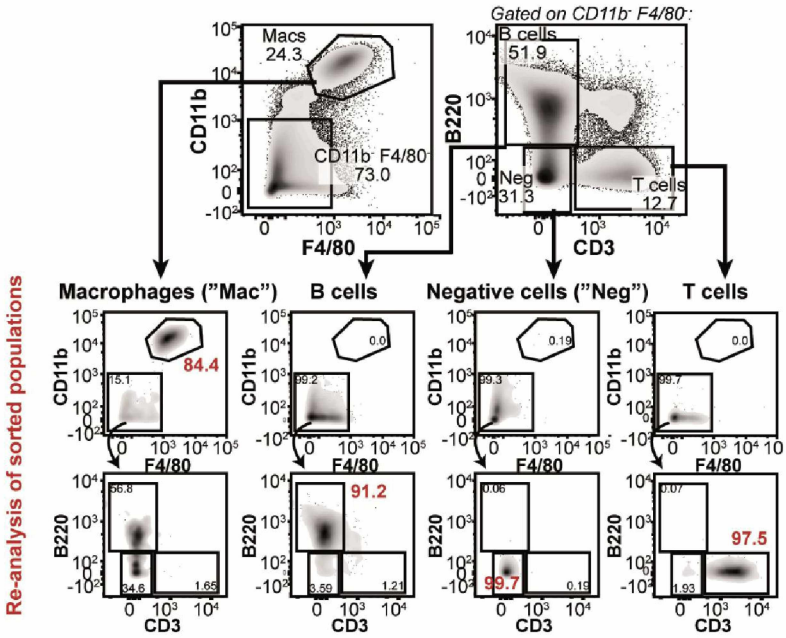

Figure 30. Gating strategy for the isolation of the desired PEC immune populations. Following the gating of macrophages ("Mac"; $CD11b^{+}F4/80^{+}$), cells were then gated on $CD11b^{-}F4/80^{-}$ and subsequently sorted as $B220^{+}$ (B cells), $CD3^{+}$ (T cells) or $B220^{-}CD3^{-}$ (Negative cells; "Neg"). The final purity of each sorted population was re-analysed (red) by flow cytometry and is shown below, where macrophages were >85%, and all other populations were >90%. Figure shows representative flow cytometry plots

In contrast to experiment 1, however, sorting of a pure (>85%) peritoneal macrophage population uncovered a clear trend of lower *Ym1* expression by macrophages under HSD (p=0.07) (Figure 31) which was not detectable in experiment 1. Negative cells showed no trend for decreased *Ym1* expression under high dietary salt loading, which suggests that salt affects different cell populations in a very specific way. In conclusion, the findings from experiment 1 and 2 suggest that high dietary salt intake also affects the activation of M2 macrophages *in vivo.*

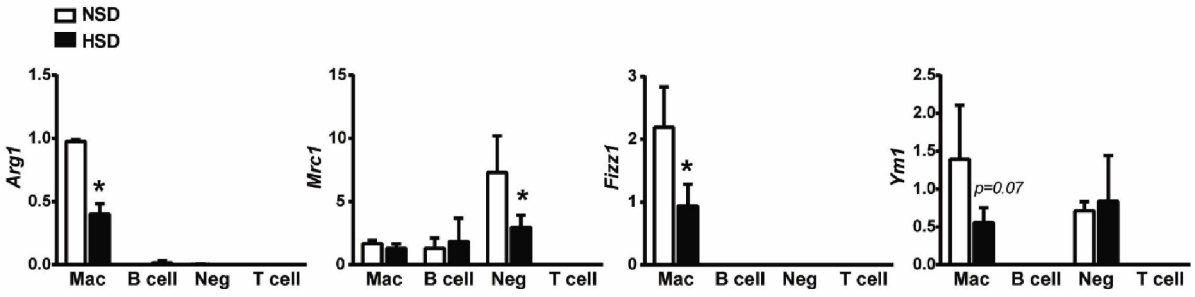

Figure 31. High dietary salt intake blunts M2 macrophage activation in vivo. The expression of M2 signature genes in immune cell populations sorted from PECs as described in (Figure 30) was determined by qPCR. NSD: normal salt diet; HSD: high salt diet. *p<0.05 by 2-way ANOVA.

3.1.4. High dietary salt intake impairs wound healing

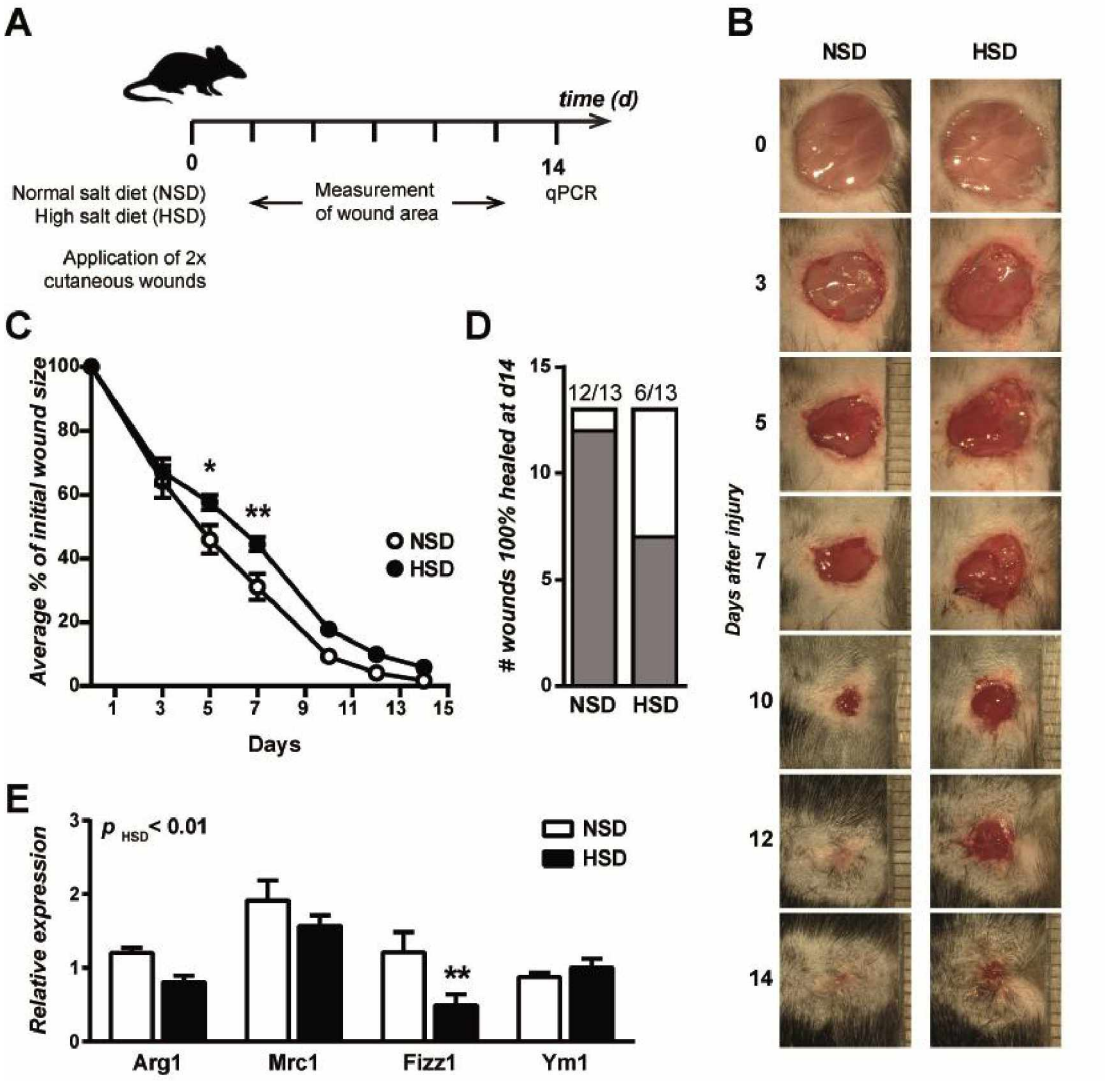

Figure 32. High dietary salt intake causes delayed wound healing. A: Two cutaneous wounds were applied to the back of mice, which were then fed a NSD or HSD for 14 days. The closure of the wounds was monitored at the desired times during a 14 day period, at the end of which skin samples from the wounded area were subjected to qPCR analysis. **B:** Representative images of wounds from mice on a NSD and HSD during 14 days after wounding. **C:** The change in wound area (percent of initial wound area) is plotted over time. The experiment was repeated twice independently, at which point the values from 7 individual mice were pooled (N=13 wounds per group). *p<0.05, **p<0.01 by 2-way ANOVA. **D:** The number of wounds completely (grey) vs. incompletely (white) healed at the end of the experiment (14 days). **E:** Real-time qPCR analysis of M2 signature genes at wound sites from mice on a NSD and HSD. The p value shown for the effect of HSD was calculated by 2-way ANOVA. **p<0.01. N=5 (biological).

Wound healing is a major effector function attributed to M2 macrophages (Mosser and Edwards, 2008). Indeed, genetic ablation of M2 macrophage activation was associated with impaired dermal wound healing (Liao et al., 2011). To test the effect of salt on this process, two cutaneous back wounds were inflicted to WT mice. Mice were then fed NSD and HSD, which did not cause major adverse health effects (Figure 13), and the closure of the wounds was monitored for 14 days (Figure 32 A). There was no difference between the diet groups in the rate of wound healing in the initial phase (0-3 days). During later stages, animals on HSD showed a significant delay in wound healing (3-7 days) (Figure 32 B-C). After 1 week, mice on a NSD exhibited a 69% reduction in wound area, whilst mice fed a HSD showed a delayed wound closure (only 56%). The difference between mice fed a NSD and HSD was not significant during the remaining observation period. However, only 6/13 wounds were completely healed after 14 days on HSD, whilst 12/13 wounds of mice on NSD healed completely during the same period (Figure 32 D). The expression of M(IL-4+IL-13) signature genes in wound samples was also examined by qPCR. RNA samples from wound sites were only available for a single late time point (day 14). Nonetheless, by 2-way ANOVA a significant effect of HSD was observed and *Fizz1* expression was significantly reduced (Figure 32 E).

Collectively, the data presented here suggest that high dietary salt intake delays dermal wound healing *in vivo* to a similar degree as observed in genetic models of impaired M2 activation (Liao et al., 2011), and furthermore reduces the on-site expression of M(IL-4+IL-13) signature genes. However, it is highly plausible that HSD affects many other cell types important for wound healing (e.g. neutrophils, fibroblasts), and so I cannot safely conclude that high salt impairs *in vivo* wound healing exclusively by reducing M2 activation.

3.1.5. High salt reduces the suppressive capacity of M(IL-4+IL-13) *in vitro*

To substantiate that high salt affects the function of M2 macrophages, the ability of M(IL-4+IL-13) macrophages to suppress T cell proliferation *in vitro* was tested. A macrophage/T-cell co-culture suppression assay has been described earlier and showed dose-dependent inhibition of T-cell proliferation by M(IL-4) macrophages (Huber et al., 2010). Briefly, total splenocytes were isolated, labelled with CFSE and incubated with plate-bound anti-CD3 and anti-CD28 for 24 hours to initiate T cell proliferation. BMDM were

simultaneously and separately activated with IL-4+IL-13 in the absence or presence of an additional 40mM NaCl for 24 hours. After this period, activated macrophages were washed extensively to remove interleukins and salt before addition to T cell cultures at different ratios (Figure 33 A). After co-incubation for a further 3.5 days, cell proliferation was assessed by flow cytometry. First, viable cells were identified by exclusion of a live/dead stain. Then, the two major T cell populations were identified by their expression of the surface markers CD4 and CD8. The proliferation of $CD4^+$ cells was then analysed by taking advantage of there being equal CFSE dilution among daughter cells during cell proliferation (Figure 33 B).

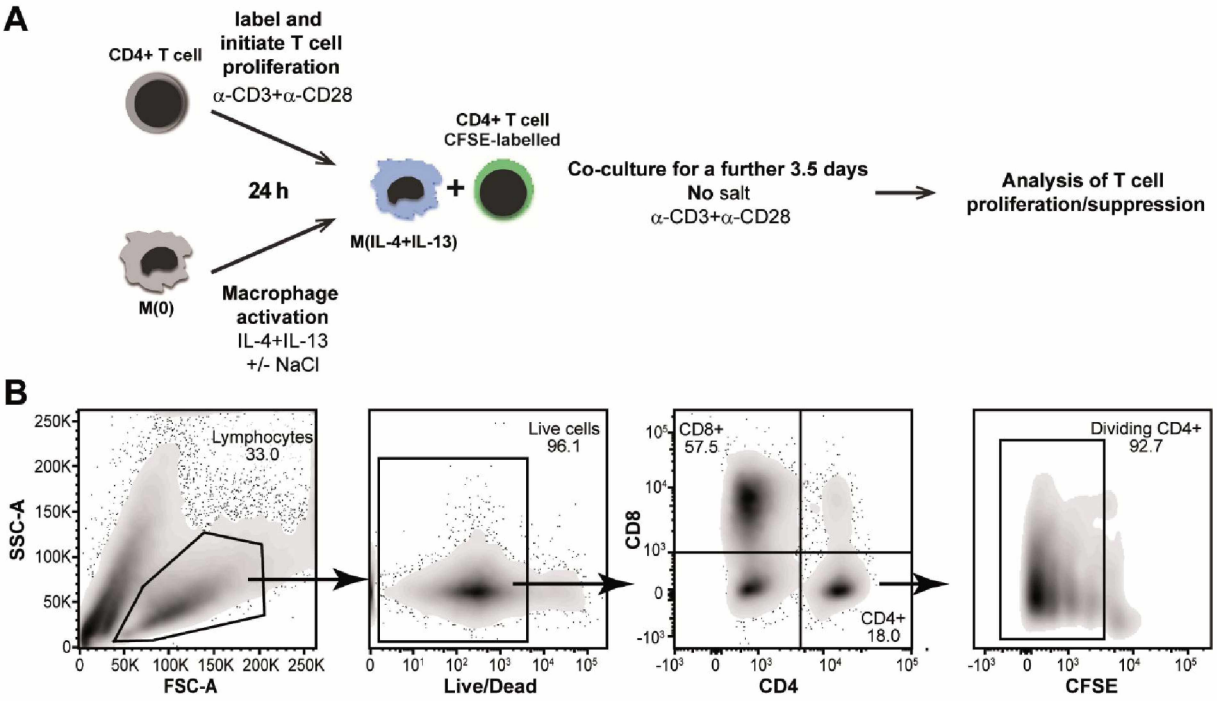

Figure 33. Experimental layout and gating strategy of the *in vitro* co-culture assay. A: Schematic of the in vitro co-culture assay. Briefly, macrophages were activated into M(IL-4+IL-13) with/without an additional 40mM NaCl for 24 hours. Excess salt was then removed by repeated washing of the cells. Co-culture of CFSE-labelled $CD4^+$ T cells (from whole splenocytes) and pre-activated macrophages occurred in the presence of plate-bound α-CD3+α-CD28, but without any additional salt. $CD4^+$ T cell proliferation was monitored by flow cytometry. **B:** Representative flow cytometry plots of the gating strategy for the analysis of $CD4^+$ T cell proliferation are shown.

At a macrophage:T cell ratio of 1:6, M(0) macrophages did not affect $CD4^+$ T cell proliferation compared to no-macrophage controls (not shown) while M(IL-4+IL-13) macrophages showed a strong capacity to suppress $CD4^+$ T cell proliferation; of note, M(IL-4+IL-13) macrophages activated in the presence of an additional 40mM NaCl had a

markedly reduced ability to suppress CD4+ T cell proliferation (Figure 34 A). The suppression of CD4+ T cell proliferation by M(IL-4+IL-13) macrophages was dose-dependent and high salt impaired this important function significantly over a range of macrophage:T cell ratios (Figure 34 B). A similar suppressive function of M(IL-4+IL-13) macrophages on CD8+ T cells was obvious in my experiments (not shown) and described earlier (Huber et al., 2010). However, the effect of pre-activation of M(IL-4+IL-13) macrophages with high salt on CD8+ T cell suppression was not conclusive.

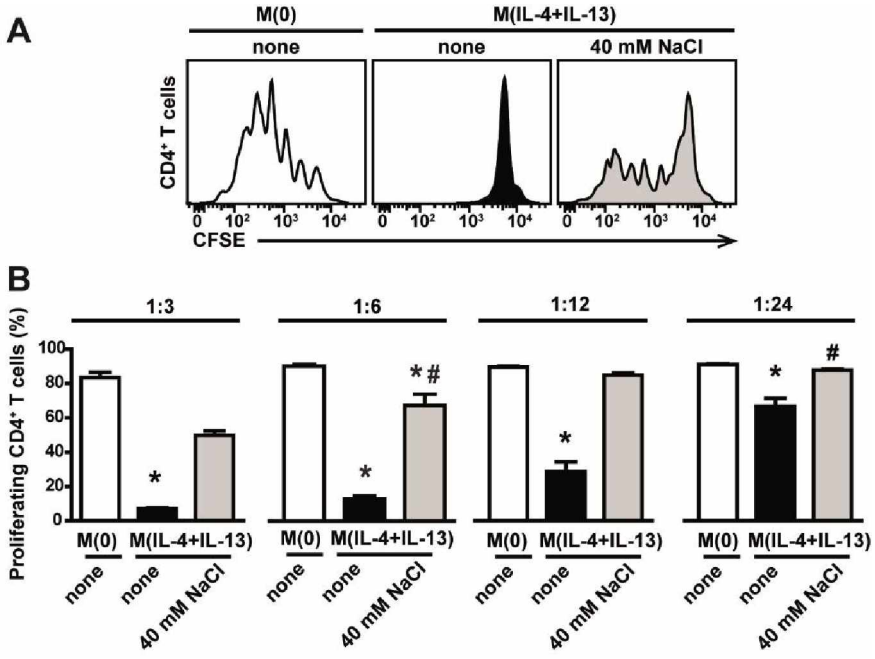

Figure 34. High salt reduces the suppressive capacity of M(IL-4+IL-13) macrophages. A: CFSE fluorescence histograms of gated CD4+ T cells incubated with macrophages at a ratio of 1:6 (macrophage:T cell). Macrophages were un-activated (M(0)) or activated with IL-4+IL-13 in the absence (none) or with high salt. **B:** Quantification of (**A**). Bars show the mean % of proliferating CD4+ T cells at macrophage:T cell ratios of 1:3, 1:6, 1:12, 1:24. *p<0.05 vs M(0); #p<0.05 vs M(IL-4+IL-13) none.

Programmed death 1 ligand 2 (PD-L2) is a cell surface molecule that inhibits CD4+T cell proliferation (Latchman et al., 2001) and constitutes a major effector molecule to mediate cell contact-dependent suppression of T cell proliferation by M2 macrophages (Huber et al., 2010). I hypothesized that high salt impairs the suppressive capacity of M(IL-4+IL-13) macrophages by affecting PD-L2 expression. Indeed, high salt repeatedly reduced PD-L2 gene expression levels (Figure 35 A). By flow cytometry, PD-L2 surface expression was induced upon activation of macrophages with IL-4+IL-13, with high salt reducing this induction (Figure 35 B). Combined, these results suggest that the blunted expression of a

major M2 T cell-suppressive effector molecule is a possible mechanism by which high salt impairs M2 function *in vitro*. Taken together, the aberrant M(IL-4+IL-13) activation with high salt observed *in vitro* translated to altered *in vitro* function and an effect of high salt on M2 macrophages was also apparent when investigating respective *in vivo* models.

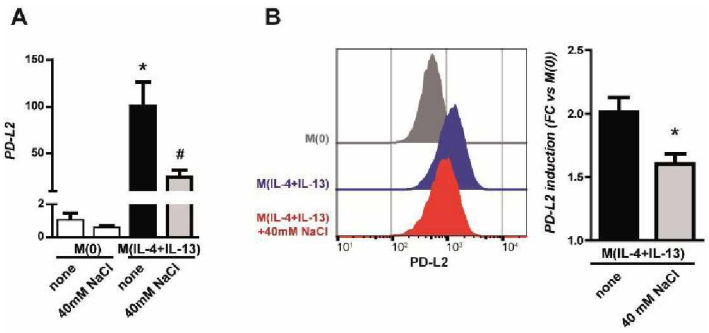

Figure 35. High salt blunts the gene and protein expression of PD-L2. Macrophages were unactivated (M(0)) or activated with IL-4+IL-13 in the absence (none) or with high salt. **A:** PD-L2 expression was then determined by qPCR for gene expression levels. *p<0.05 vs M(0); #p<0.05 vs M(IL-4+IL13). **B:** Surface PD-L2 protein was measured by flow cytometry and representative fluorescence histograms are shown. The bar graph shows the quantification of fold change (vs M(0)) of geometric mean PD-L2 fluorescence intensity. *p<0.05 vs M(IL-4+IL-13).

3.2. The effect of high salt on M(IL-4+IL-13) macrophages: genome wide analysis

In the previous chapters, I have shown that high salt has a significant effect on M(IL-4+IL13) macrophage activation and function *in vitro* and *in vivo*. This effect seems to be independent of initial STAT6 phosphorylation and is not *via* osmo-stress-related signalling cascades (Nfat5, Sgk1), that were essential to mediate the effect of high salt on pro-inflammatory macrophages and T cells as previously shown (Jantsch et al., 2015; Kleinewietfeld et al., 2013). During M2 activation, epigenetic modifications of the Irf4 locus are essential to induce *Irf4* expression and subsequently a full M2 phenotype (Ishii et al., 2009; Satoh et al., 2010). As the expression of *Irf4* and a second essential M2 TF (*Klf4*) was significantly blunted by high salt (Figure 19 C), I hypothesized that aberrant M(IL-4+IL-13) activation may be *via* altered histone modifications. To test this hypothesis and to unveil additional mechanisms, I used genome-wide approaches to characterize M(IL-4+IL-13) macrophage activation and the effect of high salt. To this end, BMDM were stimulated as before with IL-4+IL-13 in the absence or presence of an additional 40mM NaCl for 24 hours

and used to generate a set of genomic gene expression and H3K4me3/H4ac histone modification data by microarray and ChIP-seq, respectively.

3.2.1. *In vitro* activation of M(IL-4+IL-13) macrophages

Before addressing the effect of high salt, I first characterized the genome-wide changes that occurred upon *in vitro* activation of M(IL-4+IL-13). Three M(IL-4+IL-13) gene sets were generated: a set of genes in which the expression was changed upon activation and similarly a set of genes with differential H3K4me3 and H4ac. Analysing all three gene sets together, a total of 3560 genes were differential (induced or reduced; FDR<0.05) upon stimulation of BMDM with IL-4+IL-13 in normal, isotonic media. More specifically, 2604, 1763 and 494 genes were identified to have differential expression, H3K4me3 and H4ac, respectively (Figure 36). The overlap between the three differential gene sets at 24 hours was surprisingly low; 213 genes showed significant changes in all three variables while 1644 genes were differential for expression without significant changes in histone marks. How gene expression changes contribute to M(IL-4+IL-13) activation and function can be intuitively interpreted. The meaning of significant histone mark changes without concordant expression changes, however, is less intelligible. For ease, all further gene analyses were therefore based on first identifying if there were changes in gene expression, followed by integration of the ChIP-seq data.

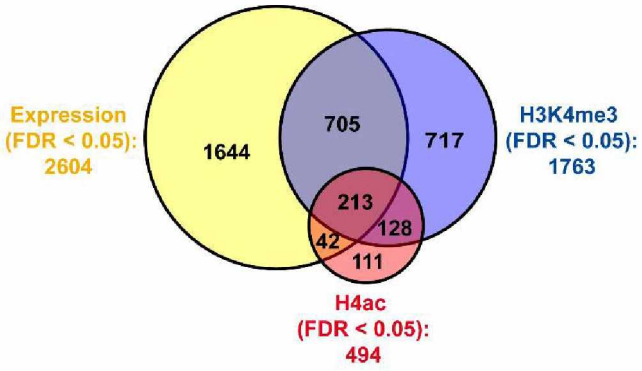

Figure 36. A *de novo* M(IL-4+IL-13) gene set defined by expression, H3K4me3 and H4ac. Differential genes (FDR<0.05) upon M(IL-4+IL-13) activation of BMDM for 24 hours in isotonic media were determined for gene expression, H3K4me3 and H4ac. In total, a set of 3560 M(IL-4+IL-13) genes were identified. The overlap between the three individual gene sets (expression: 2604 genes, yellow; H3K4me3: 1763 genes, blue; H4ac: 494 genes, red) is shown as Venn diagram.

Upon M(IL-4+IL-13) activation, of the 2604 genes with differential expression, 807 (expression; FDR<0.05) were increased more than 1.3-fold and 799 genes showed a reduced expression (FC>1.3) compared to unstimulated M(0) macrophages (Figure 37 A). The top 50 (by expression FC) induced and reduced genes are shown in Table 3 and Table 4 (see appendix 5.1), respectively. To characterize pathways and/or cellular functions affected by M(IL-4+IL13) activation, gene ontology (GO) term analysis of the 807 upregulated or the 799 downregulated (FC>1.3) expression genes was performed. This analysis yielded a plethora of significant (FDR<0.05) GO biological process terms for genes with both upregulated (FC>1.3) (Figure 37 B) and downregulated (FC>1.3) expression (Figure 37 C) genes. For upregulated M(IL-4+IL-13) genes, terms related to the immune response and cellular metabolism, specifically *metabolic process*, *mitochondrion organization*, *cellular respiration* and *cellular lipid metabolic process*, were significantly enriched (Figure 37 B; red terms). Of note, oxidative breakdown of fatty acids is a characterizing feature of M(IL-4+IL-13) activation. Additional GO terms corroborating the cellular metabolism associated with M(IL-4+IL-13) activation in the present data set are shown Table 1. For the 799 down-regulated genes, GO terms (FDR<0.05) related to cell death and nitric oxide metabolism were identified. The latter is in line with the reduced ability of M(IL-4+IL-13) activated cells to produce NO compared to pro-inflammatory murine macrophages.

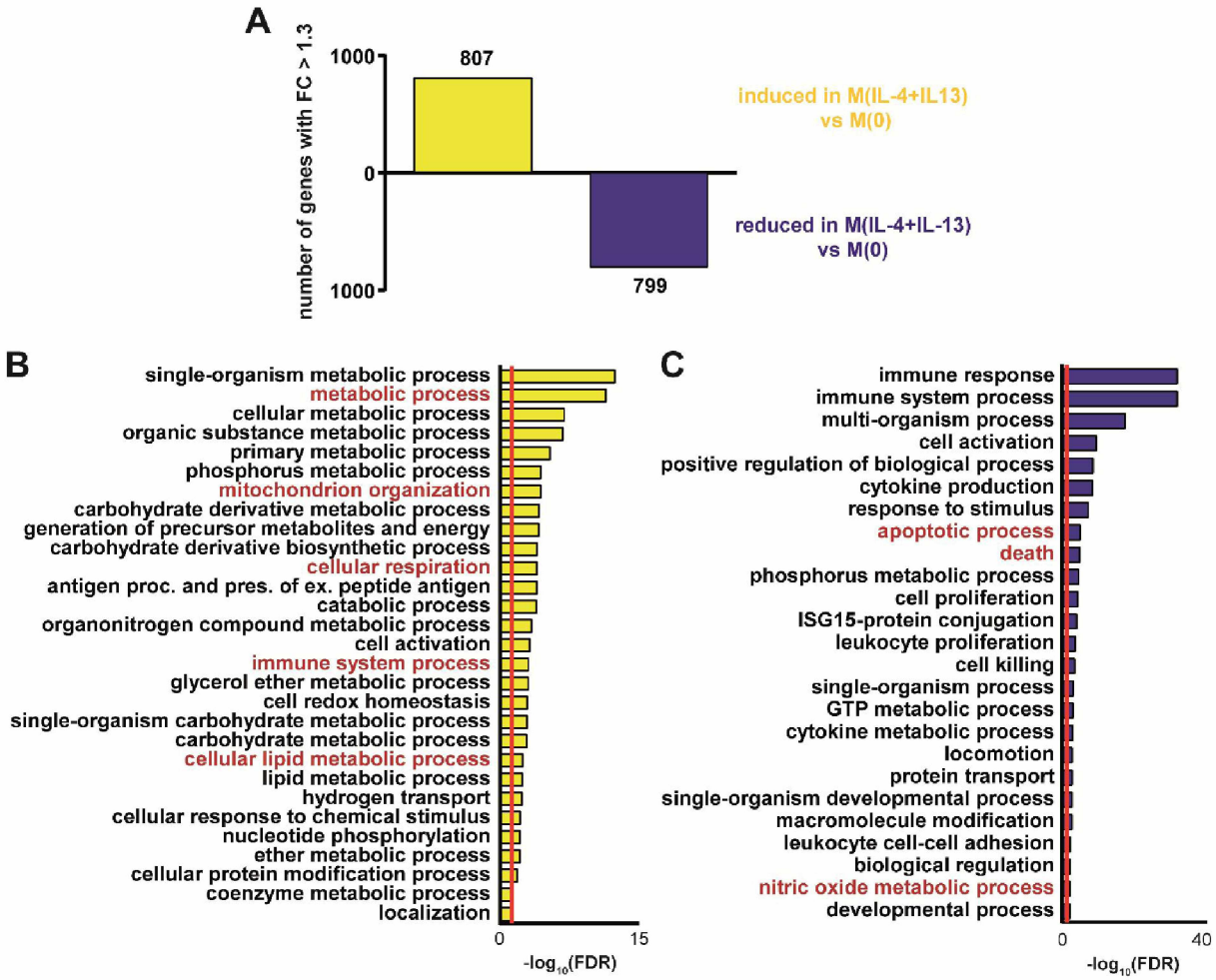

Figure 37. Global gene expression analysis of *in vitro* M(IL-4+IL-13) activation. BMDM were activated with IL-4+IL-13 for 24 hours or unstimulated (M(0)). **A:** Global gene expression changes were determined by microarray. The bars represent the number of induced (yellow) and reduced (blue) M(IL-4+IL-13) genes (FDR<0.05) with a fold change (FC)>1.3. **B+C:** Gene ontology (GO) term analysis of induced (**B**) and reduced (**C**) M(IL-4+IL-13) genes from (**A**) was performed to identify pathways and/or cellular programs induced (**B**) or reduced (**C**) upon M(IL-4+IL-13) activation. Significant (FDR<0.05) GO terms were summarized using REVIGO (Supek et al., 2011); all terms with a dispensability<0.2 are shown. Red lines in (**B+C**) indicate FDR cut off of 0.05.

Table 1. Additional (FDR<0.05) GO terms for all 807 M(IL-4+IL-13)-induced genes.

GO term ID	Description	$-\log_{10}$ (FDR)
GO:0015980	energy derivation by oxidation of organic compounds	3.5612
GO:0006635	fatty acid beta-oxidation	1.424
GO:0006631	fatty acid metabolic process	2.3647
GO:0006119	oxidative phosphorylation	2.4377
GO:0022904	respiratory electron transport chain	1.3067
GO:0006099	tricarboxylic acid cycle	2.0599

For simplification, all further analysis was focused on the 807 genes identified to have increased (FC>1.3) expression upon activation to M(IL-4+IL-13). This set of genes will be hereafter referred to as "M(IL-4+IL-13) signature genes". In agreement with the literature and my own data, typical M2 signature genes such as *Arg1*, Fizz1 (*Retnla*), Ym1 (*Chi3l3*), PD-L2 (*Pdcd1lg2*), *Irf4*, *Ccl24* and *Ccl17* were among the top 50 induced M(IL-4+IL-13) signature genes (Table 3; 5.1). *Mrc1* was induced 2-fold upon activation (not shown). Interestingly, *Socs2* was also one of the top 50 induced genes; this may indicate the activation of negative feedback signalling upon continuous IL-4+IL-13 stimulation (Alexander and Hilton, 2004).

Of these typical M2 genes, I next examined if there were concordant changes in H3K4me3 and H4ac modifications upon stimulation. ChIP-seq analysis revealed a strong association between the abundance of activating histone modifications (Figure 38 A) and increased gene expression levels (Figure 38 B) for *Arg1*, *Ccl24*, *PD-L2*, *Fizz1* and *Socs2*. For *Ym1*, H4ac levels were also clearly increased upon stimulation. For H3K4me3, *Ym1* showed a considerable FC increase (18-fold) but the actual counts were extremely low at this locus compared to the other genes mentioned above.

I next examined the two chromatin modifications on a global level for the 807 M(IL-4+IL-13) signature genes. Here, the association between gene expression and activating H3K4me3 and H4ac histone modifications was considerably weak. Interestingly, 245/273 genes showed even (slightly) decreased levels of H3K4me3/H4ac, while at the same time their gene expression was increased at least 1.3-fold (Figure 39 A). The majority of genes, i.e. 562 and 534 for H3K4me3 and H4ac, respectively, showed concordant changes of gene expression and activating histone modifications. The correlation between expression changes and H3K4me3 changes (Spearman r= 0.41) or expression changes and H4ac changes (Spearman r=0.32) upon M(IL-4+IL-13) activation was – even though statistically highly significant (both $p<0.0001$) – therefore very low (Mukaka, 2012).

This may be partly due to the fact that – globally – histone marks changed much more moderately upon M(IL-4+IL-13) activation than did gene expression. When plotting the frequency of observed gene expression, H3K4me3 and H4ac changes (M(IL-4+IL-13) vs M(0) upon activation) as density distributions, gene expression showed a clear right shift (Figure 39 B). Thus, the magnitude of changes is much higher for gene expression than for histone marks for most of the M(IL-4+IL-13) signature genes.

Comparison of the two histone marks with each other also revealed only a low positive correlation (Spearman r=0.41; p<0.0001) (Figure 39 C).

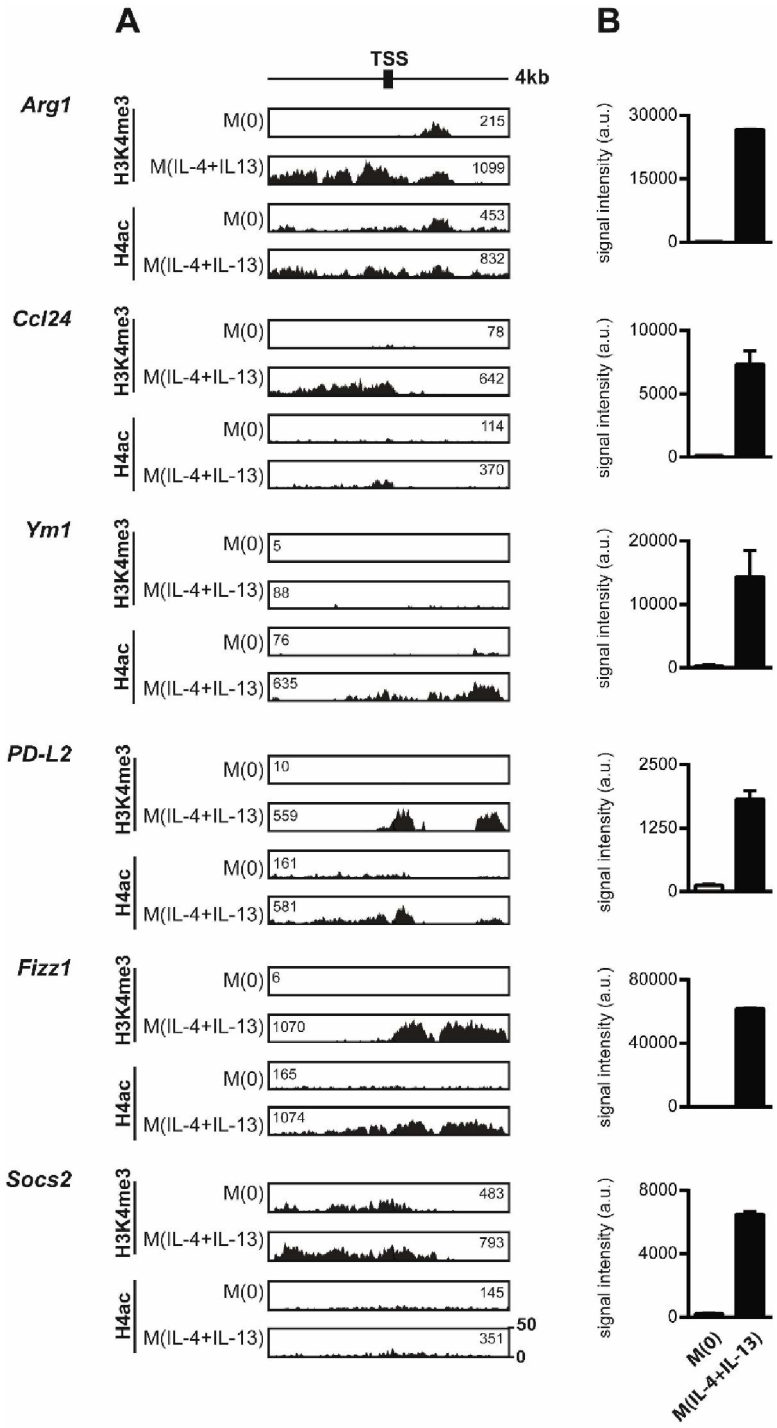

Figure 38. H3K4me3 and H4ac histone modification of M(IL-4+IL-13) signature genes. BMDM were activated as before. **A:** ChIP-seq signature tracks of H3K4me3 and H4ac histone marks are shown spanning 2kb upstream and downstream around the annotated transcription start site (TSS) of the respective gene. Mean counts are indicated for each track. **B:** Bar graphs show gene expression levels for M(0) and M(IL-4+IL-13) cells as determined by microarray.

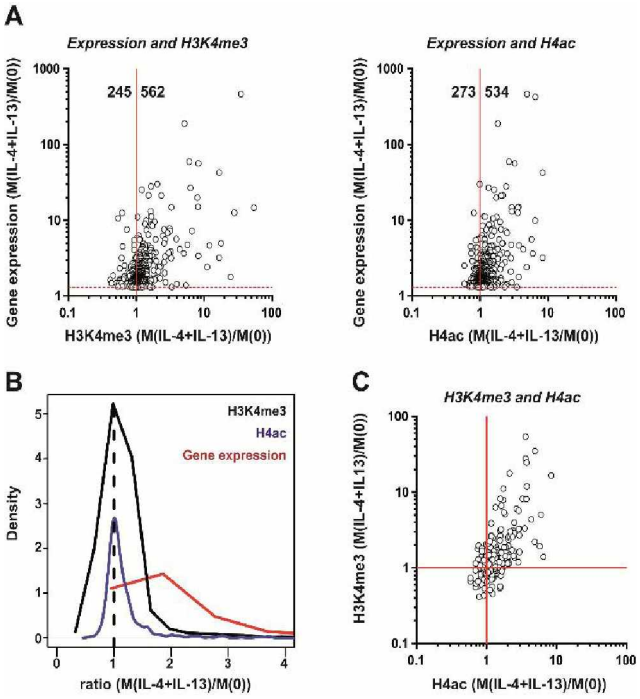

Figure 39. Correlation of expression and histone marks upon M(IL-4+IL-13) activation. A: Gene expression changes (expressed as M(IL-4+IL-13)/M(0) ratio) upon M(IL-3+IL-13) activation are plotted against the corresponding changes in H3K4me3 (left panel) or H4ac (right panel) for each of the 807 induced M(IL-4+IL-13) signature genes. Histone modification counts used to calculate M(IL-4+IL-13)/M(0) ratios span 2kb upstream and downstream of the annotated transcription start site. The dotted red line indicates the expression fold change cut off (1.3). Spearman r=0.41 (left panel) and 0.32 (right panel); p<0.0001 (both). **B:** Distribution of gene expression (red), H3K4me3 (black) and H4ac (blue) changes (expressed as M(IL-4+IL-13)/M(0) ratio) upon M(IL-4+IL-13) activation are plotted as density. Dashed black line: [x=1]. 92% of all 807 induced M(IL-4+IL-13) signature genes are covered by an X-axis FC limit of 4. **C:** H3K4me3 changes (expressed as M(IL-4+IL-13)/M(0) ratio) upon M(IL-4+IL-13) activation plotted against the corresponding H4ac changes for all 807 induced M(IL-4+IL-13) signature genes. Spearman r = 0.41; p<0.0001.

3.2.2. Adding salt to the genome-wide analysis of M(IL-4+IL-13) activation

The previous section summarizes my identification of a set of genes with differentially induced expression upon activation from M(0) to M(IL-4+IL-13). My next aim was to analyse the effect of high salt on this gene set. To this end, I compared the expression levels of M(IL-4+IL-13) signature genes in the absence and presence of an additional 40mM NaCl using microarray data. For all 807 M(IL-4+IL-13) signature genes, ratios were calculated for M(IL-4+IL-13)+40mM NaCl vs M(IL-4+IL-13) microarray signal intensities and the top 50 (by M(IL-4+IL-13) vs M(IL-4+IL-13) expression FC) salt-sensitive M(IL-4+IL-13) signature genes are presented in Table 5 and Table 6 (see appendix 5.1) for

further increased or decreased genes, respectively. The global effect of high salt on all 807 M(IL-4+IL-13) signature genes is presented in Figure 40 A by plotting microarray signal intensities detected after M(IL-4+IL-13) activation for 24 hours with or without salt. The most salt-sensitive and the previously described M(IL-4+IL-13) marker genes *Arg1*, *Fizz1*, *Mrc1* and *Ym1* are highlighted. Gene expression levels for highlighted genes are shown in Figure 40 B. Here, using the microarray data, the blunting effect of high salt on the expression of *Arg1*, *Fizz1* and *Mrc1* as determined by qPCR earlier was not detectable, while *Ym1*, *Mgl2* and *Slamf1* showed a trend to have blunted expression with high salt. Unsurprisingly, a gene mediating the uptake of compatible osmolytes (*Slc6a12*) was the most upregulated with activation in high salt. Stearoyl CoA desaturase 1 (*Scd1*) – a second highly increased salt-sensitive gene – is the rate-limiting enzyme in the synthesis of monounsaturated fatty acids (Nakaya et al., 2013). It has also been connected to inflammation and cellular stress in macrophages (Liu et al., 2011).

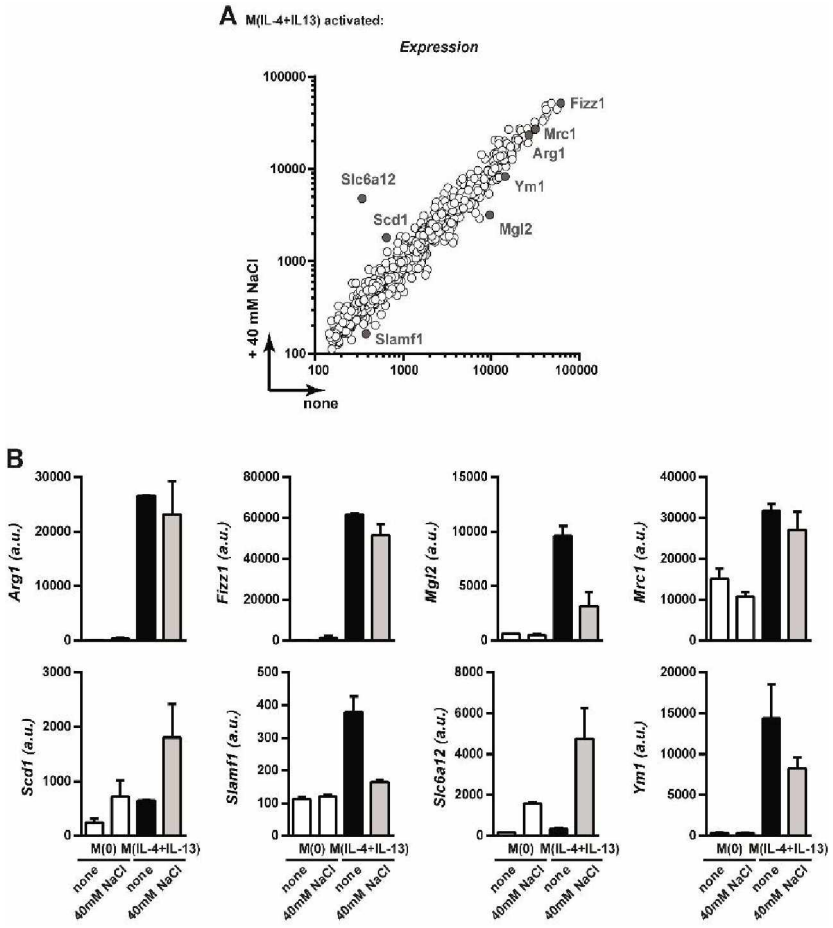

Figure 40. The effect of high salt on the expression of M(IL-4+IL-13) signature genes. BMDM were activated with IL-4+IL-13 (M(IL-4+IL-13)) in the absence (none) or presence of an additional 40mM NaCl for 24

hours. Unstimulated macrophages (M(0)) were treated similarly. **A:** The effect of high salt on M(IL-4+IL13) signature gene expression as determined by microarray is shown. Highly salt-sensitive genes are indicated (grey dots with gene names). **B:** Bar graphs show the expression level of genes highlighted in (**A**) as determined by microarray.

The trend for salt having a strong blunting effect on the expression of the two M(IL-4+IL-13) signature genes *Mgl2* and *Slamf1* (Figure 40 B) was independently confirmed by qPCR analysis of *in vitro* activated BMDM (Figure 41 A). Of note, the blunted expression of both *Mgl2* and *Slamf1* was independent of tonicity (Figure 41 B) and signaling molecules mediating the salt effect on pro-inflammatory T cells and M(LPS) macrophages (Figure 41 C) as described earlier for other M(IL-4+IL-13) marker genes. *Slamf1* is particularly interesting as its expression level was reduced by high salt in M(IL-4+IL-13) macrophages while high salt at the same time boosted *Slamf1* expression in M(LPS) activated macrophages (not shown). Additionally, *Ccl24* and *Ccl17* – two typical M2 chemotactic molecules (Murray et al., 2014) – and PD-L2 (*Pdcd1lg2*) were among the top 50 salt-reduced M(IL-4+IL-13) signature genes (Table 6, see 5.1; for PD-L2 see also Figure 35); Ccl24 induces eosinophilia, a typical functional feature of M2 macrophages (White et al., 1997) while PD-L2 – as described earlier – is a major M2 surface effector molecule to restrict T cell proliferation (Huber et al., 2010).

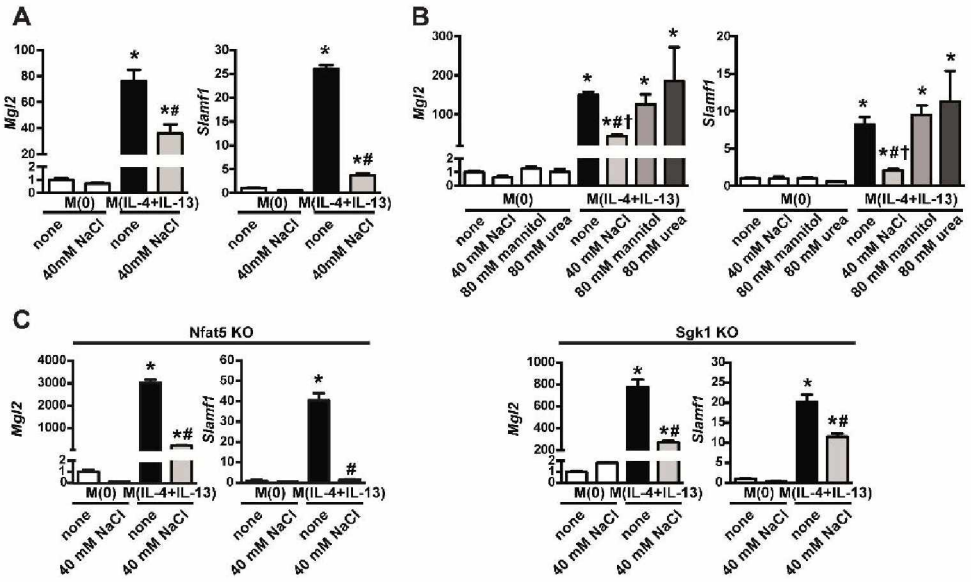

Figure 41. High salt blunts the expression of additional M(IL-4+IL-13) signature genes. BMDM were activated with IL-4+IL-13 (M(IL-4+IL-13) in the absence (none) or presence of an additional 40mM NaCl for 24 hours. Unstimulated macrophages (M(0)) were treated similarly. **A:** Gene expression was determined by qPCR. *p<0.05 vs M(0); #p<0.05 vs M(IL-4+IL-13) none. **B:** BMDM were activated as in (**A**) or in the presence of an additional 80mM urea or mannitol as tonicity controls before analysing gene expression by qPCR. *p<0.05 vs M(0); #p<0.05 vs M(IL-4+IL-13) none and M(IL4+IL-13)+mannitol; †p<0.05 vs M(IL-4+IL-13)+urea. **C:** BMDM

were generated from the bone marrow of *Nfat5* myeloid-specific knockout mice (left panel) or *Sgk1* total knockout mice (right panel), and activated as in (A). The expression of M(IL-4+IL-13) signature genes was determined by qPCR. *p<0.05 vs M(0); #p<0.05 vs M(IL-4+IL-13) none.

The effect of high salt on the histone modification levels of all 807 M(IL-4+IL-13) signature genes was also analyzed. The global effect on H3K4me3 and H4ac is presented in Figure 42 and Figure 43, respectively. Genes with high salt sensitivity in the previous gene expression analysis and the M(IL-4+IL-13) marker genes *Arg1*, *Fizz1*, *Mrc1* and *Ym1* are also indicated. According to the weak salt effect on *Arg1*, *Fizz1* and *Mrc1* expression (Figure 40), H3K4me3 levels around their respective transcription start sites were marginally affected by salt; only *Fizz1* showed a mild reduction (Figure 42 B). As mentioned before, H3K4me3 levels were generally very low for *Ym1* and also not affected by salt. The remaining salt-sensitive genes showed clear (*Slamf1*, *Slc6a12*) or mild (*Mgl2*, *Scd1*) concordant changes for H3K4me3 modification and gene expression levels. For H4ac, *Scd1*, *Slamf1*, *Slc6a12* and *Ym1* showed a mild salt effect that mirrored microarray gene expression changes of M(IL-4+IL-13) activated macrophages in the absence or presence of an additional 40mM NaCl. For *Arg1*, *Fizz1*, *Mgl2* and *Mrc1*, H4ac levels were unchanged or even slightly increased (Figure 43 B). Collectively, the data presented here do not justify – as initially hypothesized – to conclude that high salt was affecting M(IL-4+IL-13) activation and function via H3K4me3 or H4ac histone modifications as a general mechanism.

As no significant changes in chromatin modifications were identified, a more detailed analysis of salt-induced changes in the transcriptional program was performed, with the aim to eventually identify disturbances in pathways or individual genes which may account for the salt-blunted activation observed before. Of all 807 M(IL-4+IL-13) signature genes, the expression of 136 genes was further increased (FC>1.2) while the expression of 166 genes was decreased (FC>1.2) by salt (Figure 44 A). GO term analysis was performed using these 302 salt-sensitive M(IL-4+IL-13) signature genes as input. Results (FDR<0.1) were summarized using REVIGO as before and are presented in Figure 44 B.

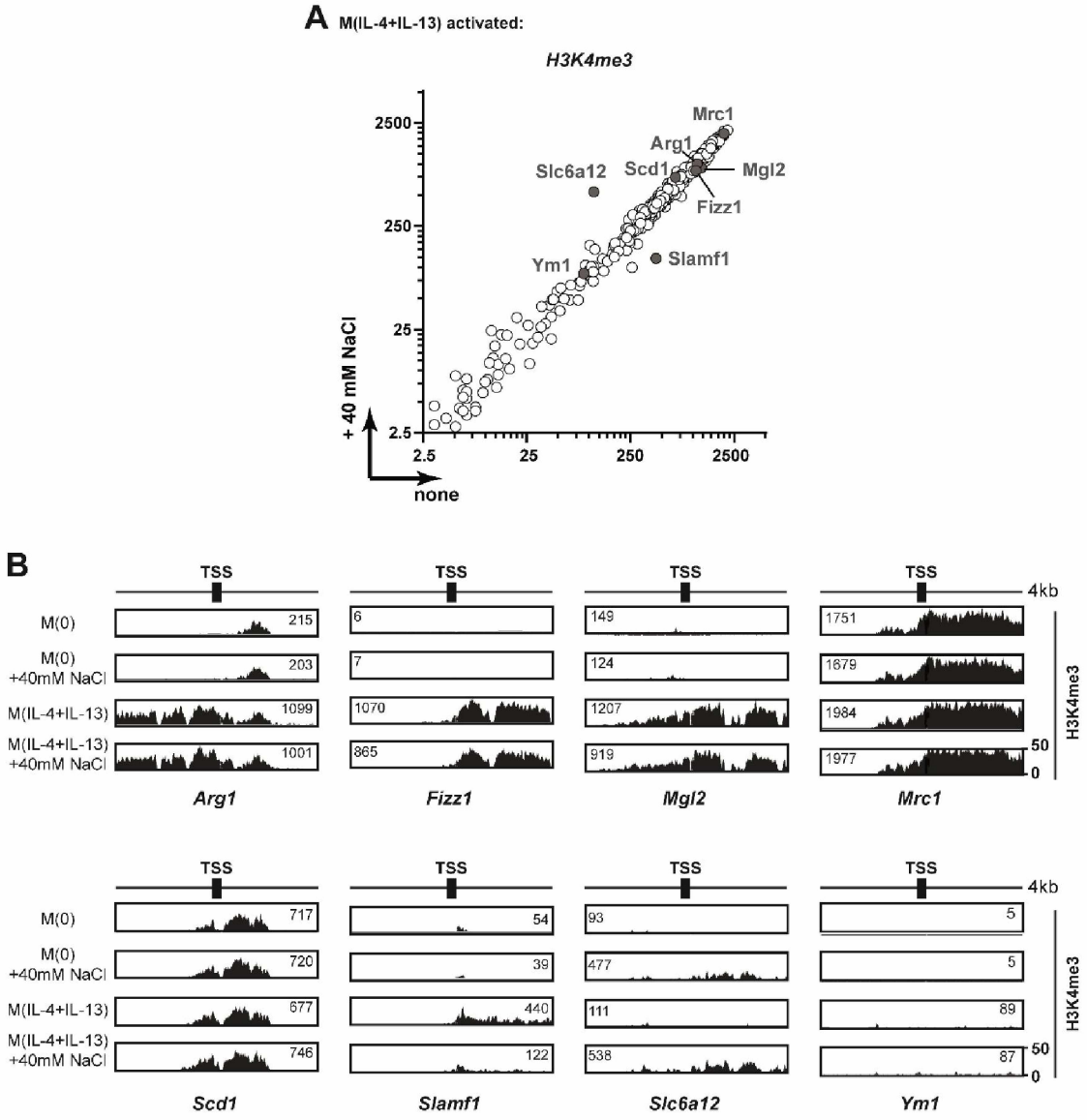

Figure 42. The effect of high salt on H3K4me3 levels of M(IL-4+IL-13) signature genes. BMDM were activated as before. Histone modification levels were determined by ChIP-seq spanning 4kb around the annotated transcription start site (TSS) **A:** The effect of high salt on H3K4me3 levels of all 807 M(IL-4+IL-13) signature genes is shown. Individual genes from Figure 40 are indicated (grey). **B:** Representative H3K4me3 signature tracks for highlighted genes from (**A**) are shown. Mean counts are indicated for each track.

Many terms related to immune cell activation and proliferation as well as *response to wounding* were identified as being affected upon activation in the presence of high salt (Figure 44 B) (note that *T cell proliferation* was also identified (FDR<0.05) (not shown)). Changes in these terms therefore supports the functional results presented earlier (sections 3.1.4; 3.1.5).

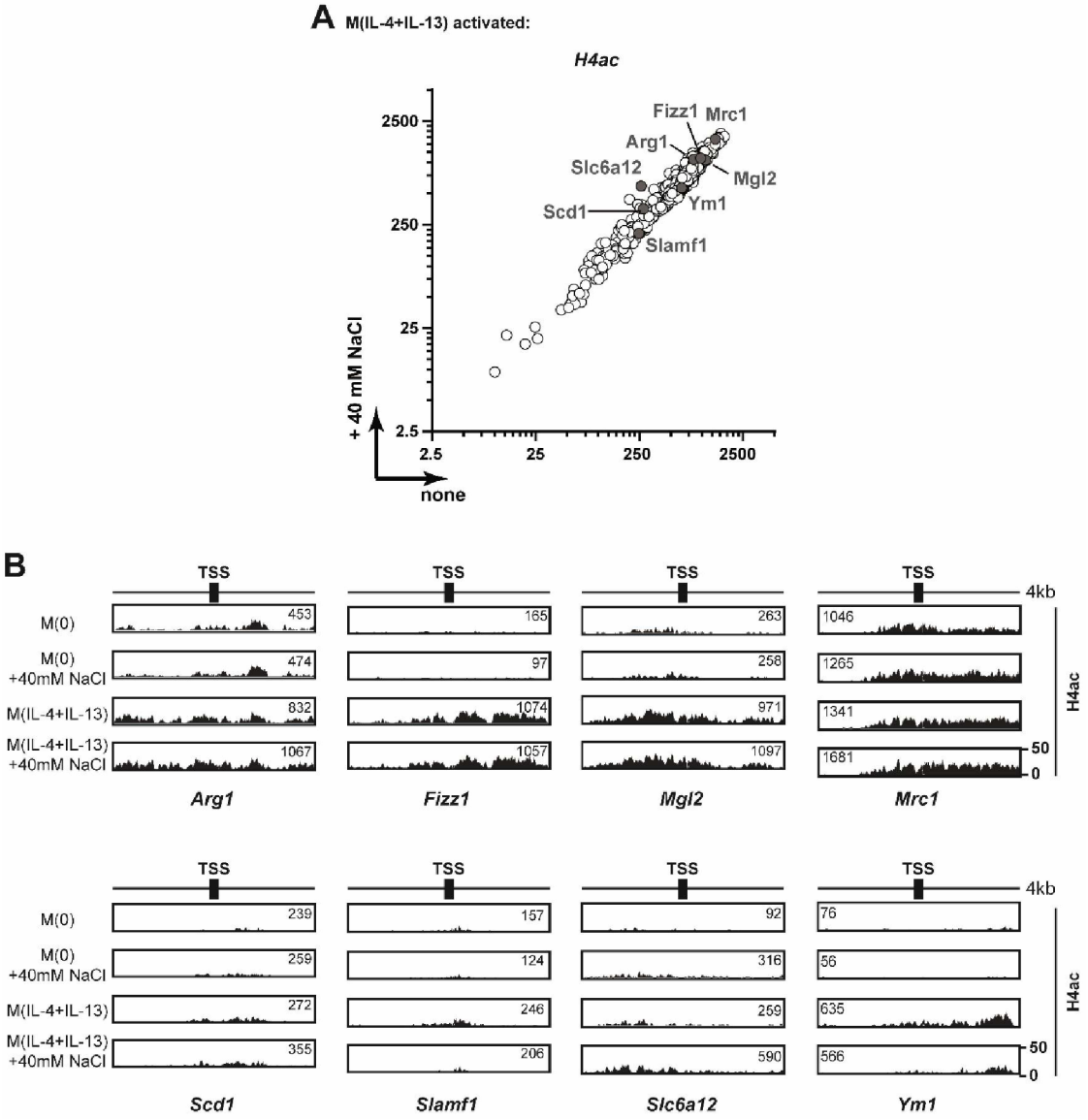

Figure 43. The effect of high salt on H4mac levels of M(IL-4+IL-13) signature genes. BMDM were activated as before. Histone modification levels were determined by ChIP-seq spanning 4kb around the annotated transcription start site (TSS) **A:** The effect of high salt on H4ac levels of all 807 M(IL-4+IL-13) signature genes is shown. Individual genes from Figure 40 are indicated (grey). **B:** Representative H3K4me3 signature tracks for highlighted genes from (**A**) are shown. Mean counts are indicated for each track.

Additionally, several terms related to cellular metabolism were identified (*metabolic process*, *single-organism metabolic* and *negative regulation of mitochondrion organization*). Adaption of cellular metabolism is a hallmark of immune cell activation (Pearce and Pearce, 2013; Tan et al., 2015). Many cells substantially re-wire their metabolic programs upon activation and show a strong commitment towards primarily using either glycolysis or oxidative phosphorylation. This is also the case for macrophages: while M(LPS) macrophages use glycolysis to meet their energetic needs, M(IL-4+IL-13) macrophages

predominantly rely on oxidative phosphorylation using fatty acids as their main source of energy (Huang et al., 2014a). According to the genome-wide analysis presented above, I next hypothesized that high salt may affect M(IL-4+IL-13) activation via cellular metabolism (Figure 45).

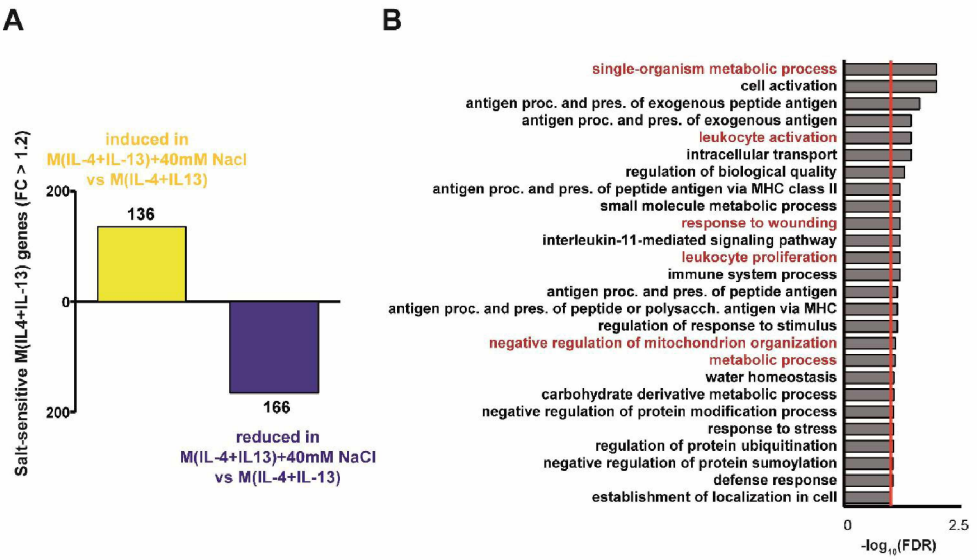

Figure 44. The functional effect of high salt on M(IL-4+IL-13) signature gene expression. BMDM were activated as before. **A:** The effect of high salt on the expression of all 807 M(IL-4+IL-13) signature genes was determined by microarray. Bars represent the number of genes that differ (FC>1.2) in their expression whether or not an additional 40mM NaCl was present during activation. **B:** Gene ontology (GO) analysis of genes from (**A**) was performed. GO terms (FDR<0.1) were summarized using REVIGO (Supek et al., 2011). Proc.: processing; pres.: presentation. Red line indicates FDR cut off of 0.1.

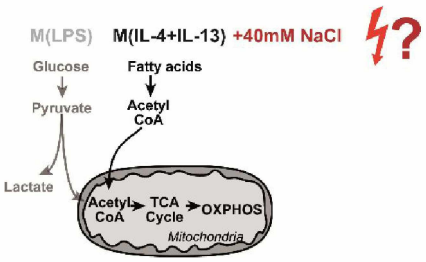

Figure 45. Scheme of metabolism hypothesis of the salt effect on M(IL-4+IL-13). Full M(IL-4+IL-13) activation relies on a re-wiring of cellular metabolism leading to increased oxidative phosphorylation using fatty acids as a main substrate to meet the energetic needs of activated M(IL-4+IL-13) macrophages. As aberrant metabolic adaption leads to impaired M2 polarization, metabolism was identified as a possible working point for high salt to blunt M(IL-4+IL-13) activation according to the previous analysis of salt-sensitive M(IL-4+IL-13) signature genes.

3.2.3. Salt modulates M(IL-4+IL13) cellular metabolism *via* Akt and mTOR

Extracellular flux analyses were conducted to test the effect of high salt on M(IL-4+IL-13) macrophage metabolism. First, BMDM were activated to M(IL-4+IL-13) in the presence or absence of an additional 40mM NaCl for 24 hours. The oxygen consumption rate (OCR) was then monitored over time, in the absence of interleukins or salt, for 150 minutes. To test mitochondrial function, cells were sequentially treated with oligomycin (to inhibit mitochondrial respiration (Penefsky, 1985)), carbonyl cyanide-4-(trifluoromethoxy)phenylhydrazone (FCCP) (to detect maximal respiration by uncoupling mitochondria (Heytler and Prichard, 1962)) and rotenone plus antimycin A (Rot+A) (to determine non-mitochondrial respiration) (Figure 46 A). In agreement with the earlier described metabolic adaptions of M(IL-4) macrophages (Huang et al., 2014a), the basal OCR was increased upon M(IL-4+IL-13) activation. However, in the presence of an additional 40mM NaCl, the spare respiratory capacity (SRC), which provides information as to the maximal mitochondrial respiration of the cell, was significantly reduced. This indicated that NaCl indeed blunted the metabolic capacity of mitochondria of M(IL-4+IL-13) macrophages. Interestingly, when unstimulated M(0) macrophages were incubated with high salt, their SRC was instead increased. Activation of BMDM to M(IL4+IL-13) also increased the basal extracellular acidification rate (ECAR), a surrogate for lactate-dependent acidification of the cell culture medium by glycolysis. No salt effect on ECAR was obvious under these basal conditions (Figure 46 B).

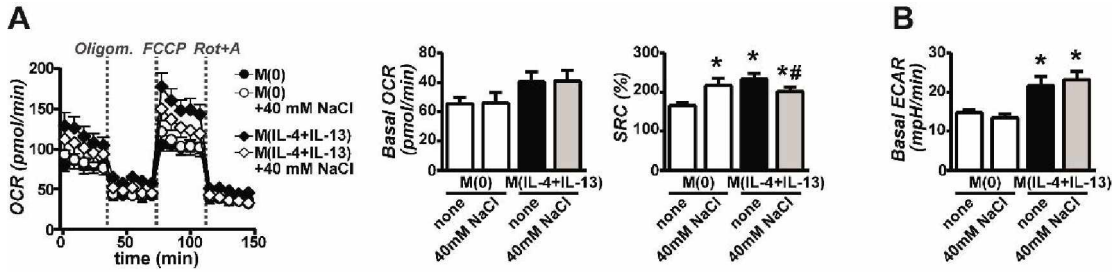

Figure 46. Salt affects mitochondrial and metabolic function of M(IL-4+IL-3) cells. A: Oxygen consumption rate (OCR) of unstimulated (M(0)) or M(IL-4+IL-13) activated macrophages without (none) or with high salt for 24 hours, followed by sequential treatment with oligomycin (to inhibit mitochondrial respiration), FCCP (to elucidate maximal respiration), and rotenone plus antimycin A (Rot+A) (to measure non-mitochondrial respiration). The basal OCR and spare respiratory capacity (SRC) are also shown. *p<0.05 vs M(0); #p<0.05 vs M(IL-4+IL-13). **B:** BMDM were activated as in (**A**) and the basal extracellular acidification rate (ECAR) was determined by flux analysis. *p<0.05 vs M(0).

The observed changes in OXPHOS could be due to a functional impairment of mitochondria or a general reduction in mitochondrial content after activation with salt for 24 hours. To address this question, I next tested whether salt decreased the mitochondrial content of M(IL-4+IL-13) macrophages activated in the presence of an additional 40mM NaCl. Two independent experimental approaches, one taking advantage of a mitochondrial dye and one relying on nucleic acid analysis, showed that the changes observed with salt were, however, not associated with a decreased mitochondrial content (Figure 47 A and B). Quantification of mitochondrial content by qPCR of mitochondrial (mt) DNA suggested a slight reduction for M(IL-4+IL-13) cells versus M(0) which was, however, not statistically significant (Figure 47 B).

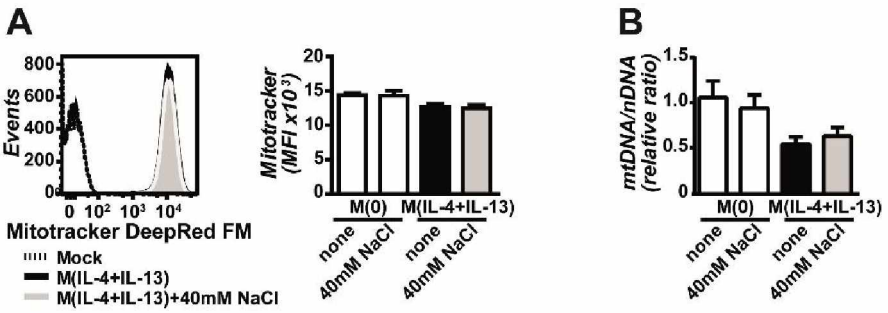

Figure 47. The effect of high salt on M(IL-4+IL-13) mitochondrial content. BMDM were activated as before. **A:** Mitochondrial mass was quantified by staining cells with Mitotracker red and analysis by flow cytometry. A representative flow cytometry plot (left panel) and the quantification of flow cytometry data (right panel) are shown. **B:** Mitochondrial content was measured by the ratio of mitochondrial (mt) DNA to nuclear (n) DNA.

The significant increase in ECAR (Figure 46 B) indicated that M(IL-4+IL-13) activated macrophages had increased rates of glycolysis under the activation conditions applied here. Therefore, I next explored in greater detail whether glycolysis was similarly affected by high salt. Extracellular flux analyses were again performed of M(0) and M(IL-4+IL-13) macrophages activated for 24 hours in the absence or presence of an additional 40mM NaCl. Before performing the measurements, macrophages were exchanged into glucose-free media and then the maximal response of the cells upon re-addition of glucose was used as a measure of the rate of glycolysis (Figure 48 A). Activation with IL-4+IL-13 under isotonic conditions was again associated with a significant increase in glycolytic flux in comparison to M(0), indicating that M(IL-4+IL-13) macrophages are

generally more glycolytically active than resting cells. M(IL-4+IL-13) cells activated with an additional 40mM NaCl had a decreased rate of glycolysis. High salt increased the SRC of M(0) macrophages before (Figure 46 A). Similarly, high salt increased the rate of glycolysis of M(0) cells (Figure 48 A). This opposing effect of high salt on the SRC and the rate of glycolysis of unstimulated or M(IL-4+IL-13) macrophages argues for a very specific effect of high salt on different activation phenotypes.

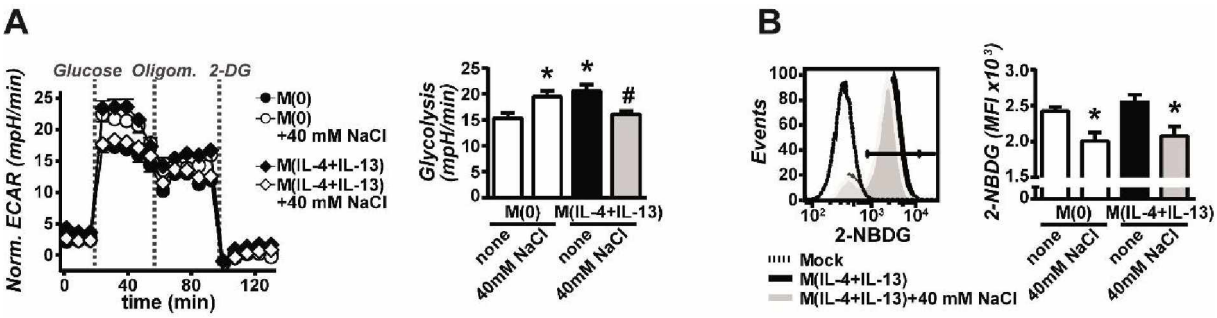

Figure 48. The effect of salt on the glycolytic flux of M(IL-4+IL13) cells. A: Extracellular acidification rate (ECAR) of unstimulated (M(0)) or M(IL-4+IL-13) activated macrophages without (none) or with high salt for 24 hours, followed by sequential treatment with glucose (to initiate glycolysis), oligomycin (to inhibit mitochondrial respiration), and 2-deoxy glucose (DG) (to inhibit glycolysis). The rate of glycolysis was calculated based on the difference between basal ECAR and the maximal ECAR following glucose stimulation. *p<0.05 vs M(0); #p<0.05 vs M(IL-4+IL-13). **B:** Glucose uptake of macrophages activated as in (**A**), followed by incubation of the cells with 2-NBDG for one hour, and analysis by flow cytometry. *p<0.05 vs M(0) none.

The decrease in glycolytic flux in M(IL-4+IL-13) cells with salt could be due to a salt-impaired uptake of glucose. Therefore, I analyzed glucose uptake of M(IL-4+IL-13) cells activated in high salt for 24 hours vs isotonic conditions by incubation with the fluorescent D-glucose derivate 2-(N-(7-nitrobenz-2-oxa-1,3-diazol-4-yl)amino)-2-deoxyglucose (2-NBDG) (Yamada et al., 2007; Yoshioka et al., 1996) for one hour and subsequent flow cytometric analysis (Figure 48 B). In line with the salt-blunted glycolytic flux observed previously, M(IL-4+IL-13) cells activated with an additional 40mM NaCl took up significantly less 2-NBDG . Surprisingly, glucose uptake was similarly impaired in M(0) cells incubated with high salt albeit glycolysis vs M(0) none was increased in these cells previously (Figure 48 A). Collectively, the metabolic analyses presented here indicate that high NaCl blunts the increase in OXPHOS and glycolysis necessary for full M(IL-4+IL-13) activation.

As both the analysis of gene expression data and the extracellular flux experiments revealed that high salt affects M(IL-4+IL-13) cellular metabolism, I hypothesized that this might be *via* aberrant Akt/mTOR signaling. These signaling pathways are known to be important for nutrient sensing and orchestrating the metabolic re-wiring associated with immune cell activation and fate decisions (Chi, 2012; Palmer et al., 2015; Zeng et al., 2013). Of note, mTOR has recently been identified to regulate the inflammatory response of innate immune cells such as macrophages and dendritic cells (Weichhart et al., 2008; Weichhart and Saemann, 2008). Akt signaling, which is itself upstream of mTOR (Hay and Sonenberg, 2004), was shown to synergize with STAT6 to induce full M2 macrophage activation (Byles et al., 2013). To investigate this, BMDM were pretreated in isotonic media or high salt for five minutes before stimulation with IL-4+IL-13 for 15, 30 and 60 minutes and detection by western blotting of the phosphorylation of Akt^{S473} and $p70S6K^{T389}$, a downstream target of mTOR signaling (Hay and Sonenberg, 2004), which is itself downstream of pAkt signaling. Despite serum starvation, BMDM showed considerable phosphorylation of Akt, which was further increased upon stimulation with IL-4+IL-13 (Figure 49 A). Pre-incubation of BMDM with an additional 40mM NaCl significantly blunted interleukin-induced Akt phosphorylation at all times analyzed. Basal phosphorylation of p70S6K was low and strongly increased by IL-4+IL-13 stimulation over time (Figure 49 B). This increase was almost completely abrogated with high salt pre-treatment. To corroborate the importance of Akt signaling for M(IL-4+IL-13) activation, BMDM were activated with IL-4+IL-14 for 24 hours while Akt signaling was chemically inhibited. Inhibition of Akt signaling with the small molecule LY294002 blunted the expression of M(IL-4+IL-13) signature genes significantly (not shown). This result was similar to that observed previously with M(IL-4) macrophages (Byles et al., 2013) and mimicked the effect of high salt. Collectively, the results suggested that high salt affects M(IL-4+IL-13) activation and metabolism *via* its effect on Akt/mTOR signaling.

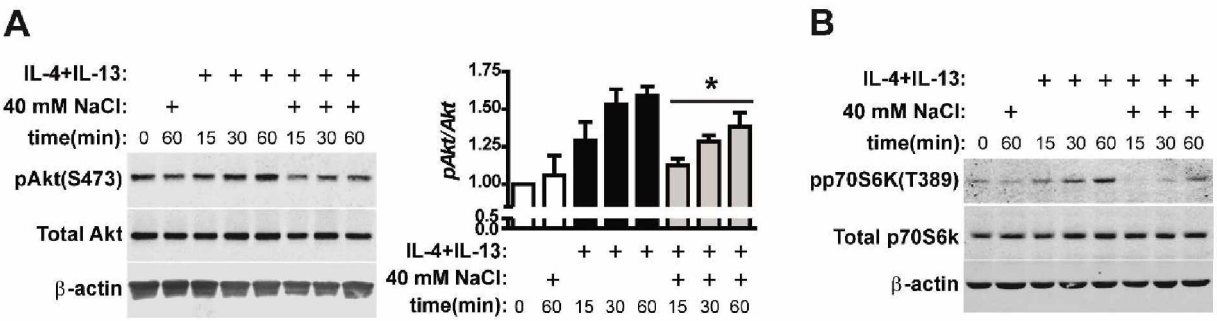

Figure 49. The effect of high salt on IL-4+IL-13-induced Akt and mTOR signaling. BMDM were serum-starved overnight and then pre-treated with 40mM NaCl for 5 minutes, prior to stimulation with IL-4+IL-13. **A:** phospho-Akt (pAkt) levels were determined by western blotting after 15, 30 or 60 minutes. The levels of total Akt were determined in a separate blot with β-actin as a loading control. Bar graphs show the quantification of pAkt/total Akt levels normalized to t=0. *p<0.05 vs M(IL-4+IL13) none by 2-way-ANOVA. **B:** BMDM were treated as in (**A**). phospho-p70S6K levels were determined by western blotting after 15, 30 or 60 minutes. The levels of total p70S6K were determined in a separate blot with β-actin as loading control.

If the effect of high salt on M(IL-4+IL-13) activation was mechanistically due to the effect of salt on Akt signaling described previously, experimental restoration of Akt signaling during M(IL-4+IL-13) activation in the presence of high salt might attenuate the salt phenotype. To test this hypothesis, BMDM were generated from transgenic mice which express a constitutively active Akt isoform (caAkt) to test whether this would rescue the blunting-effect of high salt on M(IL-4+IL-13) activation. In this model, caAkt expression is inducible by Cre recombinase. Bone marrow cells were first differentiated into BMDM in the absence of Cre to ensure normal differentiation (caAkt^{inactive}). After differentiation, recombinant TAT-Cre was added to induce caAkt expression (caAkt^{active}). WT BMDM were treated similarly as controls (Figure 50 A). WT BMDM treated with TAT-Cre showed detectable Akt phosphorylation (Figure 50 B). Importantly, Akt phosphorylation was highly increased in caAkt BMDM after TAT-Cre treatment as expected. Adherent caAkt^{active} and WT BMDM were then left unstimulated, or stimulated with IL-4+IL-13 alone or with an additional 40mM NaCl for 24 hours. Next, the expression of M(IL-4+IL-13) signature genes was measured by qPCR. As before, WT BMDM revealed a significantly reduced induction of the genes *Mrc1, Ym1* and *Mgl2* when stimulated with IL-4+IL-13 in the presence of an additional 40mM NaCl. This blunted expression by high salt was rescued in caAkt^{active} BMDM (Figure 50 C). Interestingly, *Arg1* expression, which unexpectedly was also salt sensitive in this case, was further enhanced by high salt in caAkt^{active} cells.

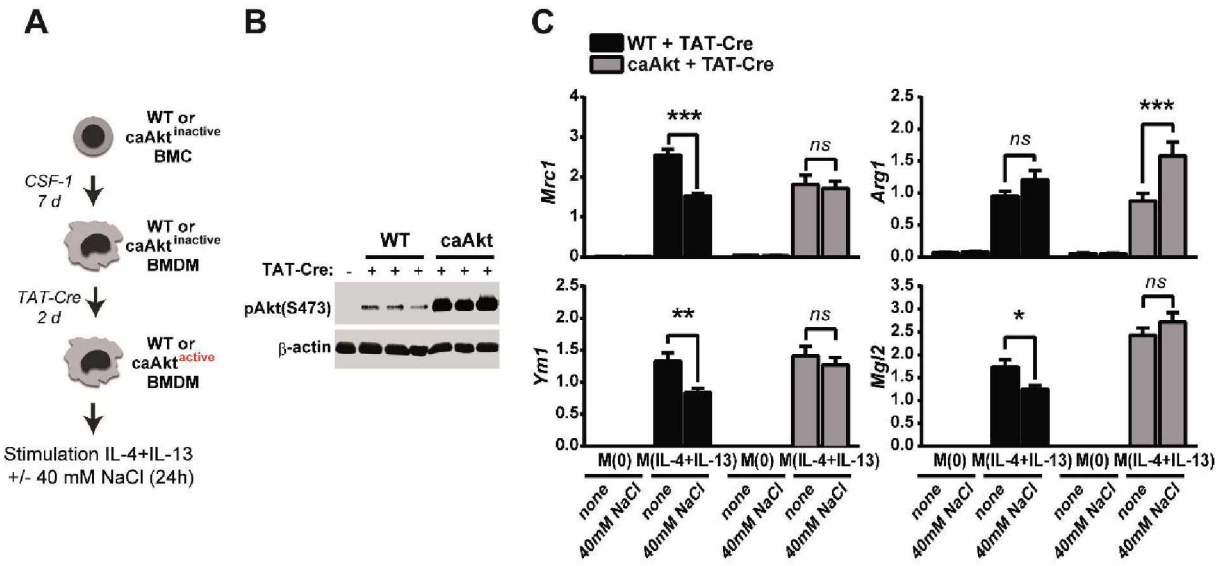

Figure 50. Constitutively active (ca) Akt rescues the salt effect on M(IL-4+IL-13) cells. A: Schematic for the generation of BMDM with caAkt (NH(2)-terminally myristoylation signal-attached Akt). After differentiation of caAkt^{inactive} or WT BMDM from the respective bone marrow cells (BMC), macrophages were incubated with TAT-Cre to induce caAkt expression (caAkt^{active}) or as controls. **B:** Western blot of phospho-Akt shows a robust induction of phosphorylated Akt after treatment of BMDM caAkt macrophages with TAT-Cre for 2 days (lanes 5-7). WT macrophages treated with TAT-Cre similarly are also shown (lanes 2-4). **C:** WT and caAkt^{active} BMDM were stimulated with IL-4+IL-13 in the absence (none) or with an additional 40mM NaCl for 24 hours and signature gene expression was analyzed by qPCR. *p<0.05; **p<0.01; ***p<0.001 by 2-way ANOVA.

In summary, these results support the view that high salt blunts Akt signaling and thereby affects other downstream signaling molecules (mTOR) and, ultimately, the necessary metabolic adaptions of M(IL-4+IL-13) macrophages. An effect of high salt on cellular metabolism was also identified by the genome-wide expression analysis (Figure 44 B). This therefore suggests a novel mechanism by which high salt might affect immune cell activation and function.

3.3. The effect of high salt on M(LPS) macrophages: genome wide analysis

An effect of high salt on pro-inflammatory M(LPS) macrophage activation and function was demonstrated recently (Jantsch et al., 2015). Here, high salt boosted the expression of inflammatory mediators and bactericidal effector molecules leading to an increased killing of L. major *in vitro* and *in vivo*. In contrast to M(IL-4+IL-13) activation, the effect of high salt on M(LPS) macrophages was mediated via Nfat5. To elucidate additional mechanisms and to increase our understanding of how high salt affects the activation of

pro-inflammatory macrophages, I used genome-wide approaches to characterize M(LPS) macrophage activation in the absence or presence of an additional 40mM NaCl. The approach described was performed as per my previous M(IL-4+IL-13) analysis (see 3.2).

3.3.1. *In vitro* activation of pro-inflammatory macrophages

To characterize the *in vitro* generation of pro-inflammatory macrophages, BMDM were allowed to attach and then activated with 10ng/ml LPS for 24 hours. Again, three data sets were generated: one with differentially expressed genes, one set with differential H3K4me3 genes and one set with differential H4ac genes upon M(LPS) activation of BMDM for 24 hours. Analysing all three gene sets together, a total of 7030 genes were differential (FDR<0.05) upon activation to M(LPS) in normal, isotonic media. The expression, H3K4me3 and H4ac gene sets comprised 4029, 3099 and 2783 differential genes, respectively. As previously for M(IL-4+IL-13), the overlap between the three gene sets was low (Figure 51). For the reasons discussed previously (see 3.2.1), all further analyses were based on genes with differential expression upon M(LPS) activation, followed by the integration of ChIP-seq data.

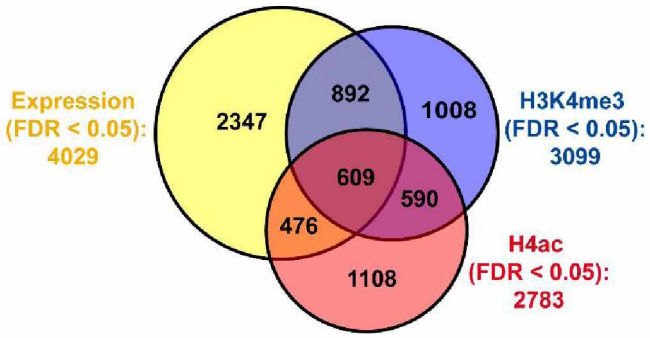

Figure 51. A *de novo* M(LPS) gene set defined by expression, H3K4me3 and H4ac. Differential genes (FDR<0.05) upon M(LPS) activation of BMDM for 24 hours in isotonic media were determined for gene expression, H3K4me3 and H4ac. In total, a set of 7030 *de novo* M(LPS) genes was identified. The overlap between the three individual gene sets (expression: 4029 genes, yellow; H3K4me3: 3099 genes, blue; H4ac: 2783 genes, red) is shown as a Venn diagram.

Upon M(LPS) activation, 1235 of the 4029 differential M(LPS) expression genes (FDR<0.05) were induced more than 1.3-fold, while the expression of 1325 genes was downregulated more than 1.3-fold compared to unstimulated M(0) macrophages (Figure 52 A). The top 50 up- and downregulated genes (by expression FC) upon M(LPS) activation

are shown in Table 7 and Table 8 (see appendix 5.1), respectively. To characterize cellular functions associated with the 1235 upregulated and 1325 downregulated M(LPS) genes, GO term analysis was performed and significant results (FDR<0.05) are shown. For the 1235 upregulated M(LPS) genes (Figure 52 B), terms related to the immune response and cellular metabolism, specifically *cellular carbohydrate catabolic process* were significantly enriched. *Hexose catabolic process*, *glucose catabolic process* and *glycolytic process* were also detected (FDR<0.05) (not shown). Terms related to apoptosis and cell death are also shown. Additional features of pro-inflammatory activation were identified and are listed in Table 2. For the 1325 downregulated M(LPS) genes (Figure 52 C), terms related to cell division and metabolism were identified.

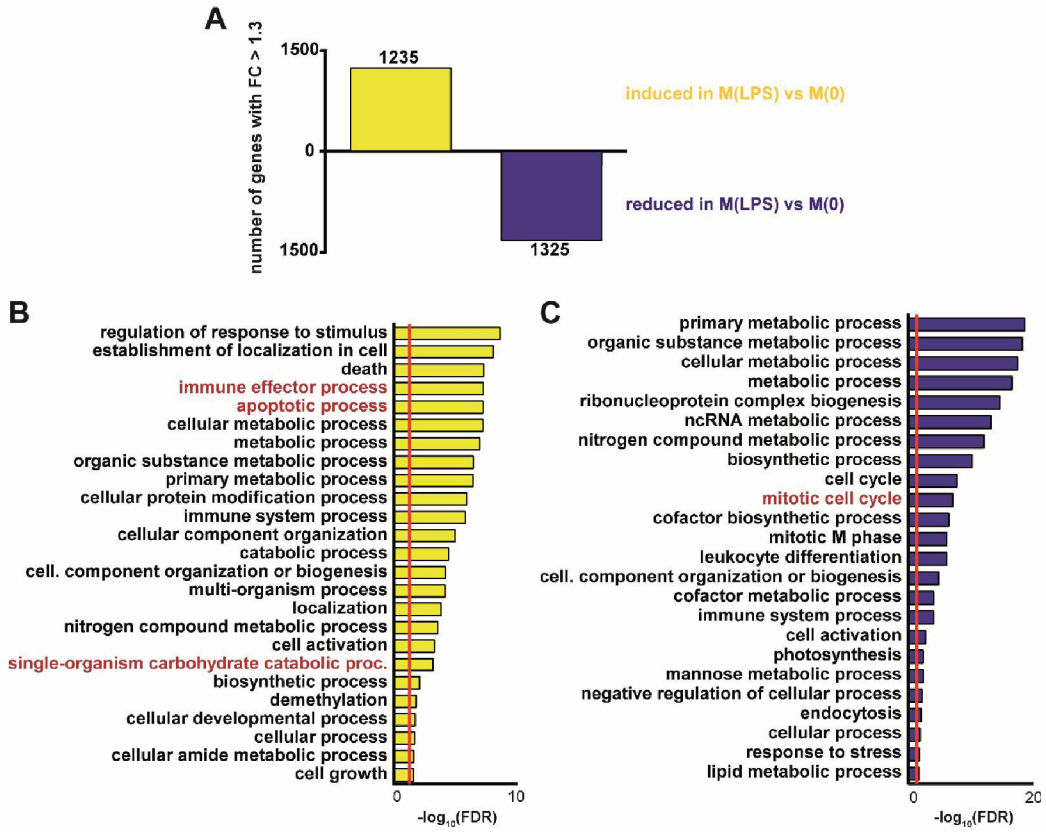

Figure 52. Global gene expression analysis of *in vitro* M(LPS) activation. BMDM were activated with LPS for 24 hours M(LPS) or unstimulated (M(0)). **A:** Global gene expression changes were determined by microarray. The bars represent the number of induced (yellow) and reduced (blue) M(LPS) genes (FDR < 0.05) with a fold change (FC)>1.3. **B+C:** Gene ontology (GO) term analysis of induced (**B**) and reduced (**C**) M(LPS) genes from (**A**) was performed to identify pathways and/or cellular programs induced (**B**) or reduced (**C**) upon M(LPS) activation. Significant (FDR<0.05) GO terms were summarized using REVIGO (Supek et al., 2011); all terms with a dispensability<0.1 are shown. Red lines in (**B+C**) indicate FDR cut off of 0.05.

Table 2. Additional GO terms (FDR<0.05) for 1235 upregulated (FC>1.3) M(LPS) genes.

GO term ID	Description	-log$_{10}$ (FDR)
GO:0071222	cellular response to lipopolysaccharide	3.3244
GO:0071356	cellular response to tumor necrosis factor	1.7967
GO:0016570	histone modification	1.5466
GO:0031349	positive regulation of defense response	1.6043
GO:0043123	positive regulation of I-kappaB kinase/NF-kappaB signaling	3.6103
GO:1900745	positive regulation of p38MAPK cascade	1.6429
GO:0001666	response to hypoxia	2.2717
GO:0070555	response to interleukin-1	3.7356

In line with the approach used for M(IL-4+IL-13) macrophages, my further analysis was focused only on genes which were induced (FC>1.3) upon M(LPS) activation and this set of genes will be hereafter be referred to as "M(LPS) signature genes". Of note, the GO term *histone modification* was also significantly (FDR<0.05) enriched for these M(LPS) signature genes (Table 2). Histone methyltransferases (*Dot1l*), demethylases (*Kdm1a, Kdm3a, Kdm6b*), deacetylases (*Hdac4, Hdac7*) and members of the polycomb silencing complex (*Pcgf1*) were among the genes identified (not shown). This corroborated earlier reports by others showing the importance of histone modifications to regulate M1 macrophage activation (Nicodeme et al., 2010). Both genes for metabolic adaption (enolase 2 (*Eno2*)) and pro-inflammatory mediators (chemokine (C-C) ligand 5 (*Ccl5*) and interleukin 1 alpha (*Il1a*)) were among the top 50 induced M(LPS) gene hits (Table 7; appendix 5.1). The silver medalist of the list, lipocalin 2 (*Lcn2*) is routinely used as a kidney damage marker in the clinic (Bennett et al., 2008). Here, however, it is probably simply part of a conserved antibacterial defense program due to its ability to sequester iron necessary for bacterial growth (Flo et al., 2004; Schmidt-Ott et al., 2007). Suppressor of cytokine signaling 3 (*Socs3*) was among the top hits likewise. This might again indicate activation of negative feedback loops upon continuous LPS-signaling to restrict – under physiological conditions – overshooting inflammation (Song and Shuai, 1998; Yoshimura et al., 2005). Negative feedback signaling via SOCS proteins may also explain why *Cd14*, a major component of the cellular LPS recognition machinery (Lacroix et al., 1998), and the surface pattern recognition receptor toll-like receptor 2 (*Tlr2*) (Liu et al., 2014; Yoshida et al., 2009) are among the top 50 downregulated genes upon M(LPS) activation (Table 8; appendix 5.1).

Again, parallel analysis of H3K4me3 and H4ac histone marks by ChIP-seq revealed a strong association between the abundance of activating histone modifications and gene expression levels for some M(LPS) signature genes. For *Il1a*, *Ccl5* and *Lcn2*, histone modification (Figure 53 A) and gene expression (Figure 53 B) changes upon M(LPS) activation are shown. Similar to M(IL-4+IL-13) activation, this association was weak when looking at all M(LPS) signature genes and the overall statistical correlation between expression and histone modification changes was negligible (not shown).

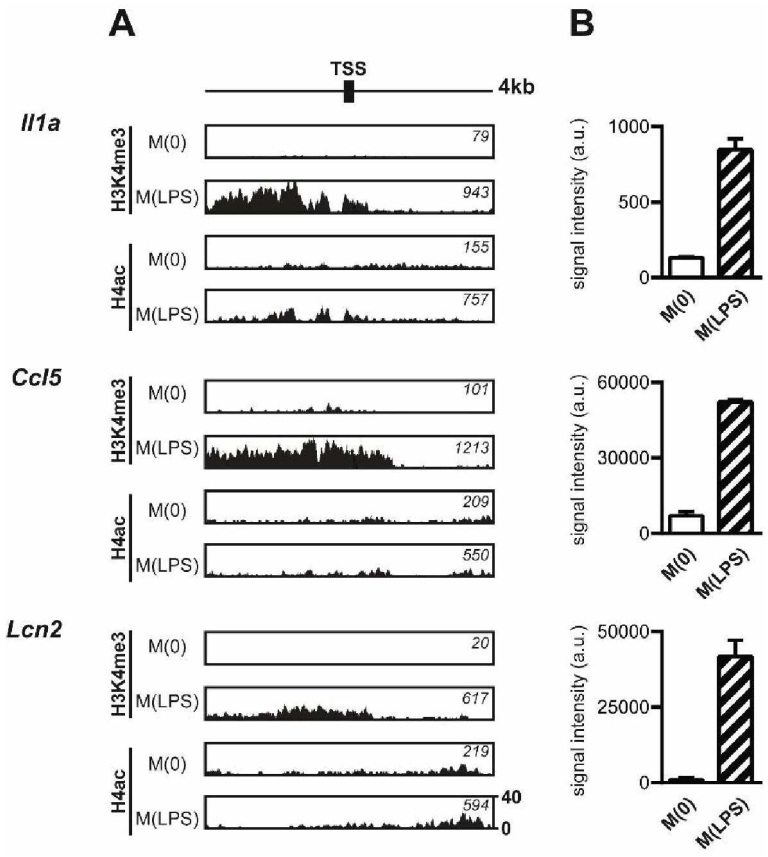

Figure 53. H3K4me3 and H4ac histone modifications of M(LPS) signature genes. BMDM were activated as before. **A:** ChIP-seq signature tracks of H3K4me3 and H4ac histone marks are shown spanning 2kb upstream and downstream around the annotated transcription start site (TSS). Mean counts are indicated for each track. **B:** Bar graphs show gene expression levels for M(0) and M(LPS) as determined by microarray.

3.3.2. Adding salt to the genome-wide analysis of M(LPS) activation

After establishing a reference dataset of 1235 genes induced upon M(LPS) activation, my next aim was, again, to characterize the effect of high salt on gene expression and histone modification levels. Therefore, the expression of the 1235 M(LPS) signature genes as determined previously was compared to their respective expression

levels when M(LPS) cells were activated in the presence of an additional 40mM NaCl using microarray data. The top 50 (by expression FC) salt-sensitive M(LPS) signature genes are presented in Table 9 and Table 10 (see appendix 5.1) for further increased and decreased genes, respectively, and the expression levels with or without salt is presented in Figure 54 as a scatter plot. Some of the most salt-sensitive genes are highlighted in Figure 54. Genes mediating the adaption to osmotic stress such as compatible osmolyte channels (*Slc6a12*) and heat shock proteins (*Hspa1a*, *Hsph1*) were increased further by high salt. M(LPS) immune effector genes (*Nos2*), regulators of the immune answer (*Socs3*) and genes involved in glucose metabolism (*Slc2a1*) also expressed at higher levels in the presence of high salt. *Ctsk*, a cysteine protease which participates in fighting infection by its ability to activate TLR signaling (Abou Fakher et al., 2009; Asagiri et al., 2008; Blum and Cresswell, 1988; Manoury, 2013) was increased, while the expression of protease inhibitor (*Cst7*), *bona fide* lactate channel (*Slc16a6*) (Bonen et al., 2006; Hugo et al., 2012) and cell cycle (*Ccng1*) genes was decreased. Further immune mediators (*Il19*, *Ccl2*) and *Malt1*, an important regulator of NF-κB signaling (Afonina et al., 2015; Wegener and Krappmann, 2007), were also boosted by high salt (Table 9; see appendix 5.1).

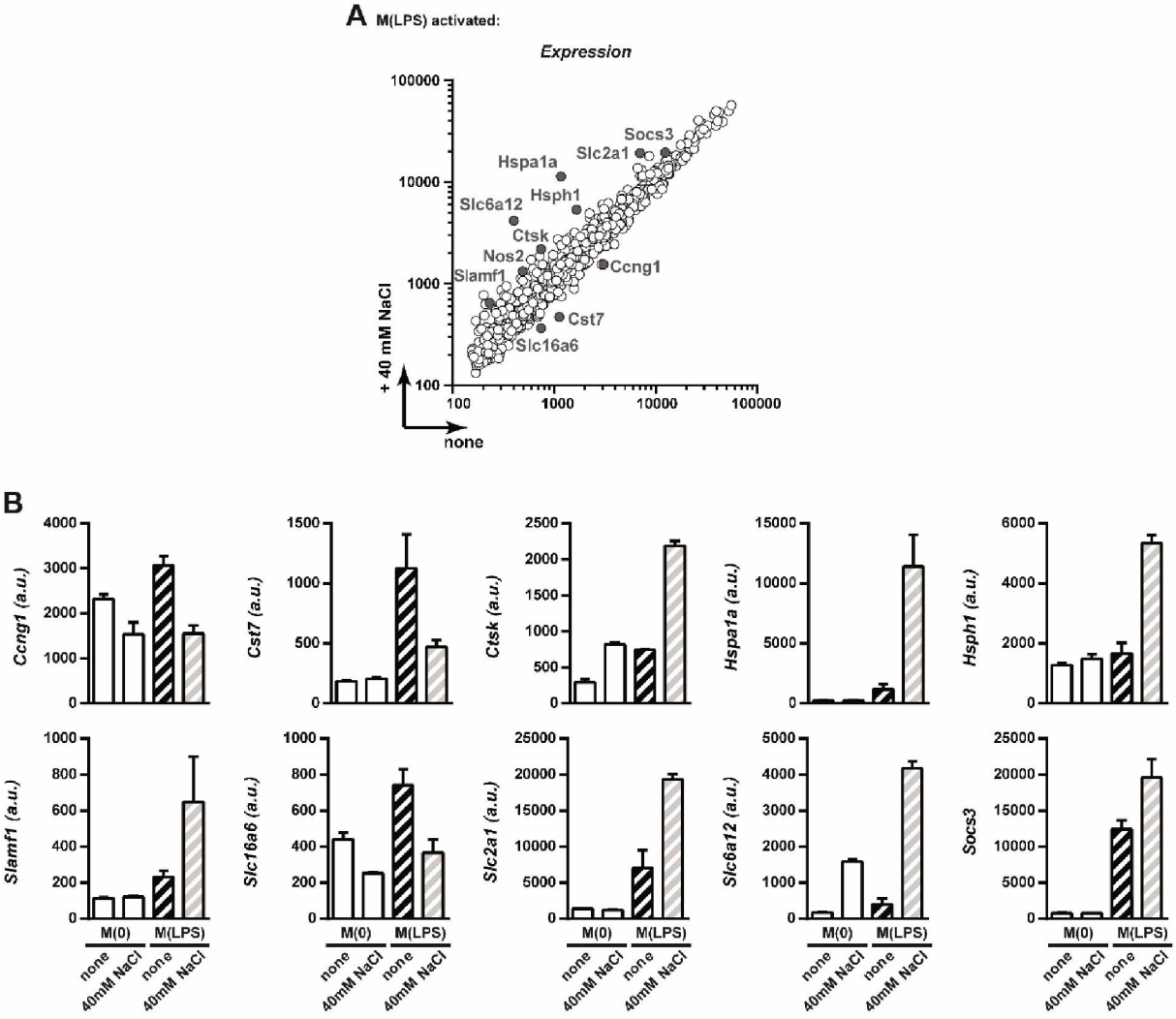

Figure 54. The effect of high salt on the expression of M(LPS)-induced signature genes. BMDM were activated with LPS (M(LPS)) in the absence (none) or presence of an additional 40mM NaCl for 24 hours. Unstimulated macrophages (M(0)) were treated similarly. **A:** The effect of high salt on M(LPS) signature gene expression as determined by microarray is shown. Highly salt-sensitive genes are indicated (grey dots with gene names). **B:** Bar graphs show the expression level of genes highlighted in (**A**) by microarray.

Next, the effect of high salt H3K4me3 and H4ac modification levels was analyzed (Figure 55 A and Figure 56 A, respectively). Genes that showed salt sensitivity in the previous gene expression analysis (Figure 54) are indicated on the plots. Especially, *Cst7*, *Ctsk*, *Slamf1*, *Slc6a12* and *Socs3* showed changes in H3K4me3 levels concordant to gene expression (Figure 55 B). For H4ac, *Hspa1a*, *Hsph1*, *Slc2a1*, *Slc6a12* and *Socs3* showed increased modification when macrophages were activated with LPS in the presence of an additional 40mM NaCl. Interestingly, a considerable increase of H4ac was detected around the TSS of *Slc16a6* even though its expression was decreased in the presence of high salt (Figure 56 B).

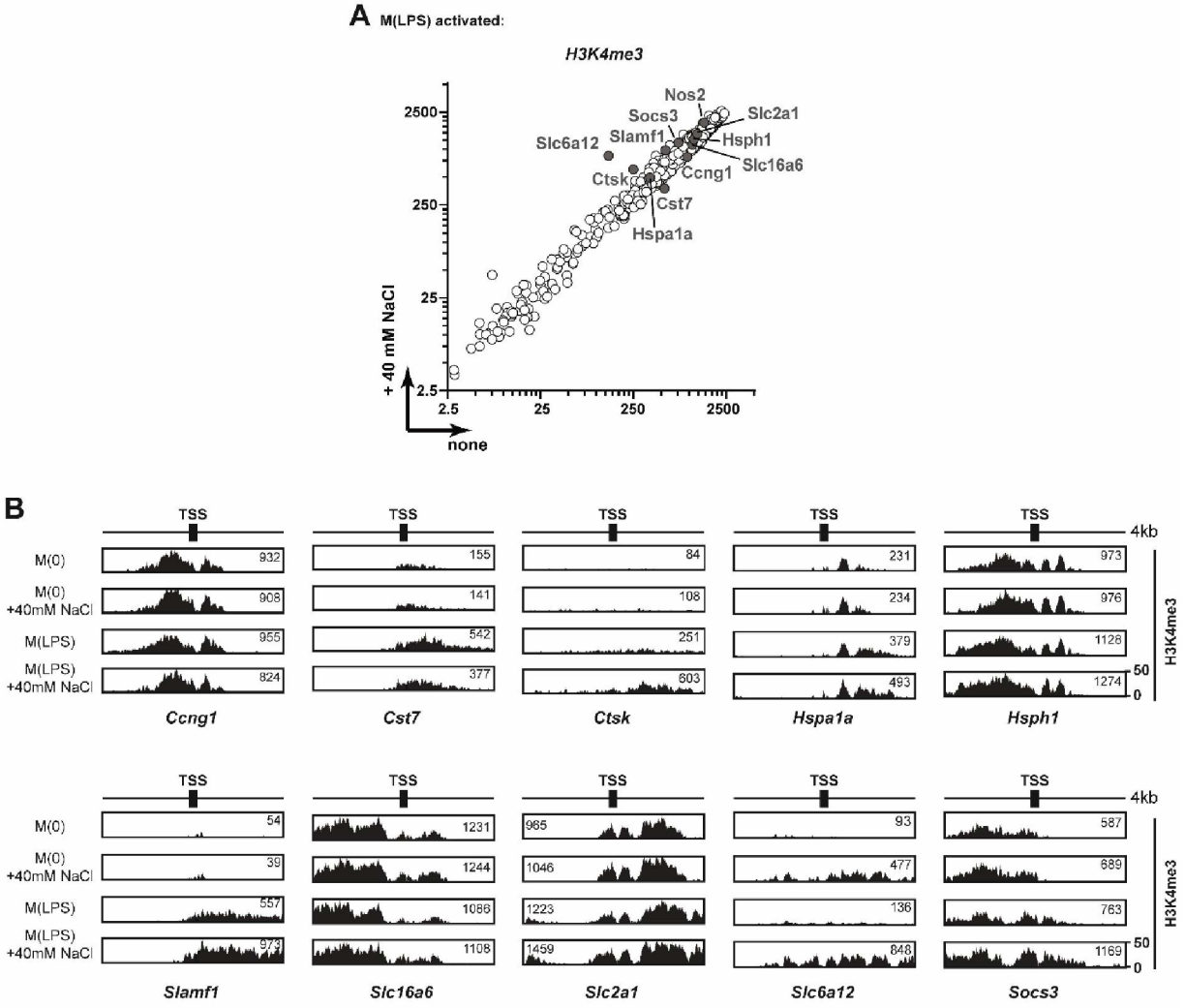

Figure 55. The effect of high salt on H3K4me3 levels of M(LPS) signature genes. BMDM were activated as before. Histone modification levels were determined by ChIP-seq spanning 4kb around the annotated transcription start site (TSS) **A:** The effect of high salt on H3K4me3 levels of M(LPS) signature genes is shown. Individual genes from Figure 54 are indicated (grey). **B:** Representative H3K4me3 signature tracks for highlighted genes from (**A**) are shown. Mean counts are indicated for each track.

The induction of Nos2 and NO production constitutes an important murine M(LPS) macrophage effector mechanism (Bogdan et al., 2000; MacMicking et al., 1997). Activation in the presence of high salt significantly increased both *Nos2* gene expression (Figure 18 A; Figure 57 A) and NO production (Figure 18 B). This led to increased killing of intracellular pathogens (Jantsch et al., 2015). The effect of high salt on activating histone marks (H3K4me3) around the *Nos2* TSS was tested by ChIP-seq and qPCR of immune-precipitated DNA. By ChIP-seq, increased H3K4me3 modification levels were visible around the *Nos2* TSS (Figure 57 B). The same trend was obvious using qPCR even though the number of replicates (N=3) was not sufficient to show significance (Figure 57 C).

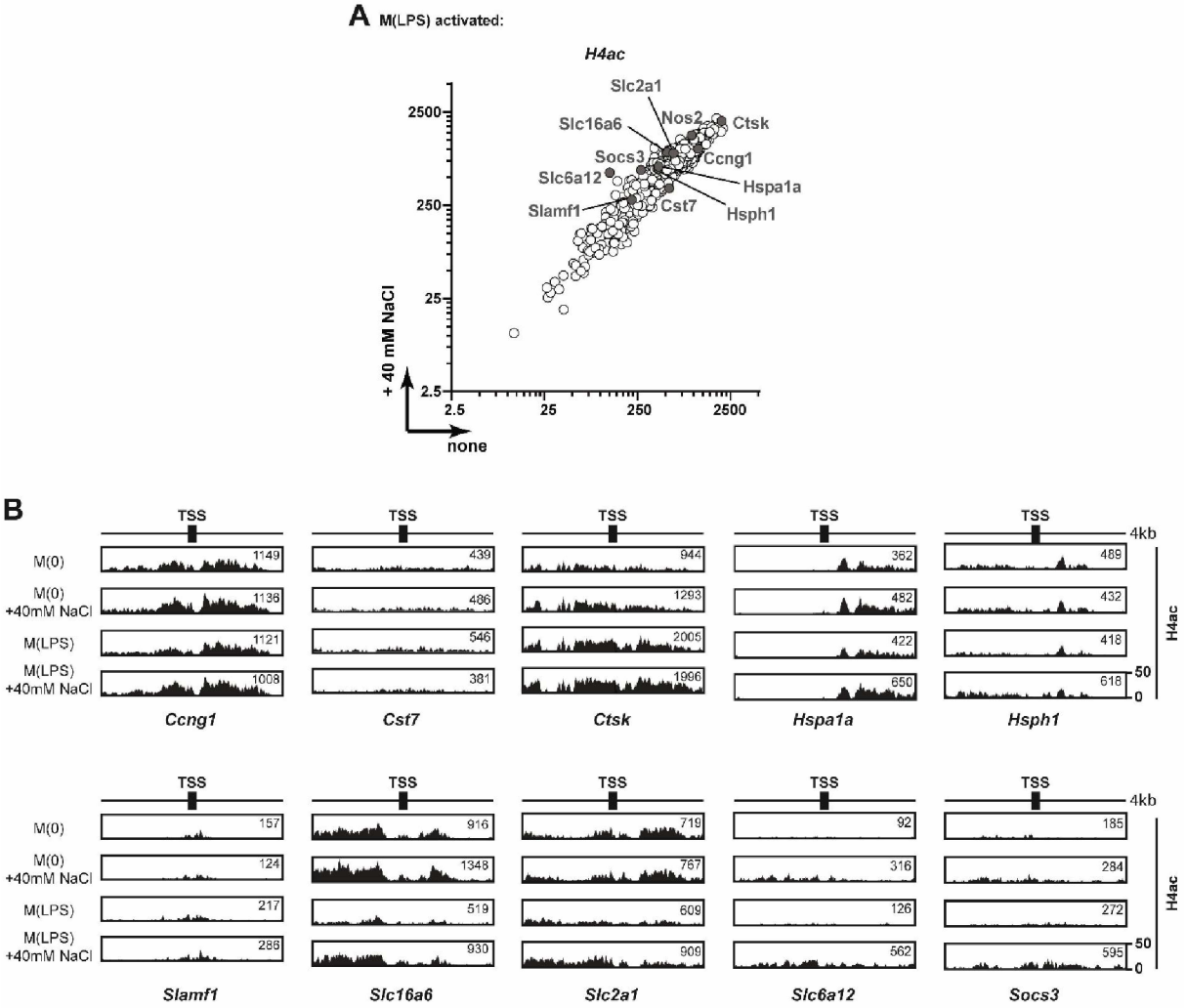

Figure 56. The effect of high salt on H4ac levels of M(LPS) signature genes. BMDM were activated and histone modification levels determined as before. **A:** The effect of high salt on H4ac levels of M(LPS) signature genes is shown. Individual genes from Figure 54 are indicated (grey). **B:** Representative H4ac signature tracks for highlighted genes from (**A**) are shown. Mean counts are indicated for each track.

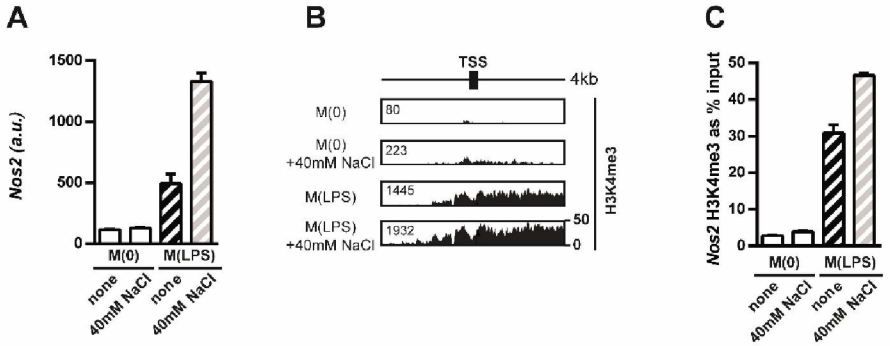

Figure 57. High salt increases H3K4me3 at the *Nos2* promoter. BMDM were activated as before. **A:** Bar graphs show *Nos2* gene expression levels as determined by microarray. **B:** Representative H3K4me3 signature tracks by Chip-seq around the *Nos2* transcription start site (TSS) are shown. Mean counts are indicated for each track. **C:** Bar graphs show H3K4me3 levels at the *Nos2* promoter determined by qPCR of immuno-precipitated DNA.

The effect of high salt on M(LPS) signature genes was determined using a similar approach as for M(IL-4+IL-13). Out of the 1235 M(LPS) signature genes, 343 genes increased (FC>1.2) with high salt while 89 genes were decreased (FC>1.2) (Figure 58 A). GO term analysis was then performed using these 432 salt- sensitive genes as the input. Significant results (FDR<0.05) are shown in Figure 58 B. Under high salt conditions, *apoptotic process* and *death* were again identified, indicating that salt further modifies these processes which were already present in the M(LPS) dataset. In agreement with the observed increase in NO production by high salt (Figure 18 B; (Jantsch et al., 2015)), *arginine metabolic process* was also identified to be affected by salt. Most interestingly, the GO term analysis results suggested that high salt also affected cellular metabolism of M(LPS) macrophages, a result similar to M(IL-4+IL-13) (Figure 44 and section 3.2.3). Especially, high salt seemed to affect the glycolytic breakdown of glucose (*hexose catabolic process*, *metabolic process*) which is a hallmark of inflammatory macrophages (Cramer et al., 2003).

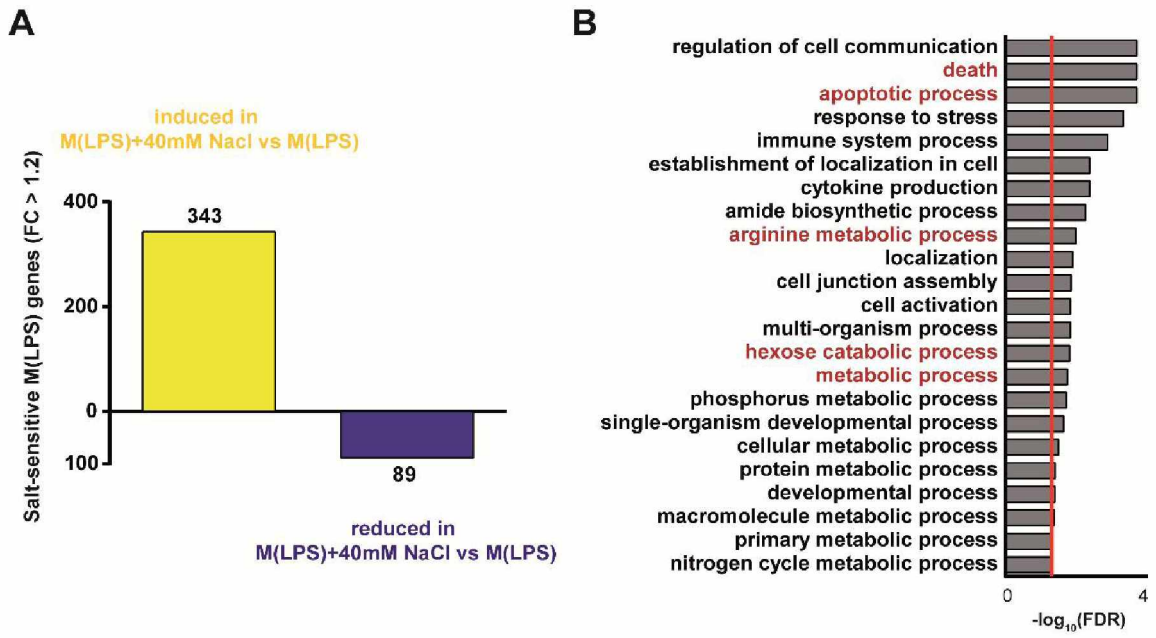

Figure 58. The functional effect of high salt on M(LPS) signature gene expression. BMDM were activated as before. **A:** The effect of high salt on the expression of all 1235 M(LPS) signature genes was determined by microarray. Bars represent the number of genes that differ (FC > 1.2) in their expression whether or not an additional 40mM NaCl was present during M(LPS) activation. **B:** Gene ontology (GO) analysis of genes from (**A**) was performed. Significant (FDR < 0.05) GO terms were summarized using REVIGO (Supek et al., 2011); all terms with a dispensability < 0.2 are shown. Red line indicates FDR cut off of 0.05.

The genes within the GO term *glycolytic process* were analyzed in more detail (Figure 59). The expression of *glycolytic process* genes were found to be further increased by the presence of an additional 40mM NaCl, compared to M(LPS) activation alone. This increase was mostly accompanied with concordant changes in H3K4me3 and H4ac modifications (Figure 59). Collectively, these data suggest that high salt promotes the expression of metabolic genes which mediate the metabolic changes associated with pro-inflammatory macrophage activation.

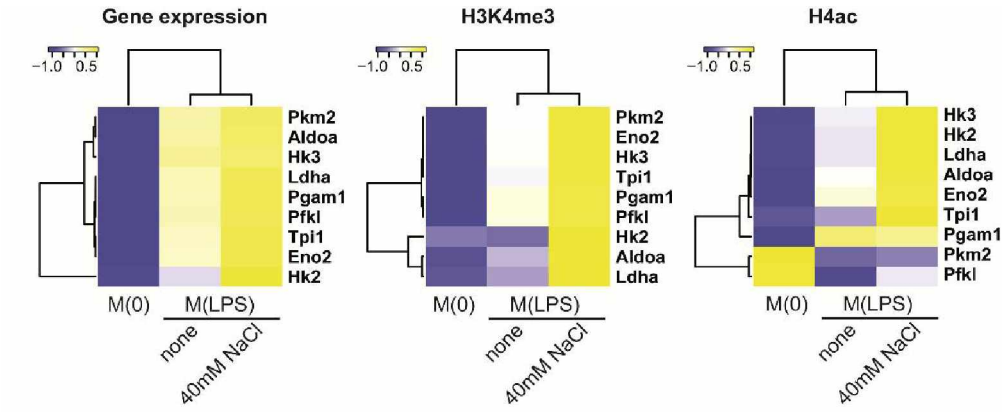

Figure 59. The effect of high salt on GO *glycolytic process* M(LPS) signature genes. BMDM were activated as previously. Mean gene expression (microarray), H3K4me3 and H4ac (both Chip-seq) data for genes annotated with *GO:0006096 glycolytic process* of all 1235 M(LPS) signature genes are presented as heatmaps. Data were scaled and centered around 0 row-wise.

3.3.3. High salt increases the glycolytic capacity of M(LPS) macrophages

As the bioinformatics results suggested that high salt increased the glycolytic flux of M(LPS) macrophages, I tested this hypothesis by a series of wet-lab approaches, i.e. determination of the expression of glycolysis genes by qPCR and measurement of lactate production of M(LPS) cells activated in the absence or presence of an additional 40mM NaCl. First, the boost in expression by high salt of the glycolysis genes hexokinase 2 (*Hk2*), phosphoglycerate mutase 1 (*Pgam1*), lactate dehydrogenase A (*Ldha*) and the glucose transporter GLUT-1 (*Slc2a1*) was confirmed by qPCR (Figure 60 A+B). The expression of all four genes was significantly enhanced by high salt. Next, glycolytic activity was determined by measuring lactate levels. BMDM were activated with LPS for 24 hours in the absence or presence of an additional 40mM NaCl. Intracellular lactate was then measured from cell lysates (Figure 60 C upper panel). To determine glycolytic flux

after LPS-activation +/-40mM NaCl, macrophages were washed free of LPS+/-40mM NaCl and lactate was determined in one-hour cell culture supernatants (extracellular; Figure 60 C lower panel). In both cases, activation of macrophages with LPS led to a significant increase in lactate production compared to unstimulated macrophages. High salt additionally boosted lactate production of M(LPS) cells. Taking together the bioinformatics, qPCR results and lactate measurements, high salt seems to induce an increased glycolytic flux in M(LPS) macrophages. As metabolic switching towards glycolysis is essential for pro-inflammatory macrophage activation and to survive in hostile NO-loaded environments (Everts et al., 2012), this salt-induced increase of glycolysis likely constitutes an additional mechanism by which high salt mediates the previously described boost of M(LPS) activation (Jantsch et al., 2015).

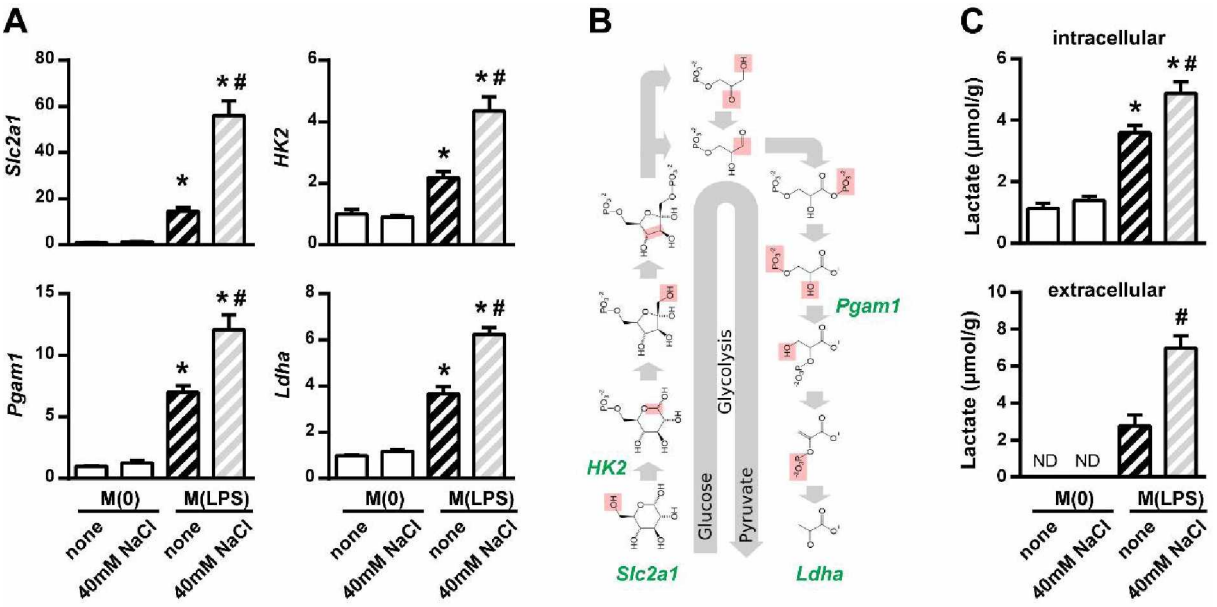

Figure 60. High salt increases glycolysis of M(LPS) macrophages. Macrophages were stimulated with LPS (M(LPS)) in the absence (none) or with an additional 40mM NaCl for 24 hours. Unstimulated (M(0)) macrophages were treated similarly. **A:** The expression of glycolysis genes was determined by qPCR. *p<0.05 vs M(0); #p<0.05 vs M(LPS). **B:** Schematic of the glycolysis pathway. Steps, which showed enhanced gene expression in (**A**) are indicated in green (faithfully adapted from https://upload.wikimedia.org/wikipedia/commons/thumb/0/0b/Glycolysis_metabolic_pathway.svg/2000px-Glycolysis_metabolic_pathway.svg.png as of 14th Sep 2015). **C:** Bar graphs show intracellular (upper panel) and extracellular (lower panel) lactate levels after activation. Values were normalized to total protein. *p<0.05 vs M(0); #p<0.05 vs M(LPS).

4. Discussion

The continued imbalance of host-destructive immune effector, and host-protective regulatory immune mechanisms, is a major threat to human health and contributes to a variety of autoimmune disorders which constitute a serious health burden (Dejaco et al., 2006; Doherty, 2015; Rosenblum et al., 2015). Other common and costly disease entities such as cardiovascular disease are similarly associated with altered immune function (McMaster et al., 2015; Schiffrin, 2014; Spirig et al., 2012). Thus, a better understanding of factors which influence immune homeostasis will be essential in order to develop novel strategies for disease prevention and treatment.

The data presented here showed a significant blunting of M(IL-4+IL-13) activation by a modest and physiologically relevant (Jantsch et al., 2015; Machnik et al., 2010; Wiig et al., 2013) increase in salt (NaCl). The salt-induced blunting of M(IL-4+IL-13) activation caused a similar functional impairment of M(IL-4+IL-13) macrophages *in vitro* and *in vivo*. In stark contrast to previous studies with pro-inflammatory M(LPS) macrophages (Jantsch et al., 2015) or Th17 cells (Kleinewietfeld et al., 2013; Wu et al., 2013), this effect was not mediated *via* Nfat5 or Sgk1.

Histone modifications are crucial for macrophage activation (Ishii et al., 2009; Satoh et al., 2010). The histone modifications analysed here (H3K4me3 and H4ac), were only mildly affected by salt upon stimulation with IL-4+IL-13 or LPS. However, genome-wide analysis of gene expression data suggested a marked influence of high salt on the cellular metabolism of unstimulated (M(0)), M(IL-4+IL-13) and M(LPS) macrophages. As cellular metabolism controls the activation and effector functions of various other immune cells (Chang et al., 2013; Everts et al., 2014), the effect of salt on M(IL-4+IL-13) and M(LPS) macrophage metabolism was further analysed.

Indeed, high salt blunted the metabolic activation and increase in oxidative phosphorylation of M(IL-4+IL-13) cells. This was associated with aberrant Akt and mTOR signalling and likely contributed to the phenotypic and functional alterations of M(IL-4+IL-13) activation observed with high salt. In contrast, high salt increased glycolysis in M(LPS) macrophages which may account for the boosting effect of high salt on pro-inflammatory macrophage activation (in addition to the previously identified mechanisms *via* Nfat5 signalling (Jantsch et al., 2015)).

Collectively, these data suggested cellular metabolism as a novel mechanism by which high salt affects macrophage activation. Interestingly, as similarly observed for gene expression and function, the effect of salt on macrophage cellular metabolism was not uniform, but differential according to the stimuli used to activate macrophages, i.e. IL-4+IL-13 or LPS. By reducing non-inflammatory (M(IL-4+IL-13) and augmenting pro-inflammatory (M(LPS)) macrophage activation (Figure 61), I hypothesize that high salt might considerably influence immune balance *in vivo* and possibly aggravate autoimmune and cardiovascular diseases.

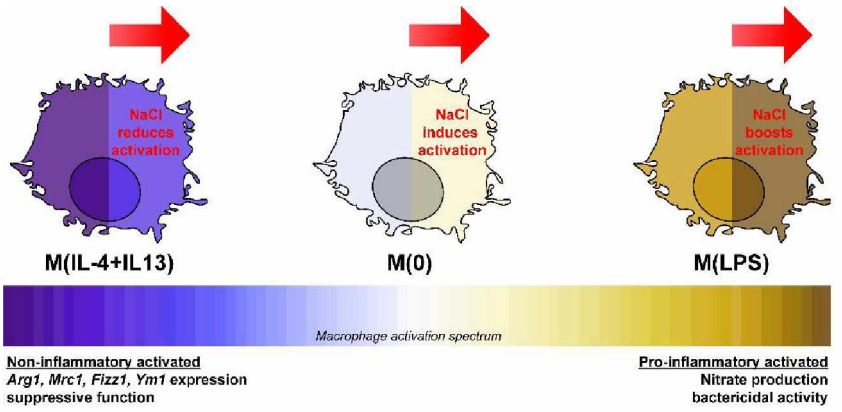

Figure 61. Summary of the effect of high NaCl on the activation of macrophages. In the presence of non-inflammatory signals (e.g. IL-4 and IL-13), NaCl reduces macrophage activation (this thesis). In contrast, with a pro-inflammatory stimuli (e.g. LPS), salt augments macrophage activation ((Jantsch et al., 2015) and this thesis). Furthermore, without a stimulus, M(0) macrophages exhibit an altered homeostasis (Ip and Medzhitov, 2015). Together, NaCl does not seem to have a general and non-specific effect on macrophages homeostasis, but rather, its effect is orchestrated by differentially modulating specific signaling pathways and cellular processes essential for macrophage activation.

4.1. Exploring the mechanisms by which high salt affects M(IL-4+IL-13) activation

In this study, high salt significantly blunted the activation of murine M(IL-4+IL-13) macrophages, as determined by the gene and protein expression of a typical set of signature genes (Murray et al., 2014; Raes et al., 2002; Raes et al., 2005) of M(IL-4+IL-13). The boosted activation of M(LPS) macrophages (Jantsch et al., 2015) was corroborated, and LPS-induced genes involved in bacterial killing (*Slamf1*) (Berger et al., 2010) were newly identified to be augmented by salt. Similar to recent studies addressing the effect of salt on pro-inflammatory Th17 cells (Kleinewietfeld et al., 2013) or M(LPS) (Jantsch et al., 2015), the

blunted activation of M(IL-4+IL-13) cells with salt was not mimicked by tonicity control experiments. This indicates that sodium chloride may affect cells *via* very specific mechanisms independent of the general osmotic stress response. First, the hypothesis that high salt may affect M(IL-4+IL-13) activation *via* histone modifications was explored.

4.1.1. Histone modifications

Differential modification of histones is an established epigenetic mechanism regulating gene expression and immune cell activation (Chang et al., 2014; Kouzarides, 2007). Histone modifications, particularly acetylation and methylation marks on histone tails, are crucial to regulate the activation of both alternatively activated M2 (Ishii et al., 2009; Mullican et al., 2011; Satoh et al., 2010) and pro-inflammatory M1 macrophages (Grabiec et al., 2010; Nicodeme et al., 2010). Our understanding of how environmental factors such as air pollution, smoking, toxins, engineered nanoparticles, drugs and diet affect cellular functions and ultimately health and disease *via* different epigenetic mechanisms is constantly increasing (Alegria-Torres et al., 2011; Barnes et al., 2005; Cooney et al., 2002; Dik et al., 2012; Edwards and Myers, 2007; Jirtle and Skinner, 2007; Smolkova et al., 2014). Furthermore, deliberate interference with epigenetic mechanisms is currently investigated in preclinical and clinical studies (Asangani et al., 2014; Bandukwala et al., 2012; Boi et al., 2015; Herait et al., 2015; Lochrin et al., 2014; Mele et al., 2013; Schones and Zhao, 2008). The effect of high salt on two activating histone marks (H3K4me3 and H4ac) upon stimulation of BMDM with IL-4+IL-13 or LPS was therefore examined using ChIP-seq (with parallel gene expression analysis by microarray) to elucidate, if high salt affected macrophage activation *via* epigenetic mechanisms. For both M(IL-4+IL-13) and M(LPS) macrophages the induction of several highly regulated signature genes was found to be associated with a marked increase in H3K4me3 and/or H4ac, corroborating the established function of these two histone marks for active gene expression (Kouzarides, 2007; Pokholok et al., 2005). On the other hand, a number of induced genes showed no substantial induction, or even a slight reduction, in H3K4me3 and/or Ha4c. This finding may indicate other histone modifications not analyzed here, such as H3K27me3 (Satoh et al., 2010), are important for regulating gene expression at these *loci*. Alternatively, this may simply reflect the dynamic nature of histone modifications (Clayton et al., 2006; Greer and Shi, 2012; Katan-Khaykovich and Struhl, 2002; Shi and Whetstine, 2007). A number of

recent studies suggested that histone marks at promoters and enhancers establish epigenetic landscapes, which foreshadow how cells are poised to respond to future stimuli. Alternatively, these marks depict past activation states (Lara-Astiaso et al., 2014; Lavin et al., 2014; Schones and Zhao, 2008; Winter and Amit, 2014). This fact may explain some of the discrepancies identified when comparing gene expression and H3K4me3/H4ac modification levels at a single time point: genes that were marked with H3K4me3/H4ac early after stimulation with IL-4+IL-13 or LPS, may maintain these histone modifications for a sustained period, whilst contrastingly, gene expression may have decreased and/or ceased. Activated macrophages might also initiate late gene expression programs, for example those which are initiated by negative feedback loops (Alexander and Hilton, 2004; Alexander et al., 1999; Cheng et al., 2014a; Song and Shuai, 1998; Yoshimura et al., 2005), and thus poised genes are established, which have modified histones but are not expressed (yet). Recent studies showing that posttranslational histone modifications can propagate across the cell cycle (Alabert et al., 2015), and how H3K4me3 mark breadth influences epigenetic regulation (Benayoun et al., 2014; Mukhopadhyay et al., 2014), emphasize both the relevance and complexity of the matter. Thus, additional and time-resolved studies are proposed to derive a fully comprehensive picture of the role of histone modifications during macrophage activation. Moreover, the study of additional histone marks, such as H3K4me1 or H3K27me3, demarcating gene enhancers or suppressed genes (Heintzman et al., 2007; Satoh et al., 2010; Schones and Zhao, 2008), respectively, is desirable to further clarify the contribution of epigenetic mechanisms on the effect of high salt on macrophage activation.

In this study, H3K4me3 and/or H4ac levels of M(IL-4+IL-13) signature genes were only mildly affected by salt even though salt significantly blunted the expression of these genes. The picture was similar for M(LPS) macrophages where most salt sensitive signature genes showed only a moderate modulation of H3K4me3/H4ac levels by salt. However, H3K4me3/H4ac levels of highly induced tonicity response genes were substantially increased in both M(IL-4+IL-13) and M(LPS) macrophages, and a number of significantly induced (expression) glycolysis genes in M(LPS) cells. Interestingly, the establishment of a highly glycolytic cellular metabolic state *via* histone modifications of glycolytic genes has recently been identified as one molecular mechanism of "trained immunity", i.e. the memory-like ability of innate immune cells to mount a stronger immune response upon reinfection (Cheng et al., 2014b; Netea, 2013; Quintin et al., 2012; Topfer et

al., 2015). The priming or silencing of specific gene sets during endotoxin tolerance, i.e. the refractory state of innate immune cells upon secondary endotoxin challenge, is also achieved *via* histone modifications (Biswas and Lopez-Collazo, 2009; Foster et al., 2007). The increase of histone marks of M(LPS) metabolic and effector genes observed here is therefore highly likely to contribute to the mechanisms by which high salt boosts M(LPS) activation (Jantsch et al., 2015).

4.1.2. Sgk1-Nfat5 signaling

Sgk1-Nfat5 signaling mediated the effect of high salt on pro-inflammatory Th17 cells and M(LPS) macrophages (Jantsch et al., 2015; Kleinewietfeld et al., 2013; Wu et al., 2013). In stark contrast, using genetic knock out models, signaling *via* Nfat5 or Sgk1 was not essential to mediate the effect of high salt on M(IL-4+IL-13) macrophage activation. Osmotic stress triggers signaling via the MAP kinase p38 (Denkert et al., 1998; Han et al., 1994), and both Sgk1 and Nfat5 are subsequently activated downstream of p38 to orchestrate the cellular response to hypertonicity (Aramburu et al., 2006; Kleinewietfeld et al., 2013; Küper et al., 2007; Lang et al., 2006; Meng et al., 2005; Zarubin and Han, 2005). Signaling *via* p38 is also activated in response to pathogen-associated bacterial infection and promotes inflammation (Han et al., 1994; Schieven, 2005; Schindler et al., 2007). Similarly, pro-inflammatory stimuli trigger Sgk1 and Nfat5 signaling independent of osmotic stress (Weintz et al., 2010; Wu et al., 2013) and there is substantial overlap between pro-inflammatory and osmotic stress signaling pathways. Indeed, hyperosmotic stress by high salt alone induced pro-inflammatory cytokine production in human peripheral blood mononuclear cells *via* p38 *in vitro* (Shapiro and Dinarello, 1995, 1997). For murine macrophages, it has recently been shown that increased tonicity by high salt is sufficient to induce a modest pro-inflammatory phenotype *via* p38 (Zhang et al., 2015) or inflammasome activation (Ip and Medzhitov, 2015) in the absence of additional pro-inflammatory signals. The previously described boosting of pro-inflammatory M(LPS) macrophages (Jantsch et al., 2015; Zhang et al., 2015) or T cells (Kleinewietfeld et al., 2013; Wu et al., 2013) by high salt further corroborated this interweaving of tonicity and inflammatory signaling. The contribution of hyperosmotic stress to inflammation and human disease is therefore intensively debated (Brocker et al., 2012; Dinarello, 2009; Neuhofer, 2010) and novel strategies to modulate inflammation *via* p38 and Nfat TF

signaling are currently explored for therapeutic use (Escolano et al., 2014; Schultze, 2014). In contrast, M(IL-4+IL-13) macrophages are not considered to be pro-inflammatory and signaling upon IL-4+IL-13 stimulation activates completely different pathways (Gordon, 2003; Murray et al., 2014). In a murine macrophage cell line, pre-activation with IL-4 even suppressed p38 activation in response to LPS (Hunt et al., 2002). The opposite (blunting) effect of high salt on the non-inflammatory immune cell type described here and by (Zhang et al., 2015) is therefore not surprising. Interestingly, two other recent studies addressing the effect of high salt on non-inflammatory immune cells concluded that Sgk1 was essential to mediate their blunted activation by salt (Hernandez et al., 2015; Safa et al., 2015). However, these studies investigated the effect of salt on regulatory T cells. While both regulatory T cells and M(IL-4+IL-13) activated macrophages are considered to be non-inflammatory and to possess immune regulatory properties (Huber et al., 2010; Sakaguchi et al., 2009; Yamaguchi et al., 2011), there is considerable morphological and functional differences between these cell types, which also employ discrete activation signaling pathways (Antov et al., 2003; Levine et al., 2014). Taking together the findings by (Hernandez et al., 2015; Jantsch et al., 2015; Kleinewietfeld et al., 2013) and the contributions made by the present study, a picture is emerging where high salt as one environmental factor could bias the immune system towards pro-inflammatory responses while the activation of non-inflammatory and regulatory cells is dampened. This would have significant implications for the development and treatment of a variety of diseases.

4.1.3. STAT6 signaling

STAT6 is a master TF of M2 macrophage activation downstream of the IL-4 receptor *in vitro* and *in vivo* (Burgis and Gessner, 2007; Gordon and Martinez, 2010; Mishra et al., 2011). Upon receptor activation by IL-4, STAT6 becomes phosphorylated, accumulates in the nucleus (Chen and Reich, 2010) and orchestrates the M2 transcriptional program. No effect of high salt on early STAT6 phosphorylation was detected in this thesis, while late phosphorylation was significantly blunted. STAT6 phosphorylation is sustained upon continuous IL-4 signaling *in vitro* and *in vivo* (Comfort and Haugh, 2008; Hanson et al., 2003; Perona-Wright et al., 2010). Similar to the results presented here, Zhang et al. have shown that high salt at a concentration similar to the one used here significantly blunted late STAT6 phosphorylation in murine BMDM activated with IL-4 (Zhang et al., 2015). In

their study, reconstitution of STAT6 signaling rescued the salt-blunted activation of M(IL-4) macrophages. Taken together, the results presented here and by Zhang et al. suggest a so far underappreciated role for sustained STAT6 signaling, which is vulnerable to osmotic stress by high salt, to support full M2 macrophage activation.

While Zhang et al. found an Erk1/2-STAT6 signaling cascade to mediate the salt effect on M(IL-4) macrophage activation (Zhang et al., 2015), additional signaling pathways by which high salt affects M(IL-4+IL-13) cell activation were identified in this study. IL-4 receptor downstream signaling *via* Akt synergizes with STAT6 to acquire full M2 macrophage activation *in vitro* and *in vivo*, and a significantly blunted M2 activation was observed upon experimental inhibition of Akt signaling (Byles et al., 2013; Ruckerl et al., 2012). Byles *et al.* identified mTOR, a downstream target of Akt signaling, as an additional regulator of IL-4-induced macrophage activation (Byles et al., 2013). In the experiments conducted for this thesis, high salt significantly blunted both Akt and mTOR activation of BMDM upon IL-4+IL-13 activation. Importantly, experimental reconstitution of Akt signaling upon stimulation with salt rescued the salt effect. Collectively, these data suggest that the impairment of Akt-mTOR signaling by salt constitutes a major and novel mechanism by which high salt may affect M(IL-4+IL-13) activation. Similar to these data, a pro-inflammatory shift was observed in monocytes, macrophages and dendritic cells with experimental inhibition of mTOR, which was reversible upon reconstitution of mTOR activity (Weichhart et al., 2008; Weichhart and Saemann, 2008). Of note, the salt-dependent blunting of mTOR signaling and M(IL-4+IL-13) activation in murine macrophages described in this thesis are in line with a study addressing the effect of prolonged rapamycin, an inhibitor of mTOR activation, treatment in humans where M2 macrophage activation was similarly decreased in favor of an M1 phenotypical bias (Mercalli et al., 2013).

4.2. The effect of high salt on macrophage metabolism

Since Akt-mTOR signaling is a known regulator of the cellular responses to changes in nutrient and energy availability (Byles et al., 2013; Haissaguerre et al., 2014; Schmelzle and Hall, 2000) and the gene expression analysis also indicated an effect of high salt on metabolic pathways, it was next analyzed whether the blunted signaling observed with high salt translated to changes in cellular metabolism. Different activation states of immune cells are characterized by bold differences in cellular metabolism (Haschemi et al.,

2012; O'Neill and Hardie, 2013; Rodriguez-Prados et al., 2010; Tan et al., 2015). Upon activation, M2 macrophages considerably increase their rate of OXPHOS using initially glucose (Tan et al., 2015) and later predominantly PPARγ-induced fatty acid oxidation to fuel mitochondrial respiration (Huang et al., 2014b; Odegaard et al., 2007; Vats et al., 2006). Importantly, M2 activation was also associated with enhanced mitochondrial metabolism in a murine helminth infection model *in vivo* (Thomas et al., 2012). Human primary monocytes were similarly primed into a non-inflammatory M2-like phenotype by PPARγ activation (Bouhlel et al., 2007; Charo, 2007), even though the precise contribution of fatty acid oxidation is less well understood for human M2 macrophages (Namgaladze and Brune, 2014). Similar to previous studies with M(IL-4) cells (Huang et al., 2014b), IL-4+IL13 activation led to increased OXPHOS; additionally glycolysis was significantly induced upon activation to M(IL-4+IL-13). While high salt did not influence the basal OCR of M(IL-4+IL-13) cells, it significantly reduced the mitochondrial respiratory reserve, glucose uptake and glycolytic flux of these cells. Collectively, these findings suggest a reduced energy availability necessary to support full M(IL-4+IL-13) activation in the presence of high salt. Mimicking these results, it was previously shown that chemical inhibition of fatty acid oxidation was shown to inhibit mitochondrial oxidation, marker gene expression and function of M(IL-4) macrophages (Huang et al., 2014b). This supports the proposed mechanism that high salt blunts M(IL-4+IL-13) activation by perturbing the metabolic adaptions necessary for full activation. Interestingly, a second non-inflammatory immune cell type, regulatory T cells, show decreased activation in the presence of high salt (Hernandez et al., 2015; Safa et al., 2015) and likewise utilize predominantly OXPHOS (Barbi et al., 2013; Michalek et al., 2011; Shi et al., 2011). Analysis of the effect of high salt on the metabolism of regulatory T cells would determine if this is a general mechanism, or specific to M(IL-4+IL-13) OXPHOS.

Pro-inflammatory M(LPS) macrophages and Th17 cells instead predominantly utilize glycolysis to meet their energetic needs (Barbi et al., 2013; Cramer et al., 2003; Garedew and Moncada, 2008; Shi et al., 2011), and, as mentioned before, the activation of both cell types was boosted by salt (Jantsch et al., 2014a; Kleinewietfeld et al., 2013). In this thesis, M(LPS) showed significantly increased expression of glycolysis genes and glycolytic flux in the presence of high salt. Thus, in contrast to M(IL-4+IL-13) cells, high salt supported the cellular adaptions necessary to fulfil the metabolic requirements of pro-inflammatory M(LPS) macrophages. NO is a major defense molecule of murine M(LPS) cells

and both *Nos2* gene expression and NO production were significantly increased by salt (Jantsch et al., 2015). Interestingly, excessive NO is thought to induce a state of "functional" hypoxia (Albina and Mastrofrancesco, 1993; Mateo et al., 1995) by its ability to inhibit the mitochondrial respiratory chain (Cassina and Radi, 1996; Cleeter et al., 1994; Maneiro et al., 2005; Moncada, 2000; Yamasaki et al., 2001). It is therefore not surprising that HIF-1α, a TF induced in response to hypoxia, is a major regulator of the activation of pro-inflammatory immune cells, such as M(LPS), and their associated metabolic adaptions (Cheng et al., 2014b; Cramer et al., 2003; Garedew and Moncada, 2008; Shi et al., 2011). Elevated NO concentrations can be sufficient to induce cell death of the same cells producing this NO, and/or neighboring cells (Albina et al., 1993; Stuehr and Nathan, 1989; Sveinbjornsson et al., 1996); this might be reflected by the GO analysis of M(LPS) gene expression analysis using GO terms where cell death related terms were identified even in the absence of salt. Taking into account that M(LPS) cells have increased NO production with high salt (Jantsch et al., 2015), it is possible that the boosted rate of glycolysis shown in this thesis, constitutes a crucial mechanism for salt-boosted M(LPS) cells to survive within a hostile microenvironment. Similar to this, glycolysis has recently been shown to sustain survival of NO-producing murine dendritic cells, which show a comparable glycolytic reprograming upon TLR activation (Everts et al., 2014; Everts et al., 2012). Taking into account many recent publications showing that the proper activation and functions of many different immune cell types depends on fine-tuned adaptions of cellular metabolism (Chang et al., 2013; Everts et al., 2014; Haschemi et al., 2012; Huang et al., 2014b; Man et al., 2013; O'Sullivan and Pearce, 2014; O'Sullivan et al., 2014), the results presented here suggest a mechanism by which a moderate increase in extracellular salt could affect a wide range of immune cells by its effect on cellular metabolism.

Besides NaCl, a number of additional components of the cellular environment, such as small metabolites, have been shown to substantially affect the activation of immune cells that experience this altered environment (Chang et al., 2013; Colegio et al., 2014; Tannahill et al., 2013). Macrophages, in particular, have been shown to be highly sensitive to their local environment and to integrate a wide range of input signals to yield a plethora of activation states (Ip and Medzhitov, 2015; Kratz et al., 2014; Lavin et al., 2014; Lumeng et al., 2007; Xue et al., 2014). The "Western" diet is not only rich in salt but also fat, protein and sugar (Manzel et al., 2014). It will therefore be essential to study the effect of different combinations of stimuli that might shape the behavior of a

given immune cell type in order to develop a more comprehensive picture. Additionally, a more detailed *in vivo* analysis of the electrolyte and metabolite composition of microenvironments where immune cells reside in would be highly desirable.

4.3. Exploring the functional implications of salt-blunted M(IL-4+IL-13) activation

To address the functional consequences of the observed salt-blunted M(IL-4+IL-13) activation, the ability of M(IL-4+IL13) macrophages activated in the absence or presence of salt to suppress T cell proliferation *in vitro* was compared. T effector cell suppression *via* PD-L2 is an established function of M2 activated macrophages (Carter et al., 2002; Huber et al., 2010; Latchman et al., 2001; Schebesch et al., 1997). Similar to previous results (Huber et al., 2010), M(IL-4+IL-13) cells dose-dependently suppressed T cell proliferation. Cells activated in the presence of salt had a significantly reduced ability to suppress $CD4^+$ T cell proliferation. Macrophages activated with IL-4+IL-13 in the absence or presence of salt additionally suppressed $CD8^+$ T cell proliferation as observed earlier (Huber et al., 2010). The effect of salt on $CD8^+$ T cell suppression by M(IL-4+IL-13) macrophages was not conclusive, however, most likely because $CD8^+$ T cell proliferation does not occur independently under the chosen conditions. Instead, it depends on $CD4^+$ T cell proliferation as a source of IL-2 (D'Souza and Lefrancois, 2003, 2004; Keene and Forman, 1982; Lai et al., 2009) which was – in contrast to (Huber et al., 2010) – not supplemented in the assays described here. The importance of the suppressive function of M2 macrophages was demonstrated in a murine *Schistosoma mansoni* infection model (Herbert et al., 2004). Here, M2 macrophages dampened the initial inflammatory response during acute infection and the experimental abrogation of M2 macrophages caused 100% early-phase mortality by uncontrolled inflammation (Herbert et al., 2004). As several mechanisms triggered by worm infection *in vivo* are conserved between rodents and humans (He et al., 2008; Marquet et al., 1996; Peisong et al., 2004; Perrigoue et al., 2008; Thomas et al., 2012), it is plausible that high salt influences anti-helminth immune responses in humans. It is important to emphasize here that the effect of salt on immune cell activation may not always be adverse. For example, while the salt-induced boost of pro-inflammatory Th17 cells aggravated experimental autoimmune encephalomyelitis (Kleinewietfeld et al., 2013), Th17 cells also possess physiological functions in fighting

bacterial, fungal and viral infections (Peck and Mellins, 2010; van de Veerdonk et al., 2009), and thus enhanced activation may prove beneficial under these circumstances. For macrophages, the salt-augmented activation of M(LPS) was beneficial to combat experimental *L. major* infection (Jantsch et al., 2015); again evidence for the beneficial effect of high salt. Furthermore, it was shown that patients with infected tissue had an accumulation of sodium at these sites, and thus salt loading might represent a mechanism to increase the barrier function of the skin *via* increased activation of pro-inflammatory immune cells (Jantsch et al., 2015).

To test the relevance of salt-blunted M(IL-4+IL-13) activation *in vivo*, the effect of an experimental high salt diet (HSD) on a chitin-induced peritoneal M2 activation model and on dermal wound healing was tested. Chitin is found in both infectious worms and their egg shells (Perrigoue et al., 2008), and it was shown that the injection of homogenized chitin into the peritoneal cavity induces M2 macrophage activation in an IL-4-dependent manner (Reese et al., 2007). Several recent publications used this model to study M2 macrophage activation *in vivo* (Byles et al., 2013; Satoh et al., 2010). In line with the *in vitro* observations, prolonged (14 day) HSD prior to chitin injection significantly blunted the expression of M2-associated marker genes specifically in peritoneal macrophages, while the general composition of the peritoneal immune exudate upon chitin administration was not affected by dietary salt intake. This indicates that high salt attenuates M2 activation *in vivo*. The question remains, however, whether dietary salt affects peritoneal macrophages directly or indirectly. It is plausible to assume that a prolonged HSD might affect other immune cell types and physiological processes *in vivo*. Eosinophils are of special interest here. Whilst M2 activated macrophages are known to recruit this innate immune cell type (Kreider et al., 2007; Reese et al., 2007; Voehringer et al., 2007), eosinophils in turn have been shown to sustain resident M2 macrophages in tissues and to constitute a major source of tissue IL-4 (Wu et al., 2011). This complex interplay makes it a very interesting question to examine whether and how high salt would affect this innate immune cell type. Considering the fundamental role of IL-4/IL-13 signaling in shaping Th2 immunity *in vivo* (Shimoda et al., 1996), with substantial implications for host protection against helminth infection and for the development of allergies (O'Shea et al., 2002; Paul and Zhu, 2010), additional experiments to test the effect of high salt on other IL-4+IL-13-activated immune cell types is necessary. This will

especially help to establish if the molecular mechanism elucidated in this thesis for M(IL-4+IL-13) macrophages holds true for other IL-4+IL-13-activated cells.

Wound healing is a complex process requiring different cell types and functions at different times to resolve initial inflammation and to repair the injured tissue (Agaiby and Dyson, 1999; Martin, 1997). Wound healing has been described as a major effector function of M2 macrophages and they are believed to contribute to the resolution of inflammation (Deonarine et al., 2007; Mosser and Edwards, 2008), even though it is now known that they are not solely responsible (Martin et al., 2003; Stout, 2010). To test the effect of high salt on this process, two cutaneous back wounds were inflicted to wildtype mice. Mice were then fed a HSD or normal salt diet (NSD) and monitored for 14 days. While initially dietary salt intake did not affect wound closure, mice on HSD had significantly delayed wound healing during later stages. Importantly, while incomplete wound healing after 14 days was very rare in mice on NSD (1/13), nearly half of the wounds (6/13) of the mice on HSD were not completely healed after 14 days. These findings are very similar to a recent study where M2 activation was perturbed by a macrophage-specific knockout of *Klf4* (Liao et al., 2011). Collectively, the data presented here demonstrate that HSD delays cutaneous wound healing to a similar extent as that observed in macrophage-specific genetic models of impaired M2 activation. As HSD additionally reduced the expression of M2 signature genes in wound samples, it is plausible to assume that HSD may affect wound healing *via* impaired activation of M2 macrophages *in vivo.* However, wound healing is accomplished by the complex interplay of many different cell types (Agaiby and Dyson, 1999; Havran and Jameson, 2010; Sasaki et al., 2008; Toulon et al., 2009). Moreover, the extracellular matrix plays a pivotal role during wound healing (Olczyk et al., 2014; Raghow, 1994; Wong et al., 2012) and high dietary sodium has been hypothesized to be stored there in the skin (Farber, 1960; Farber et al., 1957; Ivanova et al., 1978; Jantsch et al., 2015; Machnik et al., 2009; Wiig et al., 2013). This extra sodium may cause alterations of the mechanical or functional properties of the extracellular matrix. It is therefore not possible to exclude that high salt may, in addition to its effect on M2 macrophages, cause the observed delay in wound healing partly by non-specific actions on other cell types or the tissue itself. Thus, to further establish the effect of high salt on M2 activation *in vivo*, it is proposed to study additional functional M2 models, such as *Schistosoma mansoni* infection (Herbert et al., 2004).

4.4. Concluding remarks and outlook

The salt-induced blunting of M(IL-4+IL-13) macrophage activation and function described in this thesis contributes to our current understanding of how and by which mechanisms environmental cues shape immune cell activation. Taking together the findings presented here and other recent studies, it is tempting to speculate that high salt modulates the two arms of the immune system differentially: there is increased activation of pro-inflammatory Th17 cells (Kleinewietfeld et al., 2013; Wu et al., 2013) and innate M(LPS) macrophages (Jantsch et al., 2015), while the activation of regulatory T cells (Hernandez et al., 2015; Safa et al., 2015) and non-inflammatory M(IL-4+IL-13) macrophages (this thesis) is blunted. This notion constitutes a putative link between high dietary salt intake and impaired immune homeostasis, leading to the increasing epidemic of human autoimmune and pro-inflammatory disorders with the "western lifestyle" (Lucca and Hafler, 2015; Manzel et al., 2014).

The relevance of the findings presented here is emphasized by the fact that salt storage also occurs *in vivo*. Hypertonic salt-loaded environments are found in experimental animals on HSD, especially in the skin interstitium, where residing macrophages act to regulate and restore interstitial electrolyte balance (Go et al., 2004; Machnik et al., 2009; Szabo and Magyar, 1982; Wiig et al., 2013). As immune cells often enter the interstitium, for example upon tissue damage or infection, it is therefore plausible to hypothesize that under conditions of dietary salt excess, the concentration of sodium that immune cells are exposed to may be high. In rats, dietary salt restriction can result in sodium being removed from these interstitial stores (Schafflhuber et al., 2007). Importantly, salt storage is also observed in humans during infection, states of perturbed electrolyte homeostasis, high blood pressure patients or with increasing age (Jantsch et al., 2015; Kopp et al., 2013b; Kopp et al., 2012a; Kopp et al., 2012b; Rakova et al., 2013). Similar to experimental animals, salt can again be mobilized from tissue stores (Dahlmann et al., 2015). First studies linking disease progression of multiple sclerosis (Farez et al., 2015) or the risk to develop rheumatoid arthritis (Sundstrom et al., 2015) to high dietary salt intake in patients hint to a similar role of salt in modulating immune cell function in humans and animals. However, care should be taken whenever findings made in experimental animals are to be extrapolated to the human situation, even though animal models are still considered a useful research tool (Lam-Tse et al., 2002). While basic principles of the immune response are conserved between humans and experimental animals (He et al.,

2008), the biology of human immune cells and particularly macrophages is still far less understood (Martinez et al., 2006) and may show marked differences in particular cases (Gross et al., 2014; Namgaladze and Brune, 2014). A strong future focus on research with human material, healthy volunteers and patients would therefore be highly desirable, to complement the complex picture evident so far. This may pave the road towards relatively easy-to-adopt low-sodium dietary regime as a treatment option for diseases associated with disturbed immune homeostasis.

5. Appendix

5.1. Tables of gene expression data

Table 3. The top 50 induced M(IL-4+IL-13) activation genes. The top 50 induced M(IL-4+IL-13) vs M(0) genes are presented according to their expression FC (from high to low). Mean signal intensities (expression) or ChIP-seq counts 4kb around annotated transcription start sites (H3K4me3 and H4ac) are shown.

Gene symbol	Expression M(0)	Expression M(IL-4+IL-13)	H3K4me3 M(0)	H3K4me3 M(IL-4+IL13)	H4ac M(0)	H4ac M(IL-4+IL-13)
Ear11	120	55889	12	429	144	705
Retnla	145	61781	6	1070	165	1074
Arg1	141	26642	215	1099	453	832
Cldn11	110	6514	33	197	73	196
Ccl24	131	7331	78	642	114	370
Chi3l3	338	14392	5	89	76	635
Cish	215	6452	717	1459	596	584
Socs2	232	6488	483	793	145	351
Ear2	110	2941	17	109	128	171
Ear10	127	3224	165	198	168	270
Bhlhe40	210	4489	1124	1702	460	1002
F10	278	5931	43	101	546	1121
Lipn	190	3779	74	589	237	409
Mgl2	639	9626	149	1207	263	971
Gpc1	741	10985	218	715	82	241
Pdcd1lg2	124	1822	10	559	161	581
Pdlim1	139	1825	334	541	78	230
Apol7c	149	1878	9	259	51	181
Vwf	398	4982	128	79	275	222
AA467197	1064	12020	274	446	258	294
Ccl17	112	1246	39	65	90	107
Egr2	610	6734	704	737	315	552
Il31ra	110	1166	11	6	90	139
Ear14	125	1237	9	12	79	512
Hebp2	128	1216	320	596	250	494
Klf9	418	3754	966	1295	544	808
P2ry1	303	2660	880	1463	332	448
Irf4	235	1983	700	1203	373	409
Diras2	209	1618	103	317	245	383
Batf3	500	3790	472	1203	240	485
Aqp9	125	945	59	43	150	186
Snn	440	3266	348	490	212	317
Tarm1	118	853	110	730	331	535
F7	176	1262	75	233	321	766
Flt1	152	1034	357	1028	106	264
Tfrc	4933	31898	865	1298	404	466
Chchd10	468	2946	359	390	249	266
Plekhf1	165	1027	544	1338	387	570
Ppargc1b	287	1673	1016	1049	470	476
Ciita	278	1578	148	576	173	200
Msx3	112	629	675	1297	193	1106
Ddhd1	234	1316	967	1098	960	890
Slc27a3	148	824	107	286	137	159
Nfil3	1256	6975	1603	1787	685	1305
Mcf2l	133	727	185	173	157	135
Cd74	8159	40537	436	1117	477	1029
Adipoq	132	658	16	289	200	424
Pdia4	1515	7484	1304	1657	755	906
Tuba8	122	583	67	379	28	81
Ier3	2263	10613	1428	1334	738	874

Table 4. The top 50 reduced M(IL-4+IL-13) activation genes. The top 50 reduced M(IL-4+IL-13) vs M(0) genes are presented according to their expression FC (from high to low). Mean signal intensities (expression) or ChIP-seq counts 4kb around annotated transcription start sites (H3K4me3 and H4ac) are shown.

Gene symbol	Expression M(0)	Expression M(IL-4+IL-13)	H3K4me3 M(0)	H3K4me3 M(IL-4+IL13)	H4ac M(0)	H4ac M(IL-4+IL-13)
Cxcl10	5003	143	730	247	675	263
Ifit3	15477	456	784	302	693	456
Ly6a	20285	644	407	36	422	111
Fpr2	7057	225	358	63	481	203
Rsad2	27153	1141	1552	789	837	802
Ifit2	13588	662	1103	514	1042	816
Irf7	5427	360	1302	679	895	407
Nfkbiz	4005	266	917	658	713	639
Cmpk2	8001	591	1436	837	882	575
Isg15	3968	382	1457	679	1079	666
Fcgr1	8912	874	1408	828	1389	621
Slfn1	2319	238	831	246	1357	514
Cd69	1569	161	815	367	618	405
Mx2	2045	216	1695	868	1326	970
D14Ertd668e	4138	457	1040	475	998	695
Arap3	4746	559	691	273	614	364
Il1b	2072	245	157	33	259	166
Hpgds	2059	261	1448	938	1151	1012
Ifitm6	2522	324	845	140	859	368
Pilrb1	1032	142	238	24	268	53
Oasl2	4839	675	1366	957	1540	946
Fam26f	2844	398	1110	814	1079	810
Tlr2	7423	1042	1314	835	866	710
Oas2	7945	1119	1523	841	1482	895
Isg20	955	135	1444	780	1579	1071
Cp	1525	228	746	305	482	341
Oasl1	1155	173	1857	764	1532	935
Ly6e	13580	2039	1412	658	892	202
Cd14	29599	4543	1679	1209	1368	1052
Cx3cr1	817	127	235	23	192	73
Adrb2	1717	268	1675	981	689	609
St3gal6	882	138	333	286	111	112
Igfbp4	6074	961	1462	839	1037	826
Slc40a1	7951	1261	960	565	368	355
BC006779	2218	355	1183	675	744	386
Siglec1	7573	1237	1021	429	1549	1069
Slamf9	14645	2403	803	246	717	342
Igtp	7035	1164	1069	638	570	602
Plac8	1058	188	389	84	298	148
Mx1	959	178	1511	806	1376	762
Slc13a3	941	175	112	40	128	74
Ifi47	4610	889	377	168	429	246
Ddx58	2021	391	1384	1008	867	678
Irgm2	7381	1432	1202	755	819	695
Gpr162	742	151	809	257	509	235
Rtp4	1135	235	1603	1278	2154	1285
Abi3	2082	436	1368	623	714	535
Dhx58	7841	1666	1133	853	1047	811
Fnbp1l	5251	1118	1373	908	458	406
Lst1	12820	2750	1621	917	1209	1185

Table 5. The top 50 salt-sensitive (increased by salt) M(IL-4+IL-13) signature genes. The top 50 salt-sensitive (increased by high salt) M(IL-4+IL-13) signature genes are presented according to their expression FC (from high to low M(IL-4+IL-13)+40mM NaCl vs M(IL-4+IL-13)). Mean signal intensities (expression) or ChIP-seq counts 4kb around annotated transcription start sites (H3K4me3 and H4ac) are shown.

Gene symbol	Expression M(IL-4+IL-13)	Expression M(IL-4+IL-13) +40mM NaCl	H3K4me3 M(IL-4+IL13)	H3K4me3 M(IL-4+IL13) +40mM NaCl	H4ac M(IL-4+IL13)	H4ac M(IL-4+IL-13) +40mM NaCl
Slc6a12	342	4759	111	538	259	590
Scd1	649	1805	677	746	272	355
Dut	266	582	748	610	567	590
Adamtsl5	408	817	334	301	181	170
Dnase2a	929	1854	961	966	500	502
Galnt9	290	579	9	6	13	21
Mmp12	3224	6264	302	350	726	1087
Adipoq	658	1264	289	305	424	507
Gpc1	10985	20458	715	767	241	285
Chchd10	2946	5423	390	406	266	275
Hvcn1	2377	4350	42	43	190	228
Glt25d1	7805	14262	1118	1111	836	901
Slamf8	1712	3117	699	841	657	800
Large	871	1577	952	957	469	493
Igsf3	184	329	174	165	86	124
Hmg20b	1076	1844	732	755	396	405
Ctsz	15786	26879	1534	1604	1383	1483
Ctsk	1358	2295	113	149	1382	1603
Anpep	12169	20471	1372	1431	658	729
Csf2rb2	2300	3860	1378	1416	769	809
Capg	4745	7830	833	922	852	924
Acaca	1587	2614	448	389	367	340
Abcg1	2819	4613	1402	1380	646	829
Bhlhe40	4489	7255	1702	1788	1002	1404
4930471M23Rik	481	777	1570	1558	988	1018
Sgsm3	379	599	415	411	432	363
Mical1	375	592	879	885	976	987
Abcb8	538	829	503	538	913	963
Eef1a2	269	413	49	58	73	91
Dpp7	12174	18647	1196	1201	382	380
Vat1	8507	12880	1547	1463	748	692
Slc39a11	3800	5748	677	662	614	608
Atf3	5834	8797	1659	1738	1434	1743
Wdr74	858	1288	646	620	725	728
Apbb2	635	954	968	940	441	423
Dhcr7	322	479	647	596	672	681
Csf2ra	2761	4104	443	445	600	660
Vps18	2999	4442	1071	1045	840	873
Mvd	1827	2705	1317	1277	506	474
Tmem120b	406	601	10	8	95	93
Scgb1a1	153	226	16	13	147	144
Inpp5a	2291	3364	1084	1135	589	650
Tnfrsf12a	321	469	843	919	344	330
Ryr1	373	545	52	51	58	59
Isyna1	935	1365	429	406	302	280
Taf6l	306	445	527	506	343	371
Rrp12	899	1291	718	652	715	636
Stac2	661	948	466	499	402	524
Pi4ka	923	1322	1628	1499	594	469
Fastk	368	528	640	555	493	463

Table 6. The top 50 salt-sensitive (decreased by salt) M(IL-4+IL-13) signature genes. The top 50 salt-sensitive (decreased by high salt) M(IL-4+IL-13) signature genes are presented according to their expression FC (from high to low M(IL-4+IL-13)+40mM NaCl vs M(IL-4+IL-13)). Mean signal intensities (expression) or ChIP-seq counts 4kb around annotated transcription start sites (H3K4me3 and H4ac) are shown.

Gene symbol	Expression M(IL-4+IL-13)	Expression M(IL-4+IL-13) +40mM NaCl	H3K4me3 M(IL-4+IL13)	H3K4me3 M(IL-4+IL13) +40mM NaCl	H4ac M(IL-4+IL13)	H4ac M(IL-4+IL-13) +40mM NaCl
Mgl2	9626	3166	1207	919	971	1097
Lyzl4	1791	709	415	362	433	441
Ccl24	7331	2928	642	542	370	381
Slc39a12	486	204	6	4	56	44
Pdlim1	1825	778	541	385	230	182
Syngr2	3689	1589	770	735	460	417
Apol7c	1878	810	259	100	181	118
Slamf1	379	165	440	122	246	206
Gja1	1020	464	937	796	300	303
Ccl7	3811	1792	776	485	454	470
Cst7	563	265	292	168	494	465
Tarm1	853	427	730	551	535	689
Snx6	6674	3347	1244	1051	653	641
Ccl17	1246	657	65	48	107	164
Msx3	629	334	1297	1090	1106	1295
Ppbp	259	141	12	13	150	140
Uck2	936	514	768	677	337	332
Snn	3266	1817	490	397	317	292
Cbr2	3319	1863	109	73	645	739
Ear2	2941	1654	109	103	171	231
Snx9	1482	836	1422	1174	643	662
Chi3l3	14392	8245	89	87	635	566
Cytip	9395	5393	52	38	286	256
Nrg1	402	233	168	135	54	43
Tesk1	355	210	615	574	374	366
Ear10	3224	1914	198	176	270	282
Galm	1601	953	588	611	1557	1616
Diras2	1618	983	317	237	383	390
5730494M16Rik	1374	842	911	804	598	603
Batf	742	468	632	605	549	582
Socs2	6488	4102	793	754	351	407
Creld2	3373	2146	935	843	414	400
Clec10a	2923	1877	543	491	855	1022
Prkrir	684	441	1382	1229	645	624
Aqp9	945	609	43	33	186	197
Etv3	1783	1150	1466	1424	920	1173
Arl4c	1862	1206	1150	1167	820	904
Ppp1r3c	376	243	217	193	175	188
Pdcd1lg2	1822	1190	559	510	581	662
Casp6	3495	2286	913	863	549	658
Hfe	2851	1866	853	818	1025	1164
Ear14	1237	812	12	17	512	607
Cenpa	12284	8077	1015	859	855	848
Tuba8	583	384	379	282	81	112
Pdlim4	11594	7677	779	697	607	631
H2-Eb1	7407	4925	500	434	716	978
Pfkp	748	499	1323	1322	864	1028
Eif5a	5641	3769	1083	1120	1005	1127
Cish	6452	4314	1459	1368	584	599
Hebp2	1216	818	596	541	494	547

Table 7. The top 50 induced M(LPS) activation genes. The top 50 induced M(LPS) vs M(0) genes are presented according to their expression FC (from high to low). Mean signal intensities (expression) or ChIP-seq counts 4kb around annotated transcription start sites (H3K4me3 and H4ac) are shown.

Gene symbol	Expression M(0)	Expression M(LPS)	H3K4me3 M(0)	H3K4me3 M(LPS)	H4ac M(0)	H4ac M(LPS)
Arg1	141	9518	215	578	453	683
Lcn2	1029	41778	21	617	219	594
Gdf15	495	14313	434	569	460	705
Cxcl9	362	7789	22	33	108	113
F10	278	4868	43	438	546	1252
Hmox1	1344	21835	1152	1490	537	887
Socs3	767	12399	587	764	185	272
Samd8	250	3915	924	1133	623	823
2310016C08Rik	598	8638	848	1276	607	973
Hp	229	3187	88	477	325	461
AA467197	1064	13212	274	578	258	327
Gadd45b	674	7266	1446	1443	519	511
Ankrd37	292	2988	812	1225	748	868
Slpi	868	8647	65	64	74	93
Saa3	5678	55580	176	1082	376	660
Ppp1r15a	489	4647	1278	1452	901	1039
Cd274	4147	39318	1968	2100	1112	1621
Clec4e	696	6243	847	1552	689	1361
Ccrl2	332	2952	1295	1839	1025	1662
Mreg	124	1050	261	392	87	167
Gadd45g	797	6610	1273	1281	652	440
Ptges	119	953	681	799	975	1416
Eno2	296	2350	502	730	315	500
Cfb	296	2334	169	1016	305	502
Rhov	145	1105	455	899	302	342
Prss46	130	973	14	26	151	405
Ccl5	7039	52287	141	1213	209	550
Acsl1	592	4192	767	1149	589	755
2310044G17Rik	1332	9267	1756	1999	1000	1234
Bzrap1	424	2942	151	301	325	350
Rragd	165	1096	525	454	144	177
Il1a	133	848	79	944	156	757
Gm5483	335	2119	9	9	30	54
Gde1	2007	12539	628	1229	716	1127
Gadd45a	477	2960	897	892	495	482
Slc22a4	159	974	820	1463	946	1160
Ppap2b	162	989	607	837	222	287
Ifnb1	175	1066	65	156	257	354
Cst7	186	1124	156	543	439	546
Csrnp1	785	4627	675	1075	952	425
Htr2b	344	2006	217	908	408	767
Id2	265	1519	1998	2108	944	1205
Bhlhe40	210	1190	1124	1370	460	728
Pik3cb	803	4449	1133	1181	600	667
Gpc1	741	3990	218	437	82	129
Nupr1	2788	14535	458	591	1036	912
Slc2a1	1343	6999	965	1223	719	609
Pim3	582	2977	595	555	536	595
Cpeb2	189	941	1036	881	710	579
Lhfpl2	5453	27158	328	364	118	242

Table 8. The top 50 reduced M(LPS) activation genes. The top 50 reduced M(LPS) vs M(0) genes are presented according to their expression FC (from high to low). Mean signal intensities (expression) or ChIP-seq counts 4kb around annotated transcription start sites (H3K4me3 and H4ac) are shown.

Gene symbol	Expression M(0)	Expression M(LPS)	H3K4me3 M(0)	H3K4me3 M(LPS)	H4ac M(0)	H4ac M(LPS)
Slco2b1	5925	149	61	24	694	250
Mrc1	15080	773	1751	837	1046	803
Igfbp4	6074	369	1462	896	1037	433
Arap3	4746	291	691	356	614	450
Fcrls	7825	628	610	206	672	210
Cytip	5745	562	47	29	181	205
Cyp27a1	7063	716	1905	1037	1243	726
Rnase6	1442	147	647	275	759	305
Tmem176b	9041	961	919	447	612	185
Trf	9391	1008	737	266	893	309
Sepp1	9882	1155	199	154	541	433
Pbk	1006	118	490	351	269	226
Sult1a1	1148	146	105	39	727	453
Adrb2	1717	230	1675	1251	689	481
Sesn1	2214	299	1682	1472	650	566
Clec10a	868	128	389	170	732	231
Tfrc	4933	750	865	560	404	306
Rnd3	1164	180	1073	925	405	288
St6gal1	10973	1704	1343	1031	835	520
Birc5	1053	166	1134	1044	1054	795
Mcm5	3469	585	759	582	569	516
St3gal6	882	149	333	212	111	68
Abcb1b	1441	245	787	655	560	525
Fgd2	4989	871	1027	713	501	246
Slc46a3	10815	1892	1046	763	846	574
Il16	1013	178	10	8	121	74
Lbr	1672	299	998	742	444	245
Gpr65	4511	824	1673	1346	1083	806
S100a9	2443	447	13	14	44	57
Nfkbiz	4005	749	917	988	713	635
Clec4b1	1995	381	412	71	647	231
2810417H13Rik	698	135	639	524	358	391
Cdca7	893	174	884	731	483	355
Tlr2	7423	1459	1314	1111	866	637
Hpgd	526	104	546	337	453	222
Tmem51	7230	1460	743	511	364	234
Pros1	2860	588	712	503	658	592
Dok2	6178	1271	1110	1004	549	495
Top2a	1077	229	972	843	592	466
Ptpro	1824	412	5	6	27	30
Ephx1	1917	435	11	10	74	55
Wtip	828	188	120	42	118	43
Cdc42ep3	1281	296	1188	754	513	213
Prc1	2316	535	733	678	408	464
Cyp4f18	1350	315	281	103	888	361
Man1a	584	142	1528	1217	713	572
Smagp	1020	249	759	452	452	292
Rad54b	552	135	522	426	785	843
Cd14	29599	7313	1679	1421	1368	1214
Slc9a9	854	211	1623	1079	1211	913

Table 9. The top 50 salt-sensitive (increased by salt) M(LPS) signature genes. The top 50 salt-sensitive (increased by high salt) M(LPS) signature genes are presented according to their expression FC (from high to low M(LPS)+40mM NaCl vs M(LPS)). Mean signal intensities (expression) or ChIP-seq counts 4kb around annotated transcription start sites (H3K4me3 and H4ac) are shown.

Gene symbol	Expression M(LPS)	Expression M(LPS) +40mM NaCl	H3K4me3 M(LPS)	H3K4me3 M(LPS) +40mM NaCl	H4ac M(LPS)	H4ac M(LPS) +40mM NaCl
Slc6a12	401	4170	136	848	126	562
Hspa1a	1168	11399	379	493	422	650
Flrt3	202	774	686	703	205	241
Hsph1	1666	5345	1128	1274	418	618
Il19	211	630	45	83	96	85
Ctsk	744	2191	251	603	2005	1996
1190002H23Rik	593	1718	436	640	264	378
Tnfrsf26	303	862	1632	2280	1246	1570
Slamf1	231	650	557	973	217	286
Aqp9	338	945	78	98	262	391
Slc2a1	6999	19331	1223	1459	609	909
Nos2	492	1330	1445	1932	955	1418
Tnfsf9	232	626	1409	1903	643	886
Dnmt3l	720	1870	36	31	80	78
Hamp	169	433	48	78	171	304
AC068006.1	1085	2728	8	44	152	454
Pdlim7	322	765	389	566	145	321
Niacr1	206	488	413	706	217	466
Arg2	472	1120	834	1132	368	626
Adamtsl5	619	1411	302	446	139	217
Slc7a11	338	746	1020	1232	1302	1277
Gclm	2238	4908	1137	1248	813	828
Cdkn2b	492	1067	655	708	393	335
Dcn	298	639	28	42	92	126
Slpi	8647	18066	64	84	93	131
Gadd45g	6610	13736	1281	1471	440	740
Jdp2	541	1118	1189	1460	378	814
Panx1	1170	2408	813	1053	472	673
Dedd2	621	1275	1502	1803	718	1039
Nlgn2	272	558	970	1174	511	524
Hyal1	1311	2689	901	1134	728	1010
Wdr20b	266	543	3	4	32	38
Fzd7	1393	2806	1145	1462	723	856
Hist1h2bk	1587	3197	635	702	248	313
Ankrd37	2988	5994	1225	1301	868	913
Gstm2	772	1545	61	129	257	347
Chchd10	2241	4443	343	427	259	316
Prss46	973	1919	26	54	405	716
Ambp	268	516	17	35	82	140
Mgst2	523	1000	199	315	392	435
Klhl21	673	1287	1025	1171	614	725
Procr	180	342	870	1434	657	909
Malt1	597	1131	1383	1419	1188	1210
Inhba	375	709	447	582	638	628
Ccl2	636	1202	579	891	263	392
Edn1	192	360	1262	1328	262	356
Diras2	442	826	139	185	325	394
Afg3l2	433	806	766	1156	754	919
Sell	1404	2584	376	618	329	298
Batf	806	1468	987	1258	510	635

Table 10. The top 50 salt-sensitive (decreased by salt) M(LPS) signature genes. The top 50 salt-sensitive (decreased by high salt) M(LPS) signature genes are presented according to their expression FC (from high to low M(LPS)+40mM NaCl vs M(LPS)). Mean signal intensities (expression) or ChIP-seq counts 4kb around annotated transcription start sites (H3K4me3 and H4ac) are shown.

Gene symbol	Expression M(LPS)	Expression M(LPS) +40mM NaCl	H3K4me3 M(LPS)	H3K4me3 M(LPS) +40mM NaCl	H4ac M(LPS)	H4ac M(LPS) +40mM NaCl
Cst7	1124	472	543	377	546	381
Slc16a6	741	367	1086	1108	519	930
Ccng1	3067	1557	956	825	1122	1008
Bzrap1	2942	1555	301	422	350	380
Phyhd1	1572	895	870	838	1504	1446
Samd8	3915	2448	1133	1208	823	1085
Aldh1b1	1175	753	941	915	688	644
Tspan33	285	184	281	277	122	125
Plxna2	1557	1053	843	915	384	529
Dera	688	474	671	653	488	514
Xrcc1	1776	1231	595	623	925	1064
Dtnb	355	247	509	585	422	518
Ldlrap1	709	494	1153	1262	242	412
B9d1	294	206	214	242	362	399
Gpr157	728	513	939	1011	382	542
Ass1	1602	1134	599	723	215	278
Sertad1	1540	1091	1575	1725	449	699
Rxra	547	394	374	395	156	221
Oasl1	3252	2350	2225	2304	1754	1526
Septin8	1461	1062	708	776	339	474
Mmp14	4713	3460	1018	1144	479	652
Sec13	11592	8540	747	735	1046	887
Psmb1	10359	7641	1804	1684	929	1007
Dnahc2	575	425	71	91	64	88
Adap2	5084	3758	1213	1478	755	957
Rabl3	1612	1198	833	853	1394	1243
Nosip	711	532	1020	1003	1023	931
Mreg	1050	785	392	379	167	248
Rragd	1096	827	454	440	177	268
Ccdc66	245	186	643	629	898	646
Med21	2180	1652	927	970	675	771
3110040N11Rik	1627	1234	970	1005	986	922
Tmcc3	339	257	332	390	121	123
Gpr35	304	231	815	800	1164	1112
Ppp1r3c	294	224	254	236	172	164
Tbcb	5380	4110	798	914	382	516
Lasp1	2034	1559	897	1012	293	458
Tmem65	10489	8051	1197	1186	399	617
C1rl	271	210	340	349	559	636
Cox18	1385	1073	921	895	1016	798
1700026L06Rik	472	368	544	596	427	461
Sar1b	3419	2676	855	851	913	924
Tiam2	170	133	215	267	65	64
Ttc1	3280	2579	733	729	913	827
Smurf1	640	506	517	616	198	321
Stau1	1988	1571	1221	1216	691	711
I830077J02Rik	1356	1075	947	895	608	589
Acss1	3338	2648	907	910	554	686
Mdk	232	185	27	34	180	209
Snupn	1002	798	802	777	750	642

5.2. Publications

5.2.1. Peer-reviewed publications arising from this thesis

Binger, K.J.*, **Gebhardt, M.***, Heinig, M., Rintisch, C., Schroeder, A., Neuhofer, W., Hilgers, K., Manzel, A., Schwartz, C., Kleinewietfeld, M., Voelkl, J., Schatz, V., Linker, R.A., Lang, F., Voehringer, D., Wright, M.D., Hubner, N., Dechend, R., Jantsch. J., Titze, J., Muller, D.N., (2015). High salt reduces the activation of IL-4- and IL-13-stimulated macrophages. J Clin Invest, *in press*, * joint first-author

5.2.2. Peer-reviewed publications

Geisberger, S., Maschke. U., **Gebhardt, M.**, Kleinewietfeld, M., Manzel, A., Linker, R.A., Chidgey, A., Dechend, R., Nguyen, G., Daumke, O., Muller, D.N., Wright, M.D., Binger, K.J., (2015). New role for the (pro)renin receptor in T-cell development. Blood *126(4)*, 504-7

Park, J.*, **Gebhardt, M.***, Golovchenko, S., Perez-Branguli, F., Hattori, T., Hartmann, C., Zhou, X., deCrombrugghe, B., Stock, M., Schneider, H., von der Mark, K., (2015). Dual pathways to endochondral osteoblasts: a novel chondrocyte-derived osteoprogenitor cell identified in hypertrophic cartilage. Biol Open *4(5)* 608-21; * joint first-author

Jantsch, J., Schatz, V., Friedrich, D., Schröder, A., Kopp, C., Siegert, I., Maronna, A., Wendelborn, D., Linz, P., Binger, K.J., **Gebhardt, M.**, Heinig, M., Neubert, P., Fischer, F., Teufel, S., David, J.P., Neufert, C., Cavallaro, A., Rakov,a N., Küper, C., Beck, F.X., Neuhofer, W., Muller, D.N., Schuler, G., Uder, M., Bogdan, C., Luft, F.C., Titze, J., (2015). Cutaneous Na^+ storage strengthens the antimicrobial barrier function of the skin and boosts macrophage-driven host defense. Cell Metab. *21(3)* 493-501

Balogh, A., Németh, M., Koloszár, I., Markó, L., Przybyl, L., Jinno, K., Szigeti, C., Heffer, M., **Gebhardt, M.**, Szeberényi, J., Müller, D.N., Sétáló, G. Jr, Pap, M., (2014). Overexpression of CREB protein protects from tunicamycin-induced apoptosis in various rat cell types. Apoptosis *19(7)* 1080-98

Golovchenko, S., Hattori, T., Hartmann, C., **Gebhardt, M.**, Gebhard, S., Hess, A., Pausch, F., Schlund, B., von der Mark, K., (2013) Deletion of beta catenin in hypertrophic growth plate chondrocytes impairs trabecular bone formation. Bone *55(1)* 102-12

Hölsken, A., **Gebhardt, M.**, Buchfelder, M., Fahlbusch, R., Blümcke, I., Buslei, R., (2011). EGFR signaling regulates tumor cell migration in craniopharyngiomas. Clin Cancer Res *17(13)* 4367-77

5.3. Curriculum vitae

The author's CV has been removed from the online version of this thesis due to privacy issues

6. References

Abou Fakher, F.H., Rachinel, N., Klimczak, M., Louis, J., and Doyen, N. (2009). TLR9-dependent activation of dendritic cells by DNA from Leishmania major favors Th1 cell development and the resolution of lesions. Journal of immunology (Baltimore, Md : 1950) *182*, 1386-1396.

Abramson, S.L., and Gallin, J.I. (1990). IL-4 inhibits superoxide production by human mononuclear phagocytes. Journal of immunology (Baltimore, Md : 1950) *144*, 625-630.

Adler, A.J., Taylor, F., Martin, N., Gottlieb, S., Taylor, R.S., and Ebrahim, S. (2014). Reduced dietary salt for the prevention of cardiovascular disease. The Cochrane database of systematic reviews *12*, Cd009217.

Afonina, I.S., Elton, L., Carpentier, I., and Beyaert, R. (2015). MALT1 - a universal soldier: multiple strategies to ensure NF-kappaB activation and target gene expression. The FEBS journal *282*, 3286-3297.

Agaiby, A.D., and Dyson, M. (1999). Immuno-inflammatory cell dynamics during cutaneous wound healing. Journal of anatomy *195 (Pt 4)*, 531-542.

Agger, K., Cloos, P.A., Christensen, J., Pasini, D., Rose, S., Rappsilber, J., Issaeva, I., Canaani, E., Salcini, A.E., and Helin, K. (2007). UTX and JMJD3 are histone H3K27 demethylases involved in HOX gene regulation and development. Nature *449*, 731-734.

Alabert, C., Barth, T.K., Reveron-Gomez, N., Sidoli, S., Schmidt, A., Jensen, O.N., Imhof, A., and Groth, A. (2015). Two distinct modes for propagation of histone PTMs across the cell cycle. Genes & development *29*, 585-590.

Albina, J.E., Cui, S., Mateo, R.B., and Reichner, J.S. (1993). Nitric oxide-mediated apoptosis in murine peritoneal macrophages. Journal of immunology (Baltimore, Md : 1950) *150*, 5080-5085.

Albina, J.E., and Mastrofrancesco, B. (1993). Modulation of glucose metabolism in macrophages by products of nitric oxide synthase. The American journal of physiology *264*, C1594-1599.

Alegria-Torres, J.A., Baccarelli, A., and Bollati, V. (2011). Epigenetics and lifestyle. Epigenomics *3*, 267-277.

Alexander, W.S., and Hilton, D.J. (2004). The role of suppressors of cytokine signaling (SOCS) proteins in regulation of the immune response. Annual review of immunology *22*, 503-529.

Alexander, W.S., Starr, R., Fenner, J.E., Scott, C.L., Handman, E., Sprigg, N.S., Corbin, J.E., Cornish, A.L., Darwiche, R., Owczarek, C.M., *et al.* (1999). SOCS1 is a critical inhibitor of interferon gamma signaling and prevents the potentially fatal neonatal actions of this cytokine. Cell *98*, 597-608.

Anthony, R.M., Rutitzky, L.I., Urban, J.F., Jr., Stadecker, M.J., and Gause, W.C. (2007). Protective immune mechanisms in helminth infection. Nature reviews Immunology *7*, 975-987.

Antov, A., Yang, L., Vig, M., Baltimore, D., and Van Parijs, L. (2003). Essential role for STAT5 signaling in CD25+CD4+ regulatory T cell homeostasis and the maintenance of self-tolerance. Journal of immunology (Baltimore, Md : 1950) *171*, 3435-3441.

Aramburu, J., Drews-Elger, K., Estrada-Gelonch, A., Minguillon, J., Morancho, B., Santiago, V., and Lopez-Rodriguez, C. (2006). Regulation of the hypertonic stress response and other cellular functions by the Rel-like transcription factor NFAT5. Biochemical pharmacology *72*, 1597-1604.

Asagiri, M., Hirai, T., Kunigami, T., Kamano, S., Gober, H.J., Okamoto, K., Nishikawa, K., Latz, E., Golenbock, D.T., Aoki, K., *et al.* (2008). Cathepsin K-dependent toll-like receptor 9 signaling revealed in experimental arthritis. Science (New York, NY) *319*, 624-627.

Asangani, I.A., Dommeti, V.L., Wang, X., Malik, R., Cieslik, M., Yang, R., Escara-Wilke, J., Wilder-Romans, K., Dhanireddy, S., Engelke, C., *et al.* (2014). Therapeutic targeting of BET bromodomain proteins in castration-resistant prostate cancer. Nature *510*, 278-282.

Bandukwala, H.S., Gagnon, J., Togher, S., Greenbaum, J.A., Lamperti, E.D., Parr, N.J., Molesworth, A.M., Smithers, N., Lee, K., Witherington, J., *et al.* (2012). Selective inhibition of CD4+ T-cell cytokine production and autoimmunity by BET protein and c-Myc inhibitors. Proceedings of the National Academy of Sciences of the United States of America *109*, 14532-14537.

Barbi, J., Pardoll, D., and Pan, F. (2013). Metabolic control of the Treg/Th17 axis. Immunological reviews *252*, 52-77.

Barnes, P.J., Adcock, I.M., and Ito, K. (2005). Histone acetylation and deacetylation: importance in inflammatory lung diseases. The European respiratory journal *25*, 552-563.

Benayoun, B.A., Pollina, E.A., Ucar, D., Mahmoudi, S., Karra, K., Wong, E.D., Devarajan, K., Daugherty, A.C., Kundaje, A.B., Mancini, E., *et al.* (2014). H3K4me3 Breadth Is Linked to Cell Identity and Transcriptional Consistency. Cell *158*, 673-688.

Benjamini, Y., Drai, D., Elmer, G., Kafkafi, N., and Golani, I. (2001). Controlling the false discovery rate in behavior genetics research. Behavioural brain research *125*, 279-284.

Bennett, M., Dent, C.L., Ma, Q., Dastrala, S., Grenier, F., Workman, R., Syed, H., Ali, S., Barasch, J., and Devarajan, P. (2008). Urine NGAL predicts severity of acute kidney injury after cardiac surgery: a prospective study. Clinical journal of the American Society of Nephrology : CJASN *3*, 665-673.

Berger, S.B., Romero, X., Ma, C., Wang, G., Faubion, W.A., Liao, G., Compeer, E., Keszei, M., Rameh, L., Wang, N., *et al.* (2010). SLAM is a microbial sensor that regulates bacterial phagosome functions in macrophages. Nature immunology *11*, 920-927.

Biswas, S.K., and Lopez-Collazo, E. (2009). Endotoxin tolerance: new mechanisms, molecules and clinical significance. Trends in immunology *30*, 475-487.

Bjorkbacka, H., Fitzgerald, K.A., Huet, F., Li, X., Gregory, J.A., Lee, M.A., Ordija, C.M., Dowley, N.E., Golenbock, D.T., and Freeman, M.W. (2004). The induction of macrophage gene expression by LPS predominantly utilizes Myd88-independent signaling cascades. Physiological genomics *19*, 319-330.

Blum, J.S., and Cresswell, P. (1988). Role for intracellular proteases in the processing and transport of class II HLA antigens. Proceedings of the National Academy of Sciences of the United States of America *85*, 3975-3979.

Bogdan, C., Rollinghoff, M., and Diefenbach, A. (2000). The role of nitric oxide in innate immunity. Immunological reviews *173*, 17-26.

Boi, M., Gaudio, E., Bonetti, P., Kwee, I., Bernasconi, E., Tarantelli, C., Rinaldi, A., Testoni, M., Cascione, L., Ponzoni, M., *et al.* (2015). The BET Bromodomain Inhibitor OTX015 Affects Pathogenetic Pathways in Preclinical B-cell Tumor Models and Synergizes with Targeted Drugs. Clinical cancer research : an official journal of the American Association for Cancer Research *21*, 1628-1638.

Bonen, A., Heynen, M., and Hatta, H. (2006). Distribution of monocarboxylate transporters MCT1-MCT8 in rat tissues and human skeletal muscle. Applied physiology, nutrition, and metabolism = Physiologie appliquee, nutrition et metabolisme *31*, 31-39.

Bouhlel, M.A., Derudas, B., Rigamonti, E., Dievart, R., Brozek, J., Haulon, S., Zawadzki, C., Jude, B., Torpier, G., Marx, N., *et al.* (2007). PPARgamma activation primes human monocytes into alternative M2 macrophages with anti-inflammatory properties. Cell metabolism *6*, 137-143.

Brocker, C., Thompson, D.C., and Vasiliou, V. (2012). The role of hyperosmotic stress in inflammation and disease. Biomolecular concepts *3*, 345-364.

Burg, M.B., Ferraris, J.D., and Dmitrieva, N.I. (2007). Cellular response to hyperosmotic stresses. Physiological reviews *87*, 1441-1474.

Burgis, S., and Gessner, A. (2007). Unexpected phenotype of STAT6 heterozygous mice implies distinct STAT6 dosage requirements for different IL-4 functions. International archives of allergy and immunology *143*, 263-268.

Byles, V., Covarrubias, A.J., Ben-Sahra, I., Lamming, D.W., Sabatini, D.M., Manning, B.D., and Horng, T. (2013). The TSC-mTOR pathway regulates macrophage polarization. Nature communications *4*, 2834.

Carter, L., Fouser, L.A., Jussif, J., Fitz, L., Deng, B., Wood, C.R., Collins, M., Honjo, T., Freeman, G.J., and Carreno, B.M. (2002). PD-1:PD-L inhibitory pathway affects both CD4(+) and CD8(+) T cells and is overcome by IL-2. European journal of immunology *32*, 634-643.

Cassina, A., and Radi, R. (1996). Differential inhibitory action of nitric oxide and peroxynitrite on mitochondrial electron transport. Archives of biochemistry and biophysics *328*, 309-316.

Chang, C.H., Curtis, J.D., Maggi, L.B., Jr., Faubert, B., Villarino, A.V., O'Sullivan, D., Huang, S.C., van der Windt, G.J., Blagih, J., Qiu, J., *et al.* (2013). Posttranscriptional control of T cell effector function by aerobic glycolysis. Cell *153*, 1239-1251.

Chang, J.T., Wherry, E.J., and Goldrath, A.W. (2014). Molecular regulation of effector and memory T cell differentiation. Nature immunology *15*, 1104-1115.

Chang, N.C., Hung, S.I., Hwa, K.Y., Kato, I., Chen, J.E., Liu, C.H., and Chang, A.C. (2001). A macrophage protein, Ym1, transiently expressed during inflammation is a novel mammalian lectin. The Journal of biological chemistry *276*, 17497-17506.

Charo, I.F. (2007). Macrophage polarization and insulin resistance: PPARgamma in control. Cell metabolism *6*, 96-98.

Chen, H.C., and Reich, N.C. (2010). Live cell imaging reveals continuous STAT6 nuclear trafficking. Journal of immunology (Baltimore, Md : 1950) *185*, 64-70.

Cheng, C., Huang, C., Ma, T.T., Bian, E.B., He, Y., Zhang, L., and Li, J. (2014a). SOCS1 hypermethylation mediated by DNMT1 is associated with lipopolysaccharide-induced inflammatory cytokines in macrophages. Toxicology letters *225*, 488-497.

Cheng, S.C., Quintin, J., Cramer, R.A., Shepardson, K.M., Saeed, S., Kumar, V., Giamarellos-Bourboulis, E.J., Martens, J.H., Rao, N.A., Aghajanirefah, A., *et al.* (2014b). mTOR- and HIF-1alpha-mediated aerobic glycolysis as metabolic basis for trained immunity. Science (New York, NY) *345*, 1250684.

Chi, H. (2012). Regulation and function of mTOR signalling in T cell fate decisions. Nature reviews Immunology *12*, 325-338.

Clayton, A.L., Hazzalin, C.A., and Mahadevan, L.C. (2006). Enhanced histone acetylation and transcription: a dynamic perspective. Molecular cell *23*, 289-296.

Cleeter, M.W., Cooper, J.M., Darley-Usmar, V.M., Moncada, S., and Schapira, A.H. (1994). Reversible inhibition of cytochrome c oxidase, the terminal enzyme of the mitochondrial respiratory chain, by nitric oxide. Implications for neurodegenerative diseases. FEBS letters *345*, 50-54.

Colegio, O.R., Chu, N.Q., Szabo, A.L., Chu, T., Rhebergen, A.M., Jairam, V., Cyrus, N., Brokowski, C.E., Eisenbarth, S.C., Phillips, G.M., *et al.* (2014). Functional polarization of tumour-associated macrophages by tumour-derived lactic acid. Nature *513*, 559-563.

Comfort, K.K., and Haugh, J.M. (2008). Combinatorial Signal Transduction Responses Mediated by Interleukin-2 and -4 Receptors in a Helper T Cell Line. Cellular and molecular bioengineering *1*.

Cooney, C.A., Dave, A.A., and Wolff, G.L. (2002). Maternal methyl supplements in mice affect epigenetic variation and DNA methylation of offspring. The Journal of nutrition *132*, 2393s-2400s.

Cramer, T., Yamanishi, Y., Clausen, B.E., Forster, I., Pawlinski, R., Mackman, N., Haase, V.H., Jaenisch, R., Corr, M., Nizet, V., *et al.* (2003). HIF-1alpha is essential for myeloid cell-mediated inflammation. Cell *112*, 645-657.

D'Souza, W.N., and Lefrancois, L. (2003). IL-2 is not required for the initiation of CD8 T cell cycling but sustains expansion. Journal of immunology (Baltimore, Md : 1950) *171*, 5727-5735.

D'Souza, W.N., and Lefrancois, L. (2004). Frontline: An in-depth evaluation of the production of IL-2 by antigen-specific CD8 T cells in vivo. European journal of immunology *34*, 2977-2985.

Dahlmann, A., Dorfelt, K., Eicher, F., Linz, P., Kopp, C., Mossinger, I., Horn, S., Buschges-Seraphin, B., Wabel, P., Hammon, M., *et al.* (2015). Magnetic resonance-determined sodium removal from tissue stores in hemodialysis patients. Kidney international *87*, 434-441.

de Back, D.Z., Kostova, E.B., van Kraaij, M., van den Berg, T.K., and van Bruggen, R. (2014). Of macrophages and red blood cells; a complex love story. Front Physiol *5*, 9.

Dejaco, C., Duftner, C., Grubeck-Loebenstein, B., and Schirmer, M. (2006). Imbalance of regulatory T cells in human autoimmune diseases. Immunology *117*, 289-300.

Delgoffe, G.M., and Powell, J.D. (2009). mTOR: taking cues from the immune microenvironment. Immunology *127*, 459-465.

Denkert, C., Warskulat, U., Hensel, F., and Haussinger, D. (1998). Osmolyte strategy in human monocytes and macrophages: involvement of p38MAPK in hyperosmotic induction of betaine and myoinositol transporters. Archives of biochemistry and biophysics *354*, 172-180.

Deonarine, K., Panelli, M.C., Stashower, M.E., Jin, P., Smith, K., Slade, H.B., Norwood, C., Wang, E., Marincola, F.M., and Stroncek, D.F. (2007). Gene expression profiling of cutaneous wound healing. Journal of translational medicine *5*, 11.

Dickensheets, H., Vazquez, N., Sheikh, F., Gingras, S., Murray, P.J., Ryan, J.J., and Donnelly, R.P. (2007). Suppressor of cytokine signaling-1 is an IL-4-inducible gene in macrophages and feedback inhibits IL-4 signaling. Genes and immunity *8*, 21-27.

Dietz, G.P., and Bahr, M. (2004). Delivery of bioactive molecules into the cell: the Trojan horse approach. Molecular and cellular neurosciences *27*, 85-131.

Dik, S., Scheepers, P.T., and Godderis, L. (2012). Effects of environmental stressors on histone modifications and their relevance to carcinogenesis: a systematic review. Critical reviews in toxicology *42*, 491-500.

Dinarello, C.A. (2009). Hyperosmolar sodium chloride, p38 mitogen activated protein and cytokine-mediated inflammation. Seminars in dialysis *22*, 256-259.

DiNicolantonio, J.J., Niazi, A.K., Sadaf, R., JH, O.K., Lucan, S.C., and Lavie, C.J. (2013). Dietary sodium restriction: take it with a grain of salt. The American journal of medicine *126*, 951-955.

Doherty, D.G. (2015). Immunity, tolerance and autoimmunity in the liver: A comprehensive review. Journal of autoimmunity.

Edwards, T.M., and Myers, J.P. (2007). Environmental exposures and gene regulation in disease etiology. Environmental health perspectives *115*, 1264-1270.

El Chartouni, C., Schwarzfischer, L., and Rehli, M. (2010). Interleukin-4 induced interferon regulatory factor (Irf) 4 participates in the regulation of alternative macrophage priming. Immunobiology *215*, 821-825.

Escolano, A., Martinez-Martinez, S., Alfranca, A., Urso, K., Izquierdo, H.M., Delgado, M., Martin, F., Sabio, G., Sancho, D., Gomez-del Arco, P., *et al.* (2014). Specific calcineurin targeting in macrophages confers resistance to inflammation via MKP-1 and p38. The EMBO journal *33*, 1117-1133.

Everts, B., Amiel, E., Huang, S.C., Smith, A.M., Chang, C.H., Lam, W.Y., Redmann, V., Freitas, T.C., Blagih, J., van der Windt, G.J., *et al.* (2014). TLR-driven early glycolytic reprogramming via the kinases TBK1-IKKvarepsilon supports the anabolic demands of dendritic cell activation. Nature immunology *15*, 323-332.

Everts, B., Amiel, E., van der Windt, G.J., Freitas, T.C., Chott, R., Yarasheski, K.E., Pearce, E.L., and Pearce, E.J. (2012). Commitment to glycolysis sustains survival of NO-producing inflammatory dendritic cells. Blood *120*, 1422-1431.

Falcon, S., and Gentleman, R. (2007). Using GOstats to test gene lists for GO term association. Bioinformatics (Oxford, England) *23*, 257-258.

Farber, S.J. (1960). Mucopolysaccharides and sodium metabolism. Circulation *21*, 941-947.

Farber, S.J., Schubert, M., and Schuster, N. (1957). The binding of cations by chondroitin sulfate. The Journal of clinical investigation *36*, 1715-1722.

Farez, M.F., Fiol, M.P., Gaitan, M.I., Quintana, F.J., and Correale, J. (2015). Sodium intake is associated with increased disease activity in multiple sclerosis. Journal of neurology, neurosurgery, and psychiatry *86*, 26-31.

Farh, K.K., Marson, A., Zhu, J., Kleinewietfeld, M., Housley, W.J., Beik, S., Shoresh, N., Whitton, H., Ryan, R.J., Shishkin, A.A., *et al.* (2015). Genetic and epigenetic fine mapping of causal autoimmune disease variants. Nature *518*, 337-343.

Feil, R., Wagner, J., Metzger, D., and Chambon, P. (1997). Regulation of Cre recombinase activity by mutated estrogen receptor ligand-binding domains. Biochemical and biophysical research communications *237*, 752-757.

Ferraris, J.D., Persaud, P., Williams, C.K., Chen, Y., and Burg, M.B. (2002). cAMP-independent role of PKA in tonicity-induced transactivation of tonicity-responsive enhancer/ osmotic response element-binding protein. Proceedings of the National Academy of Sciences of the United States of America *99*, 16800-16805.

Flo, T.H., Smith, K.D., Sato, S., Rodriguez, D.J., Holmes, M.A., Strong, R.K., Akira, S., and Aderem, A. (2004). Lipocalin 2 mediates an innate immune response to bacterial infection by sequestrating iron. Nature *432*, 917-921.

Foster, S.L., Hargreaves, D.C., and Medzhitov, R. (2007). Gene-specific control of inflammation by TLR-induced chromatin modifications. Nature *447*, 972-978.

Frankel, A.D., and Pabo, C.O. (1988). Cellular uptake of the tat protein from human immunodeficiency virus. Cell *55*, 1189-1193.

Fukao, T., and Koyasu, S. (2003). PI3K and negative regulation of TLR signaling. Trends in immunology *24*, 358-363.

Gabrilovich, D.I., and Nagaraj, S. (2009). Myeloid-derived suppressor cells as regulators of the immune system. Nature reviews Immunology *9*, 162-174.

Garedew, A., and Moncada, S. (2008). Mitochondrial dysfunction and HIF1alpha stabilization in inflammation. Journal of cell science *121*, 3468-3475.

Go, W.Y., Liu, X., Roti, M.A., Liu, F., and Ho, S.N. (2004). NFAT5/TonEBP mutant mice define osmotic stress as a critical feature of the lymphoid microenvironment. Proceedings of the National Academy of Sciences of the United States of America *101*, 10673-10678.

Goberdhan, D.C., and Boyd, C.A. (2009). mTOR: dissecting regulation and mechanism of action to understand human disease. Biochemical Society transactions *37*, 213-216.

Goerdt, S., and Orfanos, C.E. (1999). Other functions, other genes: alternative activation of antigen-presenting cells. Immunity *10*, 137-142.

Gordon, S. (2003). Alternative activation of macrophages. Nature reviews Immunology *3*, 23-35.

Gordon, S. (2008). Elie Metchnikoff: father of natural immunity. European journal of immunology *38*, 3257-3264.

Gordon, S., and Martinez, F.O. (2010). Alternative activation of macrophages: mechanism and functions. Immunity *32*, 593-604.

Gordy, C., Pua, H., Sempowski, G.D., and He, Y.W. (2011). Regulation of steady-state neutrophil homeostasis by macrophages. Blood *117*, 618-629.

Grabiec, A.M., Krausz, S., de Jager, W., Burakowski, T., Groot, D., Sanders, M.E., Prakken, B.J., Maslinski, W., Eldering, E., Tak, P.P., *et al.* (2010). Histone deacetylase inhibitors suppress inflammatory activation of rheumatoid arthritis patient synovial macrophages and tissue. Journal of immunology (Baltimore, Md : 1950) *184*, 2718-2728.

Green, D.R., Droin, N., and Pinkoski, M. (2003). Activation-induced cell death in T cells. Immunological reviews *193*, 70-81.

Greer, E.L., and Shi, Y. (2012). Histone methylation: a dynamic mark in health, disease and inheritance. Nature reviews Genetics *13*, 343-357.

Gross, T.J., Kremens, K., Powers, L.S., Brink, B., Knutson, T., Domann, F.E., Philibert, R.A., Milhem, M.M., and Monick, M.M. (2014). Epigenetic silencing of the human NOS2 gene: rethinking the role of nitric oxide in human macrophage inflammatory responses. Journal of immunology (Baltimore, Md : 1950) *192*, 2326-2338.

Guo, W., Jiang, L., Bhasin, S., Khan, S.M., and Swerdlow, R.H. (2009). DNA extraction procedures meaningfully influence qPCR-based mtDNA copy number determination. Mitochondrion *9*, 261-265.

Guzik, T.J., Hoch, N.E., Brown, K.A., McCann, L.A., Rahman, A., Dikalov, S., Goronzy, J., Weyand, C., and Harrison, D.G. (2007). Role of the T cell in the genesis of angiotensin II induced hypertension and vascular dysfunction. The Journal of experimental medicine *204*, 2449-2460.

Haissaguerre, M., Saucisse, N., and Cota, D. (2014). Influence of mTOR in energy and metabolic homeostasis. Molecular and cellular endocrinology *397*, 67-77.

Han, J., Lee, J.D., Bibbs, L., and Ulevitch, R.J. (1994). A MAP kinase targeted by endotoxin and hyperosmolarity in mammalian cells. Science (New York, NY) *265*, 808-811.

Hanson, E.M., Dickensheets, H., Qu, C.K., Donnelly, R.P., and Keegan, A.D. (2003). Regulation of the dephosphorylation of Stat6. Participation of Tyr-713 in the interleukin-4 receptor alpha, the tyrosine phosphatase SHP-1, and the proteasome. The Journal of biological chemistry *278*, 3903-3911.

Harms, M., and Seale, P. (2013). Brown and beige fat: development, function and therapeutic potential. Nature medicine *19*, 1252-1263.

Haschemi, A., Kosma, P., Gille, L., Evans, C.R., Burant, C.F., Starkl, P., Knapp, B., Haas, R., Schmid, J.A., Jandl, C., *et al.* (2012). The sedoheptulose kinase CARKL directs macrophage polarization through control of glucose metabolism. Cell metabolism *15*, 813-826.

Havran, W.L., and Jameson, J.M. (2010). Epidermal T cells and wound healing. Journal of immunology (Baltimore, Md : 1950) *184*, 5423-5428.

Hay, N., and Sonenberg, N. (2004). Upstream and downstream of mTOR. Genes & development *18*, 1926-1945.

He, F.J., Li, J., and Macgregor, G.A. (2013). Effect of longer-term modest salt reduction on blood pressure. The Cochrane database of systematic reviews *4*, CD004937.

He, F.J., and MacGregor, G.A. (2009). A comprehensive review on salt and health and current experience of worldwide salt reduction programmes. Journal of human hypertension *23*, 363-384.

He, H., Isnard, A., Kouriba, B., Cabantous, S., Dessein, A., Doumbo, O., and Chevillard, C. (2008). A STAT6 gene polymorphism is associated with high infection levels in urinary schistosomiasis. Genes and immunity *9*, 195-206.

Heer, M., Baisch, F., Kropp, J., Gerzer, R., and Drummer, C. (2000). High dietary sodium chloride consumption may not induce body fluid retention in humans. American journal of physiology Renal physiology *278*, F585-595.

Heintzman, N.D., Stuart, R.K., Hon, G., Fu, Y., Ching, C.W., Hawkins, R.D., Barrera, L.O., Van Calcar, S., Qu, C., Ching, K.A., *et al.* (2007). Distinct and predictive chromatin signatures of transcriptional promoters and enhancers in the human genome. Nature genetics *39*, 311-318.

Herait, P., Dombret, H., Thieblemont, C., Facon, T., Stathis, A., Cunningham, D., Palumbo, A., Vey, N., Michallet, M., Recher, C., *et al.* (2015). O7.3BET-bromodomain (BRD) inhibitor OTX015: Final results of the dose-finding part of a phase I study in hematologic malignancies. Annals of Oncology *26*, ii10.

Herbert, D.R., Holscher, C., Mohrs, M., Arendse, B., Schwegmann, A., Radwanska, M., Leeto, M., Kirsch, R., Hall, P., Mossmann, H., *et al.* (2004). Alternative macrophage activation is essential for survival during schistosomiasis and downmodulates T helper 1 responses and immunopathology. Immunity *20*, 623-635.

Hernandez, A.C., Kitz, A., Wu, C., Lowther, D.E., Rodriguez, D.M., Vudatta, N., Deng, S., Herold, K.C., Kuchroo, V.K., Kleinewietfeld, M., *et al.* (2015). Sodium chloride inhibits the suppressive function of FoxP3+ regulatory T cells (accepted). The Journal of clinical investigation *125*, XXXX-YYYY.

Heytler, P.G., and Prichard, W.W. (1962). A new class of uncoupling agents--carbonyl cyanide phenylhydrazones. Biochemical and biophysical research communications *7*, 272-275.

Hoeijmakers, W.A., Stunnenberg, H.G., and Bartfai, R. (2012). Placing the Plasmodium falciparum epigenome on the map. Trends in parasitology *28*, 486-495.

Holliday, R. (2006). Epigenetics: a historical overview. Epigenetics : official journal of the DNA Methylation Society *1*, 76-80.

Housley, W.J., Fernandez, S.D., Vera, K., Murikinati, S.R., Grutzendler, J., Cuerdon, N., Glick, L., De Jager, P.L., Mitrovic, M., Cotsapas, C., *et al.* (2015). Genetic variants associated with autoimmunity drive NFkappaB signaling and responses to inflammatory stimuli. Science translational medicine *7*, 291ra293.

Huang, S.C., Everts, B., Ivanova, Y., O'Sullivan, D., Nascimento, M., Smith, A.M., Beatty, W., Love-Gregory, L., Lam, W.Y., O'Neill, C.M., *et al.* (2014a). Cell-intrinsic lysosomal lipolysis is essential for alternative activation of macrophages. Nature immunology.

Huang, S.C., Everts, B., Ivanova, Y., O'Sullivan, D., Nascimento, M., Smith, A.M., Beatty, W., Love-Gregory, L., Lam, W.Y., O'Neill, C.M., *et al.* (2014b). Cell-intrinsic lysosomal lipolysis is essential for alternative activation of macrophages. Nature immunology *15*, 846-855.

Huber, S., Hoffmann, R., Muskens, F., and Voehringer, D. (2010). Alternatively activated macrophages inhibit T-cell proliferation by Stat6-dependent expression of PD-L2. Blood *116*, 3311-3320.

Hugo, S.E., Cruz-Garcia, L., Karanth, S., Anderson, R.M., Stainier, D.Y., and Schlegel, A. (2012). A monocarboxylate transporter required for hepatocyte secretion of ketone bodies during fasting. Genes & development *26*, 282-293.

Hunt, A.E., Williams, L.M., Lali, F.V., and Foxwell, B.M. (2002). IL-4 regulation of p38 MAPK signalling is dependent on cell type. Cytokine *18*, 295-303.

Ip, W.K., and Medzhitov, R. (2015). Macrophages monitor tissue osmolarity and induce inflammatory response through NLRP3 and NLRC4 inflammasome activation. Nature communications *6*, 6931.

Irarrazabal, C.E., Williams, C.K., Ely, M.A., Birrer, M.J., Garcia-Perez, A., Burg, M.B., and Ferraris, J.D. (2008). Activator protein-1 contributes to high NaCl-induced increase in tonicity-responsive enhancer/osmotic response element-binding protein transactivating activity. The Journal of biological chemistry *283*, 2554-2563.

Ishii, M., Wen, H., Corsa, C.A., Liu, T., Coelho, A.L., Allen, R.M., Carson, W.F.t., Cavassani, K.A., Li, X., Lukacs, N.W., *et al.* (2009). Epigenetic regulation of the alternatively activated macrophage phenotype. Blood *114*, 3244-3254.

Ivanova, L.N., Archibasova, V.K., and Shterental, I. (1978). [Sodium-depositing function of the skin in white rats]. Fiziologicheskii zhurnal SSSR imeni I M Sechenova *64*, 358-363.

Jaenisch, R., and Bird, A. (2003). Epigenetic regulation of gene expression: how the genome integrates intrinsic and environmental signals. Nature genetics *33 Suppl*, 245-254.

Jantsch, J., Binger, K., Muller, D.N., and Titze, J. (2014a). Macrophages in homeostatic immune function. Frontiers in Physiology *5*.

Jantsch, J., Binger, K.J., Muller, D.N., and Titze, J. (2014b). Macrophages in homeostatic immune function. Front Physiol *5*, 146.

Jantsch, J., Schatz, V., Friedrich, D., Schroder, A., Kopp, C., Siegert, I., Maronna, A., Wendelborn, D., Linz, P., Binger, K.J., *et al.* (2015). Cutaneous na(+) storage strengthens the antimicrobial barrier function of the skin and boosts macrophage-driven host defense. Cell metabolism *21*, 493-501.

Jenuwein, T., and Allis, C.D. (2001). Translating the histone code. Science (New York, NY) *293*, 1074-1080.

Jha, A.K., Huang, S.C., Sergushichev, A., Lampropoulou, V., Ivanova, Y., Loginicheva, E., Chmielewski, K., Stewart, K.M., Ashall, J., Everts, B., *et al.* (2015). Network Integration of Parallel Metabolic and Transcriptional Data Reveals Metabolic Modules that Regulate Macrophage Polarization. Immunity *42*, 419-430.

Jin, H.M., Copeland, N.G., Gilbert, D.J., Jenkins, N.A., Kirkpatrick, R.B., and Rosenberg, M. (1998). Genetic characterization of the murine Ym1 gene and identification of a cluster of highly homologous genes. Genomics *54*, 316-322.

Jirtle, R.L., and Skinner, M.K. (2007). Environmental epigenomics and disease susceptibility. Nature reviews Genetics *8*, 253-262.

Kang, K., Reilly, S.M., Karabacak, V., Gangl, M.R., Fitzgerald, K., Hatano, B., and Lee, C.H. (2008). Adipocyte-derived Th2 cytokines and myeloid PPARdelta regulate macrophage polarization and insulin sensitivity. Cell metabolism *7*, 485-495.

Katan-Khaykovich, Y., and Struhl, K. (2002). Dynamics of global histone acetylation and deacetylation in vivo: rapid restoration of normal histone acetylation status upon removal of activators and repressors. Genes & development *16*, 743-752.

Katoh, H., and Watanabe, M. (2015). Myeloid-Derived Suppressor Cells and Therapeutic Strategies in Cancer. Mediators of inflammation *2015*, 159269.

Keene, J.A., and Forman, J. (1982). Helper activity is required for the in vivo generation of cytotoxic T lymphocytes. The Journal of experimental medicine *155*, 768-782.

Klaus, D. (2012). [Does sodium restriction reduce cardiovascular risk?]. Deutsche medizinische Wochenschrift (1946) *137*, 14.

Kleinewietfeld, M., Manzel, A., Titze, J., Kvakan, H., Yosef, N., Linker, R.A., Muller, D.N., and Hafler, D.A. (2013). Sodium chloride drives autoimmune disease by the induction of pathogenic TH17 cells. Nature *496*, 518-522.

Kohyama, M., Ise, W., Edelson, B.T., Wilker, P.R., Hildner, K., Mejia, C., Frazier, W.A., Murphy, T.L., and Murphy, K.M. (2009). Role for Spi-C in the development of red pulp macrophages and splenic iron homeostasis. Nature *457*, 318-321.

Kopp, C., Linz, P., Dahlmann, A., Hammon, M., Jantsch, J., Muller, D.N., Schmieder, R.E., Cavallaro, A., Eckardt, K.U., Uder, M., *et al.* (2013a). 23Na Magnetic Resonance Imaging-Determined Tissue Sodium in Healthy Subjects and Hypertensive Patients. Hypertension.

Kopp, C., Linz, P., Dahlmann, A., Hammon, M., Jantsch, J., Muller, D.N., Schmieder, R.E., Cavallaro, A., Eckardt, K.U., Uder, M., *et al.* (2013b). 23Na magnetic resonance imaging-determined tissue sodium in healthy subjects and hypertensive patients. Hypertension *61*, 635-640.

Kopp, C., Linz, P., Hammon, M., Schofl, C., Grauer, M., Eckardt, K.U., Cavallaro, A., Uder, M., Luft, F.C., and Titze, J. (2012a). Seeing the sodium in a patient with hypernatremia. Kidney international *82*, 1343-1344.

Kopp, C., Linz, P., Wachsmuth, L., Dahlmann, A., Horbach, T., Schofl, C., Renz, W., Santoro, D., Niendorf, T., Muller, D.N., *et al.* (2012b). (23)Na magnetic resonance imaging of tissue sodium. Hypertension *59*, 167-172.

Kouzarides, T. (2007). Chromatin modifications and their function. Cell *128*, 693-705.

Kratz, M., Coats, B.R., Hisert, K.B., Hagman, D., Mutskov, V., Peris, E., Schoenfelt, K.Q., Kuzma, J.N., Larson, I., Billing, P.S., *et al.* (2014). Metabolic dysfunction drives a mechanistically distinct proinflammatory phenotype in adipose tissue macrophages. Cell metabolism *20*, 614-625.

Kreider, T., Anthony, R.M., Urban, J.F., Jr., and Gause, W.C. (2007). Alternatively activated macrophages in helminth infections. Current opinion in immunology *19*, 448-453.

Kuper, C., Beck, F.X., and Neuhofer, W. (2014). Generation of a conditional knockout allele for the NFAT5 gene in mice. Front Physiol *5*, 507.

Küper, C., Beck, F.X., and Neuhofer, W. (2007). Osmoadaptation of Mammalian cells - an orchestrated network of protective genes. Current genomics *8*, 209-218.

Lacroix, S., Feinstein, D., and Rivest, S. (1998). The bacterial endotoxin lipopolysaccharide has the ability to target the brain in upregulating its membrane CD14 receptor within specific cellular populations. Brain pathology (Zurich, Switzerland) *8*, 625-640.

Lai, Y.P., Lin, C.C., Liao, W.J., Tang, C.Y., and Chen, S.C. (2009). CD4+ T cell-derived IL-2 signals during early priming advances primary CD8+ T cell responses. PloS one *4*, e7766.

Lam-Tse, W.K., Lernmark, A., and Drexhage, H.A. (2002). Animal models of endocrine/organ-specific autoimmune diseases: do they really help us to understand human autoimmunity? Springer seminars in immunopathology *24*, 297-321.

Landt, S.G., Marinov, G.K., Kundaje, A., Kheradpour, P., Pauli, F., Batzoglou, S., Bernstein, B.E., Bickel, P., Brown, J.B., Cayting, P., *et al.* (2012). ChIP-seq guidelines and practices of the ENCODE and modENCODE consortia. Genome research *22*, 1813-1831.

Lang, F., Bohmer, C., Palmada, M., Seebohm, G., Strutz-Seebohm, N., and Vallon, V. (2006). (Patho)physiological significance of the serum- and glucocorticoid-inducible kinase isoforms. Physiological reviews *86*, 1151-1178.

Lara-Astiaso, D., Weiner, A., Lorenzo-Vivas, E., Zaretsky, I., Jaitin, D.A., David, E., Keren-Shaul, H., Mildner, A., Winter, D., Jung, S., *et al.* (2014). Immunogenetics. Chromatin state dynamics during blood formation. Science (New York, NY) *345*, 943-949.

Latchman, Y., Wood, C.R., Chernova, T., Chaudhary, D., Borde, M., Chernova, I., Iwai, Y., Long, A.J., Brown, J.A., Nunes, R., *et al.* (2001). PD-L2 is a second ligand for PD-1 and inhibits T cell activation. Nature immunology *2*, 261-268.

Lavin, Y., Winter, D., Blecher-Gonen, R., David, E., Keren-Shaul, H., Merad, M., Jung, S., and Amit, I. (2014). Tissue-resident macrophage enhancer landscapes are shaped by the local microenvironment. Cell *159*, 1312-1326.

Lawrence, T., and Natoli, G. (2011). Transcriptional regulation of macrophage polarization: enabling diversity with identity. Nature reviews Immunology *11*, 750-761.

Levine, A.G., Arvey, A., Jin, W., and Rudensky, A.Y. (2014). Continuous requirement for the TCR in regulatory T cell function. Nature immunology *15*, 1070-1078.

Li, B., Carey, M., and Workman, J.L. (2007). The role of chromatin during transcription. Cell *128*, 707-719.

Li, H., Handsaker, B., Wysoker, A., Fennell, T., Ruan, J., Homer, N., Marth, G., Abecasis, G., and Durbin, R. (2009). The Sequence Alignment/Map format and SAMtools. Bioinformatics (Oxford, England) *25*, 2078-2079.

Li, L., Zhang, T., Diao, W., Jin, F., Shi, L., Meng, J., Liu, H., Zhang, J., Zeng, C.H., Zhang, M.C., *et al.* (2015). Role of Myeloid-Derived Suppressor Cells in Glucocorticoid-Mediated Amelioration of FSGS. Journal of the American Society of Nephrology : JASN.

Liao, X., Sharma, N., Kapadia, F., Zhou, G., Lu, Y., Hong, H., Paruchuri, K., Mahabeleshwar, G.H., Dalmas, E., Venteclef, N., *et al.* (2011). Kruppel-like factor 4 regulates macrophage polarization. The Journal of clinical investigation *121*, 2736-2749.

Liu, X., Strable, M.S., and Ntambi, J.M. (2011). Stearoyl CoA desaturase 1: role in cellular inflammation and stress. Advances in nutrition (Bethesda, Md) *2*, 15-22.

Liu, Y., Yin, H., Zhao, M., and Lu, Q. (2014). TLR2 and TLR4 in autoimmune diseases: a comprehensive review. Clinical reviews in allergy & immunology *47*, 136-147.

Lochrin, S.E., Price, D.K., and Figg, W.D. (2014). BET bromodomain inhibitors--a novel epigenetic approach in castration-resistant prostate cancer. Cancer biology & therapy *15*, 1583-1585.

Loke, P., Nair, M.G., Parkinson, J., Guiliano, D., Blaxter, M., and Allen, J.E. (2002). IL-4 dependent alternatively-activated macrophages have a distinctive in vivo gene expression phenotype. BMC immunology *3*, 7.

Lu, C., and Thompson, C.B. (2012). Metabolic regulation of epigenetics. Cell metabolism *16*, 9-17.

Lucca, L.E., and Hafler, D.A. (2015). Sodium-activated macrophages: the salt mine expands. Cell research *25*, 885-886.

Luger, K., Mader, A.W., Richmond, R.K., Sargent, D.F., and Richmond, T.J. (1997). Crystal structure of the nucleosome core particle at 2.8 A resolution. Nature *389*, 251-260.

Lumeng, C.N., Bodzin, J.L., and Saltiel, A.R. (2007). Obesity induces a phenotypic switch in adipose tissue macrophage polarization. The Journal of clinical investigation *117*, 175-184.

Machnik, A., Dahlmann, A., Kopp, C., Goss, J., Wagner, H., van Rooijen, N., Eckardt, K.U., Muller, D.N., Park, J.K., Luft, F.C., *et al.* (2010). Mononuclear phagocyte system depletion blocks interstitial tonicity-responsive enhancer binding protein/vascular endothelial growth factor C expression and induces salt-sensitive hypertension in rats. Hypertension *55*, 755-761.

Machnik, A., Neuhofer, W., Jantsch, J., Dahlmann, A., Tammela, T., Machura, K., Park, J.K., Beck, F.X., Muller, D.N., Derer, W., *et al.* (2009). Macrophages regulate salt-dependent volume and blood pressure by a vascular endothelial growth factor-C-dependent buffering mechanism. Nature medicine *15*, 545-552.

MacMicking, J., Xie, Q.W., and Nathan, C. (1997). Nitric oxide and macrophage function. Annual review of immunology *15*, 323-350.

Man, K., Miasari, M., Shi, W., Xin, A., Henstridge, D.C., Preston, S., Pellegrini, M., Belz, G.T., Smyth, G.K., Febbraio, M.A., *et al.* (2013). The transcription factor IRF4 is essential for TCR affinity-mediated metabolic programming and clonal expansion of T cells. Nature immunology *14*, 1155-1165.

Maneiro, E., Lopez-Armada, M.J., de Andres, M.C., Carames, B., Martin, M.A., Bonilla, A., Del Hoyo, P., Galdo, F., Arenas, J., and Blanco, F.J. (2005). Effect of nitric oxide on mitochondrial respiratory activity of human articular chondrocytes. Annals of the rheumatic diseases *64*, 388-395.

Manoury, B. (2013). Proteases: essential actors in processing antigens and intracellular toll-like receptors. Frontiers in immunology *4*, 299.

Mantovani, A. (2008). From phagocyte diversity and activation to probiotics: back to Metchnikoff. European journal of immunology *38*, 3269-3273.

Manzel, A., Muller, D.N., Hafler, D.A., Erdman, S.E., Linker, R.A., and Kleinewietfeld, M. (2014). Role of "Western diet" in inflammatory autoimmune diseases. Current allergy and asthma reports *14*, 404.

Marigo, I., Bosio, E., Solito, S., Mesa, C., Fernandez, A., Dolcetti, L., Ugel, S., Sonda, N., Bicciato, S., Falisi, E., *et al.* (2010). Tumor-induced tolerance and immune suppression depend on the C/EBPbeta transcription factor. Immunity *32*, 790-802.

Marko, L., Kvakan, H., Park, J.K., Qadri, F., Spallek, B., Binger, K.J., Bowman, E.P., Kleinewietfeld, M., Fokuhl, V., Dechend, R., *et al.* (2012). Interferon-gamma signaling inhibition ameliorates angiotensin II-induced cardiac damage. Hypertension *60*, 1430-1436.

Marquet, S., Abel, L., Hillaire, D., Dessein, H., Kalil, J., Feingold, J., Weissenbach, J., and Dessein, A.J. (1996). Genetic localization of a locus controlling the intensity of infection by Schistosoma mansoni on chromosome 5q31-q33. Nature genetics *14*, 181-184.

Marson, A., Housley, W.J., and Hafler, D.A. (2015). Genetic basis of autoimmunity. The Journal of clinical investigation *125*, 2234-2241.

Martin, P. (1997). Wound healing--aiming for perfect skin regeneration. Science (New York, NY) *276*, 75-81.

Martin, P., D'Souza, D., Martin, J., Grose, R., Cooper, L., Maki, R., and McKercher, S.R. (2003). Wound healing in the PU.1 null mouse--tissue repair is not dependent on inflammatory cells. Current biology : CB *13*, 1122-1128.

Martinez, F.O., Gordon, S., Locati, M., and Mantovani, A. (2006). Transcriptional profiling of the human monocyte-to-macrophage differentiation and polarization: new molecules and patterns of gene expression. Journal of immunology (Baltimore, Md : 1950) *177*, 7303-7311.

Martinez, F.O., Helming, L., and Gordon, S. (2009). Alternative activation of macrophages: an immunologic functional perspective. Annual review of immunology *27*, 451-483.

Mateo, R.B., Reichner, J.S., Mastrofrancesco, B., Kraft-Stolar, D., and Albina, J.E. (1995). Impact of nitric oxide on macrophage glucose metabolism and glyceraldehyde-3-phosphate dehydrogenase activity. The American journal of physiology *268*, C669-675.

McGettrick, A.F., and O'Neill, L.A. (2013). How metabolism generates signals during innate immunity and inflammation. The Journal of biological chemistry *288*, 22893-22898.

McMaster, W.G., Kirabo, A., Madhur, M.S., and Harrison, D.G. (2015). Inflammation, immunity, and hypertensive end-organ damage. Circulation research *116*, 1022-1033.

Mele, D.A., Salmeron, A., Ghosh, S., Huang, H.R., Bryant, B.M., and Lora, J.M. (2013). BET bromodomain inhibition suppresses TH17-mediated pathology. The Journal of experimental medicine *210*, 2181-2190.

Meng, F., Yamagiwa, Y., Taffetani, S., Han, J., and Patel, T. (2005). IL-6 activates serum and glucocorticoid kinase via p38alpha mitogen-activated protein kinase pathway. American journal of physiology Cell physiology *289*, C971-981.

Meraz, M.A., White, J.M., Sheehan, K.C., Bach, E.A., Rodig, S.J., Dighe, A.S., Kaplan, D.H., Riley, J.K., Greenlund, A.C., Campbell, D.*, et al.* (1996). Targeted disruption of the Stat1 gene in mice reveals unexpected physiologic specificity in the JAK-STAT signaling pathway. Cell *84*, 431-442.

Mercalli, A., Calavita, I., Dugnani, E., Citro, A., Cantarelli, E., Nano, R., Melzi, R., Maffi, P., Secchi, A., Sordi, V.*, et al.* (2013). Rapamycin unbalances the polarization of human macrophages to M1. Immunology *140*, 179-190.

Michalek, R.D., Gerriets, V.A., Jacobs, S.R., Macintyre, A.N., MacIver, N.J., Mason, E.F., Sullivan, S.A., Nichols, A.G., and Rathmell, J.C. (2011). Cutting edge: distinct glycolytic and lipid oxidative metabolic programs are essential for effector and regulatory CD4+ T cell subsets. Journal of immunology (Baltimore, Md : 1950) *186*, 3299-3303.

Michelucci, A., Cordes, T., Ghelfi, J., Pailot, A., Reiling, N., Goldmann, O., Binz, T., Wegner, A., Tallam, A., Rausell, A.*, et al.* (2013). Immune-responsive gene 1 protein links metabolism to immunity by catalyzing itaconic acid production. Proceedings of the National Academy of Sciences of the United States of America *110*, 7820-7825.

Mirza, R., DiPietro, L.A., and Koh, T.J. (2009). Selective and specific macrophage ablation is detrimental to wound healing in mice. The American journal of pathology *175*, 2454-2462.

Mishra, B.B., Gundra, U.M., and Teale, J.M. (2011). STAT6(-)/(-) mice exhibit decreased cells with alternatively activated macrophage phenotypes and enhanced disease severity in murine neurocysticercosis. Journal of neuroimmunology *232*, 26-34.

Mitchell, G.F., DeStefano, A.L., Larson, M.G., Benjamin, E.J., Chen, M.H., Vasan, R.S., Vita, J.A., and Levy, D. (2005). Heritability and a genome-wide linkage scan for arterial stiffness, wave reflection, and mean arterial pressure: the Framingham Heart Study. Circulation *112*, 194-199.

Miyakawa, H., Woo, S.K., Dahl, S.C., Handler, J.S., and Kwon, H.M. (1999). Tonicity-responsive enhancer binding protein, a rel-like protein that stimulates transcription in response to hypertonicity. Proceedings of the National Academy of Sciences of the United States of America *96*, 2538-2542.

Moncada, S. (2000). Nitric oxide and cell respiration: physiology and pathology. Verhandelingen - Koninklijke Academie voor Geneeskunde van Belgie *62*, 171-179; discussion 179-181.

Mosser, D.M., and Edwards, J.P. (2008). Exploring the full spectrum of macrophage activation. Nature reviews Immunology *8*, 958-969.

Mukaka, M.M. (2012). Statistics corner: A guide to appropriate use of correlation coefficient in medical research. Malawi medical journal : the journal of Medical Association of Malawi *24*, 69-71.

Mukhopadhyay, S., Ramadass, A.S., Akoulitchev, A., and Gordon, S. (2014). Formation of distinct chromatin conformation signatures epigenetically regulate macrophage activation. International immunopharmacology *18*, 7-11.

Muller, S., Quast, T., Schroder, A., Hucke, S., Klotz, L., Jantsch, J., Gerzer, R., Hemmersbach, R., and Kolanus, W. (2013). Salt-dependent chemotaxis of macrophages. PloS one *8*, e73439.

Mullican, S.E., Gaddis, C.A., Alenghat, T., Nair, M.G., Giacomin, P.R., Everett, L.J., Feng, D., Steger, D.J., Schug, J., Artis, D.*, et al.* (2011). Histone deacetylase 3 is an epigenomic brake in macrophage alternative activation. Genes & development *25*, 2480-2488.

Murray, P.J., Allen, J.E., Biswas, S.K., Fisher, E.A., Gilroy, D.W., Goerdt, S., Gordon, S., Hamilton, J.A., Ivashkiv, L.B., Lawrence, T.*, et al.* (2014). Macrophage activation and polarization: nomenclature and experimental guidelines. Immunity *41*, 14-20.

Murray, P.J., and Wynn, T.A. (2011a). Obstacles and opportunities for understanding macrophage polarization. Journal of leukocyte biology *89*, 557-563.

Murray, P.J., and Wynn, T.A. (2011b). Protective and pathogenic functions of macrophage subsets. Nature reviews Immunology *11*, 723-737.

Nair, M.G., Gallagher, I.J., Taylor, M.D., Loke, P., Coulson, P.S., Wilson, R.A., Maizels, R.M., and Allen, J.E. (2005). Chitinase and Fizz family members are a generalized feature of nematode infection with selective upregulation of Ym1 and Fizz1 by antigen-presenting cells. Infection and immunity *73*, 385-394.

Nair, M.G., Guild, K.J., and Artis, D. (2006). Novel effector molecules in type 2 inflammation: lessons drawn from helminth infection and allergy. Journal of immunology (Baltimore, Md : 1950) *177*, 1393-1399.

Nakaya, K., Ayaori, M., Uto-Kondo, H., Sotherden, G.M., Nishida, T., Katamoto, H., Miura, Y., Takiguchi, S., Yakushiji, E., Iizuka, M.*, et al.* (2013). Overexpression of stearoyl-coenzyme A desaturase 1 in macrophages promotes reverse cholesterol transport. Biochimica et biophysica acta *1831*, 1402-1411.

Namgaladze, D., and Brune, B. (2014). Fatty acid oxidation is dispensable for human macrophage IL-4-induced polarization. Biochimica et biophysica acta *1841*, 1329-1335.

Nathan, C.F., Murray, H.W., Wiebe, M.E., and Rubin, B.Y. (1983). Identification of interferon-gamma as the lymphokine that activates human macrophage oxidative metabolism and antimicrobial activity. The Journal of experimental medicine *158*, 670-689.

Netea, M.G. (2013). Training innate immunity: the changing concept of immunological memory in innate host defence. European journal of clinical investigation *43*, 881-884.

Neuhofer, W. (2010). Role of NFAT5 in inflammatory disorders associated with osmotic stress. Current genomics *11*, 584-590.

Newsholme, P., Curi, R., Gordon, S., and Newsholme, E.A. (1986). Metabolism of glucose, glutamine, long-chain fatty acids and ketone bodies by murine macrophages. The Biochemical journal *239*, 121-125.

Nguyen, K.D., Qiu, Y., Cui, X., Goh, Y.P., Mwangi, J., David, T., Mukundan, L., Brombacher, F., Locksley, R.M., and Chawla, A. (2011). Alternatively activated macrophages produce catecholamines to sustain adaptive thermogenesis. Nature *480*, 104-108.

Nicodeme, E., Jeffrey, K.L., Schaefer, U., Beinke, S., Dewell, S., Chung, C.W., Chandwani, R., Marazzi, I., Wilson, P., Coste, H.*, et al.* (2010). Suppression of inflammation by a synthetic histone mimic. Nature *468*, 1119-1123.

O'Donnell, M., Mente, A., and Yusuf, S. (2014). Evidence relating sodium intake to blood pressure and CVD. Current cardiology reports *16*, 529.

O'Donnell, M., Mente, A., and Yusuf, S. (2015). Sodium intake and cardiovascular health. Circulation research *116*, 1046-1057.

O'Neill, L.A., and Hardie, D.G. (2013). Metabolism of inflammation limited by AMPK and pseudo-starvation. Nature *493*, 346-355.

O'Shea, J.J., Gadina, M., and Schreiber, R.D. (2002). Cytokine signaling in 2002: new surprises in the Jak/Stat pathway. Cell *109 Suppl*, S121-131.

O'Sullivan, D., and Pearce, E.L. (2014). Fatty acid synthesis tips the TH17-Treg cell balance. Nature medicine *20*, 1235-1236.

O'Sullivan, D., van der Windt, G.J., Huang, S.C., Curtis, J.D., Chang, C.H., Buck, M.D., Qiu, J., Smith, A.M., Lam, W.Y., DiPlato, L.M.*, et al.* (2014). Memory CD8(+) T cells use cell-intrinsic lipolysis to support the metabolic programming necessary for development. Immunity *41*, 75-88.

Odegaard, J.I., Ricardo-Gonzalez, R.R., Goforth, M.H., Morel, C.R., Subramanian, V., Mukundan, L., Red Eagle, A., Vats, D., Brombacher, F., Ferrante, A.W.*, et al.* (2007). Macrophage-specific PPARgamma controls alternative activation and improves insulin resistance. Nature *447*, 1116-1120.

Olczyk, P., Mencner, L., and Komosinska-Vassev, K. (2014). The role of the extracellular matrix components in cutaneous wound healing. BioMed research international *2014*, 747584.

Palmer, C.S., Ostrowski, M., Balderson, B., Christian, N., and Crowe, S.M. (2015). Glucose metabolism regulates T cell activation, differentiation, and functions. Frontiers in immunology *6*, 1.

Paul, W.E., and Zhu, J. (2010). How are T(H)2-type immune responses initiated and amplified? Nature reviews Immunology *10*, 225-235.

Pearce, E.L., and Pearce, E.J. (2013). Metabolic pathways in immune cell activation and quiescence. Immunity *38*, 633-643.

Pearce, E.L., Poffenberger, M.C., Chang, C.H., and Jones, R.G. (2013). Fueling immunity: insights into metabolism and lymphocyte function. Science (New York, NY) *342*, 1242454.

Peck, A., and Mellins, E.D. (2010). Precarious balance: Th17 cells in host defense. Infection and immunity *78*, 32-38.

Peisong, G., Yamasaki, A., Mao, X.Q., Enomoto, T., Feng, Z., Gloria-Bottini, F., Bottini, E., Shirakawa, T., Sun, D., and Hopkin, J.M. (2004). An asthma-associated genetic variant of STAT6 predicts low burden of ascaris worm infestation. Genes and immunity *5*, 58-62.

Penefsky, H.S. (1985). Mechanism of inhibition of mitochondrial adenosine triphosphatase by dicyclohexylcarbodiimide and oligomycin: relationship to ATP synthesis. Proceedings of the National Academy of Sciences of the United States of America *82*, 1589-1593.

Perona-Wright, G., Mohrs, K., and Mohrs, M. (2010). Sustained signaling by canonical helper T cell cytokines throughout the reactive lymph node. Nature immunology *11*, 520-526.

Perrigoue, J.G., Marshall, F.A., and Artis, D. (2008). On the hunt for helminths: innate immune cells in the recognition and response to helminth parasites. Cellular microbiology *10*, 1757-1764.

Pokholok, D.K., Harbison, C.T., Levine, S., Cole, M., Hannett, N.M., Lee, T.I., Bell, G.W., Walker, K., Rolfe, P.A., Herbolsheimer, E., *et al.* (2005). Genome-wide map of nucleosome acetylation and methylation in yeast. Cell *122*, 517-527.

Qiu, Y., Nguyen, K.D., Odegaard, J.I., Cui, X., Tian, X., Locksley, R.M., Palmiter, R.D., and Chawla, A. (2014). Eosinophils and type 2 cytokine signaling in macrophages orchestrate development of functional beige fat. Cell *157*, 1292-1308.

Quah, B.J., and Parish, C.R. (2010). The use of carboxyfluorescein diacetate succinimidyl ester (CFSE) to monitor lymphocyte proliferation. Journal of visualized experiments : JoVE.

Quah, B.J., Warren, H.S., and Parish, C.R. (2007). Monitoring lymphocyte proliferation in vitro and in vivo with the intracellular fluorescent dye carboxyfluorescein diacetate succinimidyl ester. Nature protocols *2*, 2049-2056.

Quintin, J., Saeed, S., Martens, J.H., Giamarellos-Bourboulis, E.J., Ifrim, D.C., Logie, C., Jacobs, L., Jansen, T., Kullberg, B.J., Wijmenga, C., *et al.* (2012). Candida albicans infection affords protection against reinfection via functional reprogramming of monocytes. Cell host & microbe *12*, 223-232.

Raes, G., De Baetselier, P., Noel, W., Beschin, A., Brombacher, F., and Hassanzadeh Gh, G. (2002). Differential expression of FIZZ1 and Ym1 in alternatively versus classically activated macrophages. Journal of leukocyte biology *71*, 597-602.

Raes, G., Van den Bergh, R., De Baetselier, P., Ghassabeh, G.H., Scotton, C., Locati, M., Mantovani, A., and Sozzani, S. (2005). Arginase-1 and Ym1 are markers for murine, but not human, alternatively activated myeloid cells. Journal of immunology (Baltimore, Md : 1950) *174*, 6561; author reply 6561-6562.

Raghow, R. (1994). The role of extracellular matrix in postinflammatory wound healing and fibrosis. FASEB journal : official publication of the Federation of American Societies for Experimental Biology *8*, 823-831.

Rakova, N., Juttner, K., Dahlmann, A., Schroder, A., Linz, P., Kopp, C., Rauh, M., Goller, U., Beck, L., Agureev, A., *et al.* (2013). Long-term space flight simulation reveals infradian rhythmicity in human na(+) balance. Cell metabolism *17*, 125-131.

Reese, T.A., Liang, H.E., Tager, A.M., Luster, A.D., Van Rooijen, N., Voehringer, D., and Locksley, R.M. (2007). Chitin induces accumulation in tissue of innate immune cells associated with allergy. Nature *447*, 92-96.

Reinke, H., and Horz, W. (2003). Histones are first hyperacetylated and then lose contact with the activated PHO5 promoter. Molecular cell *11*, 1599-1607.

Rodriguez-Prados, J.C., Traves, P.G., Cuenca, J., Rico, D., Aragones, J., Martin-Sanz, P., Cascante, M., and Bosca, L. (2010). Substrate fate in activated macrophages: a comparison between innate, classic, and alternative activation. Journal of immunology (Baltimore, Md : 1950) *185*, 605-614.

Rosenblum, M.D., Remedios, K.A., and Abbas, A.K. (2015). Mechanisms of human autoimmunity. The Journal of clinical investigation *125*, 2228-2233.

Ruben, S., Perkins, A., Purcell, R., Joung, K., Sia, R., Burghoff, R., Haseltine, W.A., and Rosen, C.A. (1989). Structural and functional characterization of human immunodeficiency virus tat protein. Journal of virology *63*, 1-8.

Ruckerl, D., Jenkins, S.J., Laqtom, N.N., Gallagher, I.J., Sutherland, T.E., Duncan, S., Buck, A.H., and Allen, J.E. (2012). Induction of IL-4Ralpha-dependent microRNAs identifies PI3K/Akt signaling as essential for IL-4-driven murine macrophage proliferation in vivo. Blood *120*, 2307-2316.

Safa, K., Ohori, S., Borges, T.J., Uehara, M., Batal, I., Shimizu, T., Magee, C.N., Belizaire, R., Abdi, R., Wu, C., *et al.* (2015). Salt Accelerates Allograft Rejection through Serum- and Glucocorticoid-Regulated Kinase-1-Dependent Inhibition of Regulatory T Cells. Journal of the American Society of Nephrology : JASN.

Sakaguchi, S., Wing, K., Onishi, Y., Prieto-Martin, P., and Yamaguchi, T. (2009). Regulatory T cells: how do they suppress immune responses? International immunology *21*, 1105-1111.

Saleh, M.A., McMaster, W.G., Wu, J., Norlander, A.E., Funt, S.A., Thabet, S.R., Kirabo, A., Xiao, L., Chen, W., Itani, H.A., *et al.* (2015). Lymphocyte adaptor protein LNK deficiency exacerbates hypertension and end-organ inflammation. The Journal of clinical investigation *125*, 1189-1202.

Sanford, K.K., Earle, W.R., and Likely, G.D. (1948). The growth in vitro of single isolated tissue cells. Journal of the National Cancer Institute *9*, 229-246.

Sasaki, M., Abe, R., Fujita, Y., Ando, S., Inokuma, D., and Shimizu, H. (2008). Mesenchymal stem cells are recruited into wounded skin and contribute to wound repair by transdifferentiation into multiple skin cell type. Journal of immunology (Baltimore, Md : 1950) *180*, 2581-2587.

Satoh, T., Takeuchi, O., Vandenbon, A., Yasuda, K., Tanaka, Y., Kumagai, Y., Miyake, T., Matsushita, K., Okazaki, T., Saitoh, T., *et al.* (2010). The Jmjd3-Irf4 axis regulates M2 macrophage polarization and host responses against helminth infection. Nature immunology *11*, 936-944.

Savill, J., Dransfield, I., Gregory, C., and Haslett, C. (2002). A blast from the past: clearance of apoptotic cells regulates immune responses. Nature reviews Immunology *2*, 965-975.

Schafflhuber, M., Volpi, N., Dahlmann, A., Hilgers, K.F., Maccari, F., Dietsch, P., Wagner, H., Luft, F.C., Eckardt, K.U., and Titze, J. (2007). Mobilization of osmotically inactive Na+ by growth and by dietary salt restriction in rats. American journal of physiology Renal physiology *292*, F1490-1500.

Schebesch, C., Kodelja, V., Muller, C., Hakij, N., Bisson, S., Orfanos, C.E., and Goerdt, S. (1997). Alternatively activated macrophages actively inhibit proliferation of peripheral blood lymphocytes and CD4+ T cells in vitro. Immunology *92*, 478-486.

Schieven, G.L. (2005). The biology of p38 kinase: a central role in inflammation. Current topics in medicinal chemistry *5*, 921-928.

Schiffrin, E.L. (2014). Immune mechanisms in hypertension and vascular injury. Clinical science (London, England : 1979) *126*, 267-274.

Schindler, J.F., Monahan, J.B., and Smith, W.G. (2007). p38 pathway kinases as anti-inflammatory drug targets. Journal of dental research *86*, 800-811.

Schmelzle, T., and Hall, M.N. (2000). TOR, a central controller of cell growth. Cell *103*, 253-262.

Schmidt-Ott, K.M., Mori, K., Li, J.Y., Kalandadze, A., Cohen, D.J., Devarajan, P., and Barasch, J. (2007). Dual action of neutrophil gelatinase-associated lipocalin. Journal of the American Society of Nephrology : JASN *18*, 407-413.

Schneider, C.A., Rasband, W.S., and Eliceiri, K.W. (2012). NIH Image to ImageJ: 25 years of image analysis. Nature methods *9*, 671-675.

Schones, D.E., and Zhao, K. (2008). Genome-wide approaches to studying chromatin modifications. Nature reviews Genetics *9*, 179-191.

Schuettengruber, B., Chourrout, D., Vervoort, M., Leblanc, B., and Cavalli, G. (2007). Genome regulation by polycomb and trithorax proteins. Cell *128*, 735-745.

Schulte, J.H., Marschall, T., Martin, M., Rosenstiel, P., Mestdagh, P., Schlierf, S., Thor, T., Vandesompele, J., Eggert, A., Schreiber, S., *et al.* (2010). Deep sequencing reveals differential expression of microRNAs in favorable versus unfavorable neuroblastoma. Nucleic acids research *38*, 5919-5928.

Schultze, J.L. (2014). Precision attack on calcineurin in macrophages: a new anti-inflammatory weapon. The EMBO journal *33*, 1087-1088.

Shapiro, L., and Dinarello, C.A. (1995). Osmotic regulation of cytokine synthesis in vitro. Proceedings of the National Academy of Sciences of the United States of America *92*, 12230-12234.

Shapiro, L., and Dinarello, C.A. (1997). Hyperosmotic stress as a stimulant for proinflammatory cytokine production. Experimental cell research *231*, 354-362.

Shi, L.Z., Wang, R., Huang, G., Vogel, P., Neale, G., Green, D.R., and Chi, H. (2011). HIF1alpha-dependent glycolytic pathway orchestrates a metabolic checkpoint for the differentiation of TH17 and Treg cells. The Journal of experimental medicine *208*, 1367-1376.

Shi, Y., and Whetstine, J.R. (2007). Dynamic regulation of histone lysine methylation by demethylases. Molecular cell *25*, 1-14.

Shimoda, K., van Deursen, J., Sangster, M.Y., Sarawar, S.R., Carson, R.T., Tripp, R.A., Chu, C., Quelle, F.W., Nosaka, T., Vignali, D.A., *et al.* (1996). Lack of IL-4-induced Th2 response and IgE class switching in mice with disrupted Stat6 gene. Nature *380*, 630-633.

Smolkova, B., El Yamani, N., Collins, A.R., Gutleb, A.C., and Dusinska, M. (2014). Nanoparticles in food. epigenetic changes induced by nanomaterials and possible impact on health. Food and chemical toxicology : an international journal published for the British Industrial Biological Research Association.

Song, M.M., and Shuai, K. (1998). The suppressor of cytokine signaling (SOCS) 1 and SOCS3 but not SOCS2 proteins inhibit interferon-mediated antiviral and antiproliferative activities. The Journal of biological chemistry *273*, 35056-35062.

Spirig, R., Tsui, J., and Shaw, S. (2012). The Emerging Role of TLR and Innate Immunity in Cardiovascular Disease. Cardiology research and practice *2012*, 181394.

Stein, M., Keshav, S., Harris, N., and Gordon, S. (1992). Interleukin 4 potently enhances murine macrophage mannose receptor activity: a marker of alternative immunologic macrophage activation. The Journal of experimental medicine *176*, 287-292.

Stockinger, B., Zal, T., Zal, A., and Gray, D. (1996). B cells solicit their own help from T cells. The Journal of experimental medicine *183*, 891-899.

Stout, R.D. (2010). Editorial: macrophage functional phenotypes: no alternatives in dermal wound healing? Journal of leukocyte biology *87*, 19-21.

Strahl, B.D., and Allis, C.D. (2000). The language of covalent histone modifications. Nature *403*, 41-45.

Stuehr, D.J., and Nathan, C.F. (1989). Nitric oxide. A macrophage product responsible for cytostasis and respiratory inhibition in tumor target cells. The Journal of experimental medicine *169*, 1543-1555.

Sundstrom, B., Johansson, I., and Rantapaa-Dahlqvist, S. (2015). Interaction between dietary sodium and smoking increases the risk for rheumatoid arthritis: results from a nested case-control study. Rheumatology (Oxford, England) *54*, 487-493.

Supek, F., Bosnjak, M., Skunca, N., and Smuc, T. (2011). REVIGO summarizes and visualizes long lists of gene ontology terms. PloS one *6*, e21800.

Sveinbjornsson, B., Olsen, R., Seternes, O.M., and Seljelid, R. (1996). Macrophage cytotoxicity against murine meth A sarcoma involves nitric oxide-mediated apoptosis. Biochemical and biophysical research communications *223*, 643-649.

Szabo, G., and Magyar, Z. (1982). Electrolyte concentrations in subcutaneous tissue fluid and lymph. Lymphology *15*, 174-177.

Takeda, K., and Akira, S. (2004). TLR signaling pathways. Seminars in immunology *16*, 3-9.

Takeda, K., Tanaka, T., Shi, W., Matsumoto, M., Minami, M., Kashiwamura, S., Nakanishi, K., Yoshida, N., Kishimoto, T., and Akira, S. (1996). Essential role of Stat6 in IL-4 signalling. Nature *380*, 627-630.

Tan, Z., Xie, N., Cui, H., Moellering, D.R., Abraham, E., Thannickal, V.J., and Liu, G. (2015). Pyruvate Dehydrogenase Kinase 1 Participates in Macrophage Polarization via Regulating Glucose Metabolism. Journal of immunology (Baltimore, Md : 1950) *194*, 6082-6089.

Tannahill, G.M., Curtis, A.M., Adamik, J., Palsson-McDermott, E.M., McGettrick, A.F., Goel, G., Frezza, C., Bernard, N.J., Kelly, B., Foley, N.H., *et al.* (2013). Succinate is an inflammatory signal that induces IL-1beta through HIF-1alpha. Nature *496*, 238-242.

Terry, J. (1994). The major electrolytes: sodium, potassium, and chloride. Journal of intravenous nursing : the official publication of the Intravenous Nurses Society *17*, 240-247.

Thomas, G.D., Ruckerl, D., Maskrey, B.H., Whitfield, P.D., Blaxter, M.L., and Allen, J.E. (2012). The biology of nematode- and IL4Ralpha-dependent murine macrophage polarization in vivo as defined by RNA-Seq and targeted lipidomics. Blood *120*, e93-e104.

Titze, J. (2014). Sodium balance is not just a renal affair. Current opinion in nephrology and hypertension *23*, 101-105.

Titze, J., Dahlmann, A., Lerchl, K., Kopp, C., Rakova, N., Schroder, A., and Luft, F.C. (2014). Spooky sodium balance. Kidney international *85*, 759-767.

Titze, J., Lang, R., Ilies, C., Schwind, K.H., Kirsch, K.A., Dietsch, P., Luft, F.C., and Hilgers, K.F. (2003). Osmotically inactive skin Na+ storage in rats. American journal of physiology Renal physiology *285*, F1108-1117.

Titze, J., and Machnik, A. (2010). Sodium sensing in the interstitium and relationship to hypertension. Current opinion in nephrology and hypertension *19*, 385-392.

Titze, J., Maillet, A., Lang, R., Gunga, H.C., Johannes, B., Gauquelin-Koch, G., Kihm, E., Larina, I., Gharib, C., and Kirsch, K.A. (2002). Long-term sodium balance in humans in a terrestrial space station simulation study. American journal of kidney diseases : the official journal of the National Kidney Foundation *40*, 508-516.

Titze, J., Shakibaei, M., Schafflhuber, M., Schulze-Tanzil, G., Porst, M., Schwind, K.H., Dietsch, P., and Hilgers, K.F. (2004). Glycosaminoglycan polymerization may enable osmotically inactive Na+ storage in the skin. American journal of physiology Heart and circulatory physiology *287*, H203-208.

Topfer, E., Boraschi, D., and Italiani, P. (2015). Innate Immune Memory: The Latest Frontier of Adjuvanticity. Journal of immunology research *2015*, 478408.

Toshchakov, V., Jones, B.W., Perera, P.Y., Thomas, K., Cody, M.J., Zhang, S., Williams, B.R., Major, J., Hamilton, T.A., Fenton, M.J., *et al.* (2002). TLR4, but not TLR2, mediates IFN-beta-induced STAT1alpha/beta-dependent gene expression in macrophages. Nature immunology *3*, 392-398.

Toulon, A., Breton, L., Taylor, K.R., Tenenhaus, M., Bhavsar, D., Lanigan, C., Rudolph, R., Jameson, J., and Havran, W.L. (2009). A role for human skin-resident T cells in wound healing. The Journal of experimental medicine *206*, 743-750.

Tugal, D., Liao, X., and Jain, M.K. (2013). Transcriptional Control of Macrophage Polarization. Arteriosclerosis, thrombosis, and vascular biology.

van de Veerdonk, F.L., Gresnigt, M.S., Kullberg, B.J., van der Meer, J.W., Joosten, L.A., and Netea, M.G. (2009). Th17 responses and host defense against microorganisms: an overview. BMB reports *42*, 776-787.

Vander Heiden, M.G., Cantley, L.C., and Thompson, C.B. (2009). Understanding the Warburg effect: the metabolic requirements of cell proliferation. Science (New York, NY) *324*, 1029-1033.

Varin, A., and Gordon, S. (2009). Alternative activation of macrophages: immune function and cellular biology. Immunobiology *214*, 630-641.

Vats, D., Mukundan, L., Odegaard, J.I., Zhang, L., Smith, K.L., Morel, C.R., Wagner, R.A., Greaves, D.R., Murray, P.J., and Chawla, A. (2006). Oxidative metabolism and PGC-1beta attenuate macrophage-mediated inflammation. Cell metabolism *4*, 13-24.

Voehringer, D., van Rooijen, N., and Locksley, R.M. (2007). Eosinophils develop in distinct stages and are recruited to peripheral sites by alternatively activated macrophages. Journal of leukocyte biology *81*, 1434-1444.

Warburg, O., Wind, F., and Negelein, E. (1927). THE METABOLISM OF TUMORS IN THE BODY. The Journal of general physiology *8*, 519-530.

Wegener, E., and Krappmann, D. (2007). CARD-Bcl10-Malt1 signalosomes: missing link to NF-kappaB. Science's STKE : signal transduction knowledge environment *2007*, pe21.

Weichhart, T., Costantino, G., Poglitsch, M., Rosner, M., Zeyda, M., Stuhlmeier, K.M., Kolbe, T., Stulnig, T.M., Horl, W.H., Hengstschlager, M., *et al.* (2008). The TSC-mTOR signaling pathway regulates the innate inflammatory response. Immunity *29*, 565-577.

Weichhart, T., and Saemann, M.D. (2008). The PI3K/Akt/mTOR pathway in innate immune cells: emerging therapeutic applications. Annals of the rheumatic diseases *67 Suppl 3*, iii70-74.

Weintraub, H., and Groudine, M. (1976). Chromosomal subunits in active genes have an altered conformation. Science (New York, NY) *193*, 848-856.

Weintz, G., Olsen, J.V., Fruhauf, K., Niedzielska, M., Amit, I., Jantsch, J., Mages, J., Frech, C., Dolken, L., Mann, M., *et al.* (2010). The phosphoproteome of toll-like receptor-activated macrophages. Molecular systems biology *6*, 371.

White, J.R., Imburgia, C., Dul, E., Appelbaum, E., O'Donnell, K., O'Shannessy, D.J., Brawner, M., Fornwald, J., Adamou, J., Elshourbagy, N.A., *et al.* (1997). Cloning and functional characterization of a novel human CC chemokine that binds to the CCR3 receptor and activates human eosinophils. Journal of leukocyte biology *62*, 667-675.

Wiig, H., Schroder, A., Neuhofer, W., Jantsch, J., Kopp, C., Karlsen, T.V., Boschmann, M., Goss, J., Bry, M., Rakova, N., *et al.* (2013). Immune cells control skin lymphatic electrolyte homeostasis and blood pressure. The Journal of clinical investigation *123*, 2803-2815.

Winter, D.R., and Amit, I. (2014). The role of chromatin dynamics in immune cell development. Immunological reviews *261*, 9-22.

Wong, V.W., Longaker, M.T., and Gurtner, G.C. (2012). Soft tissue mechanotransduction in wound healing and fibrosis. Seminars in cell & developmental biology *23*, 981-986.

Wu, C., Yosef, N., Thalhamer, T., Zhu, C., Xiao, S., Kishi, Y., Regev, A., and Kuchroo, V.K. (2013). Induction of pathogenic TH17 cells by inducible salt-sensing kinase SGK1. Nature *496*, 513-517.

Wu, D., Molofsky, A.B., Liang, H.E., Ricardo-Gonzalez, R.R., Jouihan, H.A., Bando, J.K., Chawla, A., and Locksley, R.M. (2011). Eosinophils sustain adipose alternatively activated macrophages associated with glucose homeostasis. Science (New York, NY) *332*, 243-247.

Wulff, P., Vallon, V., Huang, D.Y., Volkl, H., Yu, F., Richter, K., Jansen, M., Schlunz, M., Klingel, K., Loffing, J., *et al.* (2002). Impaired renal Na(+) retention in the sgk1-knockout mouse. The Journal of clinical investigation *110*, 1263-1268.

Xue, J., Schmidt, S.V., Sander, J., Draffehn, A., Krebs, W., Quester, I., De Nardo, D., Gohel, T.D., Emde, M., Schmidleithner, L., *et al.* (2014). Transcriptome-based network analysis reveals a spectrum model of human macrophage activation. Immunity *40*, 274-288.

Yamada, K., Saito, M., Matsuoka, H., and Inagaki, N. (2007). A real-time method of imaging glucose uptake in single, living mammalian cells. Nature protocols *2*, 753-762.

Yamaguchi, T., Wing, J.B., and Sakaguchi, S. (2011). Two modes of immune suppression by Foxp3(+) regulatory T cells under inflammatory or non-inflammatory conditions. Seminars in immunology *23*, 424-430.

Yamasaki, H., Shimoji, H., Ohshiro, Y., and Sakihama, Y. (2001). Inhibitory effects of nitric oxide on oxidative phosphorylation in plant mitochondria. Nitric oxide : biology and chemistry / official journal of the Nitric Oxide Society *5*, 261-270.

Yancey, P.H., Clark, M.E., Hand, S.C., Bowlus, R.D., and Somero, G.N. (1982). Living with water stress: evolution of osmolyte systems. Science (New York, NY) *217*, 1214-1222.

Yoshida, A., Inagawa, H., Kohchi, C., Nishizawa, T., and Soma, G. (2009). The role of toll-like receptor 2 in survival strategies of Mycobacterium tuberculosis in macrophage phagosomes. Anticancer research *29*, 907-910.

Yoshimura, A., Nishinakamura, H., Matsumura, Y., and Hanada, T. (2005). Negative regulation of cytokine signaling and immune responses by SOCS proteins. Arthritis research & therapy *7*, 100-110.

Yoshioka, K., Takahashi, H., Homma, T., Saito, M., Oh, K.B., Nemoto, Y., and Matsuoka, H. (1996). A novel fluorescent derivative of glucose applicable to the assessment of glucose uptake activity of Escherichia coli. Biochimica et biophysica acta *1289*, 5-9.

Zarubin, T., and Han, J. (2005). Activation and signaling of the p38 MAP kinase pathway. Cell research *15*, 11-18.

Zeng, H., Yang, K., Cloer, C., Neale, G., Vogel, P., and Chi, H. (2013). mTORC1 couples immune signals and metabolic programming to establish T(reg)-cell function. Nature *499*, 485-490.

Zhang, W.C., Zheng, X.J., Du, L.J., Sun, J.Y., Shen, Z.X., Shi, C., Sun, S., Zhang, Z., Chen, X.Q., Qin, M.*, et al.* (2015). High salt primes a specific activation state of macrophages, M(Na). Cell research *25*, 893-910.

Zhao, S., Guo, Y., Sheng, Q., and Shyr, Y. (2014). Advanced heat map and clustering analysis using heatmap3. BioMed research international *2014*, 986048.